NBS MONOGRAPH 38

Radiation Patterns in the Lower Ionosphere And Fresnel Zones for Elevated Antennas Over a Spherical Earth

U.S. DEPARTMENT OF COMMERCE

NATIONAL BUREAU OF STANDARDS

THE NATIONAL BUREAU OF STANDARDS

Functions and Activities

The functions of the National Bureau of Standards are set forth in the Act of Congress, March 3, 1901, as amended by Congress in Public Law 619, 1950. These include the development and maintenance of the national standards of measurement and the provision of means and methods for making measurements consistent with these standards; the determination of physical constants and properties of materials; the development of methods and instruments for testing materials, devices, and structures; advisory services to government agencies on scientific and technical problems; invention and development of devices to serve special needs of the Government; and the development of standard practices, codes, and specifications. The work includes basic and applied research, development, engineering, instrumentation, testing, evaluation, calibration services, and various consultation and information services. Research projects are also performed for other government agencies when the work relates to and supplements the basic program of the Bureau or when the Bureau's unique competence is required. The scope of activities is suggested by the listing of divisions and sections on the inside of the back cover.

Publications

The results of the Bureau's research are published either in the Bureau's own series of publications or in the journals of professional and scientific societies. The Bureau itself publishes three periodicals available from the Government Printing Office: The Journal of Research, published in four separate sections, presents complete scientific and technical papers; the Technical News Bulletin presents summary and preliminary reports on work in progress; and Basic Radio Propagation Predictions provides data for determining the best frequencies to use for radio communications throughout the world. There are also five series of nonperiodical publications: Monographs, Applied Mathematics Series, Handboks, Miscellaneous Publications, and Technical Notes.

A complete listing of the Bureau's publications can be found in National Bureau of Standards Circular 460, Publications of the National Bureau of Standards, 1901 to June 1947 ($1.25), and the Supplement to National Bureau of Standards Circular 460, July 1947 to June 1957 ($1.50), and Miscellaneous Publication 240, July 1957 to June 1960 (includes titles of papers published in outside journals 1950 to 1959) ($2.25); available from the Superintendent of Documents, Government Printing Office, Washington 25, D.C.

UNITED STATES DEPARTMENT OF COMMERCE • Luther H. Hodges, *Secretary*
NATIONAL BUREAU OF STANDARDS • A. V. Astin, *Director*

Radiation Patterns in the Lower Ionosphere and Fresnel Zones for Elevated Antennas Over a Spherical Earth

R. G. Merrill and W. V. Mansfield

National Bureau of Standards Monograph 38

Issued April 2, 1962

For sale by the Superintendent of Documents, U.S. Government Printing Office
Washington 25, D.C. - Price 70 cents

Contents

Radiation Patterns in the Lower Ionosphere and Fresnel Zones for Elevated Antennas Over a Spherical Earth

R. G. Merrill and W. V. Mansfield

Ground reflection interference patterns in the lower ionosphere have been computed for elevated antennas over a spherical earth. The computations incorporated parallax, tropospheric refraction and defocusing, spherical divergence, and near-horizon diffraction. The following antenna siting parameters for VHF scatter propagation were computed from the patterns:

1. Antenna height and elevation angle for placing the maximum of the first lobe at the path midpoint.
2. Distances from the antenna to the edges and to the quarter-wave contour of the first Fresnel zone on the earth's surface.
3. Information for determining the effects of obstacles located in the first Fresnel zone.

1. Introduction

The purpose of this work is to give the results of a detailed computation of antenna patterns in the lower ionosphere at VHF over a spherical earth. The following results are presented which have been computed from these patterns:

1. Antenna height and elevation angle for placing the maximum of the first lobe at the path midpoint; this height will henceforth be called the *lobe alinement height.*
2. Distances from the antenna to the edges and to the quarter-wave contour of the first Fresnel zone on the earth's surface.
3. Information for determining the effects of obstacles located in the first Fresnel zone. The analysis of these effects incorporates a new concept and certain refinements within the limitations of geometrical optics.

The antenna height-gain function has also been computed from these patterns.[1] [1] This function shows that there is a range of heights lower than the lobe alinement height which provides gain greater than or equal to that of the lobe alinement height.

The model used in the computations is defined by: tropospheric refraction determined by surface refractivity and a single gradient of refractivity; spherical divergence; defocusing due to refraction; a finite distance to the scattering stratum in the lower ionosphere; a near-horizon diffraction correction; and horizontally polarized antennas.

Results are presented for an ionospheric scattering layer height of 85 km at frequencies of 30 to 55 Mc; these have been found to be the most useful values [2] and they correspond to computed path lengths of 1000 to 2400 km. Parameters corresponding to "standard refraction" and a temperate over-water or tropical "wet" refraction were used.

Prior computations by Bailey, Bateman, and Kirby [2] of lobe alinement antenna heights and angles of elevation did not incorporate divergence and defocusing.

2. General Procedures

Figures 1 and 2 show the geometry used in the calculations. It is assumed that the great circle path is symmetrical about a line in the plane of propagation drawn from the center of the earth to the ionospheric scattering volume; this symmetry limits consideration to half the total path. Tropospheric refraction is incorporated using a bilinear model defined by surface refractivity and a linear gradient of refractivity. Divergence due to reflection from the curved surface of the earth is computed by means of a simplification of the van der Pol-Bremmer geometrical derivation, namely the assumption that there is no energy outside the plane of propagation (cylindrical earth). Divergence due to refractive defocusing in the atmosphere is computed analogously to divergence for the direct ray and is incorporated in the divergence of the reflected ray.

In the refractivity model, a single linear gradient is applied only up to that elevation at which the refractivity vanishes (i.e., the index of refraction becomes unity). Above this height the refractivity is defined as zero. Model atmospheres defined by Bean and Thayer [3] closely fit observed refractivity profiles, but limitations in significant figures with respect to wavelength in the computer program for ray tracing through these atmospheres do not allow these models to be used to compute the interference patterns. However, as will be shown below (sec. 4), comparison of the bilinear model used here with the exponential reference atmosphere (the simplest of the Bean and Thayer models) for the same parameters shows that the former is entirely satisfactory.

The spherical coefficient of reflection is taken to be −1.0 in accordance with Bremmer's analysis [4]. For the maximum value of the grazing angle (ψ) encountered in the present computations, the least favorable conditions give a coefficient of −0.9 at 40 Mc; for this case the gradient of the reflection coefficient is negligible through the range of ψ encountered so that the lobe position is virtually unaffected.

[1] Figures in brackets indicate the literature references on page 29.

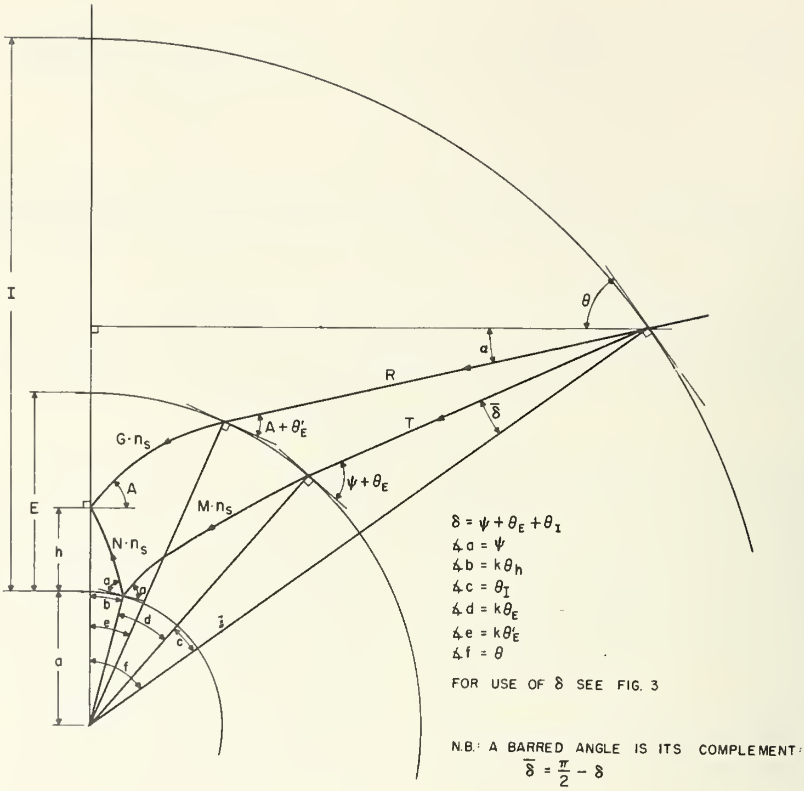

Figure 1. *The geometry in the ionosphere.*

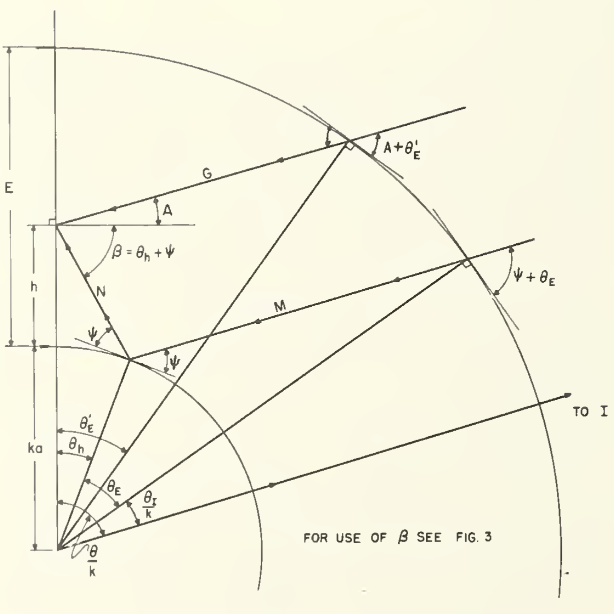

Figure 2. *The geometry in the radio troposphere.*

3. Details of Analysis

The parameters are the surface refractivity, N_s; the gradient of refractivity, ΔN; the height of the antenna, h; the height of the ionospheric scattering layer, I; and the frequency of transmission, f. The earth's radius $a=6368$ km (mean value to the nearest km) and the velocity of light in vacuo [2] $c=2.99790\cdot 10^{10}$ cm/sec.

All equations numbered below also appear in a single list as appendix VII.

Refraction. The radius of curvature of rays passing through a *linear* atmosphere may be made infinite by increasing the radius of the earth [5]. The linear atmosphere is defined and analyzed as follows. Let the variation with height, z, of the index of refraction, n, be $n=n_s+z(dn/dz)$, where n_s is the index at the surface and dn/dz is a *constant.* The modified index of refraction which takes into account the earth's curvature is defined by $m=n(1+z/a)$. Substitution gives $m=[n_s+z(dn/dz)]\ (1+z/a)$. Let this be written as $m=n_s(1+z/ka)$, where k is the effective earth's radius factor. Equating the two expressions for m we have $k=1/[\{1+(a+z)/n_s\}(dn/dz)]$. In terms of N-units (defined by $N=(n-1)\cdot 10^6$) we have $dn/dz=10^{-6}dN/dz=-\Delta N\cdot 10^{-6}$,

[2] von Ardenne, *Tabellen* 1956. In 1957 URSI and IUGG adopted $(2.997925 \pm 0.4\cdot 10^{-6})10^{10}$ cm/s.

so that $k=1/[1-\Delta N\cdot 10^{-6}(a+z)/n_s]$. It is seen that k is a function of z, but since $a>>z$ and z will be no greater than the height at which N vanishes (see eq (2) below), the effect of z is negligible. Further, for defining k, n_s is negligibly different from unity, whence we have

$$k=\frac{1}{1-\Delta N\cdot a\cdot 10^{-6}}. \tag{1}$$

For a given surface refractivity, the refractivity vanishes at a height given by

$$E=N_s/\Delta N. \tag{2}$$

The gradient, ΔN, is the change in N per kilometer as measured 1 km above the earth's surface. The height E will be called the *radio tropopause* and the linear atmosphere from the surface to E will be called the *radio troposphere*. (These must be distinguished from the *physical* tropopause, occuring at about 10 km, and the *physical* troposphere.)

Geometry. The geometry of the entire model is shown in figure 1; the geometry within the radio troposphere over the ka earth is shown in figure 2. If ψ, the angle of reflection (grazing angle), is given, the following quantities are obtained from plane geometry and trigonometry:

$$\theta_h=\cos^{-1}\left(\frac{ka}{ka+h}\cdot\cos\psi\right)-\psi; \tag{3}$$

$$N=\frac{\sin\theta_h}{\cos\psi}(ka+h); \tag{4}$$

$$\theta_E=\cos^{-1}\left(\frac{ka}{ka+E}\cdot\cos\psi\right)-\psi; \tag{5}$$

$$M=\frac{\sin\theta_E}{\cos\psi}(ka+E); \tag{6}$$

$$\theta_I=\cos^{-1}\left[\frac{a+E}{a+I}\cos(\psi+\theta_E)\right]-\psi-\theta_E; \tag{7}$$

$$T=\frac{\sin\theta_I}{\cos(\psi+\theta_E)}(a+I); \tag{8}$$

$$\theta=k(\theta_h+\theta_E)+\theta_I=\theta(\psi). \tag{9}$$

If A, the observed angle of elevation, is given, we have:

$$\theta_E'=\cos^{-1}\left(\frac{ka+h}{ka+E}\cos A\right)-A; \tag{10}$$

$$\alpha=A-\theta_E'(k-1); \tag{11}$$

$$G=\frac{\sin\theta_E'}{\cos A}(ka+E); \tag{12}$$

$$\theta'=\cos^{-1}\left[\frac{a+E}{a+I}\cos(A+\theta_E')\right]-\alpha=\theta(A); \tag{13}$$

$$R=\frac{\sin(\theta'-k\theta_E')}{\cos(A+\theta_E')}(a+I). \tag{14}$$

For the horizon case, $\psi=0$, we have:

$$\theta_E=\cos^{-1}\left(\frac{ka}{ka+E}\right); \tag{15}$$

$$\theta_h=\cos^{-1}\left(\frac{ka}{ka+h}\right)=-A_0\ (\text{horizon } A); \tag{16}$$

$$\begin{aligned}\theta_I&=\cos^{-1}\left(\frac{a+E}{a+I}\cdot\frac{ka}{ka+E}\right)-\cos^{-1}\left(\frac{ka}{ka+E}\right)\\&=\cos^{-1}\left(\frac{a+E}{a+I}\cos\theta_E'\right)-\theta_E'.\end{aligned} \tag{17}$$

The formal relationship between A and ψ is given by

$$\begin{aligned}&\cos^{-1}\left[\frac{a+E}{a+I}\cdot\frac{ka+h}{ka+E}\cdot\cos A\right]\\&\quad+(k-1)\cos^{-1}\left[\frac{ka+h}{ka+E}\cdot\cos A\right]-A\\&=(k-1)\cos^{-1}\left(\frac{ka}{ka+E}\cos\psi\right)\\&\quad+k\left[\cos^{-1}\left(\frac{ka}{ka+h}\cos_\psi\right)-2\psi\right]\\&\quad+\cos^{-1}\left(\frac{a+E}{a+I}\cdot\frac{ka}{ka+E}\cos\psi\right),\end{aligned} \tag{18}$$

and it can be shown that in the general case neither can be stated as a closed algebraic function of the other. All of these equations follow directly from the geometry and trigonometry of the problem.

Interpolation and derivative correction. In view of (18), some approximation method for relating A and ψ is necessary. Since the angle θ is the angle in common between A and ψ, and fewer steps are required to compute $\theta(A)$ than to compute $\theta(\psi)$, successive differences of $\theta(A)$ were used to compute the value A corresponding to a given ψ. The families of angles and distances associated with ψ and A were computed independently using an arithmetic progression of difference h_D for the successive values of the two angles, h_D being so chosen that the successive differences of $\theta(A)$ allow an inverse quadratic interpolation to be used to compute the A corresponding to a given ψ.

The inverse interpolation as defined by Stirling's central difference formula takes the following forms:

$$A_{n(c)}=h_D u_u+A_n; \tag{19}$$

$$u_u=\frac{-\Delta^1\theta_{n-2}'-\Delta^1\theta_n'-\sqrt{(-\Delta^1\theta_{n-1}'-\Delta^1\theta_n')^2+8\Delta^2\theta_{n-1}'(\theta_n-\theta_n')}}{2\Delta^2\theta_{n-1}'}; \tag{20}$$

$$A_{n(c)}=h_D u_l+A_{n-1}; \tag{21}$$

$$u_l=\frac{-\Delta^1\theta'_{n-2}-\Delta^1\theta'_{n-1}-\sqrt{(-\Delta^1\theta'_{n-2}-\Delta^1\theta'_{n-1})^2-8\Delta^2\theta'_{n-2}(\theta'_{n-1}-\theta_n)}}{2\Delta^2\theta'_{n-2}}; \tag{22}$$

where $\theta'_n<\theta_n<\theta'_{n+1}$, and θ_n is nearer θ'_n in (19) and (20) and nearer θ'_{n+1} in (21) and (22). The $\theta(A)$ found by this interpolation agreed with $\theta(\psi)$ in eight significant figures when the process was carried out using 10 figures throughout (this being the normal capacity of the digital computer); it was found that if agreement in 10 figures could be approached, erratic behavior in the computed voltage resultant near the horizon would be eliminated. A derivative correction was applied to the interpolated $\theta(A)$ which is given by

$$\frac{d(A_{n(c)})}{d\theta_n}\cdot\Delta\theta=\Delta A_{n(c)}; \tag{23}$$

$$A_{n(dc)}=A_{n(c)}+\Delta A_{n(c)}; \tag{24}$$

$$\Delta\theta=\theta(A_{n(c)})-\theta(\psi_n); \tag{25}$$

$$\frac{d(A_{n(c)})}{d\theta_n}=\frac{2h_D}{\Delta^1\theta'_{n-1}+\Delta^1\theta'_n+2u_u\Delta^2\theta'_{n-1}}; \tag{26}$$

$$\frac{d(A_{n(c)})}{d\theta_n}=\frac{2h_D}{\Delta^1\theta'_{n-2}+\Delta^1\theta'_{n-1}+2u_l\Delta^2\theta'_{n-2}}; \tag{27}$$

where u_u and u_l are defined by (20) and (22), respectively. The family of angles and path length segments defined by equations 10 to 17 is recomputed after each corrected interpolation. This procedure achieved the desired result: it was found that the recomputed path segments corresponded to the path segments defined by ψ with an error of ±3 mm (estimated from successive differences); this error was sufficiently small with respect to wavelength so that values of the voltage resultant lay on a smooth curve throughout.

Divergence and defocusing. The spherical divergence derived from electromagnetic theory can also be derived geometrically, as shown by van der Pol and Bremmer [4,6]. Geometrically, the divergence is the ratio of the cross section of a cone of rays at a given point after reflection from a plane surface to the cross section at the same point after reflection from a spherical surface. In the present computation the energy outside the plane of propagation is defined as zero so that linear dimensions rather than areas are used to compute the divergence. The "defocusing" of both direct and reflected rays is defined analogously: the total bending by the radio troposphere of rays at different elevation angles is different, thus, in the plane of propagation, the ratio of the distance between the ends of two "adjacent" rays of given length without bending to the corresponding distance after the rays pass through the radio troposphere defines the defocusing.

The geometry of this spherical divergence computation is shown in figure 3; refraction is included in the computation although the bending is not depicted in this figure as it was in figure 1. Figure 3A shows the shift in the rays with changing ψ if there were no reflecting surface; the plane cross section of the cone is closely approximated by the arc q_1, which is defined as the linear segment required. The rays are shown in figure 1, and β is shown in figure 2. Letting L be the length of a ray, we have $L_{1+½}=(L_1+L_2)/2$ and $q_1=(\beta_2-\beta_1)L_{1+½}$. In figure 3B, the ray lengths are the same but spherical divergence and refractive defocusing give the linear measure shown as q_2. Angle δ is shown in figure 1; since the difference (h_D) between successive values of ψ is so small that $\bar{\delta}_2-\bar{\delta}_1$ is negligible, $\bar{\delta}_1$ is taken equal to $\bar{\delta}_{1+½}$, and since $\theta_1-\theta_2$ is small enough so that the arc q_2' may be taken as the chord, we have $q_2'=(\theta_1-\theta_2)(a+I)$ and $q_2=q_2'\cos\bar{\delta}_1=q_2'\sin\delta_1$. Thus, $D_R=q_1/q_2$.

The geometry of the refractive defocusing of the direct ray is shown in figure 4. Without refraction the linear measure is as shown in figure 4A (see fig. 1) and is given by $q_1=(A_2-A_1)L_{1+½}$. After bending through the atmosphere we have the situation shown in figure 4B. Again, the spacing is such that $\overline{\alpha_{1+½}+\theta_{1+½}}$ is taken to be equal to $\overline{\alpha_1+\theta_1}$ and the chord is taken to be equal to the arc. We then have $q_2'=(\theta_1-\theta_2)(a+I)$ and $q_2=\cos(\overline{\alpha_1+\theta_1})\cdot q_2'=\sin(\alpha_1+\theta_1)\cdot q_2'$. Thus, by definition, $D_D=q_1/q_2$.

From these considerations we have the following equations for the product of the spherical divergence and the tropospheric defocusing of the reflected ray:

$$D_{R_{n+\frac{1}{2}}}=\frac{[\psi_{n+1}-\psi_n-(\theta_{h_n}-\theta_{h_{n+1}})]}{2[\sin(\psi_n+\theta_{E_n}+\theta_{I_n})]}\cdot\frac{[(N_n+N_{n+1}+M_n+M_{n+1})n_s+T_n+T_{n+1}]}{(a+I)(\theta_n-\theta_{n+1})}; \tag{28}$$

$$D_{R_n}=\tfrac{1}{2}(D_{R_{n+\frac{1}{2}}}+D_{R_{n-\frac{1}{2}}}),\ D_{R_0}\equiv 0; \tag{29}$$

and for the defocusing of the direct ray we have:

$$D_{D_{n+\frac{1}{2}}}=\frac{(A_{n+1_{(dc)}}-A_{n_{(dc)}})[(G_n+G_{n+1})n_s+R_n+R_{n+1}]}{2[\sin(\alpha_n+\theta_n)](a+I)(\theta_n-\theta_{n+1})}; \tag{30}$$

$$D_{D_n}=\tfrac{1}{2}(D_{D_{n+\frac{1}{2}}}+D_{D_{n-\frac{1}{2}}}),\ D_{D_o}\equiv D_{D_{o+\frac{1}{2}}}. \tag{31}$$

Voltage pattern in the ionosphere. The electrical path-length difference which determines the interference pattern is given by

$$L_e=(N_n+M_n)n_s+T_n-(G_n\cdot n_s+R_n), \tag{32}$$

where $n_s=1+N_s\cdot 10^{-6}$. The tropospheric segments have been multiplied by n_s, which is a geometrical correction giving the lengths of the curved rays over the earth with its normal radius (a).

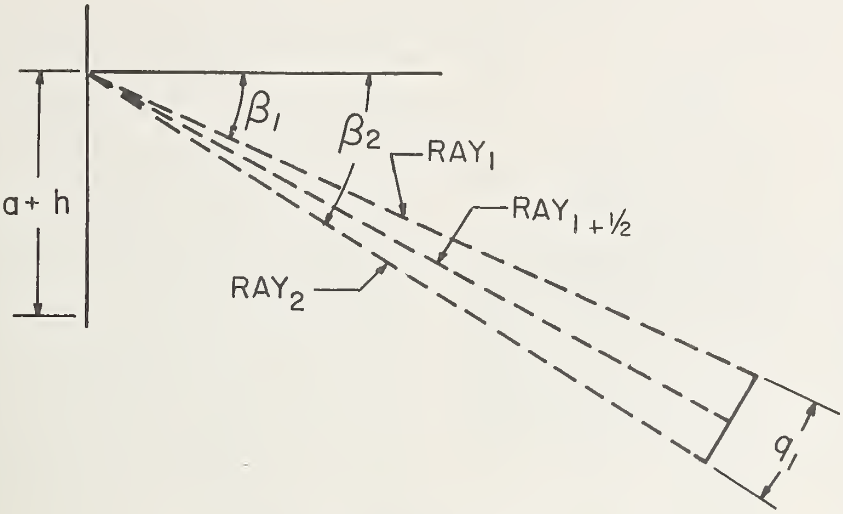

FIGURE 3A. *Linear measure before reflection:* q_1

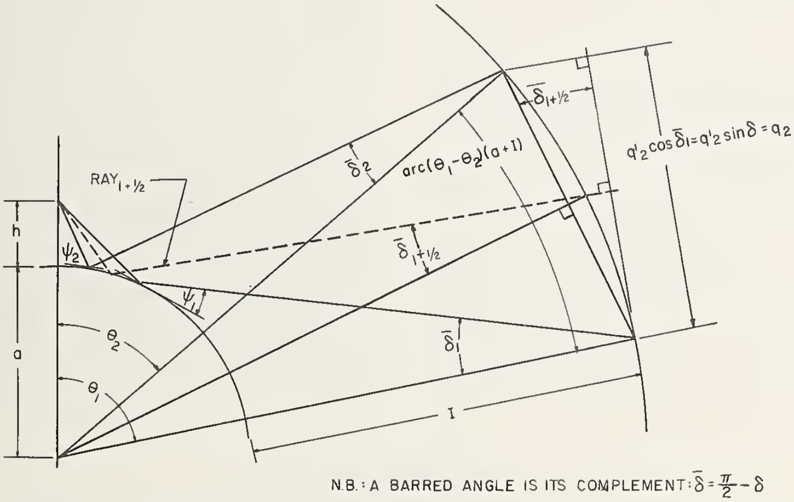

FIGURE 3B. *Linear measure after reflection:* q_2

Spherical divergence of reflected ray.

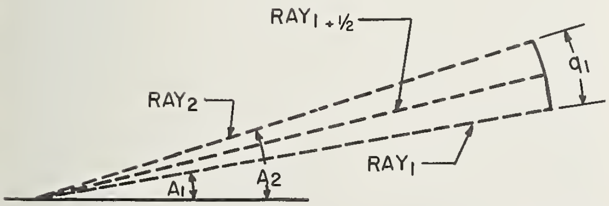

FIGURE 4A. *Linear measure without refraction:* q_1

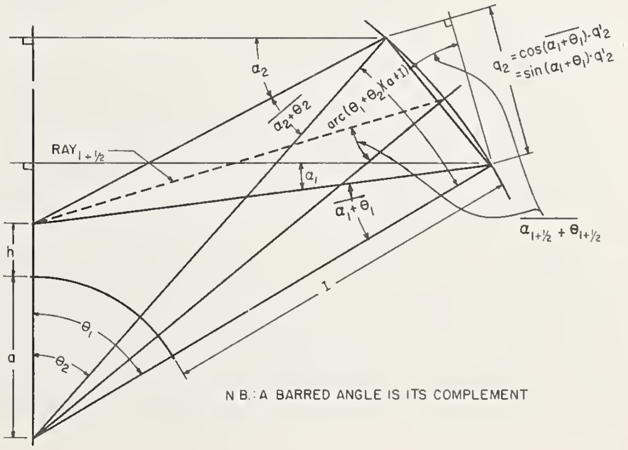

FIGURE 4B. *Linear measure with refraction:* q_2

Defocusing of direct ray (Right)

The path-length difference in wavelengths is given by

$$L_e f/c = L_w. \qquad (33)$$

The difference in electrical radians is

$$\phi = \left\{ L_w + 0.5 - [L_w + 0.5] - \binom{0.0}{1.0} \right\} 2\pi, \qquad (34)$$

where $-\pi \leq \phi \leq +\pi$, and the lobe number is $[L_w]+1$. The square brackets denote the largest integer less than the improper fraction they enclose. Since the D's represent the fraction of unit incident power remaining after divergence and defocusing, the square root of D/r^2 will represent the voltage field at a distance r from a unit power source; thus the voltage contributions made by the direct and reflected waves are given by

$$d_{D_n} = \frac{\sqrt{D_{D_n}}}{G_n \cdot n_s + R_n} \qquad (35)$$

and

$$d_{R_n} = \frac{\sqrt{D_{R_n}}}{(N_n + M_n) n_s + T_n}, \qquad (36)$$

respectively. Figure 5 shows the phase relationship between d_{D_n} and d_{R_n} in the ionosphere or at the antenna, whence we have

$$E_r = \sqrt{d_R^2 + d_D^2 + 2 d_D d_R \cos\phi} \qquad (37)$$

and

$$\phi_{ED} = \sin^{-1}\left[\frac{\sin\phi \cdot d_R}{E_r}\right] \qquad (38)$$

as the voltage resultant and its phase with respect to the direct ray.

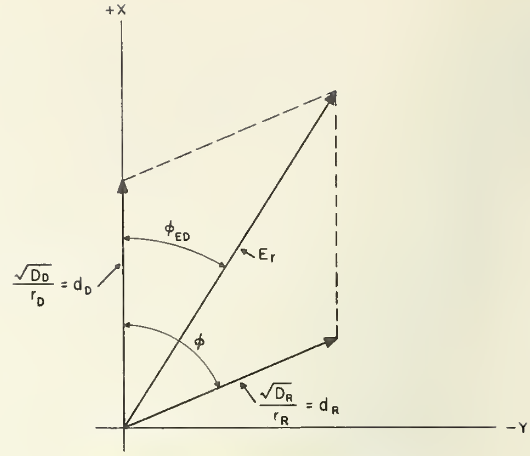

FIGURE 5. *The voltage resultant.*

Diffraction correction. $E_r = d_D$ at the radio horizon because the divergence there is zero. Thus there is a spurious rise in the interference lobe pattern at the horizon and a spurious minimum between the horizon and the first maximum. In order to eliminate this spurious portion of the pattern, an exponential decay was imposed at the point of inflection on the near side of the spurious minimum and extended to the horizon. It was shown by Domb and Pryce [7] that the field just beyond the horizon computed by diffraction theory can be merged with the free space field at the inflection point on the horizon side of the first lobe by a straight line when the patterns are plotted logarithmically; this graphical procedure was used to obtain approximate values of E_r near the horizon.

4. General Results

The analysis described in section 3 was programed for a digital computer so that, for a given set of parameters, the program could be executed for enough values of ψ to obtain a smooth curve of E_r; it could also be executed over a wider range of the parameters than was used for the present work. The diffraction correction was done graphically.

Values of E_r (37) for a given set of parameters and an arithmetic progression of increasing ψ (with difference h_D) are points on the interference lobe pattern. Patterns for the following parameters have been calculated: h=20, 50, 70, 100, 225, 500, and 1000 m for each of f=30, 35, 40, 45, 50, and 55 Mc at I=85 km and E=8 km with k_1=1.342 (ΔN=40.00, N_s=320.00) and k_2=1.467 (ΔN=50.00, N_s=400.00). The patterns so computed are given in appendixes I and II, and are compared for k_1 and k_2 in appendix III.

We shall now compare results obtained from the bilinear refractivity model described in section 3 with results obtained from the exponential reference atmosphere defined by Bean and Thayer [3]. Surface distances and slant ranges have been computed using the exponential model for various angles of elevation from a surface terminal [8]; these distances correspond to the angular distance $k\theta_E + \theta_I$ and to the slant range $M \cdot n_s + T$ in figure 1.

A direct comparison [9] of the two models was made by computing surface distances and slant ranges for the parameters defining k_1 and k_2 with both models; the results are compared in table 1. The differences in distance are much less than those given by the unbounded ka model: in the latter case, with k=4/3, the difference in surface distance is some 85 km for the lower and 75 km for the high surface refractivities at a height of 73 km where atmospheric bending becomes negligible [10].

It is now necessary to examine the difference in the positions of the antenna pattern in the ionosphere predicted by the two models. Since the ka model is virtually exact for a given ΔN and N_s in the first kilometer above the surface, and the greatest antenna height considered is 1000 m, the angular distance $k\theta_h$ will be assumed to be correct. Figures 77 and 78 of appendix III give the difference in lobe position for a 1000 m antenna at 35 and 50 Mc for k_1 and k_2. The difference in parameters represents a difference of 31 km in the position of the horizon cutoff distance and a difference of 23 km in the position of the first lobe maximum. From table 1 we may assume that the exponential atmosphere will shift the first lobe maximum less than 10 km along the scattering layer toward the antenna with respect to k_1 and less than 13 km with respect to k_2; noting that the lobes for the two refractivity profiles and a given frequency are the same size and shape (though of different amplitudes as well as at different distances), we see that the effect would be negligible in view of the fact that the vertical beamwidth of an antenna at the given distances and associated angles would prevent a horizontal shift of this amount from being detected. The differences in lobe position predicted by the exponential and the bilinear models for lower antennas may be deduced from the remainder of appendix III, keeping in mind that these differences decrease with decreasing antenna height.

Nevertheless, it may be asked why an exponential model was not used. Apart from the fact that this work was completed before the reference atmospheres were defined, the error in correspondence between the direct and reflected ray lengths must be within ± 3 mm in order to obtain a smooth pattern, regardless of the model used, and sufficient significant figures are not obtainable from the present program for ray tracing through the exponential atmosphere.

It must be understood that no model atmosphere can represent anything but an average refractivity profile or the profile at some specific time as defined by the parameters used. An estimate of the effect of changing refractivity on the position of the interference lobe may be obtained from the comparisons in appendix III and table 1 of the text, but local average refraction conditions must be known and taken into account in any particular application.

A given antenna is at the lobe alinement height for that path which is twice as long as the surface distance from the antenna to the first lobe maximum of its pattern. Thus, points on curves of path length versus lobe alinement height can be read directly from the patterns in the appendixes. Detailed results from the pattern computations were used to compute Fresnel zone information.

TABLE 1. *Bilinear versus exponential reference atmospheres*

	$N_s=320.00$, $\Delta N=40.00$, $k_1=1.342$, $E=8.00$ km			$N_s=400.00$, $\Delta N=50.00$, $k_2=1.467$, $E=8.00$ km		
	Distance, km			Distance, km		
$\psi°$*	Exp	Bilin	Diff	Exp	Bilin	Diff
0.000	1107.25	1116.38	9.13	1129.45	1142.14	12.69
.029	1102.90	1112.11	9.21	1124.65	1137.48	12.83
.057	1098.57	1107.88	9.31	1119.90	1132.85	12.95
.115	1090.04	1099.47	9.43	1110.54	1123.68	13.14
.229	1073.39	1082.91	9.52	1092.38	1105.66	13.28
.458	1041.56	1050.87	9.31	1058.01	1070.94	12.93
.859	989.93	998.12	8.19	1003.01	1014.27	11.26
1.719	892.71	898.00	5.29	901.28	908.40	7.12
3.724	714.98	716.69	1.71	718.89	721.14	2.25
5.730	584.88	585.53	0.65	536.95	537.81	0.86
11.459	365.04	365.14	.10	365.56	365.69	.13
	Slant range, km			Slant range, km		
0.000	1116.56	1125.67	9.11	1138.79	1151.46	12.67
.029	1112.20	1121.40	9.20	1133.99	1146.80	12.81
.057	1107.88	1117.16	9.28	1129.23	1142.17	12.94
.115	1099.34	1108.75	9.41	1119.87	1132.99	13.12
.229	1082.68	1092.19	9.51	1101.70	1114.97	13.27
.458	1050.85	1060.14	9.29	1067.32	1080.23	12.91
.859	999.20	1007.38	8.18	1012.30	1023.54	11.24
1.719	901.98	907.25	5.27	910.56	917.66	7.10
3.724	724.39	726.09	1.70	728.30	730.54	2.24
5.730	594.69	595.33	0.64	596.75	597.60	0.85
11.459	377.13	377.23	.10	377.64	377.77	.13

*Both models were computed in milliradians to facilitate comparison of the results.

5. Lobe Alinement Antenna Heights and Angles of Elevation and Reflection

Curves of antenna height versus the path length, which is twice the surface distance to the first lobe maximum, are given in figures 6A and 6B using the parameters defining k_1 and k_2 and $I=85$ km. The plots result from smoothing the values read from the interference patterns; this smoothing was necessary because of the error in matching the direct and reflected rays inherent in L_e (32) noted above, and the fact that the lobe maximum may fall between two computed points on the pattern (see the discussion of the inverse interpolation, sec. 3). The smoothing was done by successive difference techniques, the maximum correction being 2 km; to aid in determining curves for values other than those given, the smoothed points are listed in appendix V, tables 1A and 1B, the third differences with respect to frequency (i.e., reading horizontally) being effectively constant, while differences along a curve (i.e., reading vertically) show a nearly exponential behavior.

The angle of elevation (arrival or departure), A, corresponding to the first lobe maximum is given in figures 7A to 7D. It must be remembered that the path length in figures 7A and 7C is the lobe alinement path length and that the curves refer only to the lobe alinement antenna height, whereas figures 7B and 7D may be used with any path length for which a given antenna height provides sufficient gain (see reference 1).

The lobe alinement heights given in figure 6 differ from those given in previous calculations. The reason for this is that it is usually assumed that the interference pattern is a function of the path difference only, which means that the lobe maximums occur when the path difference in electrical radians (34) is zero; in the particular

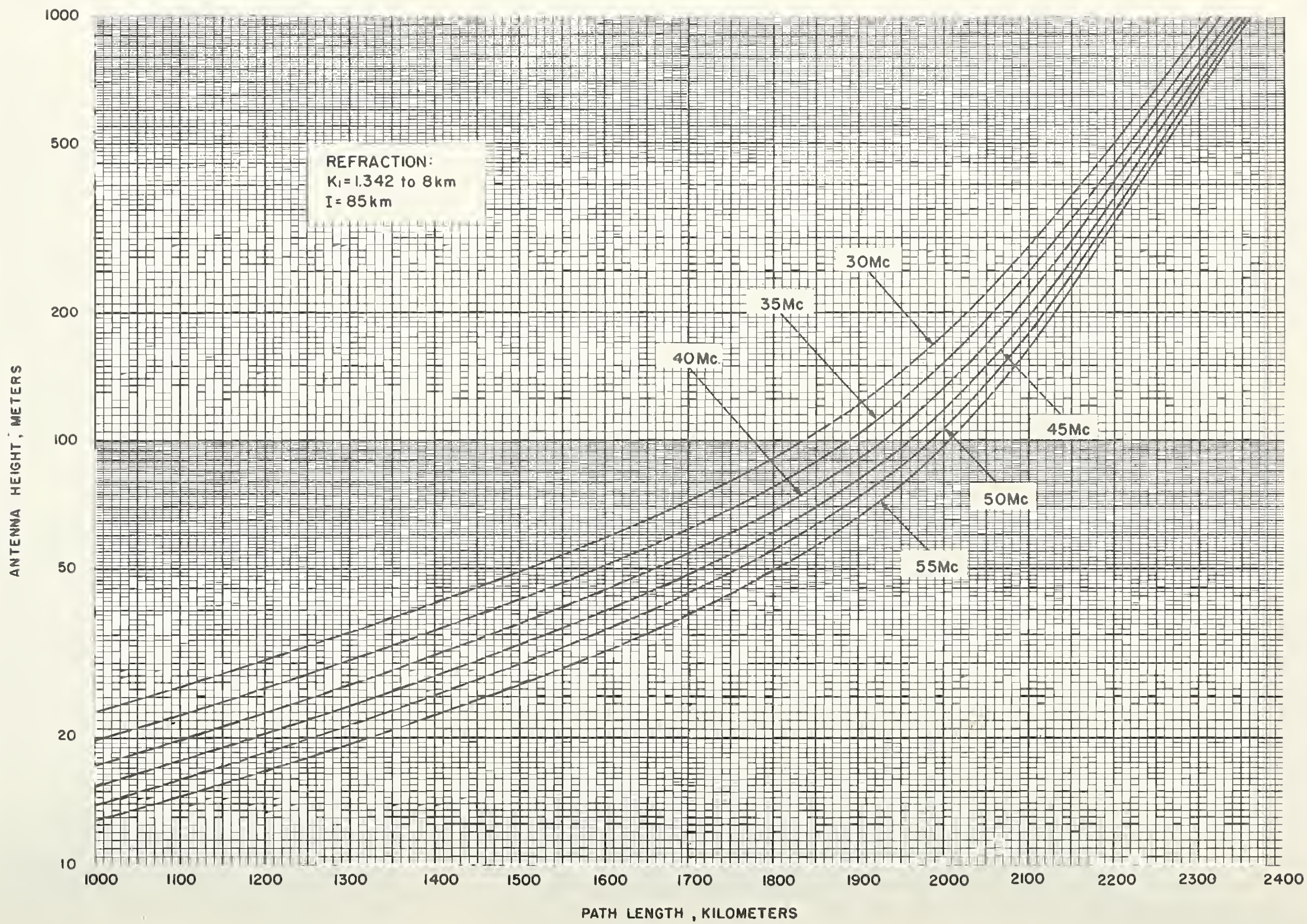

FIGURE 6A. *Lobe alinement antenna height versus path length* (k_1).

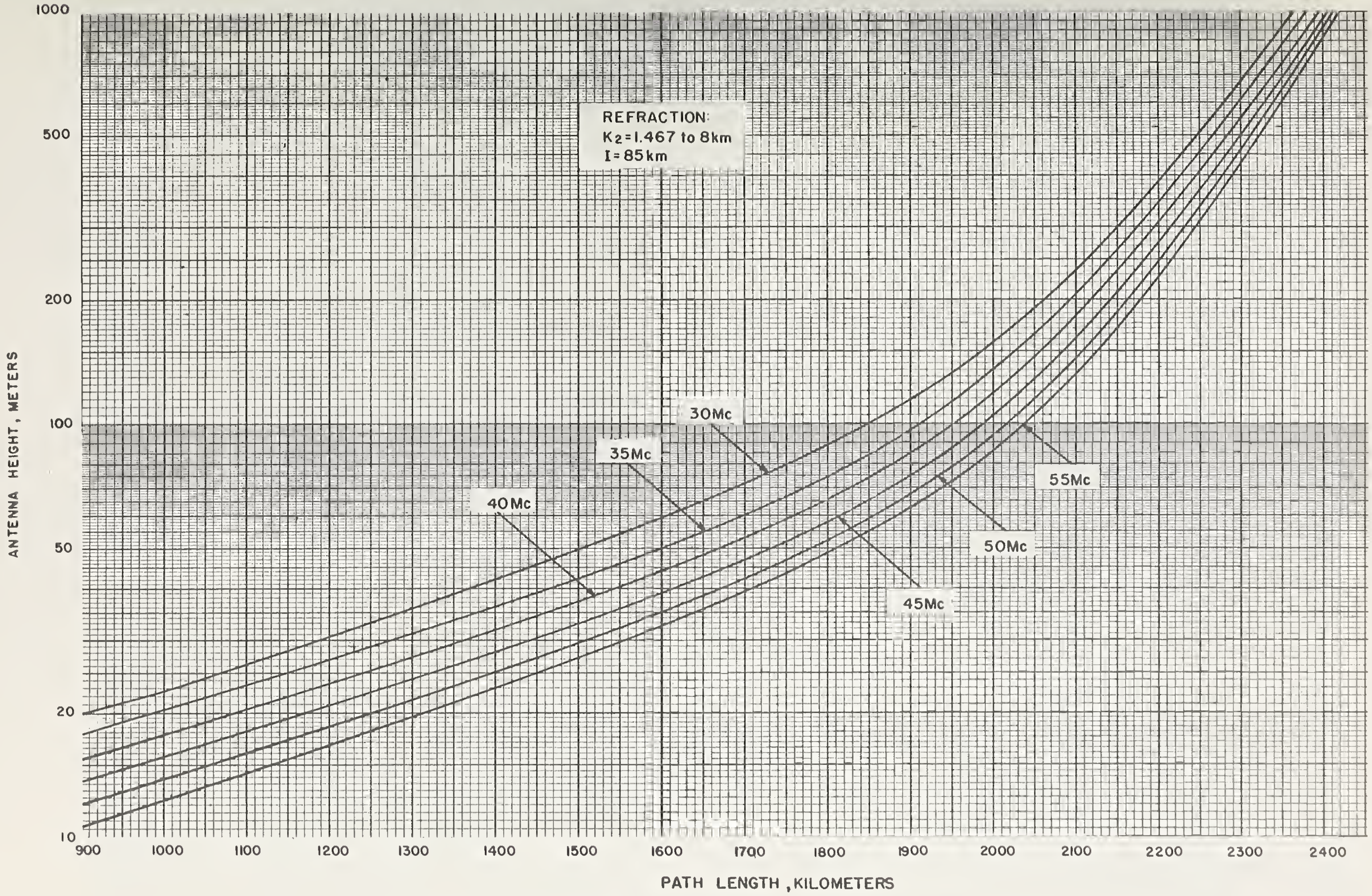

FIGURE 6B. *Lobe alinement antenna height versus path length* (k_2).

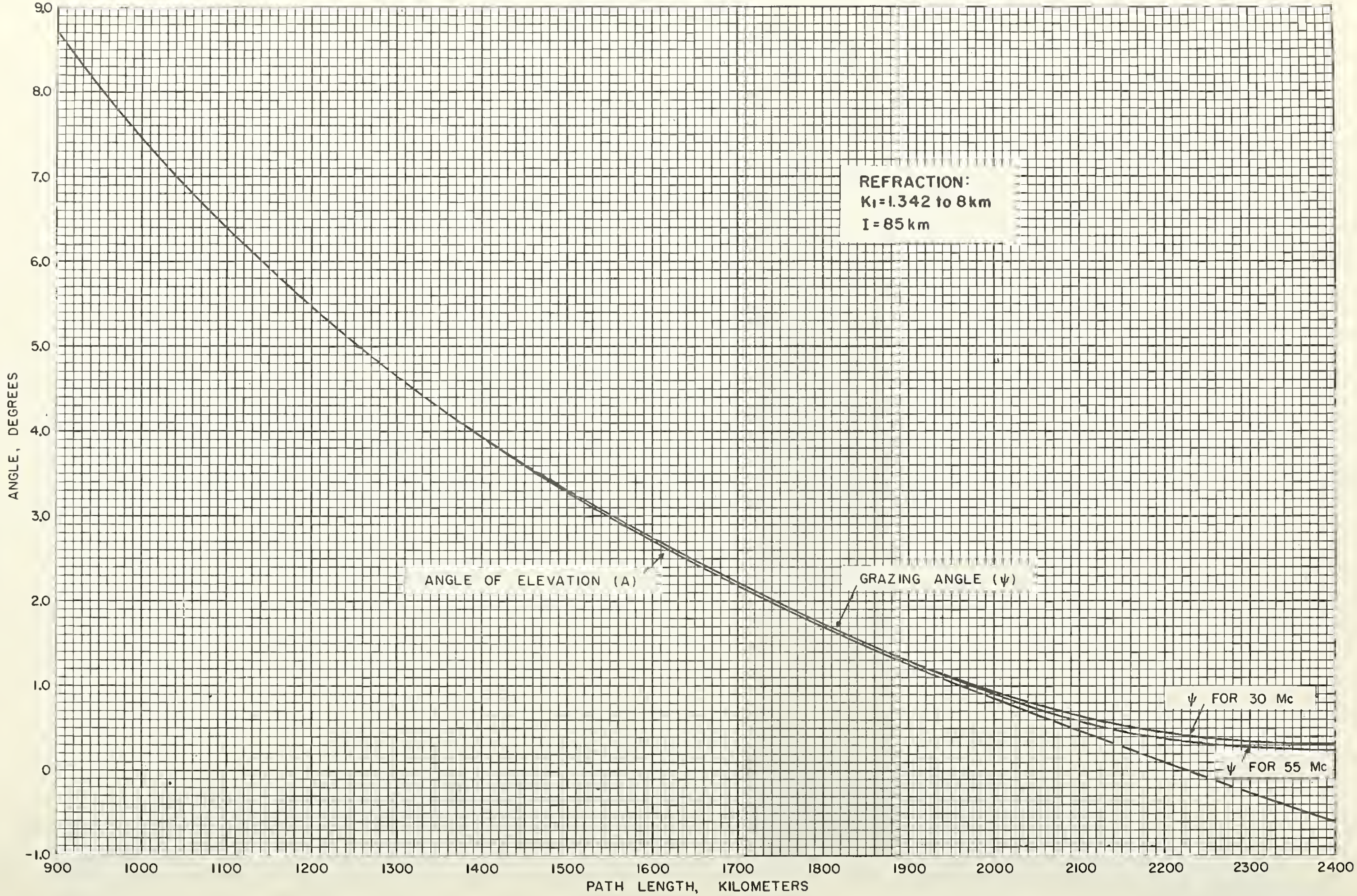

Figure 7A. *Elevation and grazing angles versus distance for lobe alinement height* (k_1).

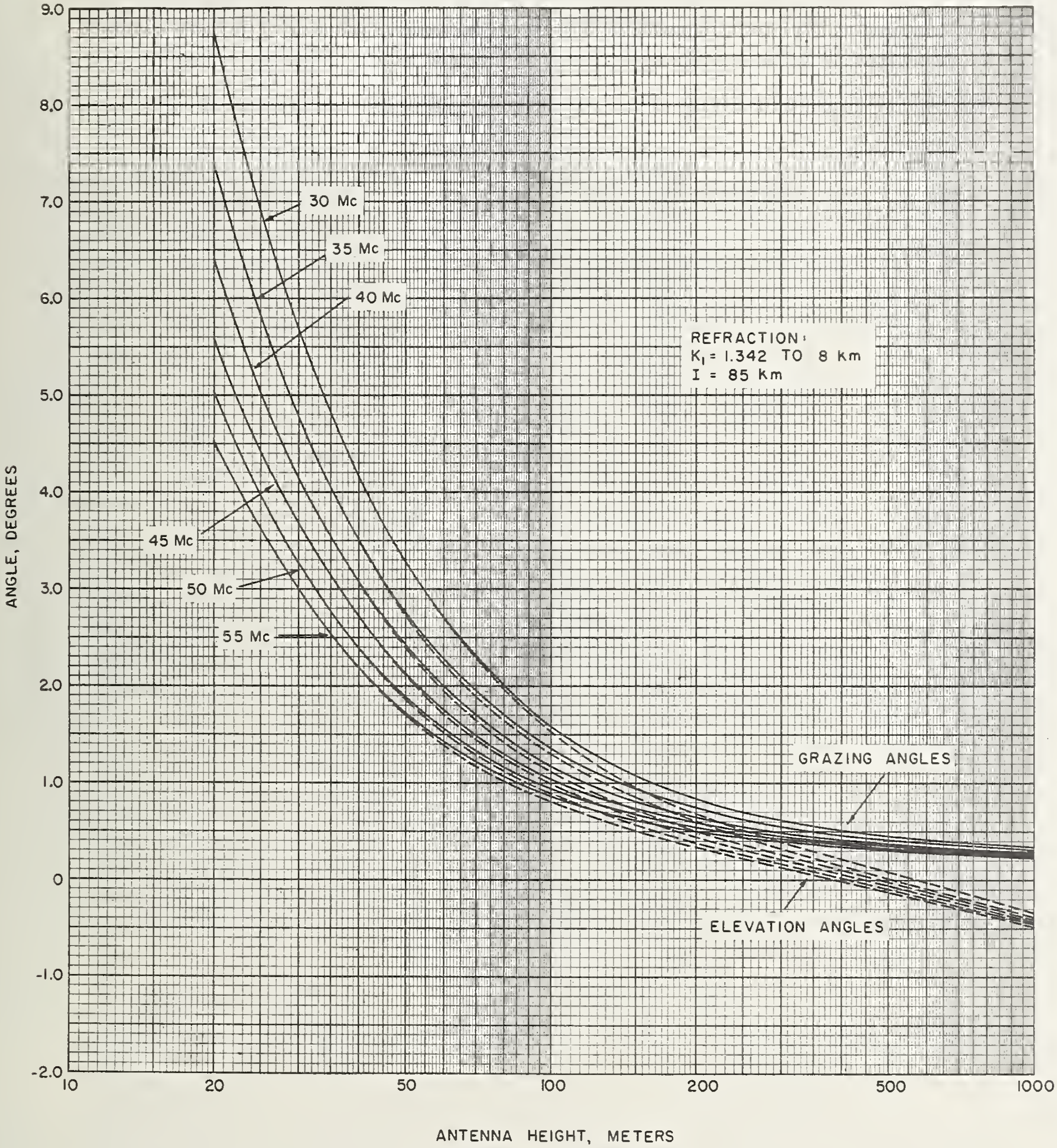

FIGURE 7B. *Elevation and grazing angles versus antenna height (k_1).*

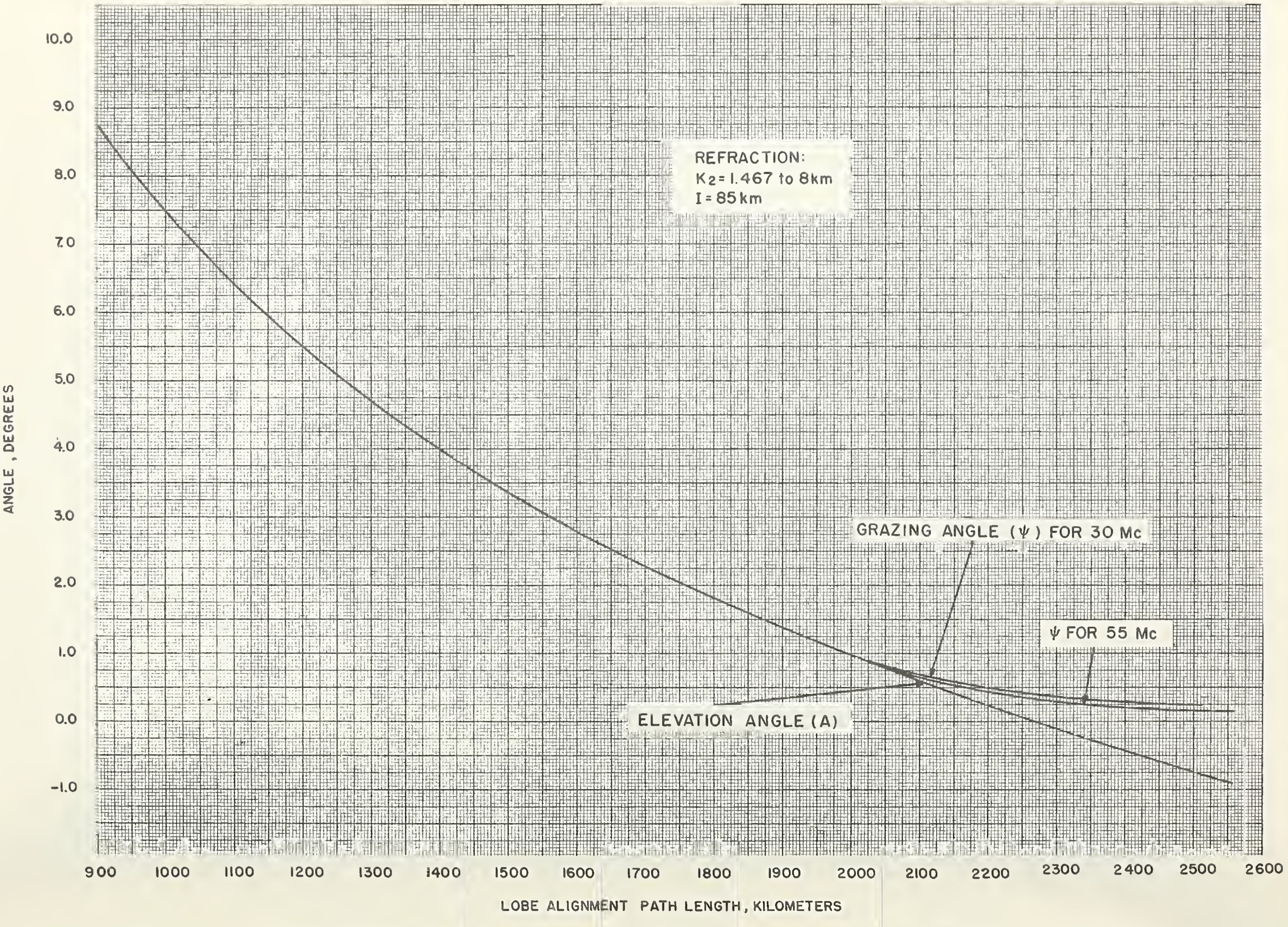

Figure 7C. *Elevation and grazing angles versus distance for lobe alinement antenna height* (k_2).

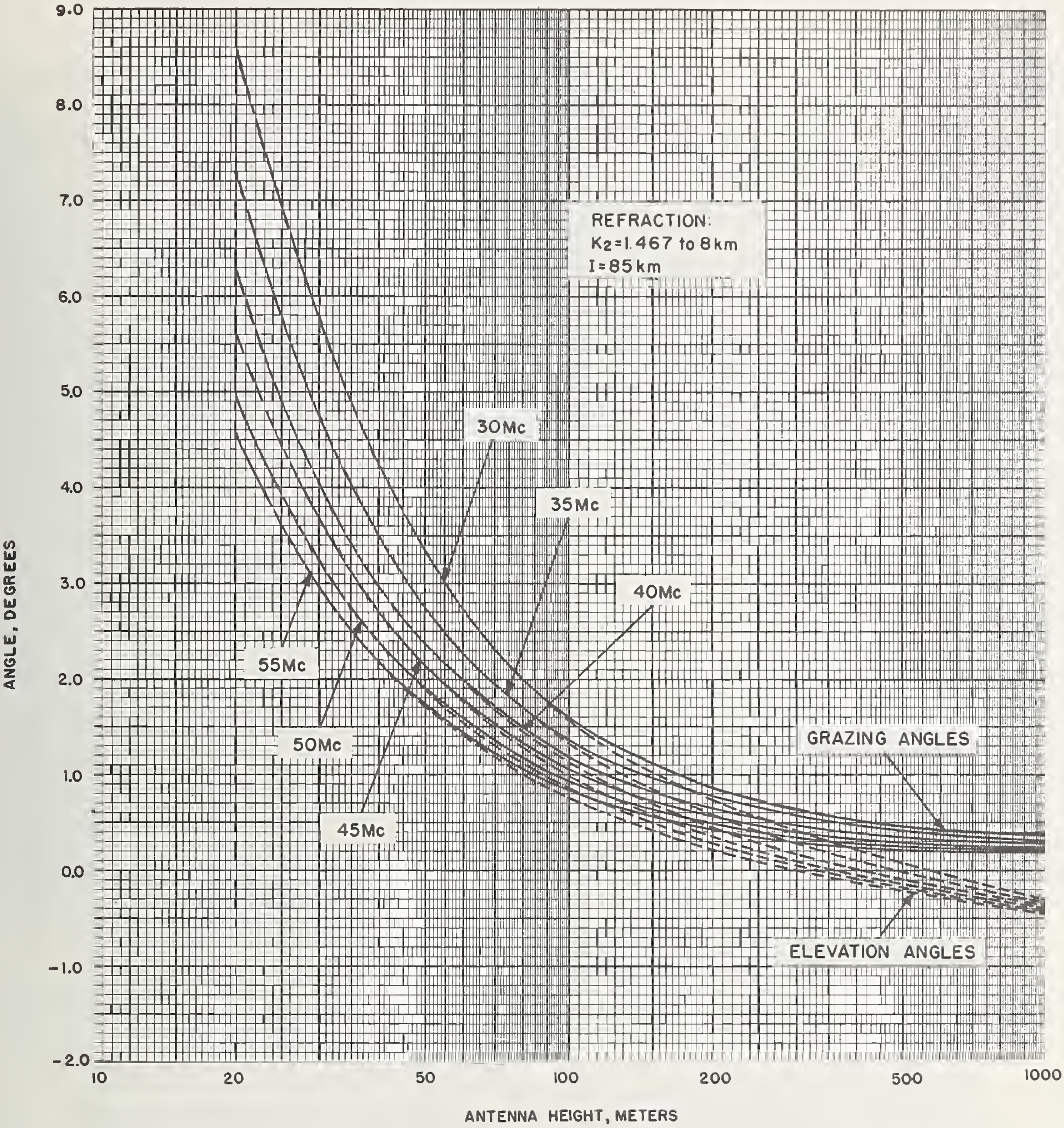

FIGURE 7D. *Elevation and grazing angles versus antenna height* (k_2).

case of reference 2, parallax and refraction corrections were applied to the least elevation angle corresponding to zero path difference. However, the present computations utilize (37), so that the resultant is directly proportional to the product of the divergence and defocusing of the reflected ray and to the defocusing of the direct ray, and inversely proportional to the ray lengths. The divergence and defocusing are shown in figure 8; their rates of change for the values of ψ obtaining throughout the first lobe cause the maximum to be seen at other than $\phi=0$, and thus shift the lobe maximum along the scattering layer toward the antenna [11].

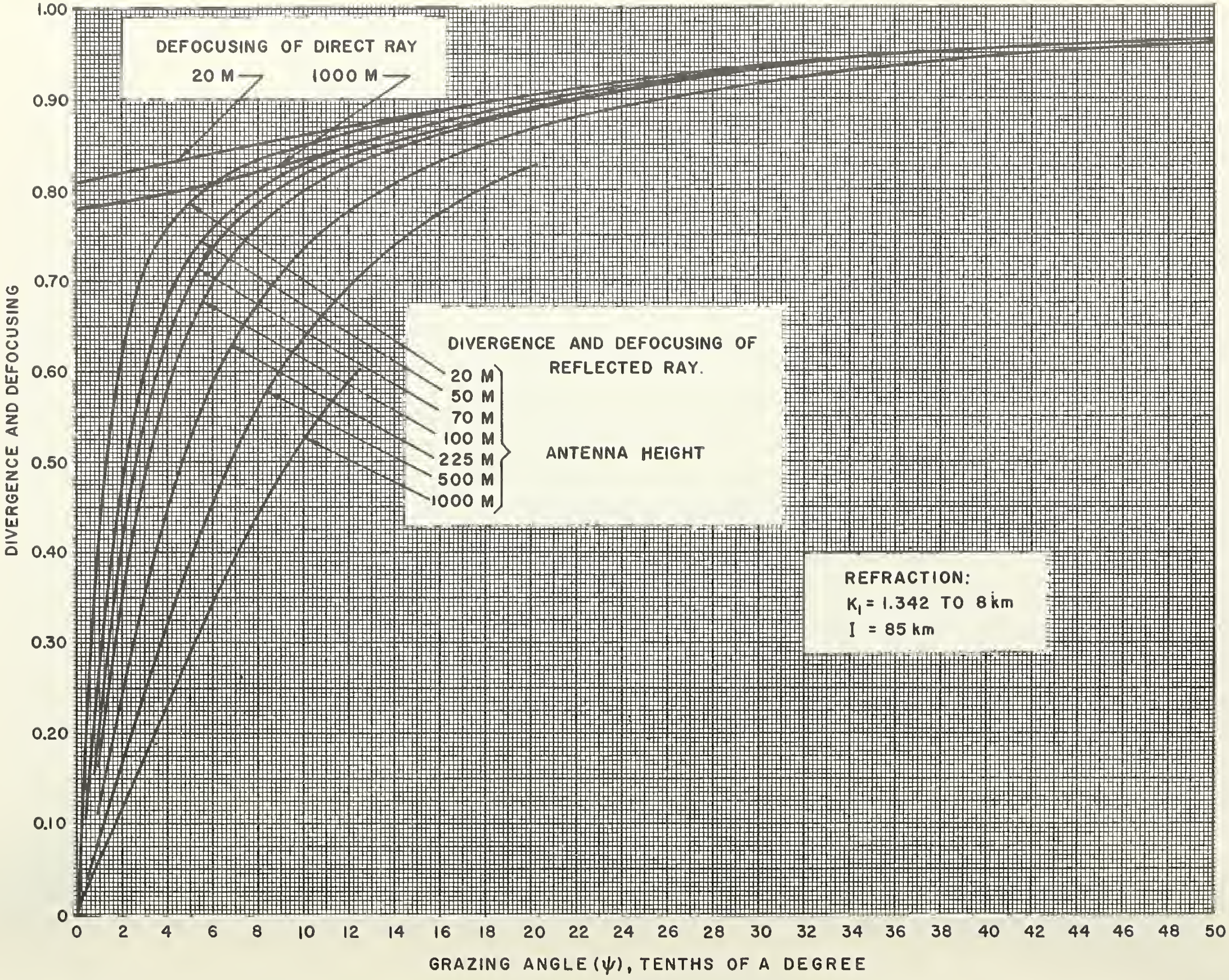

FIGURE 8A. *Divergence and defocusing versus grazing angle* (k_1).

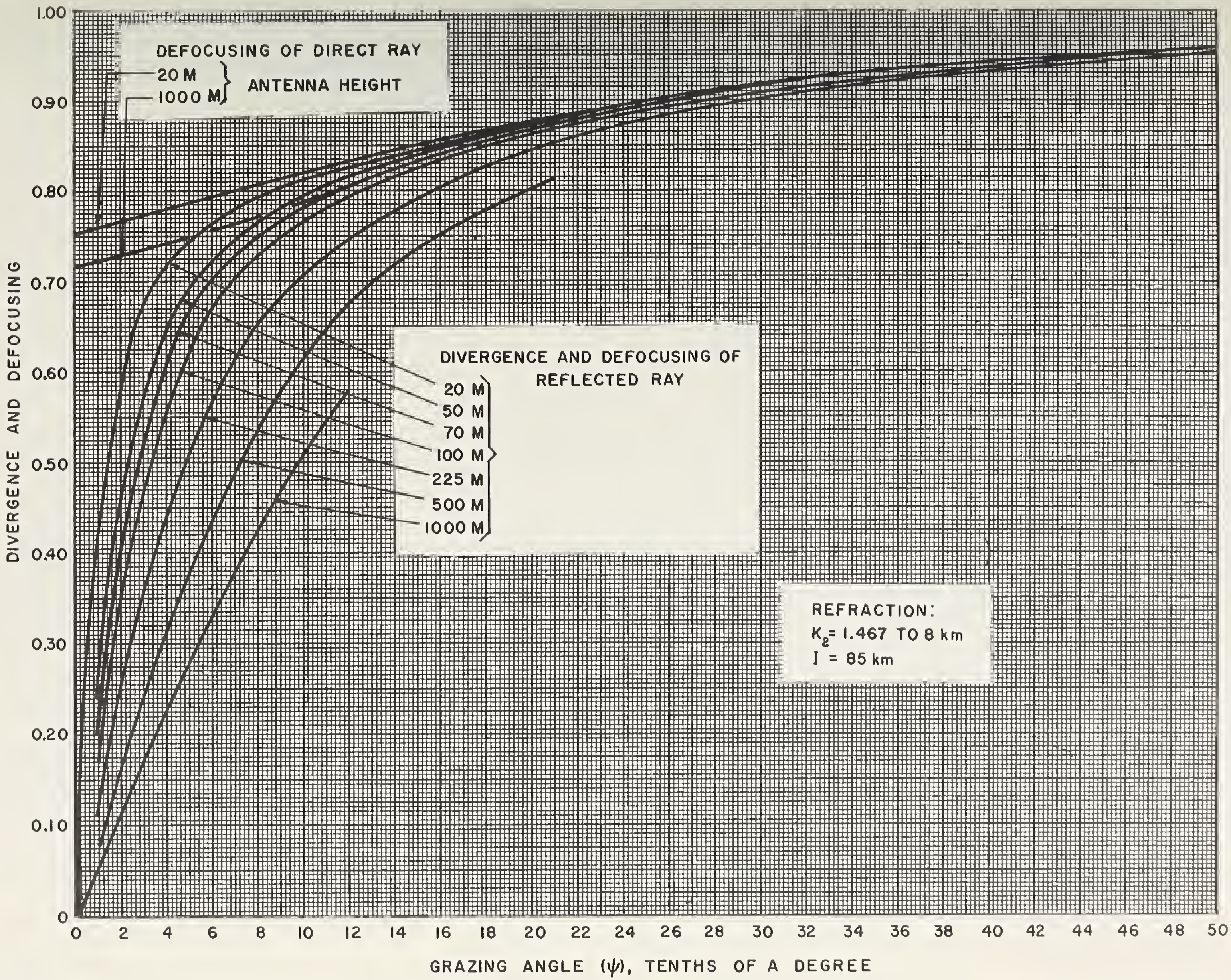

FIGURE 8B. *Divergence and defocusing versus grazing angle (k_2).*

6. The First Fresnel Zone and Obstacle Criteria

Fresnel zone distances. The ground reflection point for the value of ψ corresponding to the first lobe maximum will be called the *geometric ground reflection point* to distinguish it from other ground reflection points to be considered in studying the first Fresnel zone. The surface distance over the earth with radius a from the antenna to the geometric ground reflection point is found by multiplying (3) by ka for the proper value of ψ. These distances were subjected to finite difference smoothing: for h=20, 50, and 70 m, the relationship between distance and frequency is linear, while for h=100, 225, 500, and 1000 m, the relationship is quadratic. For antenna heights up to about 150 m, a spherical earth appears to be plane, while for higher antennas the curvature of the surface causes divergence to become significant in the computations: thus the functional relationship between frequency and the distance to the geometric ground reflection point changes from linear to quadratic with increasing height; this change will also be seen in the distances discussed below.

Distances from the antenna to the geometric ground reflection point are shown in figure 9 and the values from which the curves were drawn are listed in appendix V, table 2. The radio horizon line for k_1 satisfies the equation $H_R=4.13\sqrt{h}$, where h is in meters and the radio horizon is in kilometers; for k_2, $H_R=4.32\sqrt{h}$. For comparison, the equation $H_R=\sqrt{2h}$ expressed in miles and feet is $H_R=4.12\sqrt{h}$ expressed in kilometers and meters.

In the following discussions a reflected ray is always assumed to have one end at the antenna and the other in the ionospheric scattering volume.

The geometric ground reflection point is the center of a family of Fresnel zones on the surface of the earth. The phase at the antenna, relative to the direct ray, of a ray reflected from any other point along the great circle path can be computed using various details from the antenna pattern computations. With respect to the first Fresnel zone only, all reflection points for which the reflected rays have equal phase with respect to the direct ray define a continuous "contour" line which is an ellipse on a plane and is "egg-shaped" on a sphere; every such contour intersects the great circle path twice: once between the antenna and the ground reflection point and once between the ground reflection point and the point on the earth's surface beneath the scattering volume; the former point of intersection and its distance from the antenna will be referred to as *near*, and the latter and its distance as *far*. Distances from the antenna to the near and far points for which reflected rays have phase differences relative to the direct ray corresponding to a half-wave length ($\phi=\pi$) and to a quarter-wave length ($\phi=\pi/2$) have been computed in order to locate the first Fresnel zone on a spherical earth. The need for locating the first Fresnel zone follows from the fact that it contributes the major part of the reflected energy seen at the antenna.

The Fresnel zone distances were computed as follows. Referring to figure 1, let θ_f be the value of θ for the lobe maximum at a given frequency and let SR_f be the total length of the corresponding reflected ray. The family of angles associated with each value of ψ used in computing the antenna pattern is examined for the following conditions: $k\theta_h=\theta_f-(k\theta_E^{(n)}+\theta_I^{(n)})$ (cf. (9)), where these angles correspond to ψ_n. The $N^{(n)}$ is then computed (see fig. 1) and $SR^{(n)}=(N^{(n)}+M^{(n)})n_s+T^{(n)}$ (cf. (32)), where $M^{(n)}$ and $T^{(n)}$ are members of the family of path segments associated with ψ_n. $SR^{(n)}$ is then compared with $SR_f+\lambda/2$ and with $SR_f+\lambda/4$. When a required Fresnel distance has been bracketed by two values of $SR^{(n)}$, a second order Lagrangian interpolation is used to find the corresponding $\theta_h^{(f)}$; ka times this angle gives the required distance over the earth with radius a. This procedure was satisfactory for computing the far distances, but the near distances were undefined or inconsistent with one another because of the extremely small slope of the function $SR^{(n)}$ in the corresponding range.

In order to find the near distances, a non-parallactic model was used which is described in figure 10 (cf. figs. 1 and 2). The independent variable $\zeta=\theta_h^{(f)}-\theta_h'$, from which θ_h' and N' can immediately be computed. $W=2ka(\sin\zeta/2)$ and $P=W\sin(\psi+\zeta/2)$. The quantity compared with $\lambda/4$ or $\lambda/2$ is $SN'-N_f$, where $SN'=N'+P$. A linear interpolation is made after the required value is bracketed.

The use of SR_f in the computation implies that the divergence at the various Fresnel zone points is the same as the divergence at the geometric ground reflection point; any resulting error in the location of the computed Fresnel zone point is thus directly proportional to its distance from the ground reflection point. Rough estimates show that such an error will be detectable only in the far distances for antenna heights of 200 m and greater; however, far distances for such antenna heights are either close to or beyond the radio horizon.

The analyses for the far and near Fresnel zone distances were combined in a single digital computer program which also computed the angles relevant to the obstacle criteria which are discussed below.

Distances to the near and far edges of the Fresnel zone are presented in figure 11, while the near and far quarter-wave distances are presented in figure 12. These distances are the results of linear or quadratic (depending on antenna height)

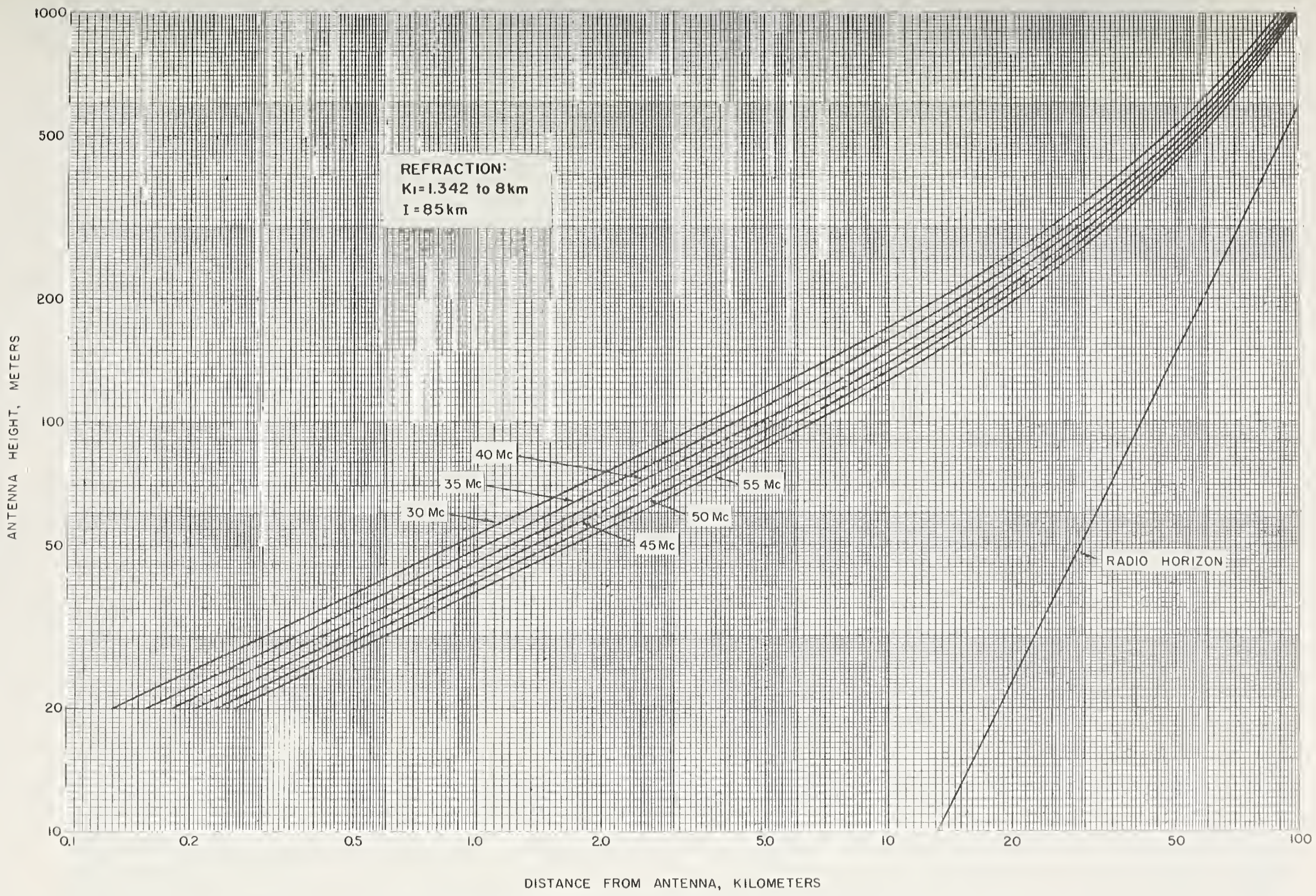

FIGURE 9A. *Geometric ground reflection point (zero phase) (k_1).*

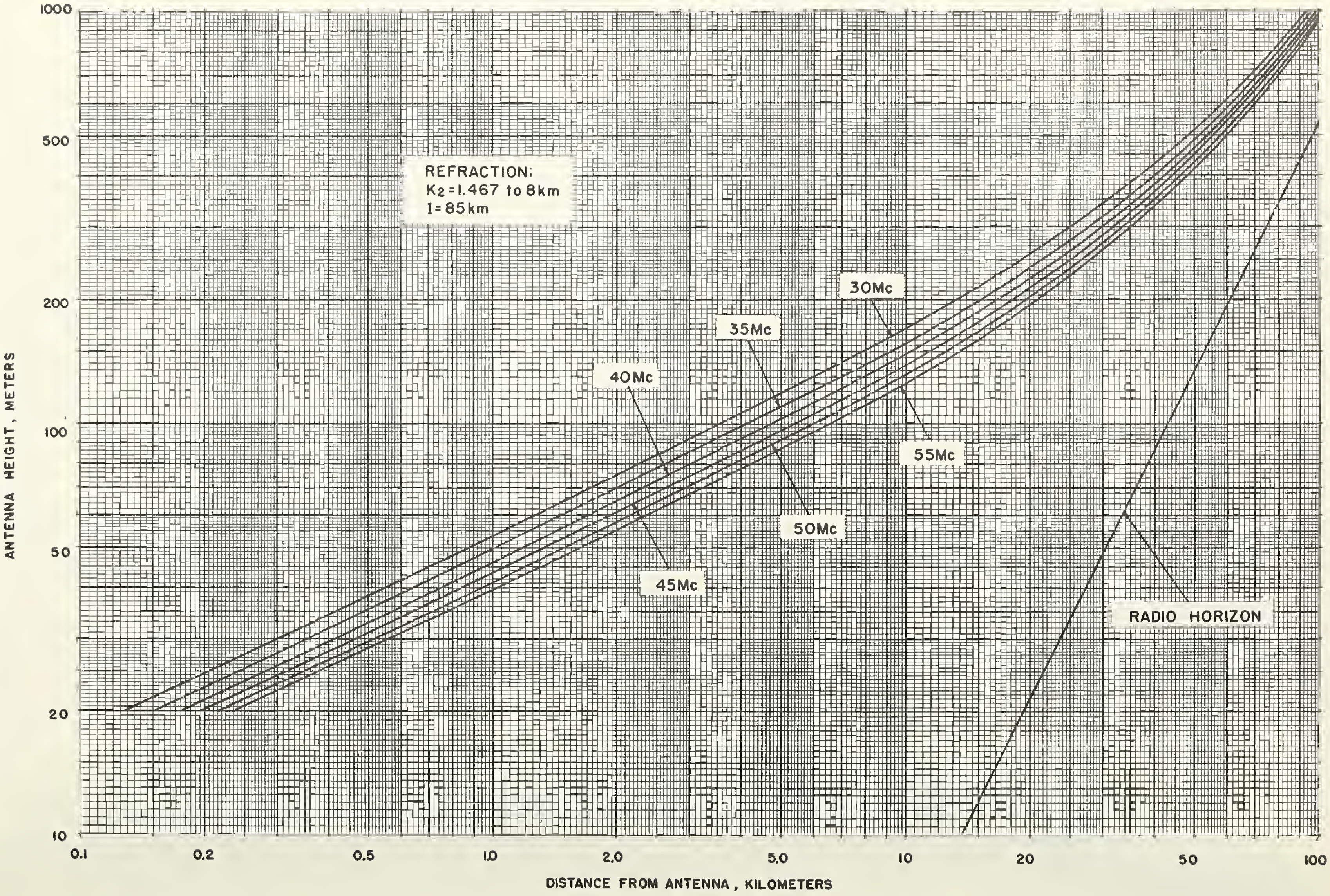

FIGURE 9B. *Geometric ground reflection point (zero phase)* (k_2).

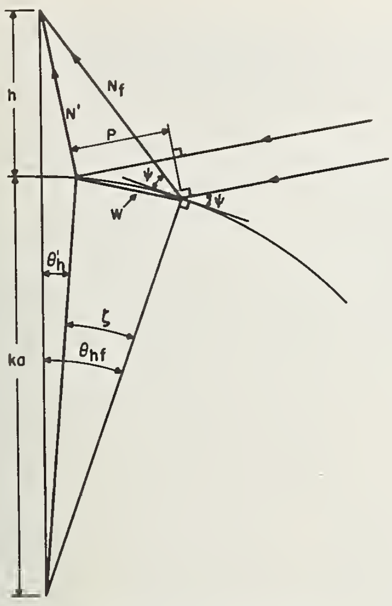

FIGURE 10. *Nonparallactic geometry.*

least squares fits to the computed values; these regressions were done on a desk-sized digital computer. The values are listed in appendix V, tables 3 through 6. An overall picture of the position of the first Fresnel zone is given in figure 13. It is emphasized that purely geometrical definitions have been used to compute these distances.

The first Fresnel zone has been located along the great circle from the antenna to the point beneath the scattering volume. Under the limitations of the model, points on the Fresnel zone boundary that are off the great circle path cannot be determined; however, upper bounds of maximum width can be found by the plane earth formula [2] for a given antenna height, viz, $w=4\sqrt{2h}$.

Obstacle criteria. The criteria for smoothness in the first Fresnel zone that have hitherto been suggested assume a plane earth, since the first zone has been completely defined for that case. Deviations from smoothness are based on the geometrical analysis in figure 14A. The path difference is $L_R=2R\sin\psi$: in terms of wavelength this is $2R\sin\psi/\lambda$, and in radians it is $4\pi R\sin\psi/\lambda$. Rayleigh's criterion for distinguishing between rough and smooth is to make this path difference less than $\pi/4$. Thus $4\pi R\sin\psi/\lambda<\pi/4$, or $R<\lambda/(16\sin\psi)$. For the plane earth, $A=\psi$ and $h=\lambda/(4\sin\psi)$; hence $R<h/4$. Kerr [12] discusses other criteria based on the path difference analysis and emphasizes its crudity.

Assuming a receiving antenna over a spherical earth, bounds for the angles of illumination (elevation of the ionospheric scattering volume) and reflection (elevation of the antenna) at any point in the first Fresnel zone along the great circle path have been obtained from a computation of these angles at the edges and at the quarter-wave points; angles of illumination are designated by ψ_F, and angles of reflection by ψ'_F. Angles of illumination were computed using the nonparallactic model (fig. 10) for both near and far distances. The angle $\psi_F=\psi+\zeta_F$, where $\zeta_F=\theta_F-\theta_h$, θ_F being the radian measure of the distance from the antenna to the point in question; ψ'_F is computed from the sine law. The computed angles are plotted in appendix IV; figure 9 of appendix IV shows how the variation of these angles throughout the length of the zone may be estimated graphically.

A criterion based merely on height considerations ignores the shape of an obstacle: an object may satisfy the height criterion mentioned above and still eliminate the major portion of the reflected energy, e.g., a building with a sloping roof, or a low hill, or just about any kind of depression. Using geometrical optics, a simple vertical wall of height R casts a shadow of length $S=R/\tan\psi_F$ in the direction of the antenna with respect to incident rays, and of length $S'=R/\psi'_F$ in the opposite direction with respect to reflected rays, where the angles may be measured at R if the shadow is short enough to be considered as lying in a plane. Thus, ignoring diffraction, an area with length $S+S'$ is eliminated from the zone as shown in figure 15.

The zero phase surface. It will be noted that the height criterion discussed above is stated in a completely negative manner, i.e., as a maximum *tolerated* deviation, even though the path from the top of the obstacle is shorter (by L_R) than that from the smooth surface at the same distance.

Consider reflection from a surface that is slightly concave upwards: the divergence factor will become a convergence factor and focusing will occur. Thus, with respect to the present problem, surfaces may be defined which, when substituted for a spherical earth, render all reflected energy exactly in phase at the antenna and in the ionospheric scattering volume. Such surfaces form a family of ellipsoids having foci at the center of the scattering volume and at the antenna: we will find points on that member of the family that is also tangent to the surface of the spherical earth at the geometric ground reflection point.

Consider a point P_F in the first Fresnel zone over a spherical earth (as previously defined geometrically), and let the phase difference between the ray reflected at P_F and that reflected at the geometric ground reflection point be ϕ: at a height $R_0=\lambda\phi/2\pi(\sin\psi_F+\sin\psi'_F)$ on the normal through P_F is a point P' such that the length of the ray reflected at P' is the same as that of the ray reflected at the geometric ground reflection point. That ellipsoidal surface which passes through all such points will be called the *zero phase surface* because any ray reflected from it will be the same length as the ray reflected at the geometric ground reflection point.

It must be remembered that any point P' on the zero phase surface is determined geometrically

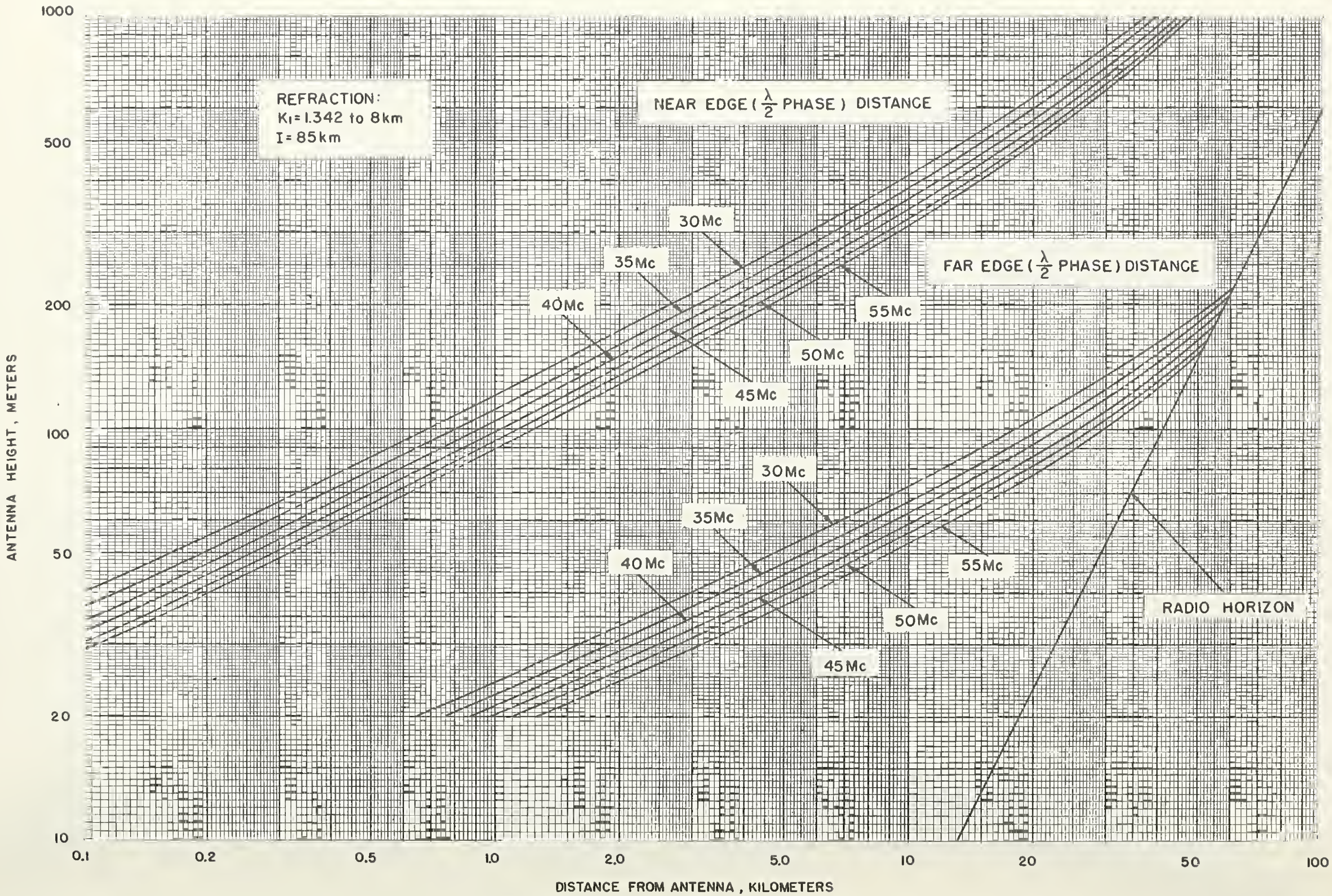

FIGURE 11A. *Edges of first Fresnel zone* (k_1).

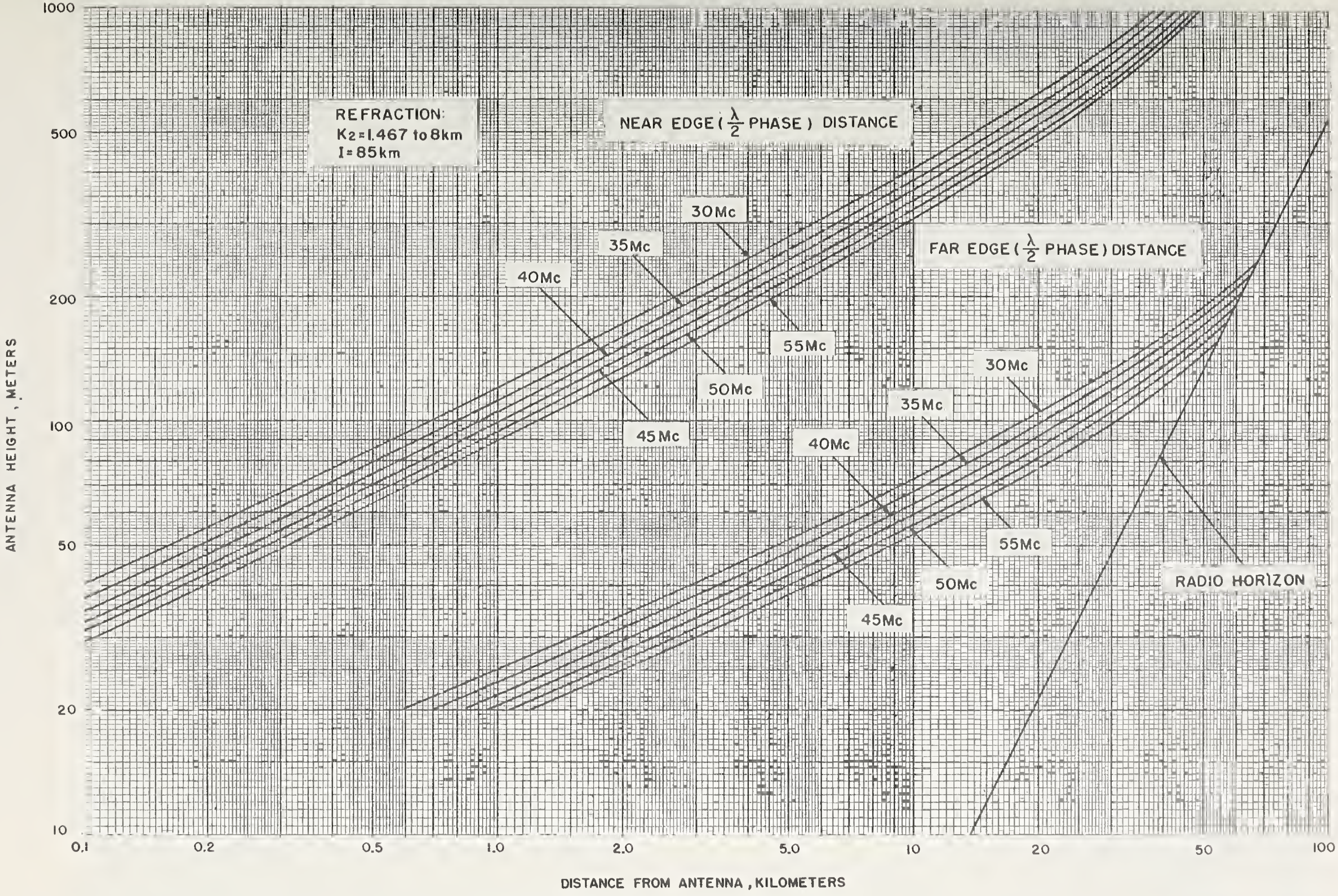

FIGURE 11B. *Edges of first Fresnel zone* (k_2).

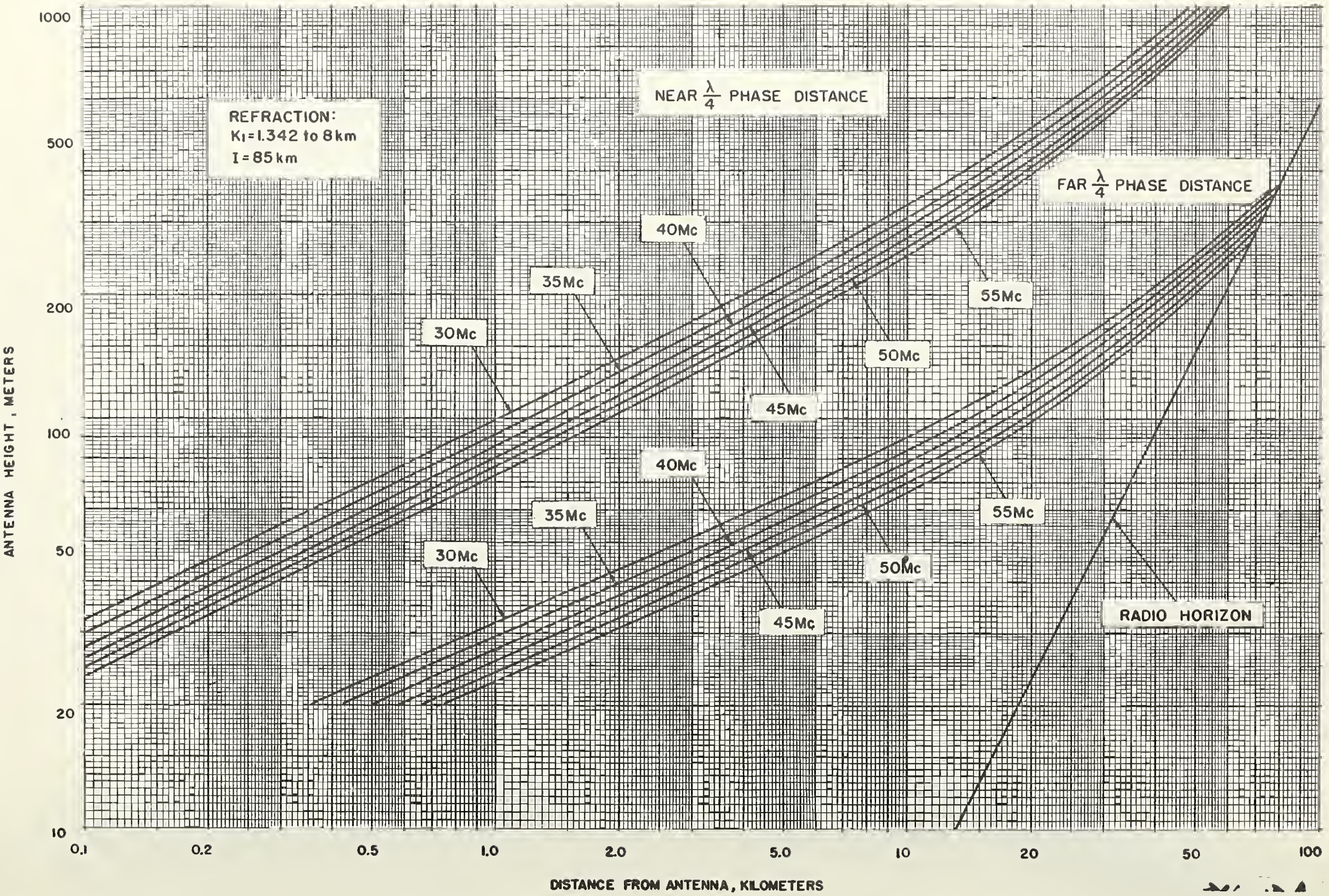

FIGURE 12A. *Quarter-wave contour in first Fresnel zone* (k_1).

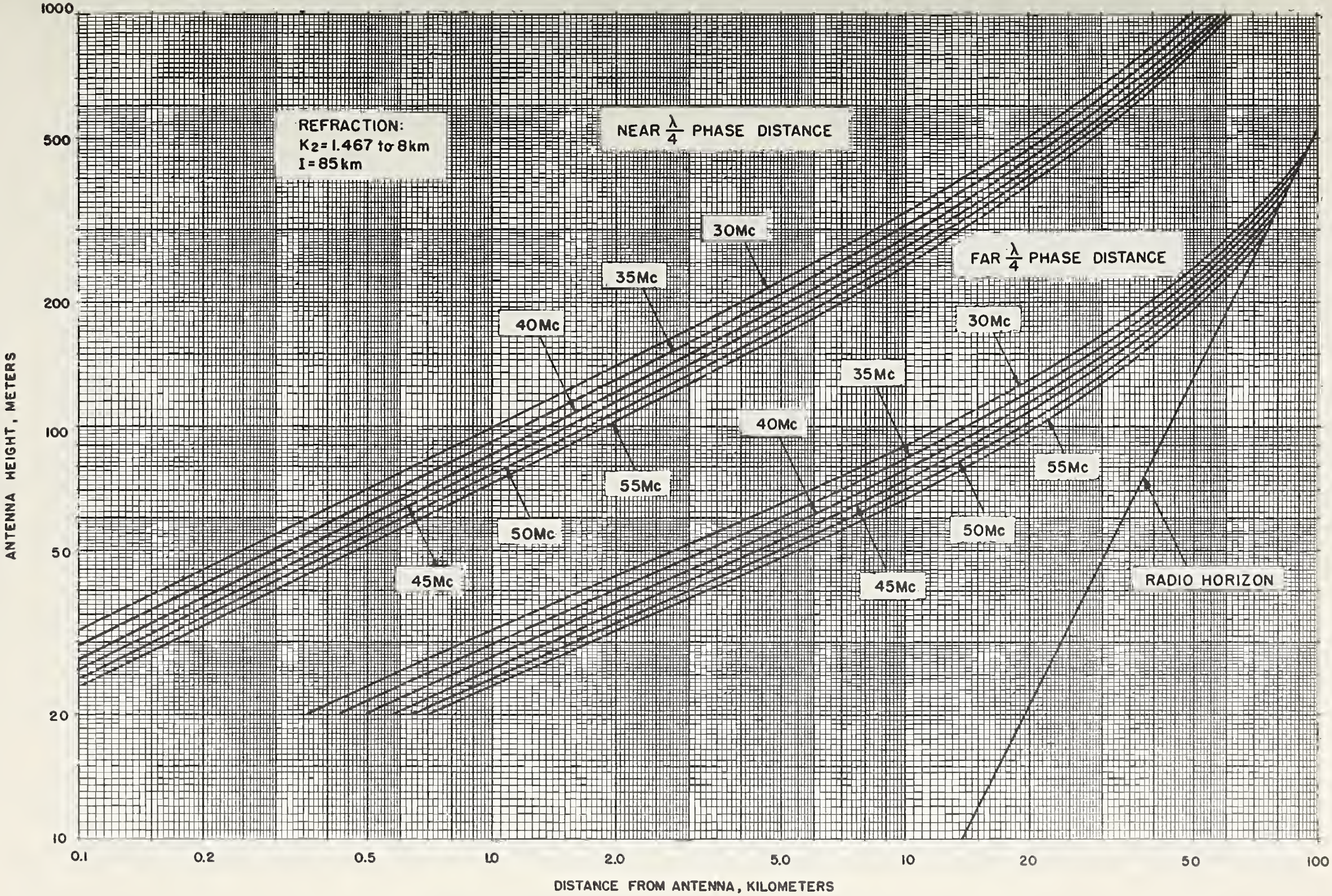

FIGURE 12B. *Quarter-wave contour in first Fresnel zone* (k_2).

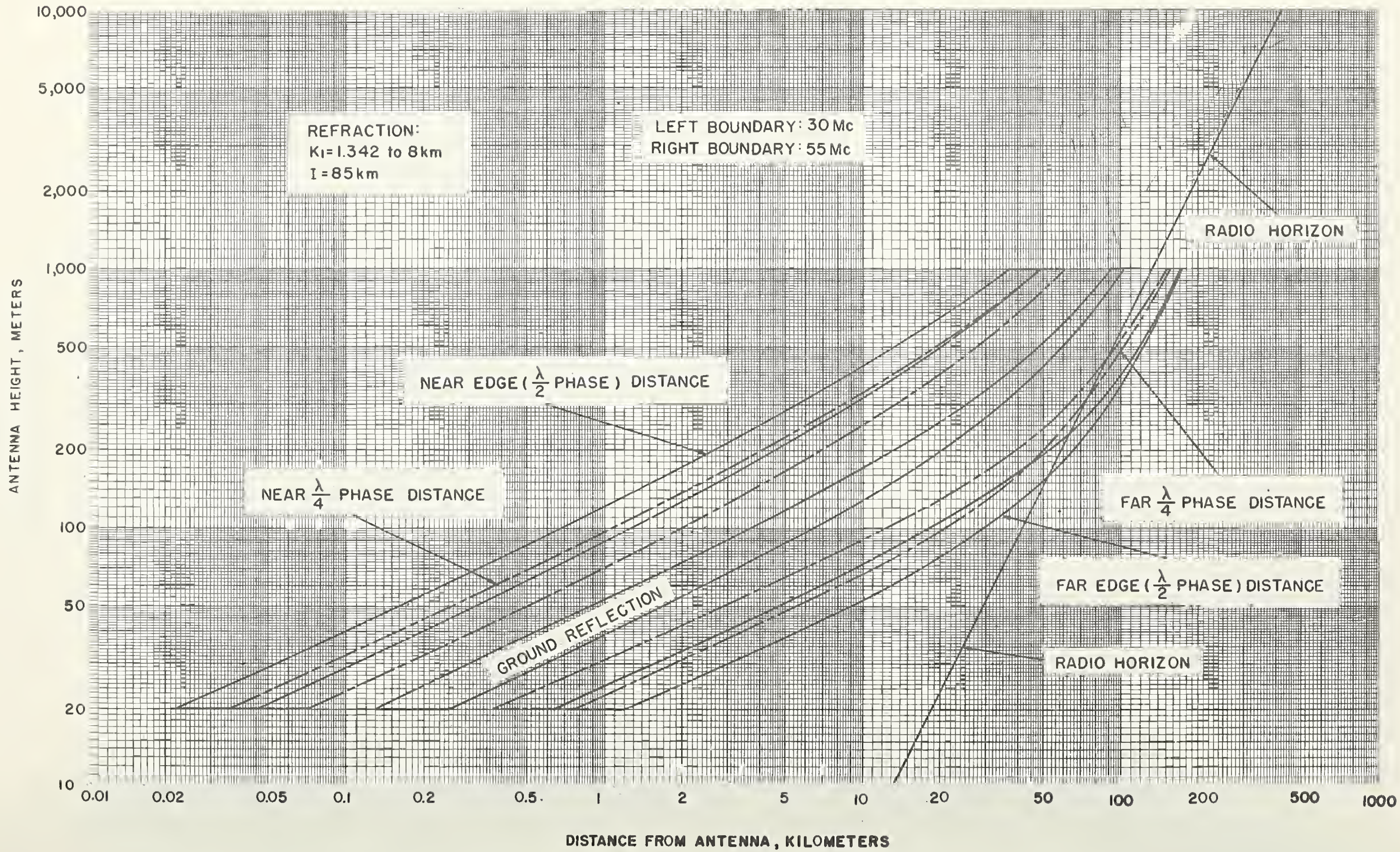

FIGURE 13A. *Summary plot of first Fresnel zone* (k_1).

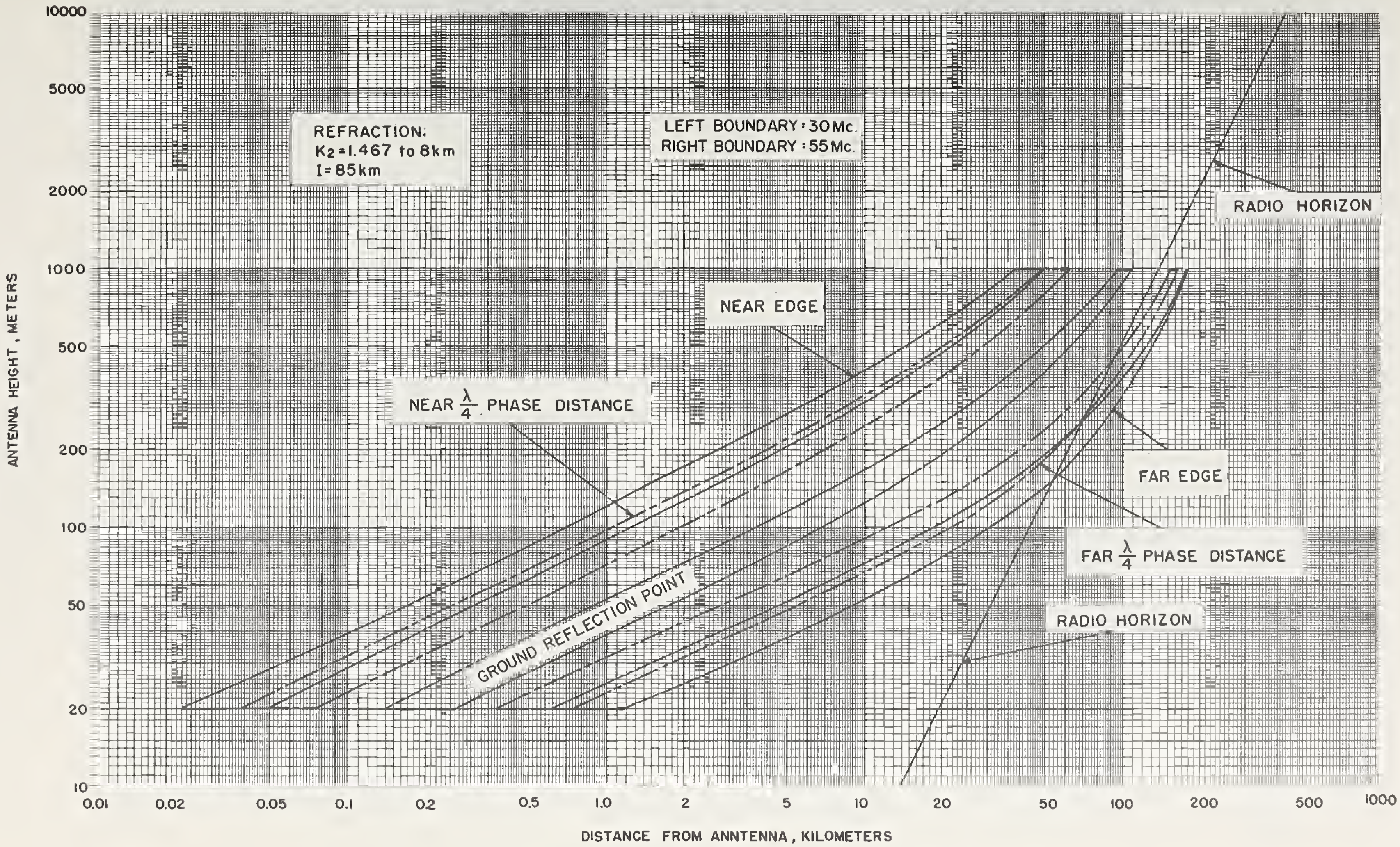

FIGURE 13B. *Summary plot of first Fresnel zone* (k_2).

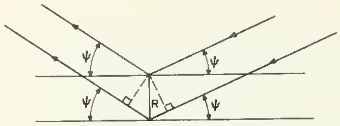

FIGURE 14A. *Obstacle geometry after Kerr.*

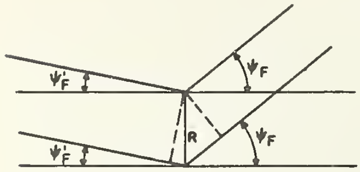

FIGURE 14B. *Generalized obstacle geometry.*

in exactly the same manner as the Fresnel zone distances. In particular, the effect of spherical divergence on the length of the ray reflected at the geometric ground reflection point has not been removed even though the zero phase surface implies convergence: this fact means that values of R_0 at far distances in the Fresnel zone will be slightly high; parallax at the antenna, which can be detected at the near distances, has not been taken into account: this means that values of R_0 for the near distances will also be slightly high (the necessary lack of significant figures in the method of calculating the angles involved prohibits the inclusion of parallax).

The elevation of the zero phase surface over the spherical earth at the previously computed Fresnel zone points is plotted in figure 16; these curves are upper bounds for deviations from the smooth spherical surface for "aiding obstacles" (see below) because parallax was not incorporated and divergence was not removed.

Applications. An obstacle of height less than R_0 may significantly add to the energy at the antenna if its upper surface has a slope between that of the smooth surface of the earth and the zero phase surface and has considerable longitudinal aspect, and its shadow doesn't extend very much into the area bounded by the quarter-wave contour. The height and lateral aspect

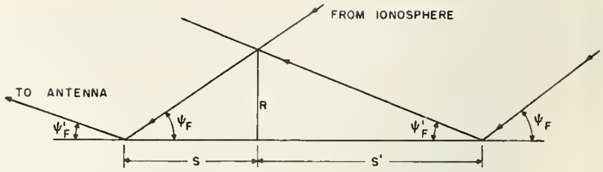

FIGURE 15. *Obstacle shadows.*

of an obstacle determine the area eliminated from the zone by shadowing (diffraction ignored).

A perfect zero phase surface above the first Fresnel zone will have a resultant field with a magnitude $\pi/2$ times that of the resultant from a Fresnel zone on a plane. An approximate integration shows that 71 percent of the energy reflected from a Fresnel zone comes from within the $\lambda/4$ contour and 50 percent from within the $\lambda/6$ contour. Upper bounds for effects of the loss of portions of the first zone may be set by assuming that the zone is of zero width; a bound for tolerated loss may be taken as a sinusoidal function of position in the zone to get a measure of the amount of surface which may be shaded or otherwise eliminated.

For holes with respect to a smooth surface and for objects higher than R_0, some such criterion as the $\pi/4$ phase difference (Rayleigh) is reasonable if combined with a knowledge of shading effects. If the area immediately around the ground reflection point is satisfactory, a variation in antenna height falling within the $\pi/4$ criterion will allow the use of a shorter antenna height apart from the considerations in reference 1. Anything which adds to the signal will also narrow the beam width, and holes, etc., will widen it; the narrowing represents a concentration of energy and should not be considered a disadvantage.

With $w=4\sqrt{2h}$ as an upper bound for the maximum width, quantitative examination of the first Fresnel zone over a spherical earth has been carried as far as the present model allows. It must be remembered that geometrical optics only was used; furthermore, energy contributions from the higher order zones have not been examined: indeed, these are unknown for the plane earth case.

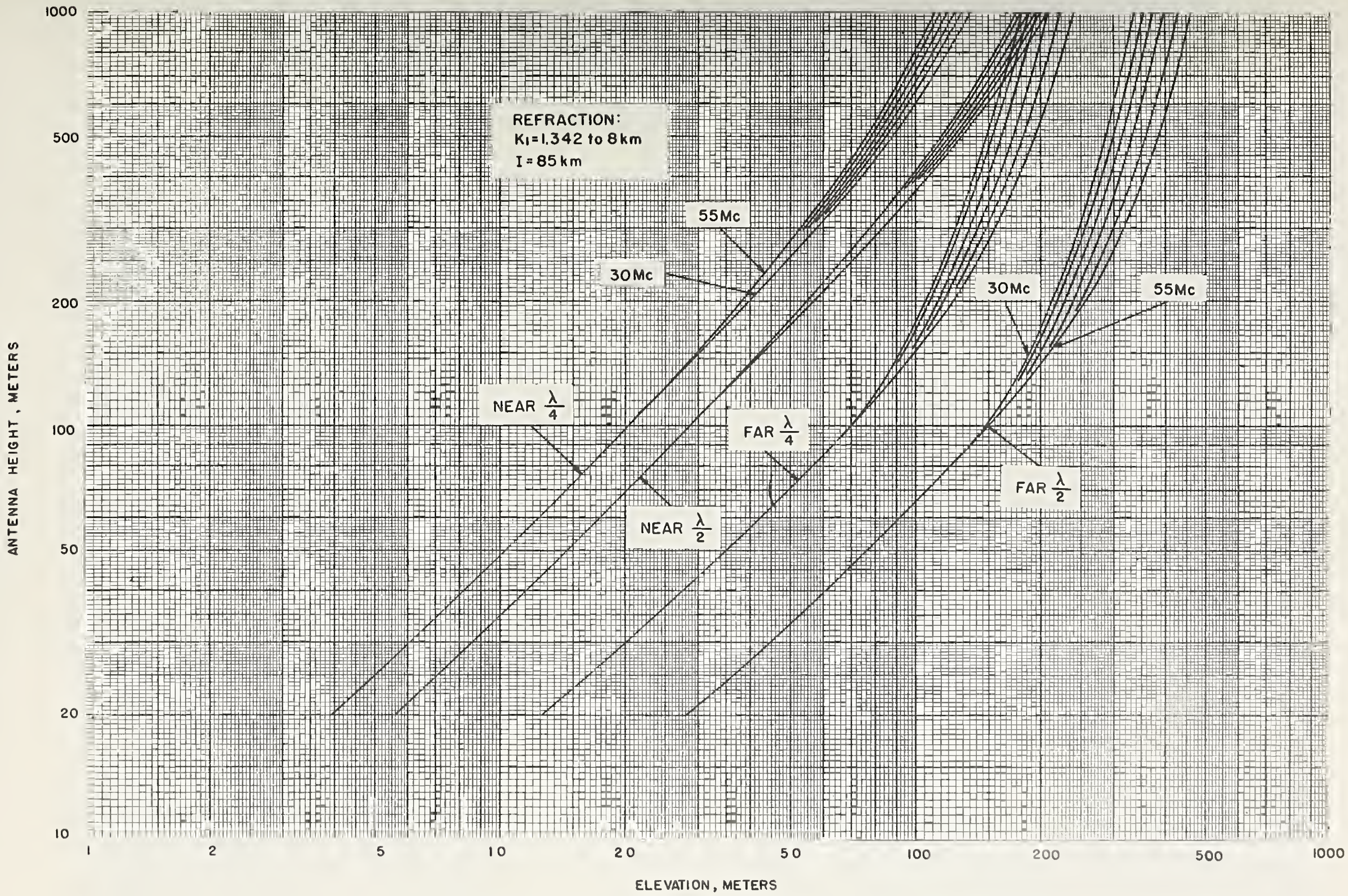

Figure 16A. *Elevation of zero phase surface* (k_1).

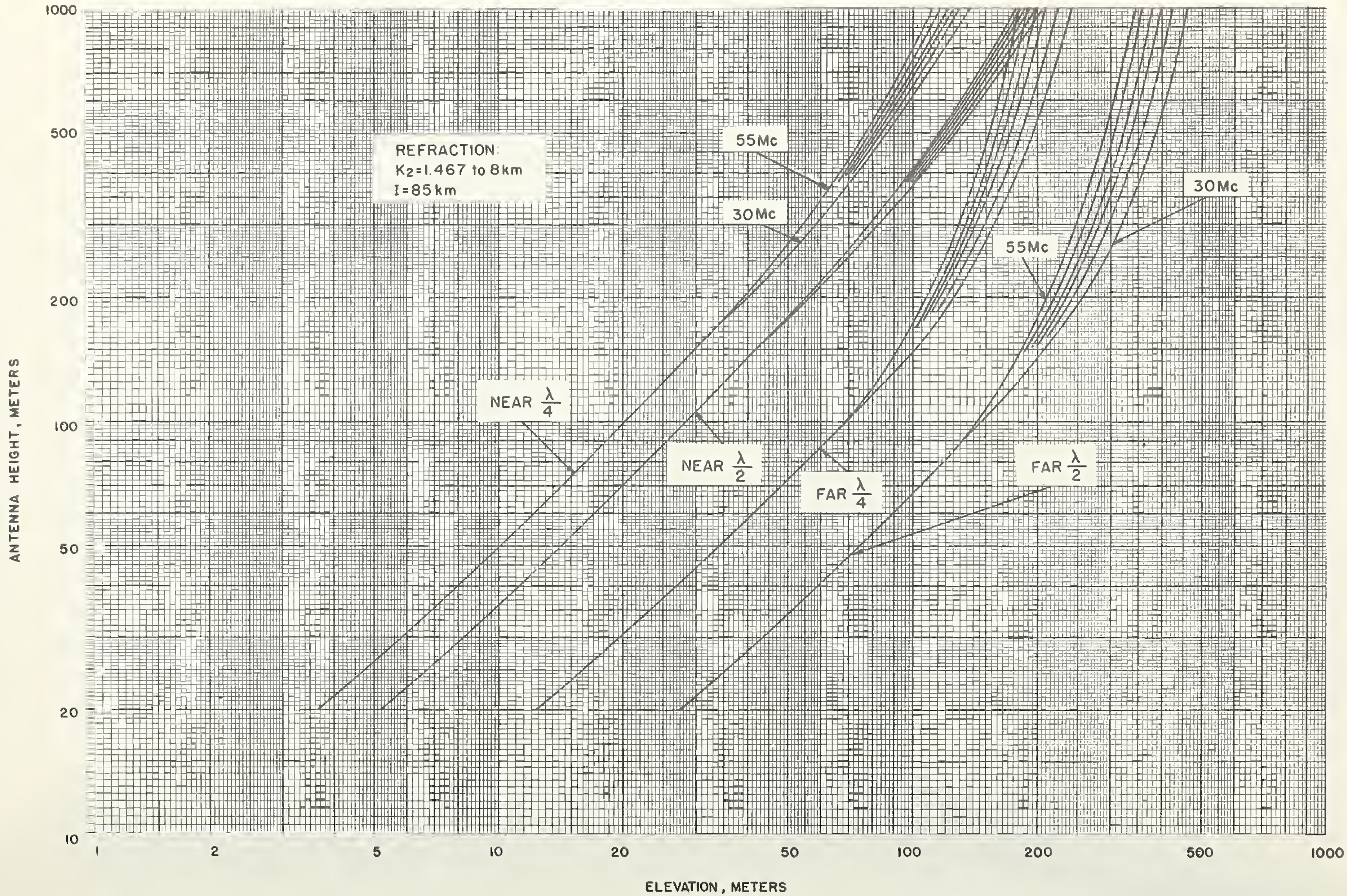

FIGURE 16B. *Elevation of zero phase surface* (k_2).

7. Summary

Antenna heights for lobe alinement at the path midpoint in an 85 km scattering stratum have been calculated at 30 through 55 Mc in steps of 5 Mc for antenna heights of 20, 50, 70, 100, 225, 500, and 1000 m and two refractivities representing "standard refraction" and temperate over-water or "wet" tropical conditions. The calculations incorporated tropospheric refraction, parallax, spherical divergence, refractive defocusing, and near-horizon diffraction. The calculations give somewhat higher antenna heights than those published in reference 2; in the latter case, divergence and defocusing were not considered and simpler allowances were made for refraction and parallax. A comparison of the refractivity model used in the present work with the exponential reference atmosphere [3, 8] shows that the two are effectively indistinguishable. The radiation patterns so computed are given in the first three appendixes.

Distances from the antenna which locate the first Fresnel zone on the spherical earth, and angles of illumination and reflection within the zone, have been given. Roughness criteria have been given with respect to the zero phase surface rather than the spherical surface of the earth.

The results of computing the antenna height-gain function have been published [1]: these show that the optimum height is *lower* than the lobe alinement height and that a broad range of lower heights is essentially equivalent in gain to the lobe alinement height.

The authors acknowledge the following contributions to this work: discussions with Richard C. Kirby, Kenneth L. Bowles, Ernest K. Smith, Bradford R. Bean, and Gordon D. Thayer; contributions to the computer program by Mrs. Marie L. West; computations and graphing by Loren P. Sims; computations by Mrs. Charlotte I. Enfield and Alvin M. Gray; extensive computer production work by Patricia R. Lollar and Bonnie M. Laubach; computer ray tracing for the refractivity model by Mrs. Betty J. Weddle; valuable critical reading of the text by Robert S. Cohen.

This work was carried out on behalf of the U.S. Air Force under support extended by the Ground Electronics Engineering and Installation Agency, Rome, N.Y.

8. References and Notes

[1] R. G. Merrill, Optimum antenna height for ionospheric scatter communication, IRE Transactions on Communications Systems **CS-8**, 14–19 (March 1960).

[2] D. K. Bailey, R. Bateman, and R. C. Kirby, Radio transmission at VHF by scattering and other processes in the lower ionosphere, Proc. IRE **43**, 1181–1230 (October 1955).

[3] B. R. Bean and G. D. Thayer, Models of the atmospheric radio refractive index, Proc. IRE **47**, 740–755 (May 1959).

[4] H. Bremmer, Terrestrial radio waves: theory of propagation, pp. 90–92 (Elsevier Publishing Co., Amsterdam, 1949).

[5] J. C. Schelleng, C. R. Burrows, and E. B. Ferrell, Ultra-short wave propagation, Proc. IRE **21**, 427–463 (March 1933).

[6] B. van der Pol and H. Bremmer, Further note on the propagation of radio waves over a finitely conducting spherical earth, Phil. Mag. [7] **27**, 261–275 (March 1939).

[7] C. Domb and M. H. L. Pryce, The calculation of field strength over a spherical earth, J. IEE **94**, 325–339 (September 1947).

[8] B. R. Bean and G. D. Thayer, CRPL exponential reference atmosphere, NBS Monograph 4 (October 29, 1959).

[9] Unpublished computation courtesy G. D. Thayer and Mrs. B. J. Weddle.

[10] Bean and Thayer, Proc. IRE, loc. cit., fig. 8, p. 748.

[11] For a more detailed discussion of this point see appendix VI.

[12] Donald E. Kerr, editor, Propagation of short radio waves, M.I.T. Radiation Laboratory Series, vol. 13 pp. 411–418 (McGraw-Hill Book Co. New York, N.Y., 1951).

9. Appendixes

Appendix I. Antenna Patterns for k_1

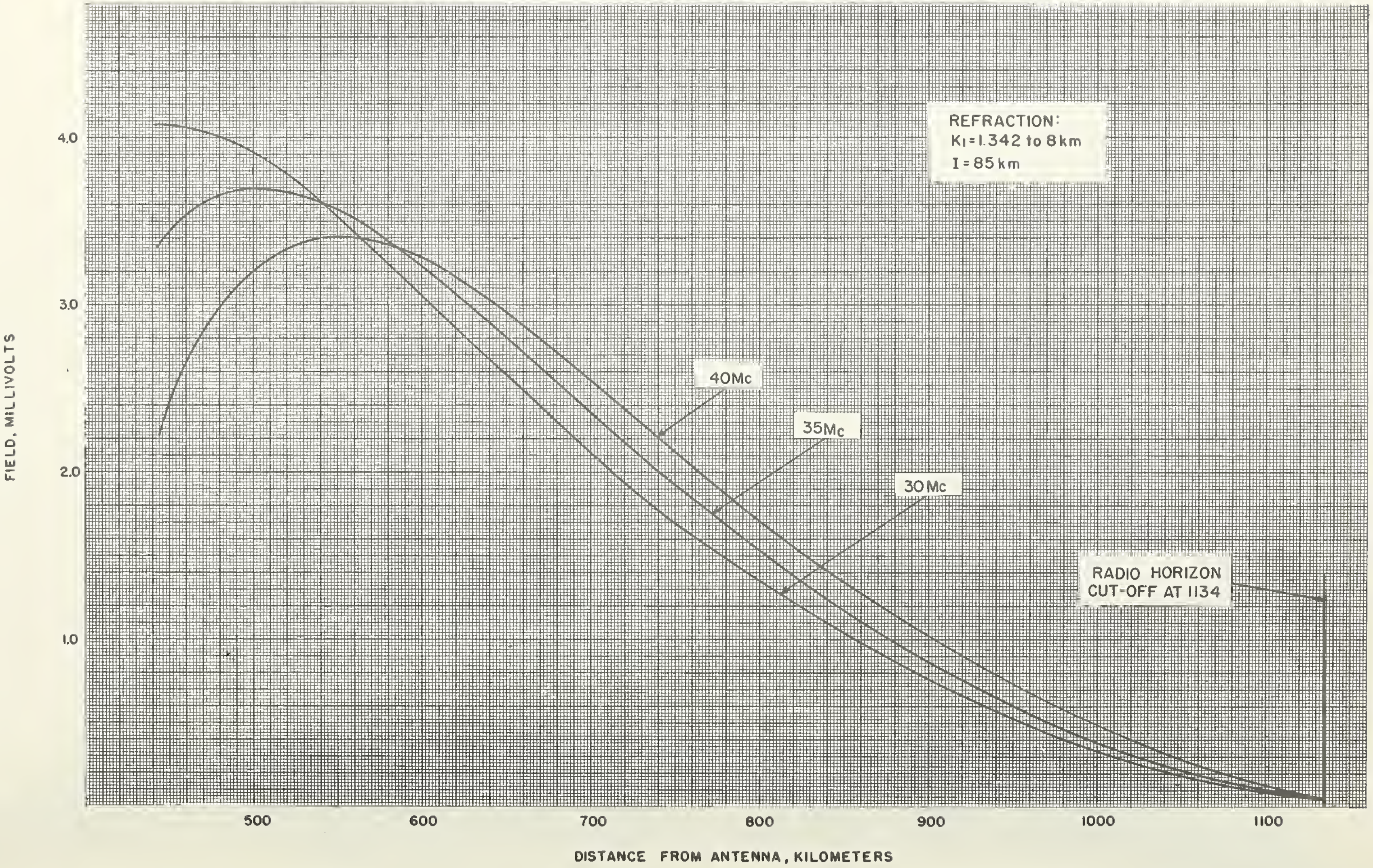

FIGURE 1. *20 meter antenna.*

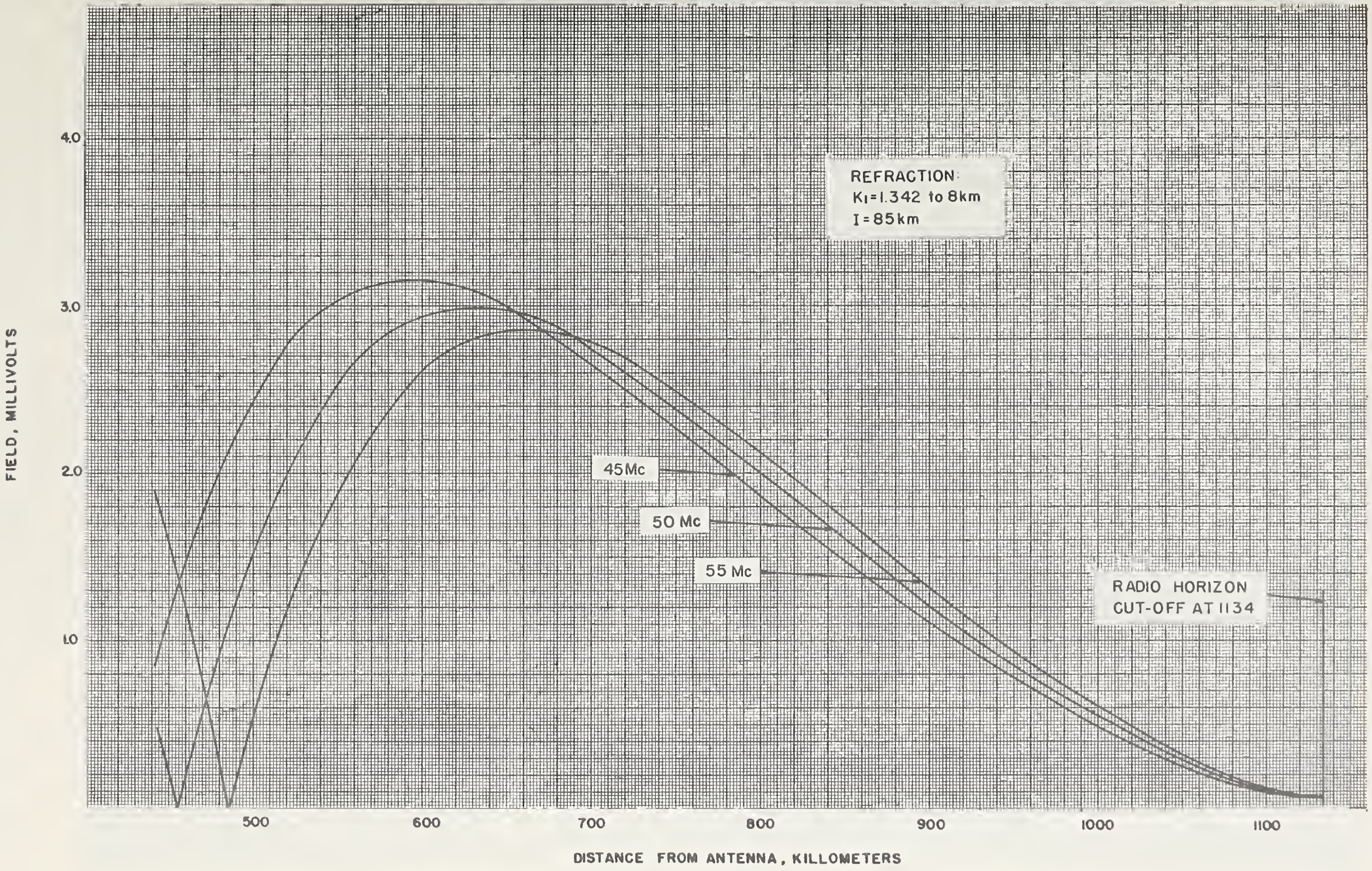

Figure 2. *20 meter antenna.*

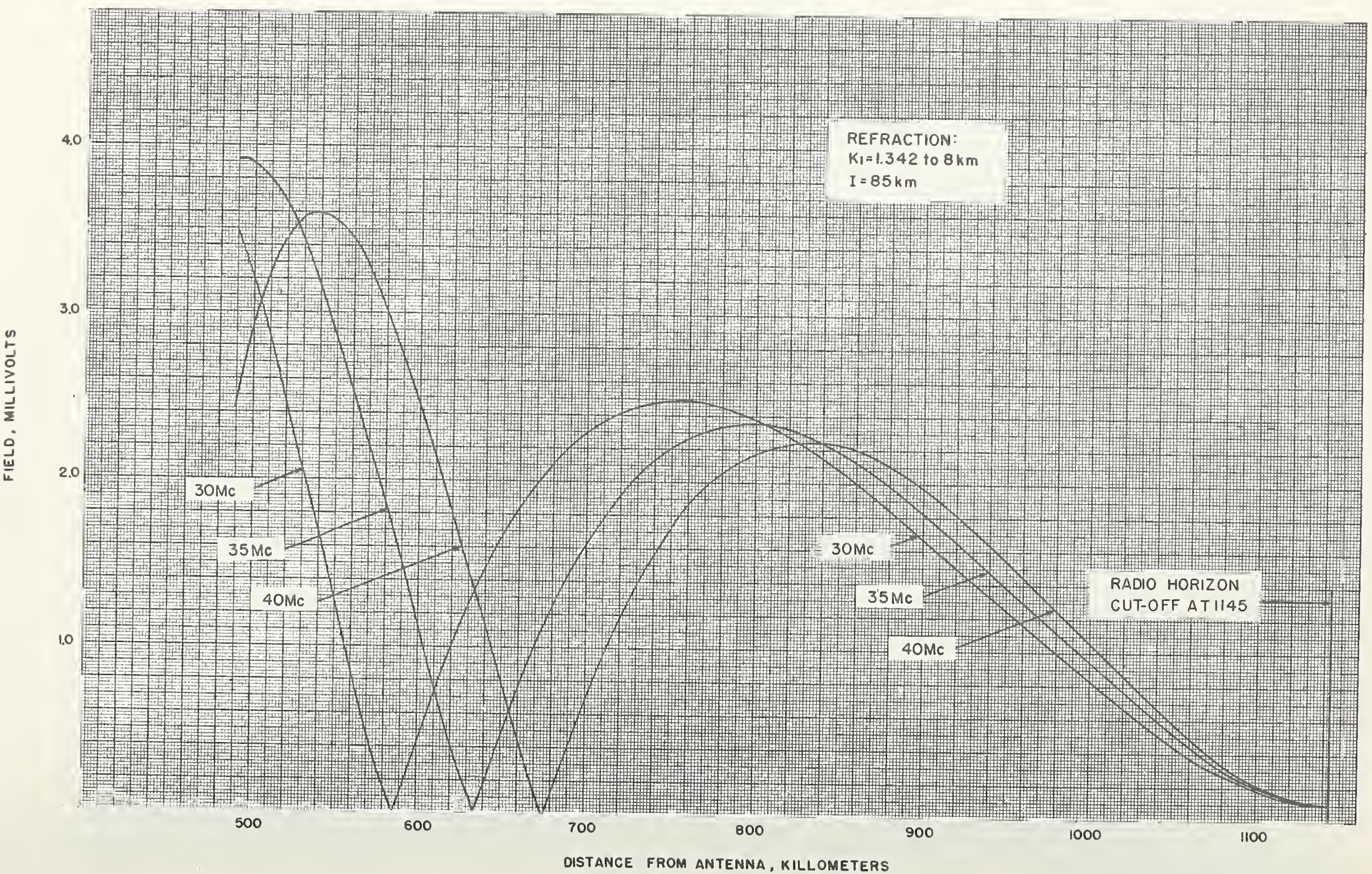

FIGURE 3. *50 meter antenna.*

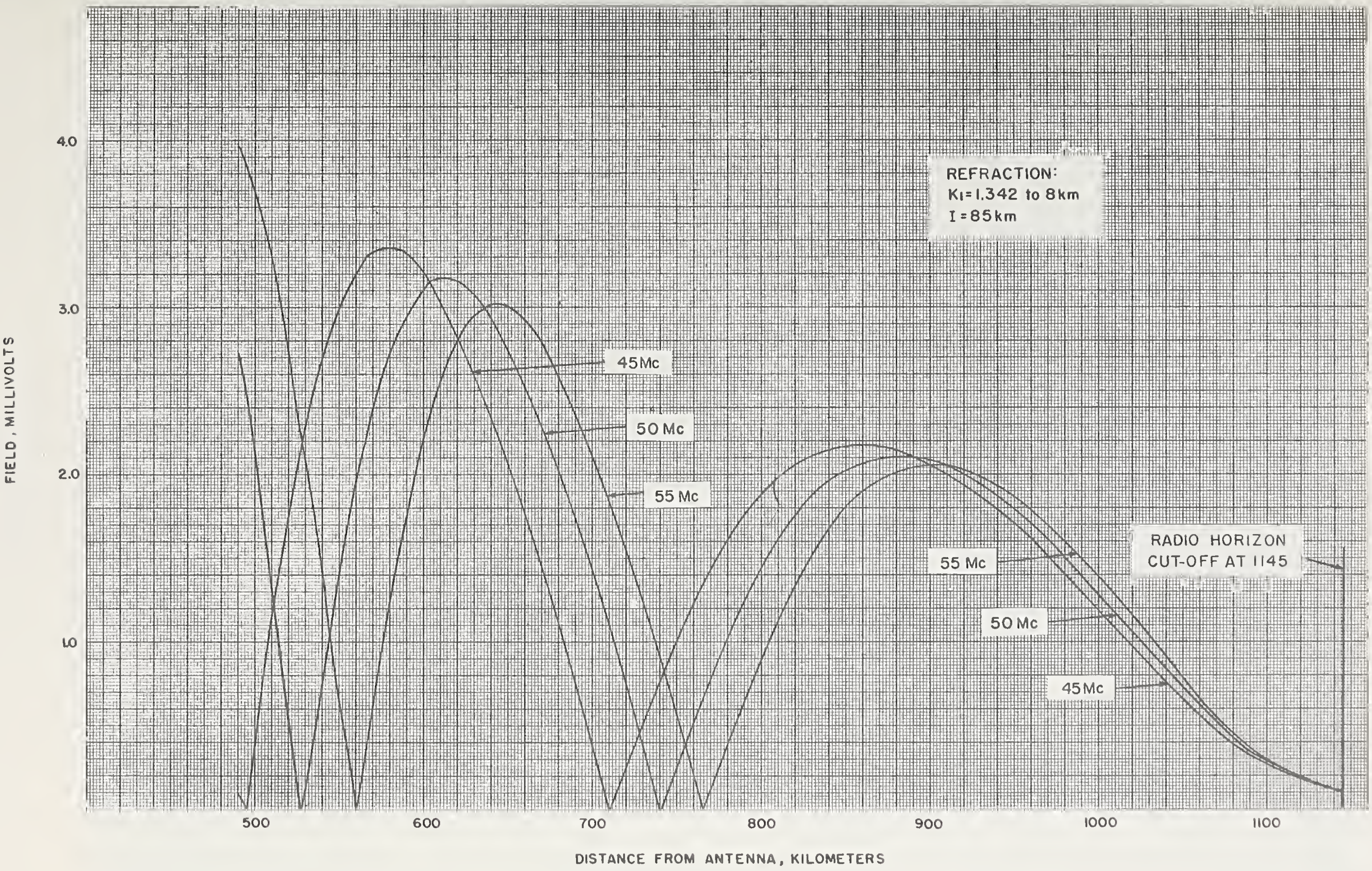

FIGURE 4. *50 meter antenna.*

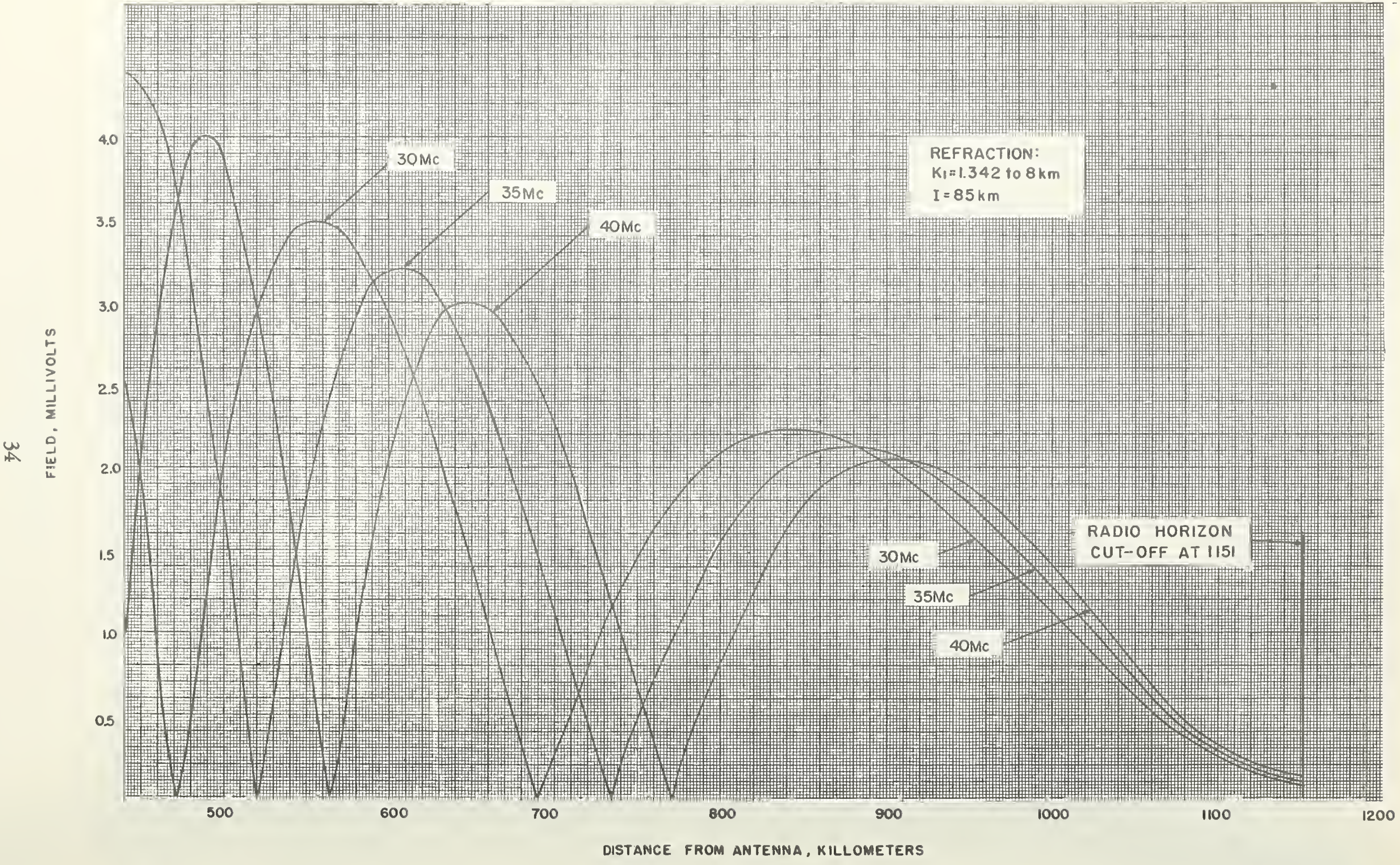

FIGURE 5. *70 meter antenna.*

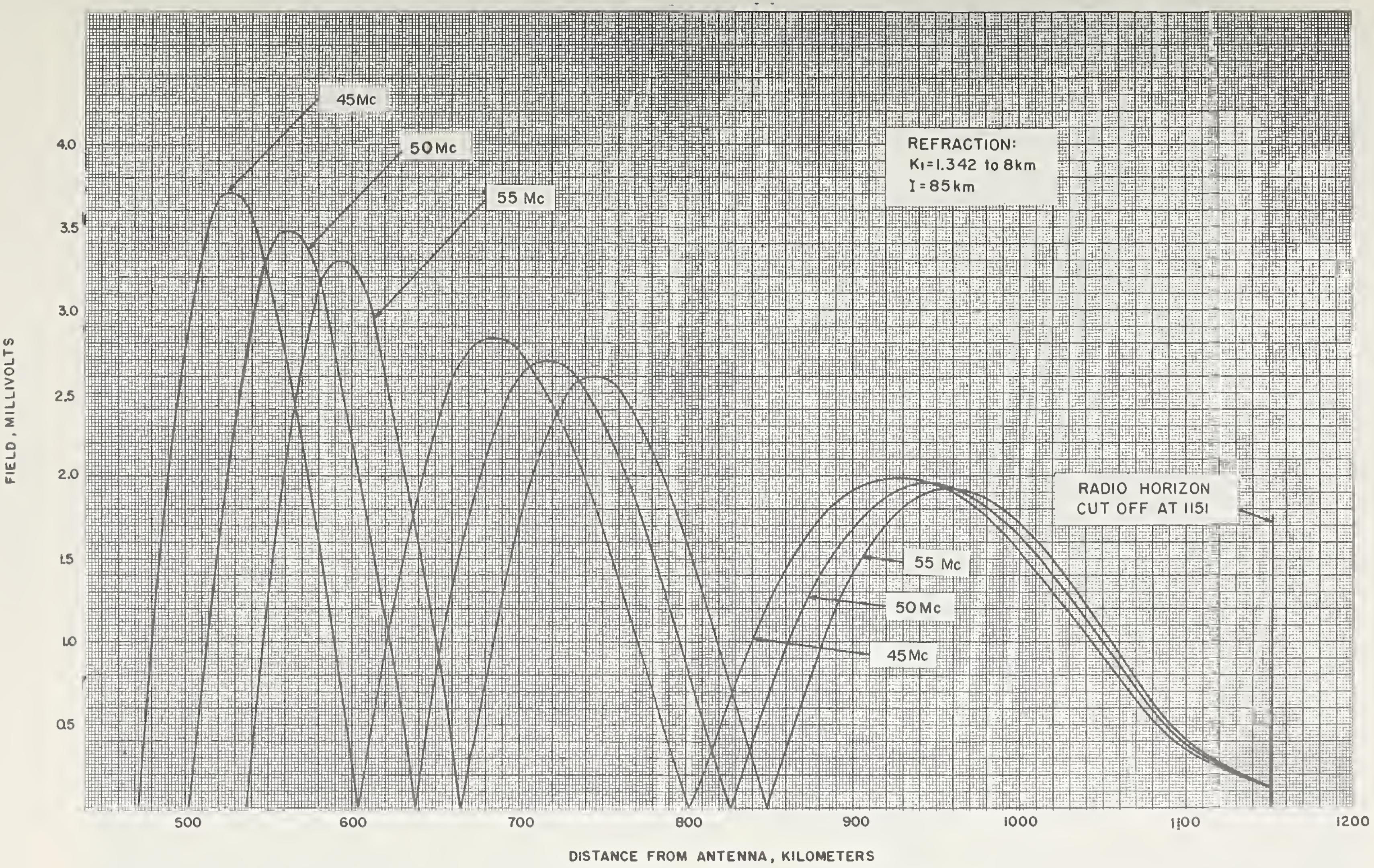

FIGURE 6. *70 meter antenna.*

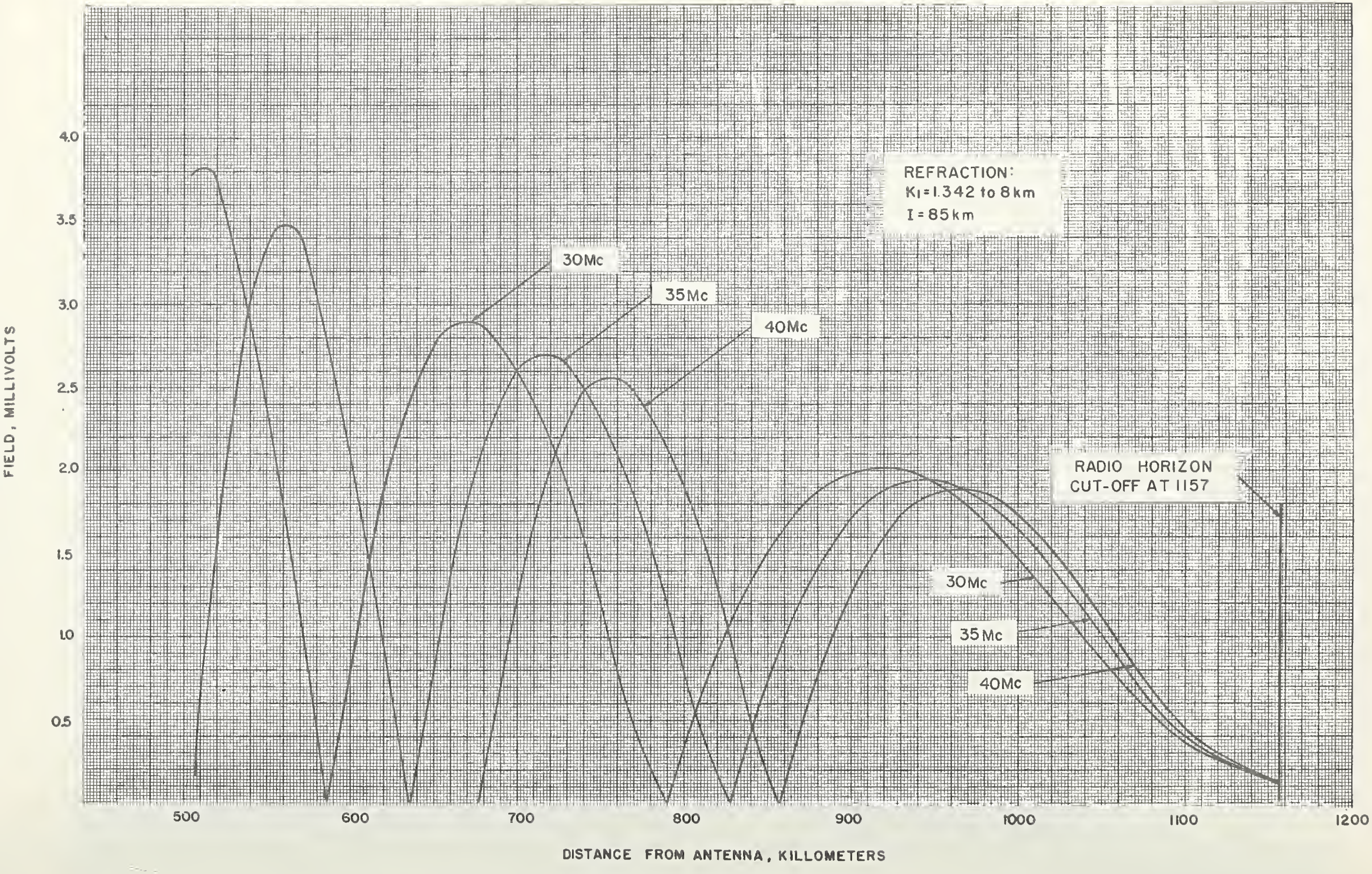

FIGURE 7. *100 meter antenna.*

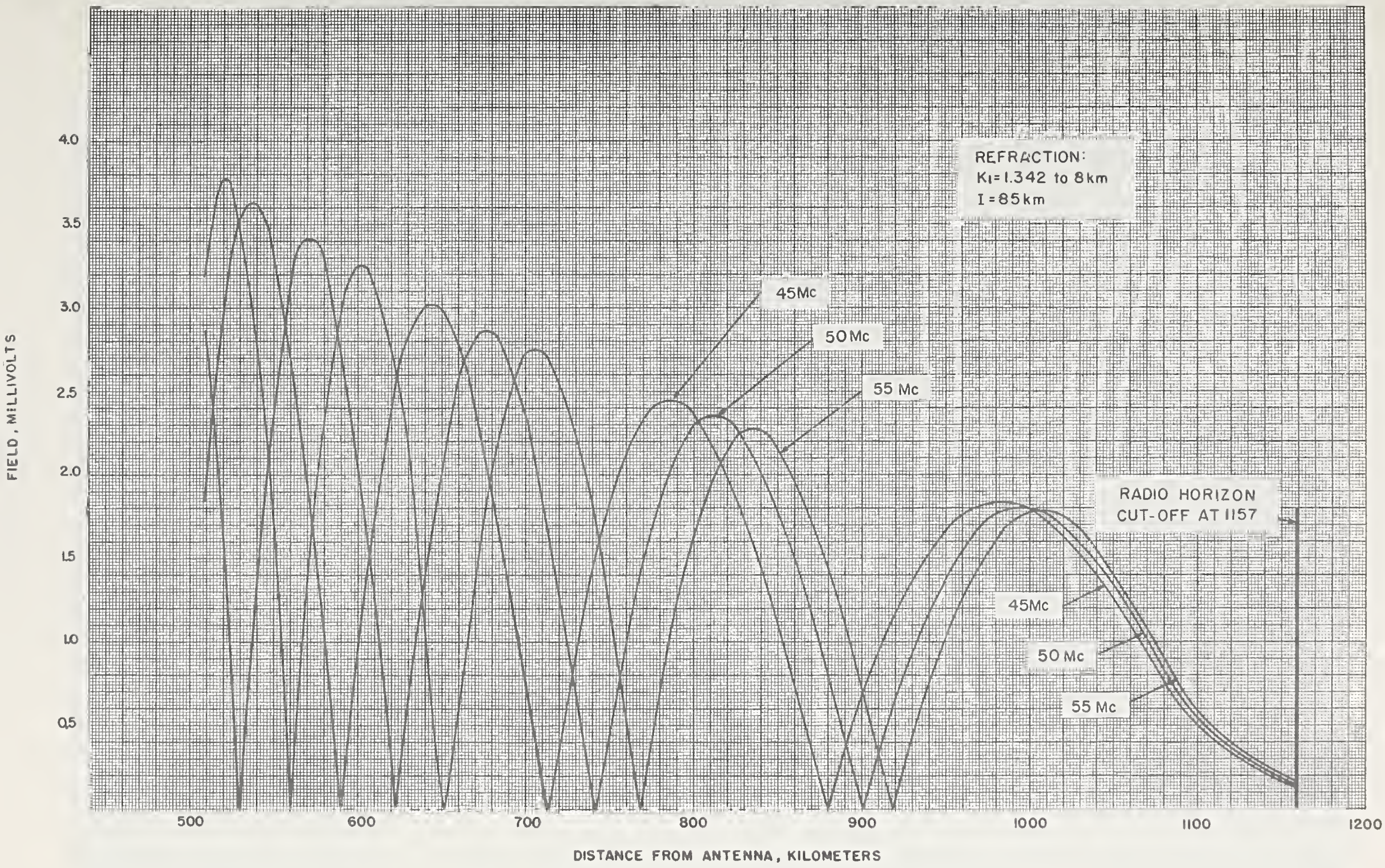

FIGURE 8. *100 meter antenna.*

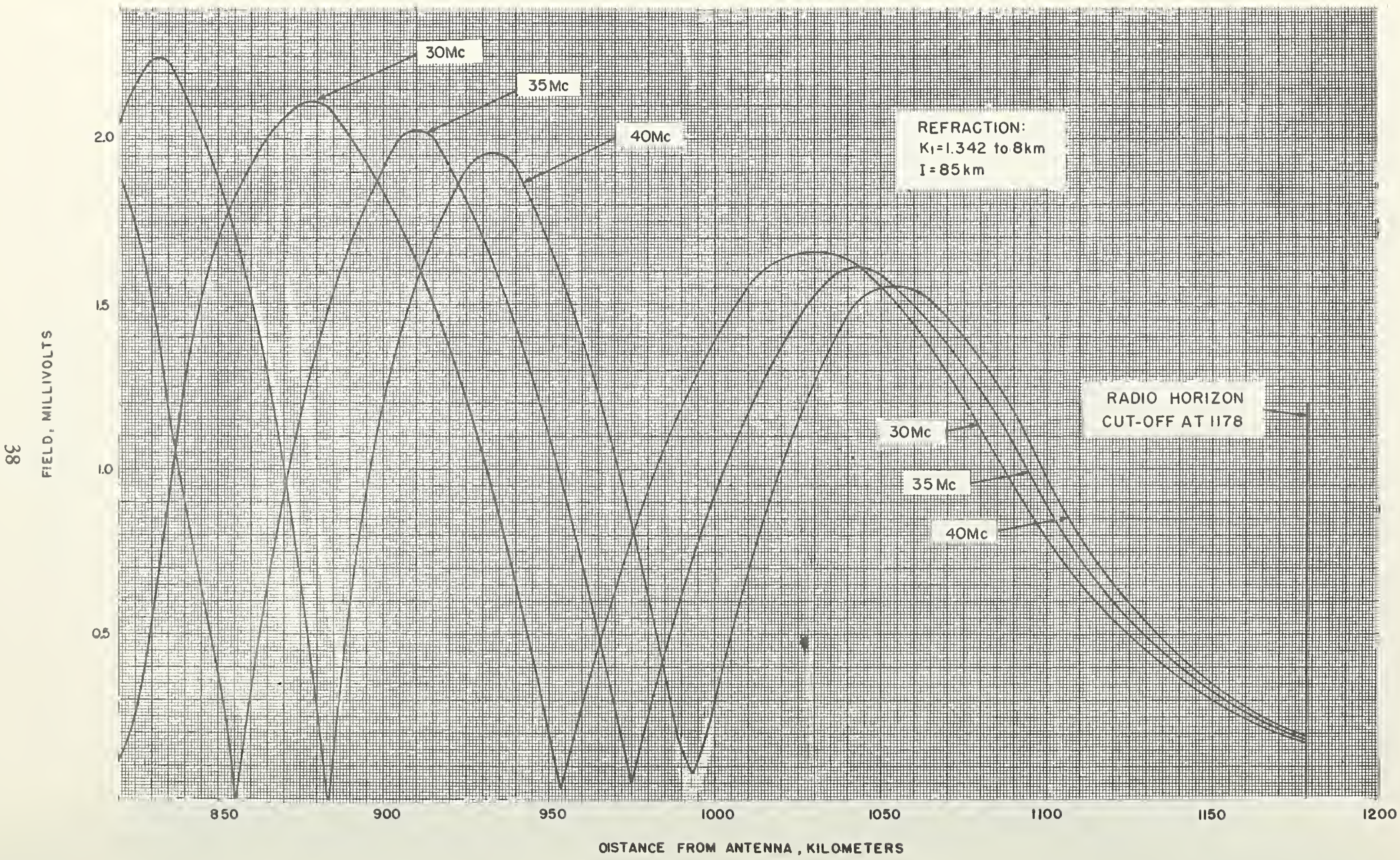

FIGURE 9. *225 meter antenna.*

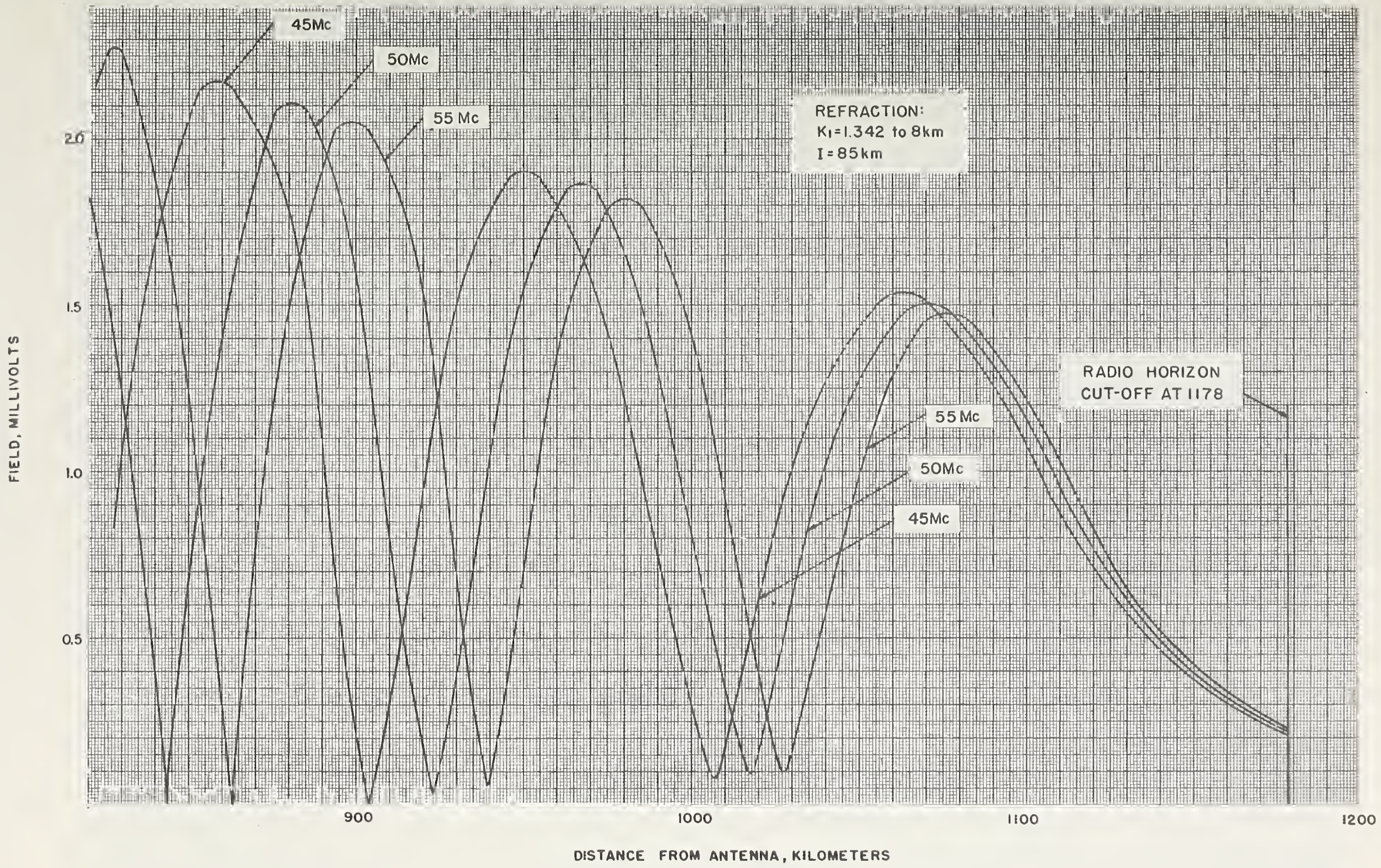

FIGURE 10. *225 meter antenna.*

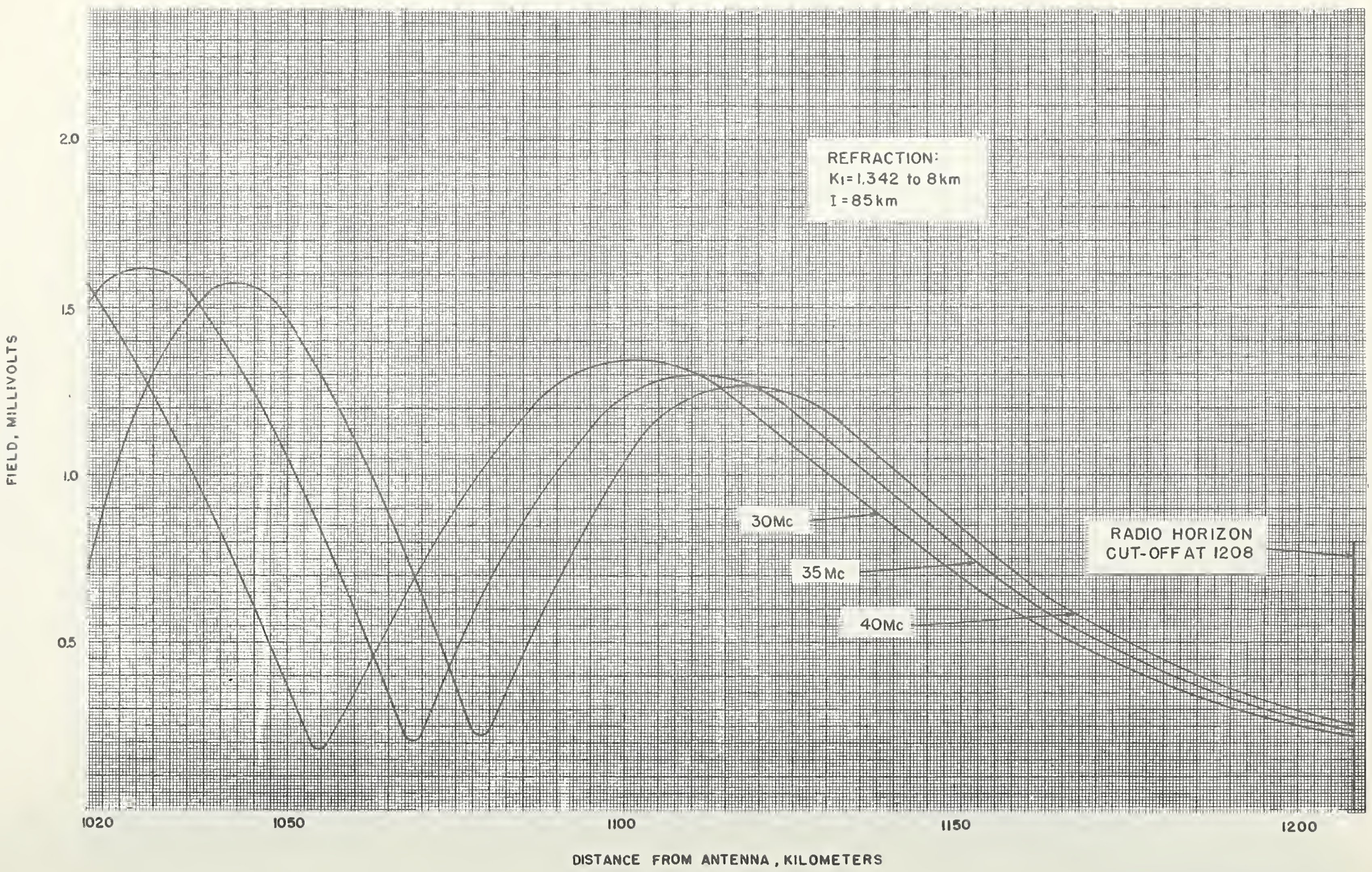

Figure 11. *500 meter antenna.*

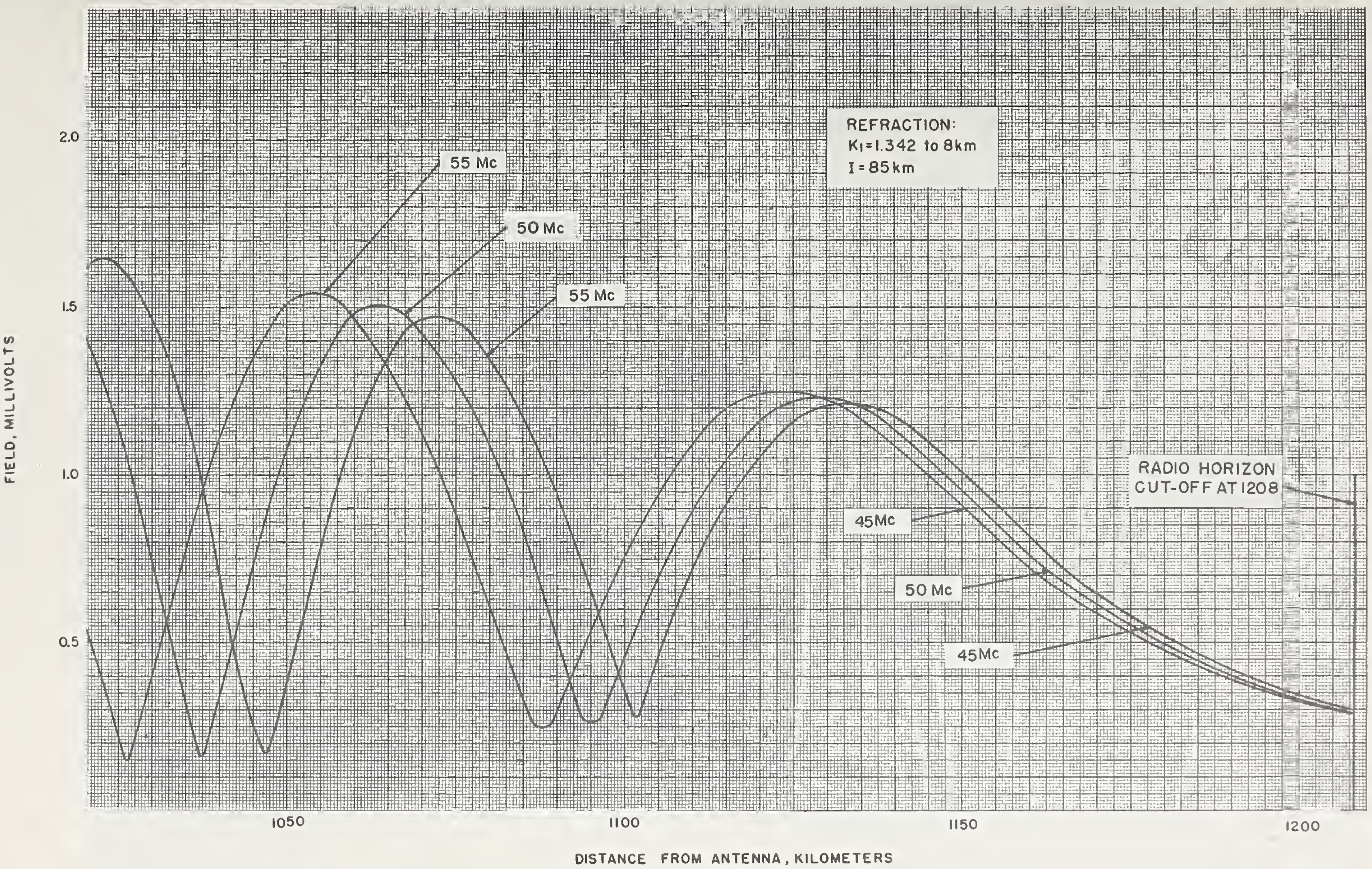

FIGURE 12. *500 meter antenna.*

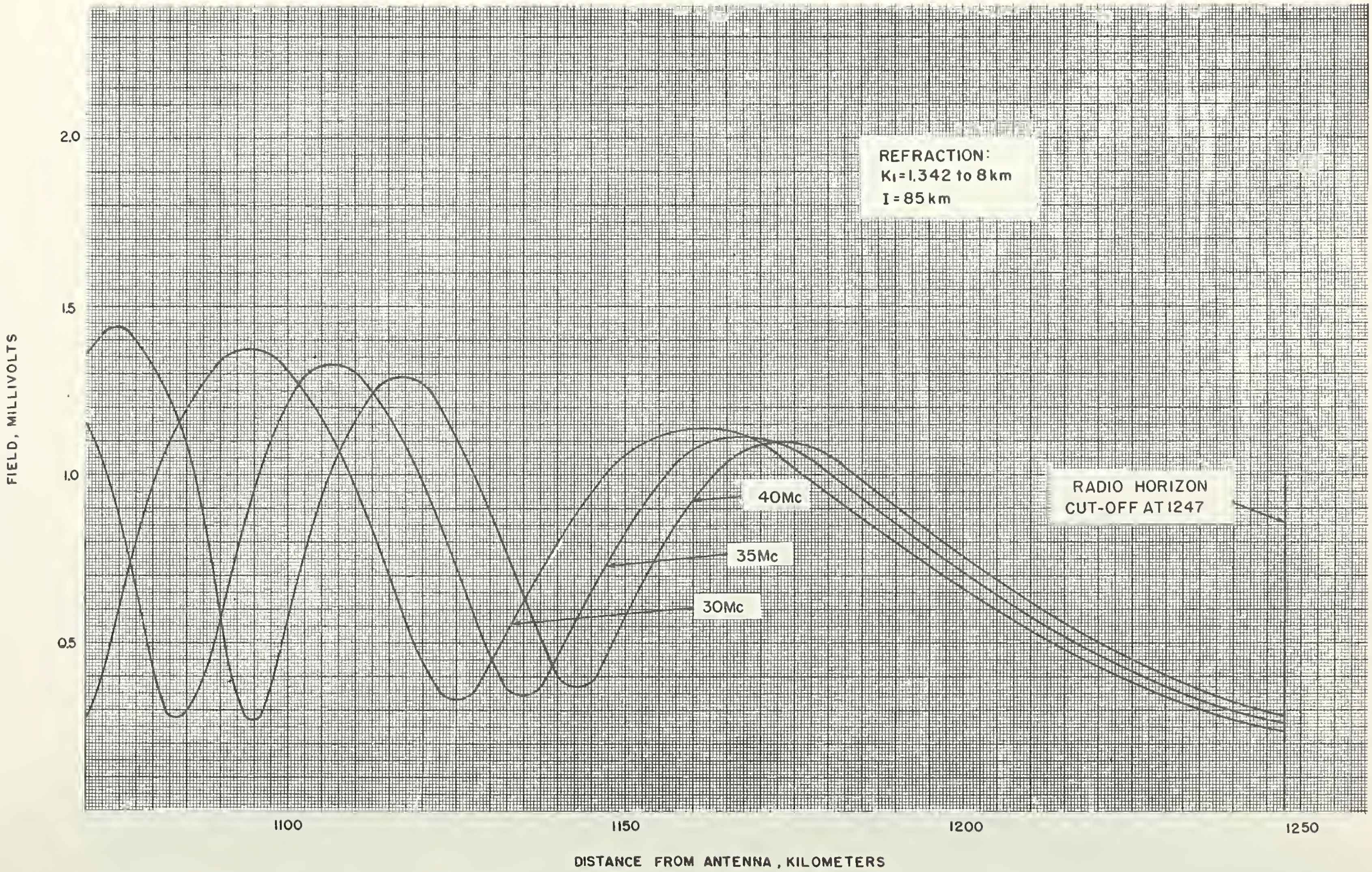

FIGURE 13. *1000 meter antenna.*

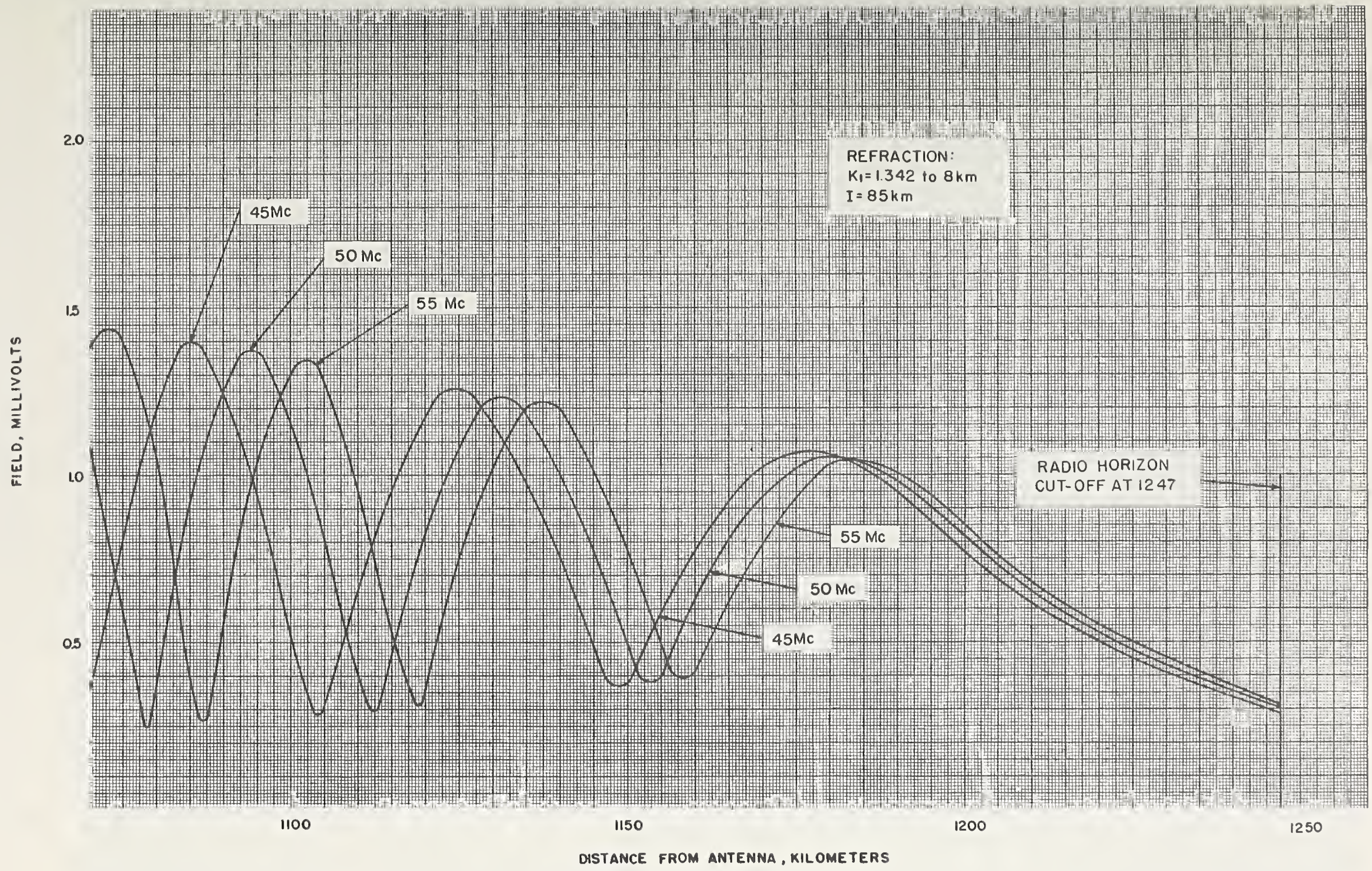

FIGURE 14. *1000 meter antenna.*

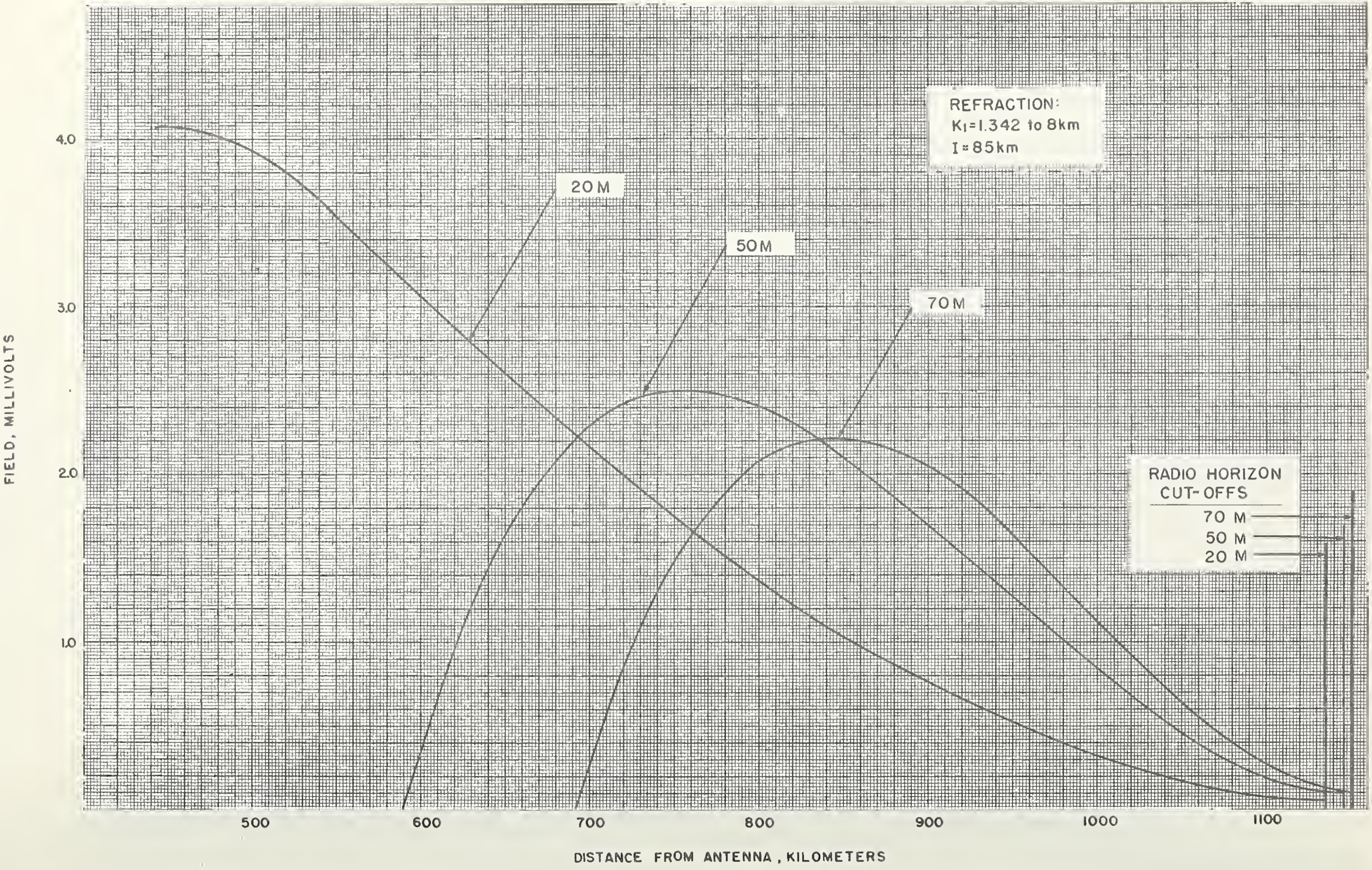

FIGURE 15. *20, 50, and 70 meter antennas at 30 Mc.*

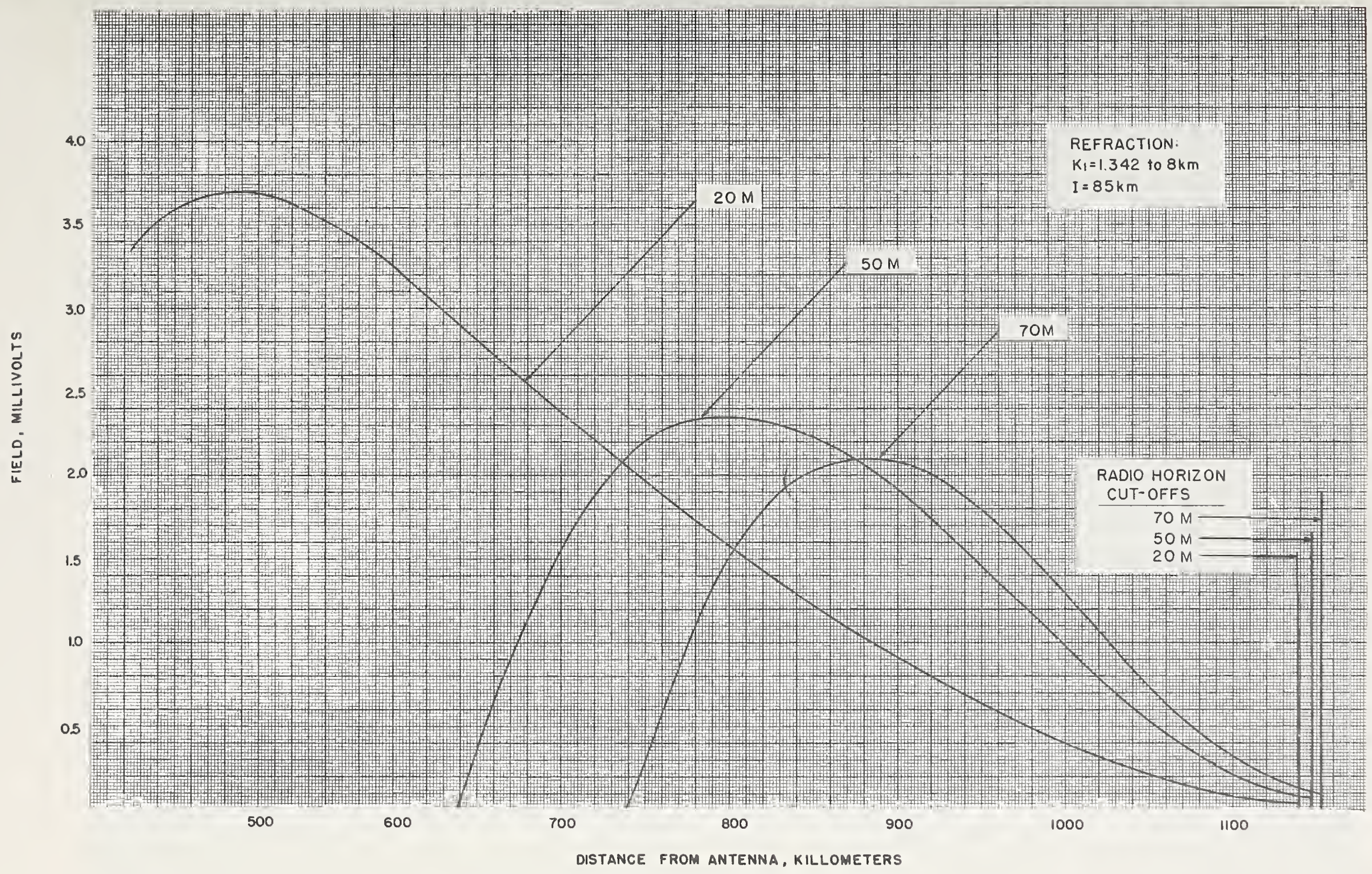

FIGURE 16. *20, 50, and 70 meter antennas at 35 Mc.*

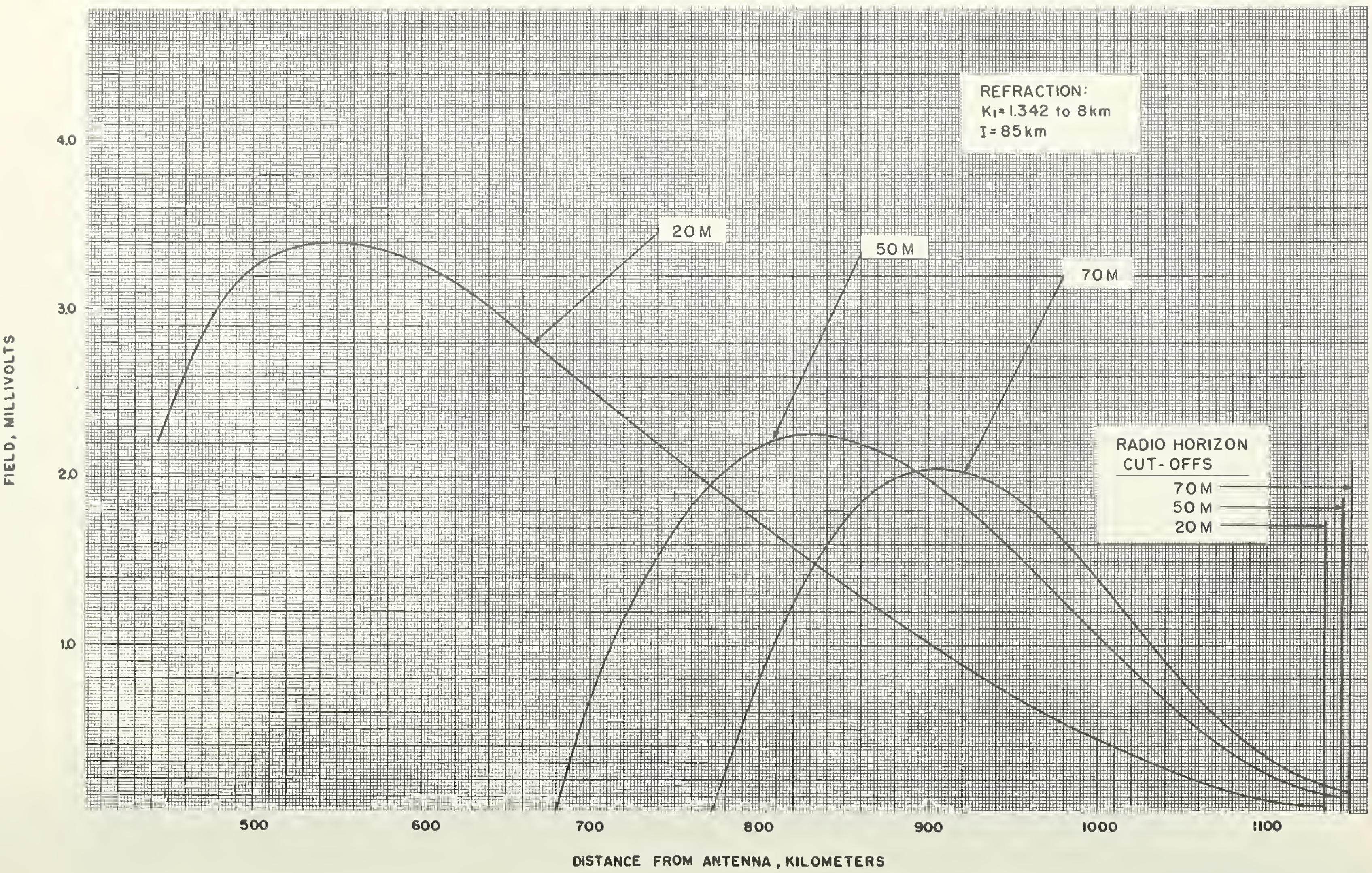

FIGURE 17. *20, 50, and 70 meter antennas at 40 Mc.*

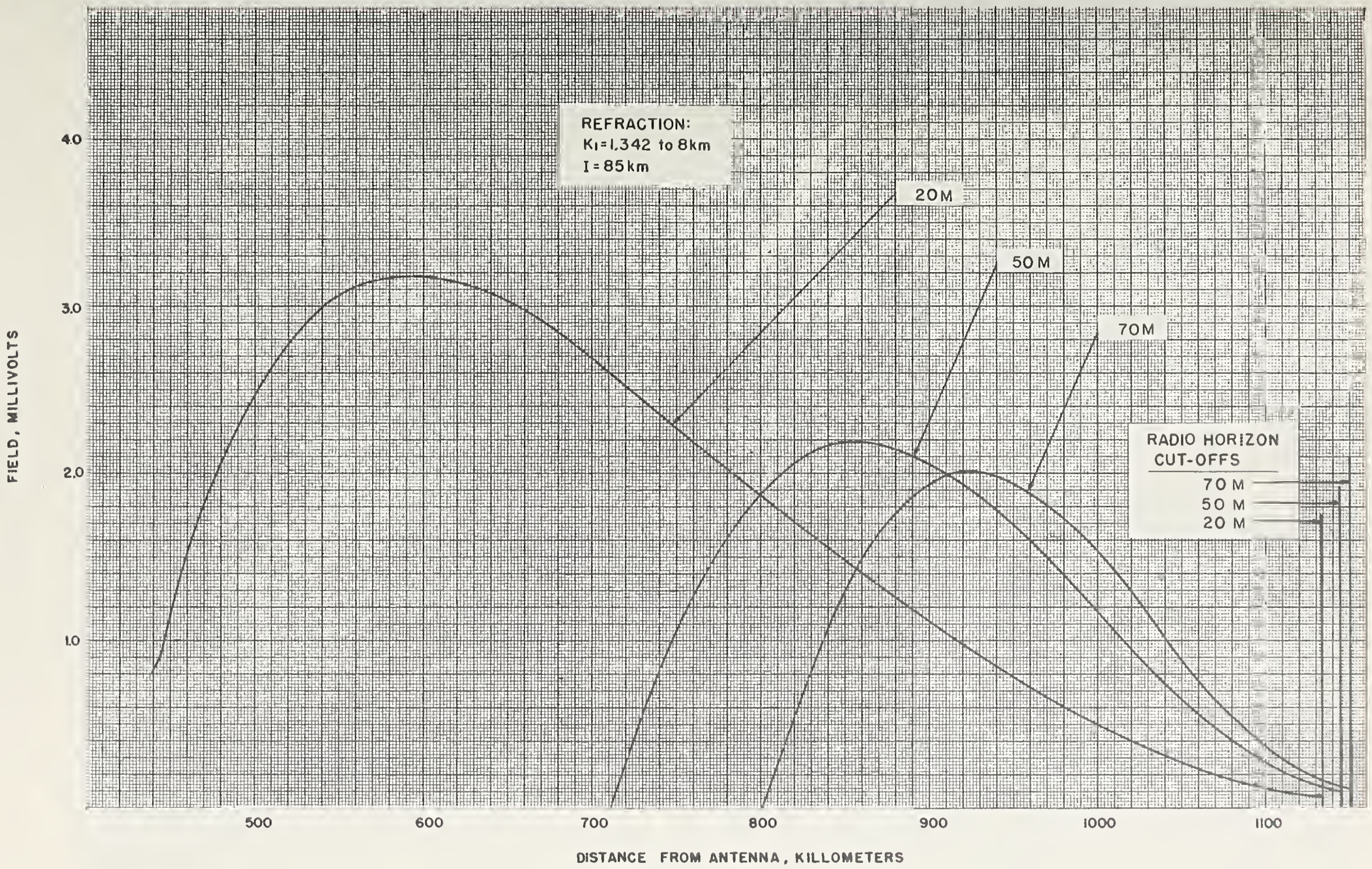

Figure 18. *20, 50, and 70 meter antennas at 45 Mc.*

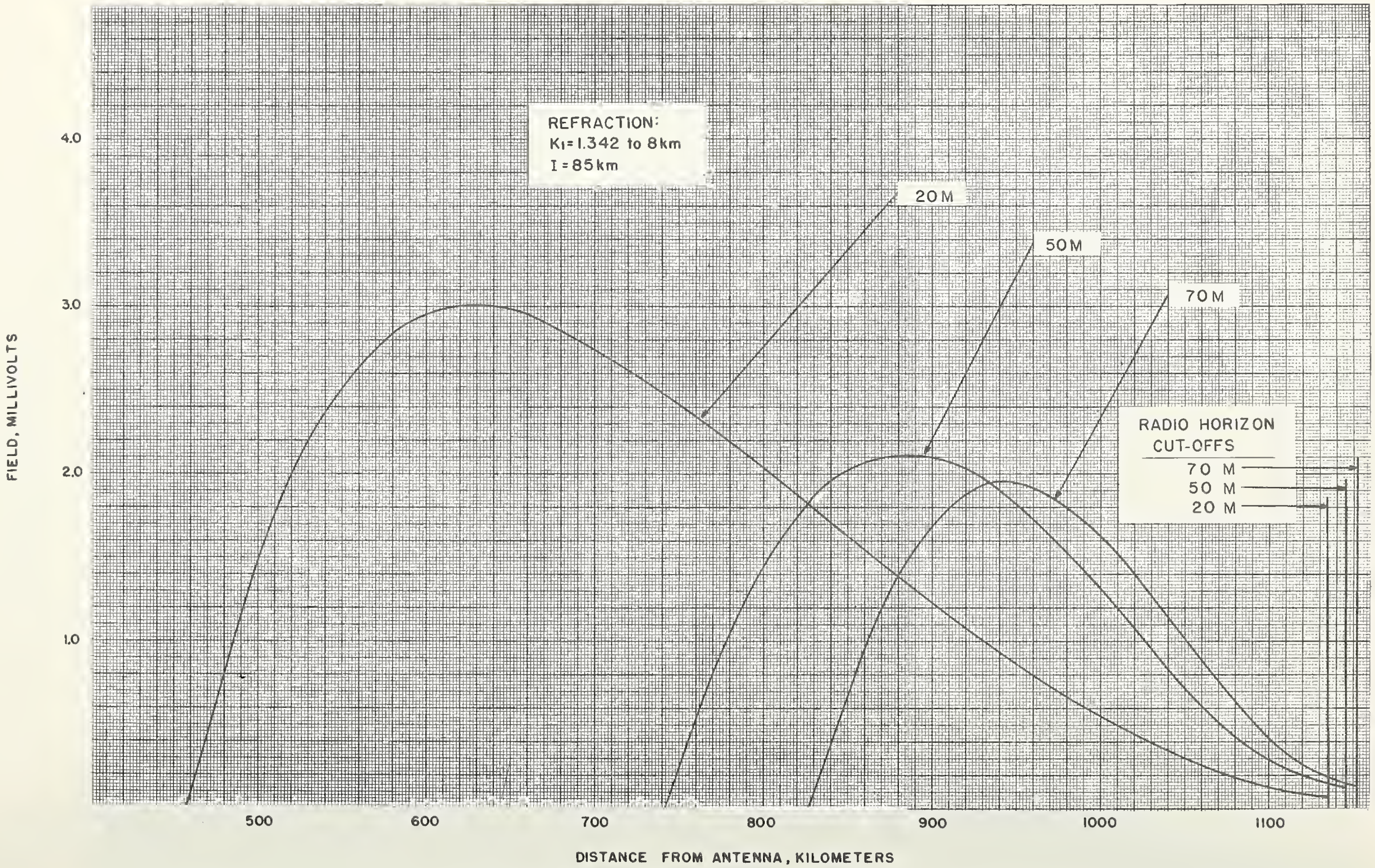

FIGURE 19. *20, 50, and 70 meter antennas at 50 Mc.*

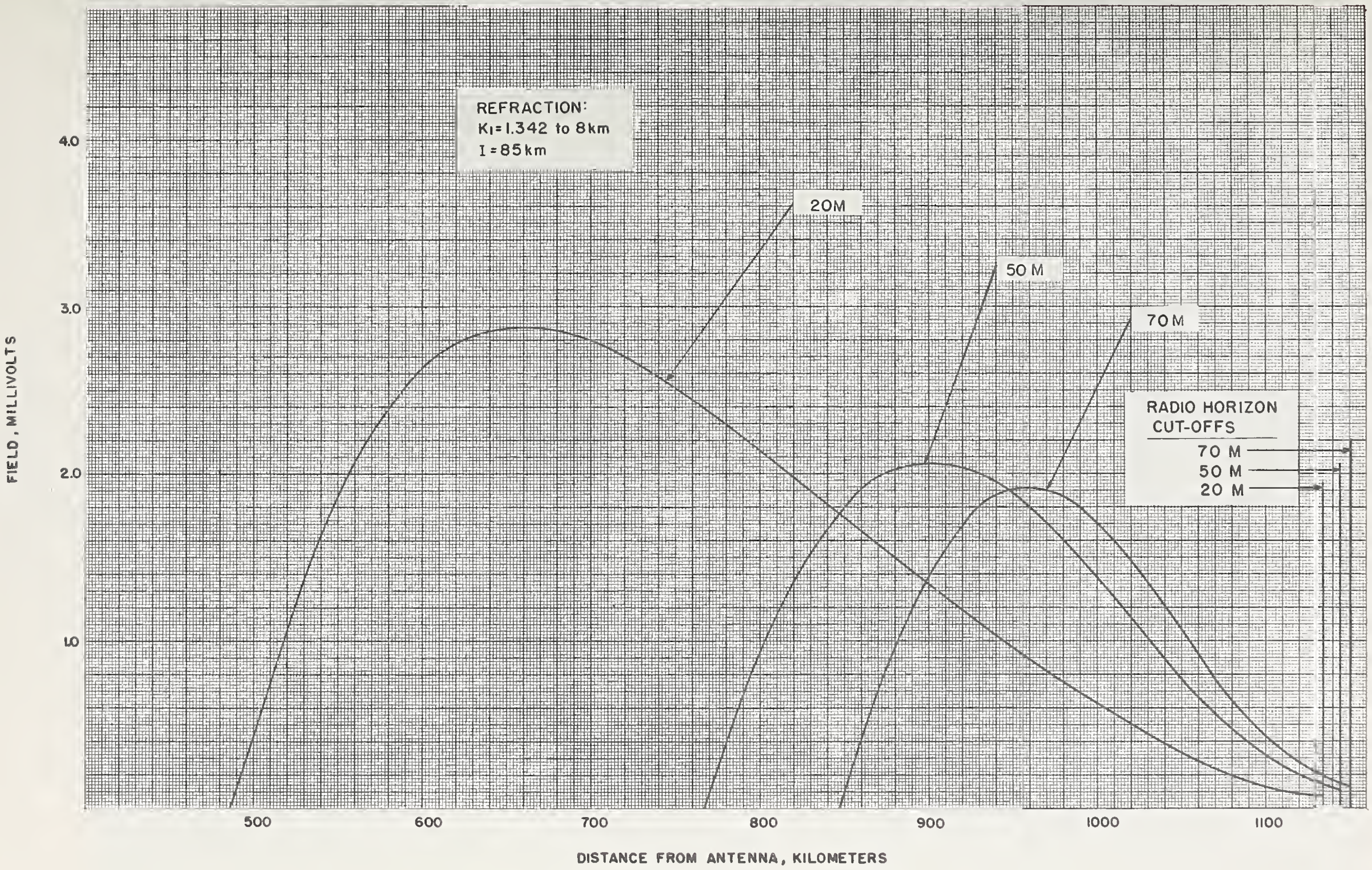

FIGURE 20. *20, 50, and 70 meter antennas at 55 Mc.*

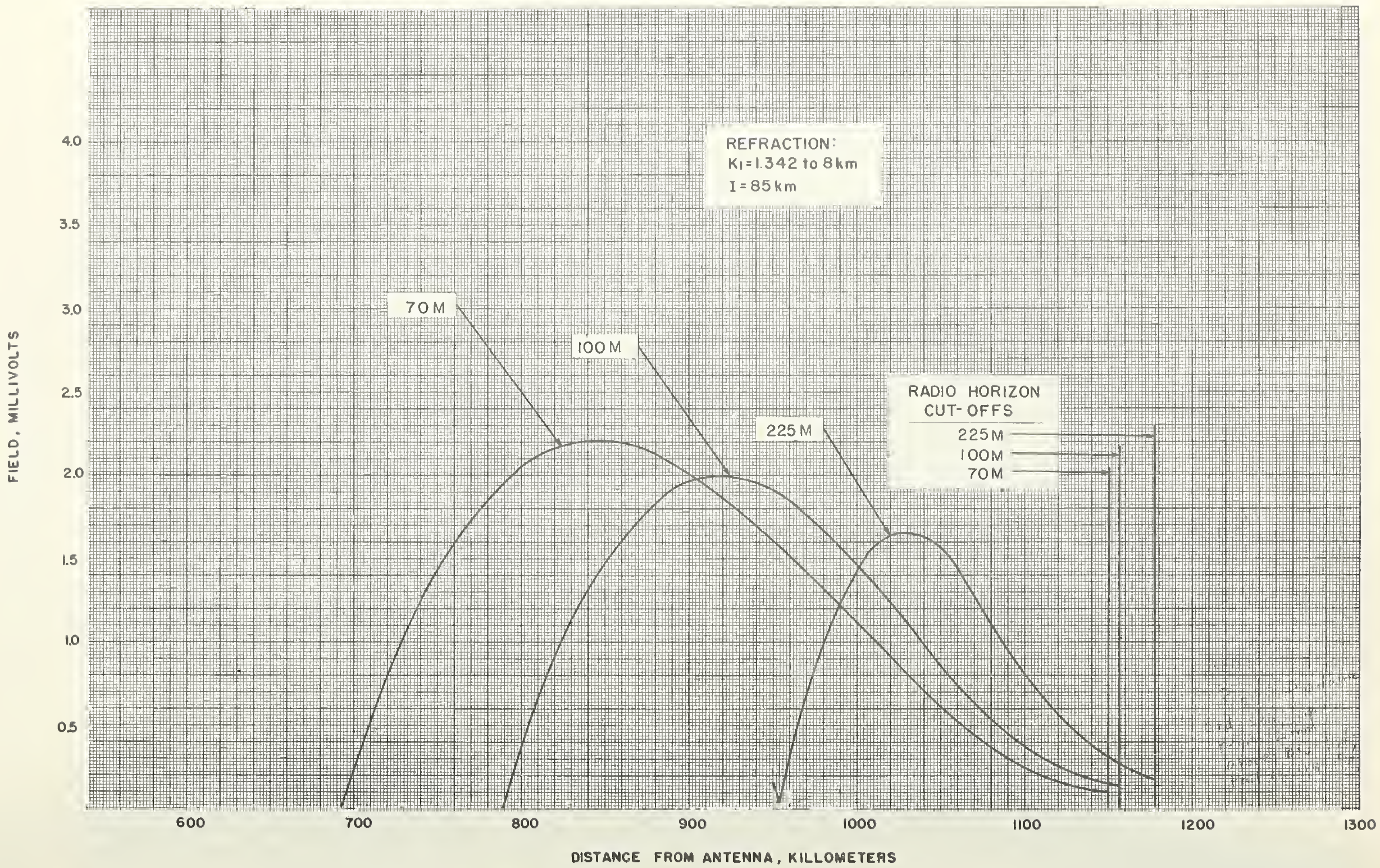

FIGURE 21. *70, 100, and 225 meter antennas at 30 Mc.*

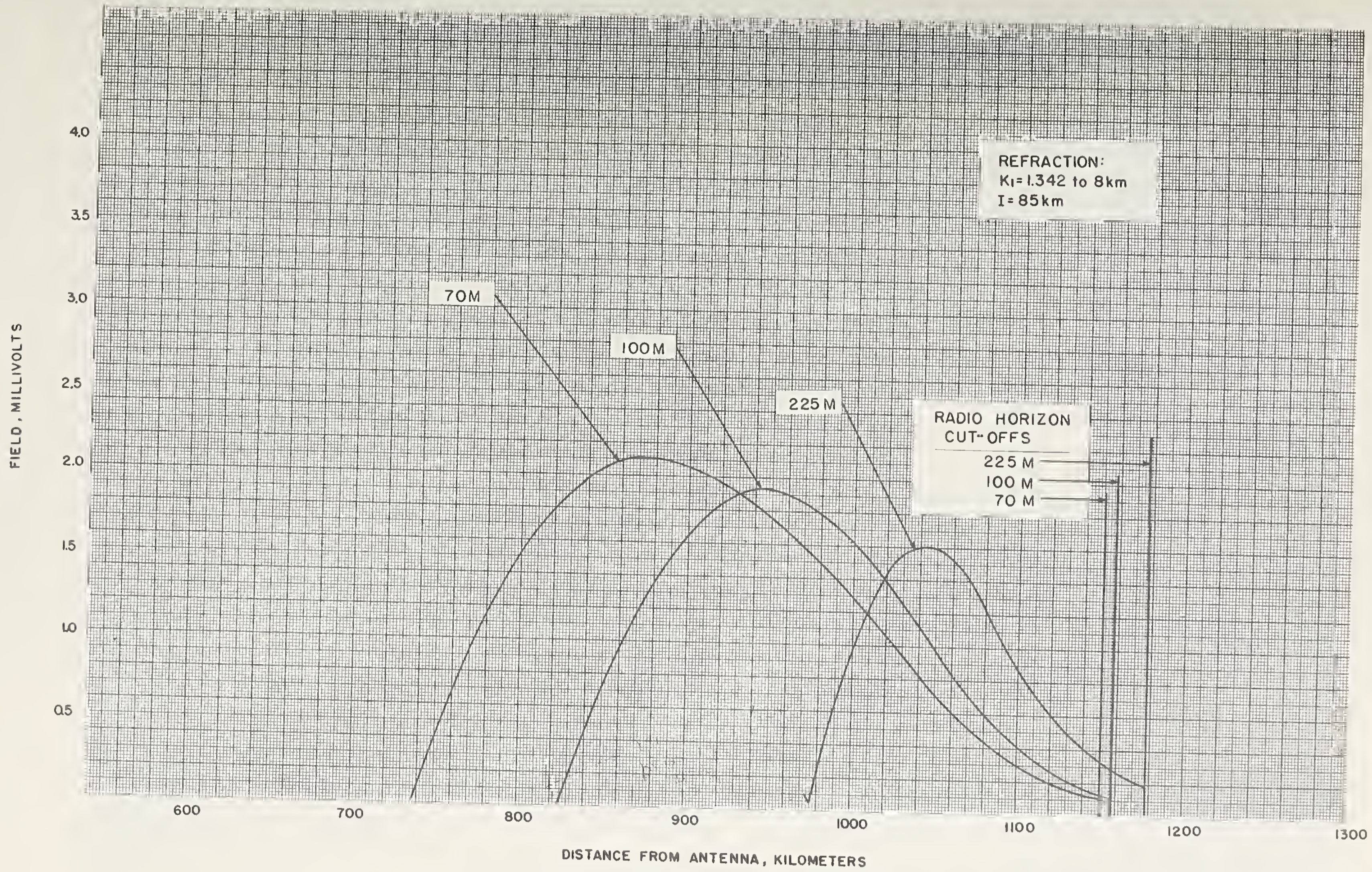

FIGURE 22. *70, 100, and 225 meter antennas at 35 Mc.*

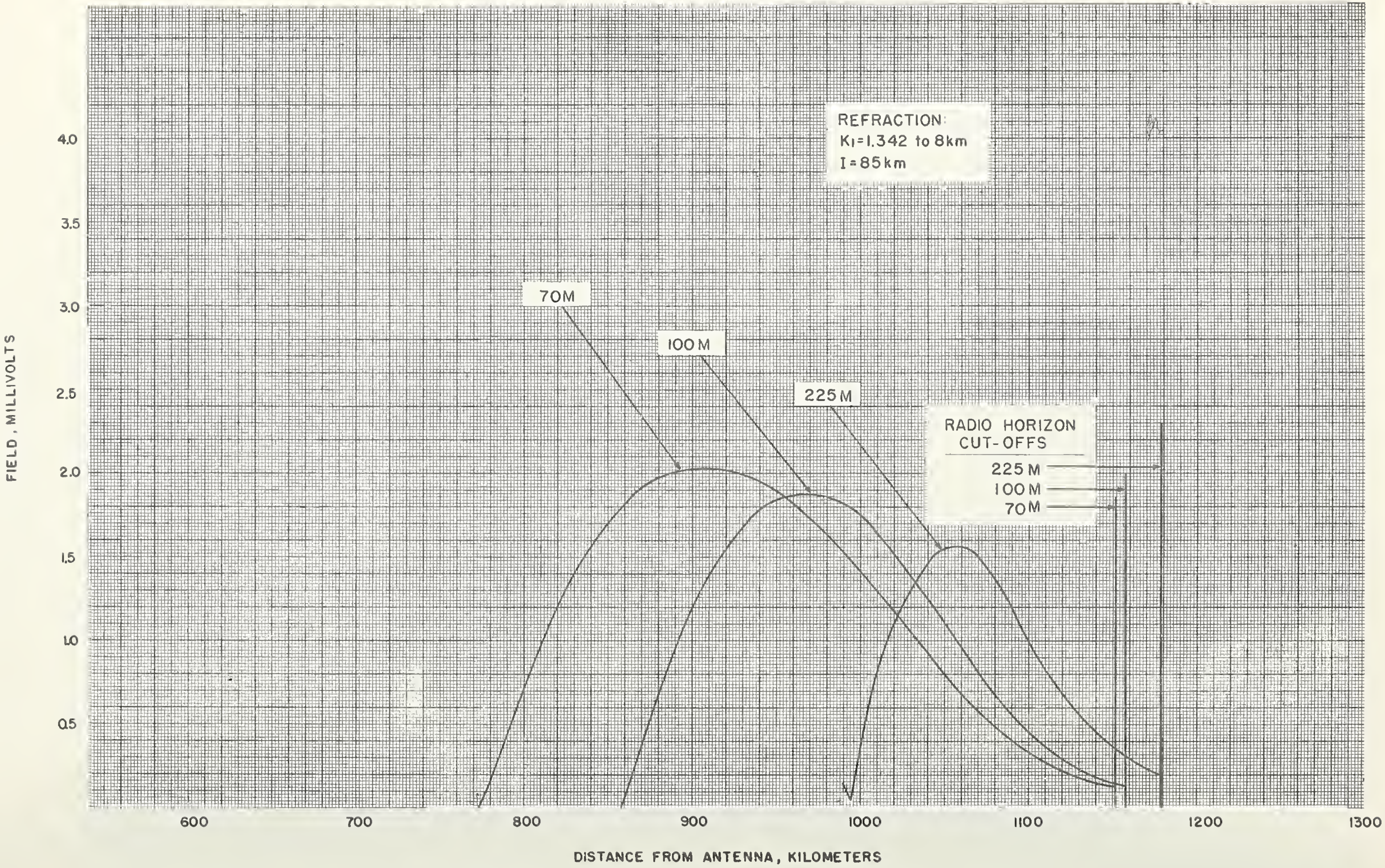

FIGURE 23. *70, 100, and 225 meter antennas at 40 Mc.*

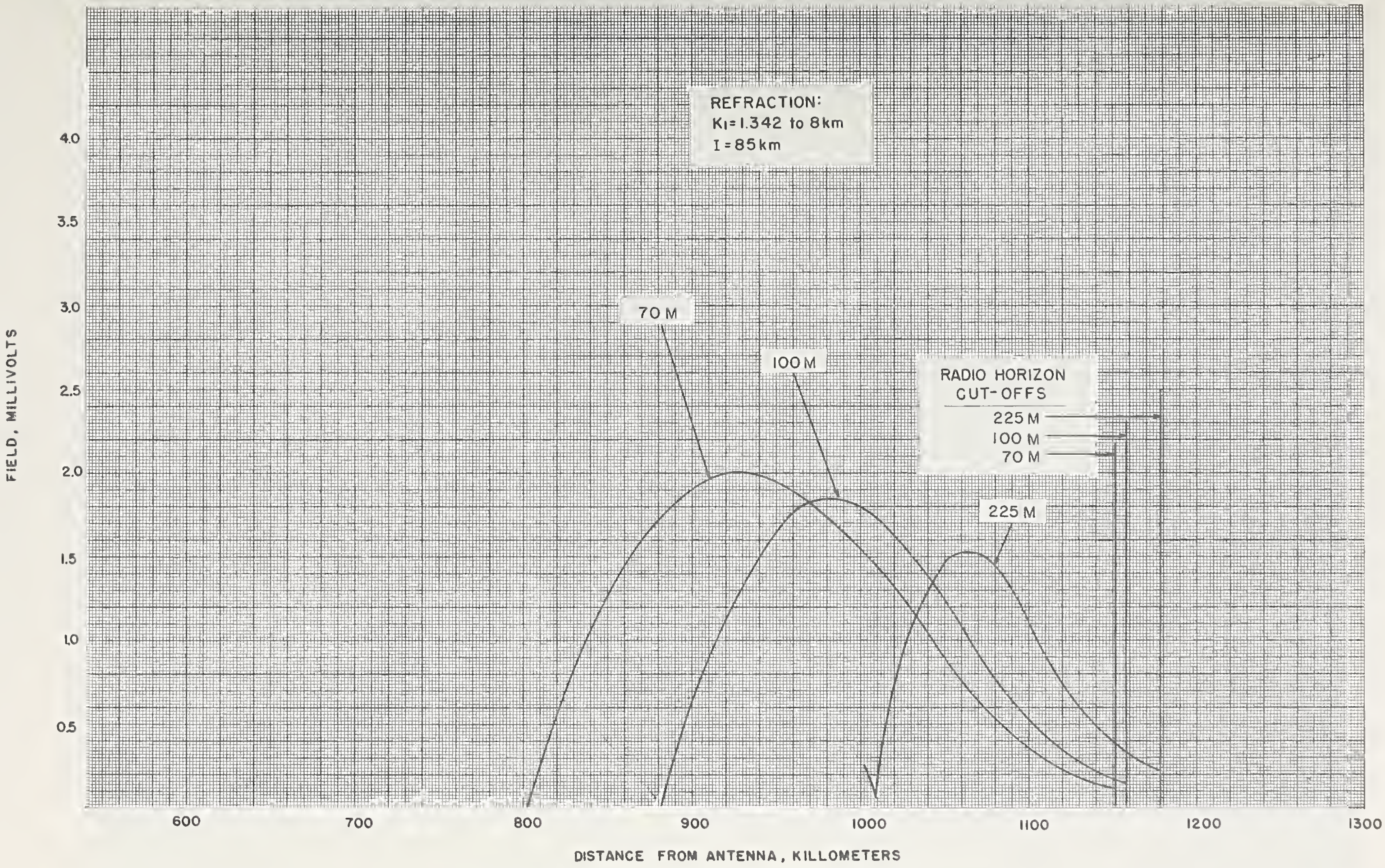

FIGURE 24. *70, 100, and 225 meter antennas at 45 Mc.*

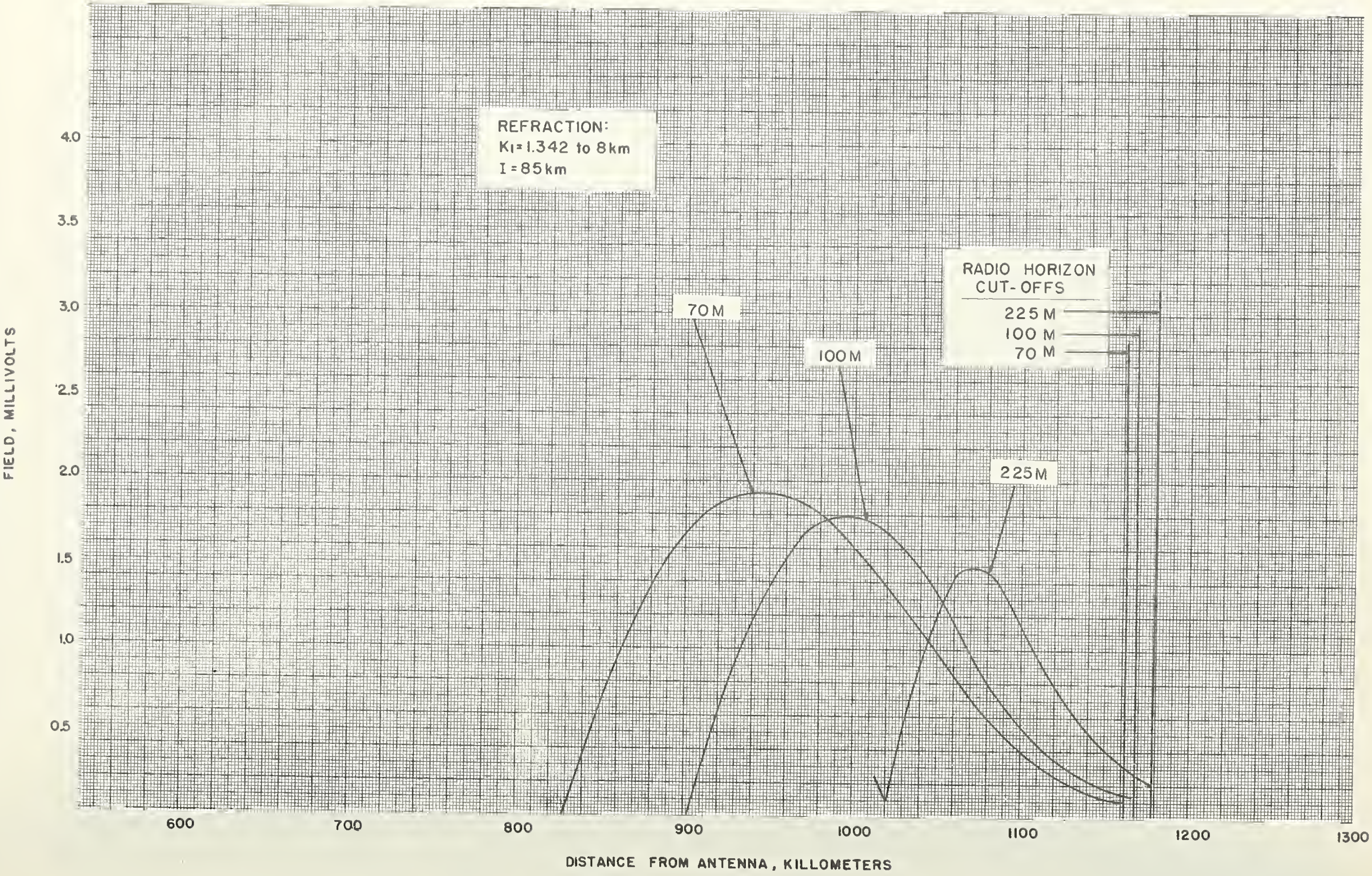

FIGURE 25. *70, 100, and 225 meter antennas at 50 Mc.*

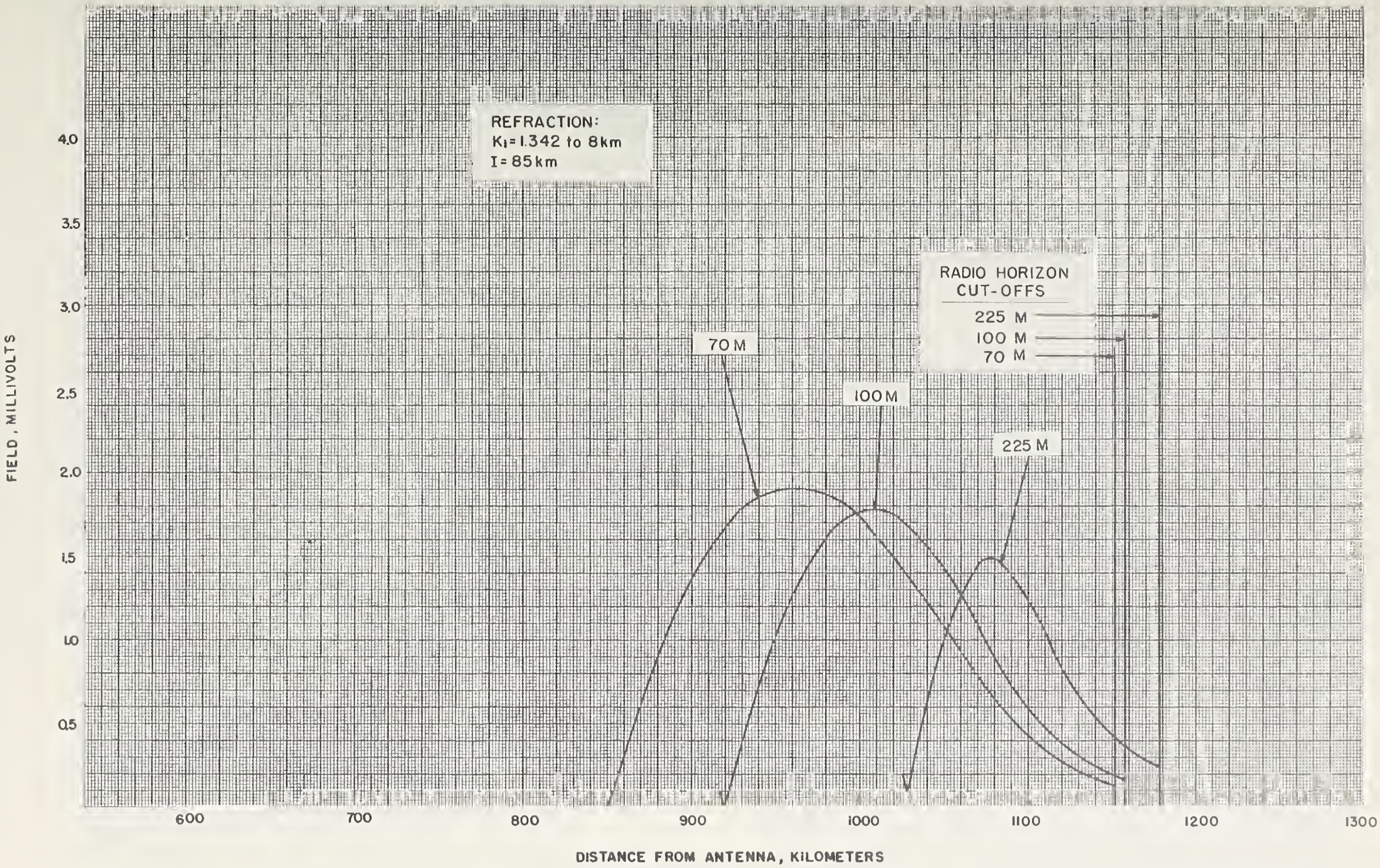

FIGURE 26. *70, 100, and 225 meter antennas at 55 Mc.*

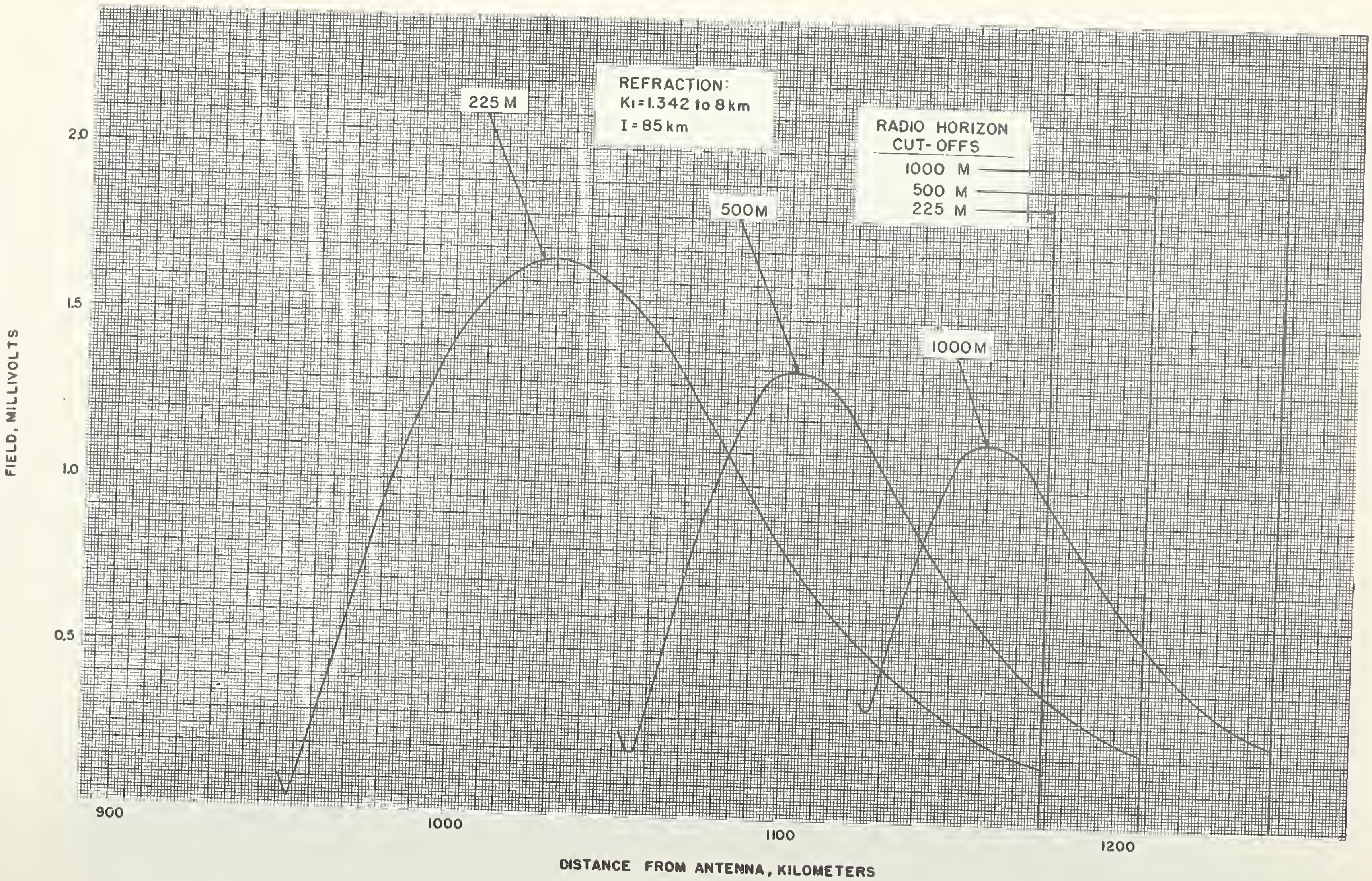

FIGURE 27. *225, 500, and 1000 meter antennas at 30 Mc.*

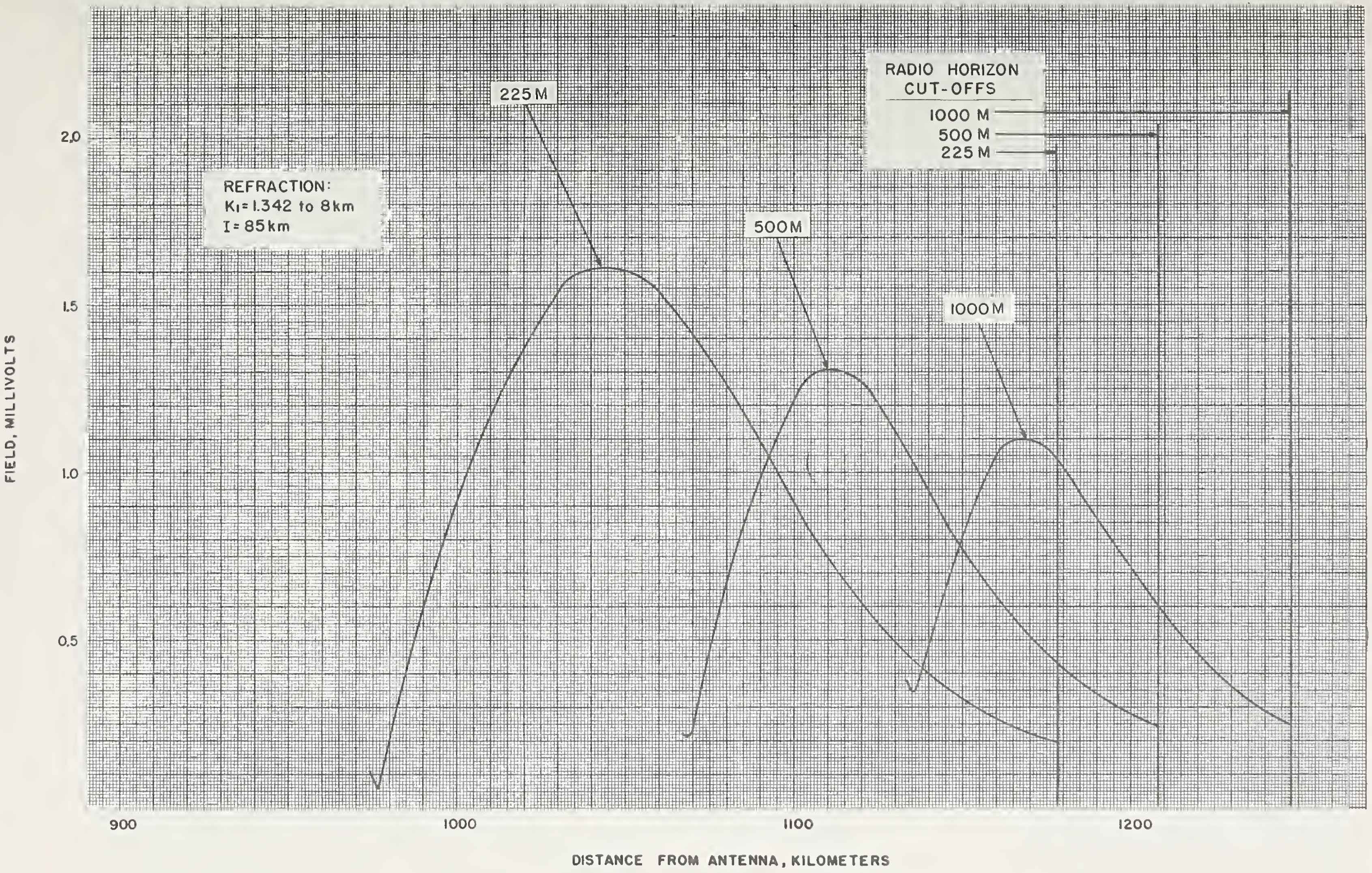

FIGURE 28. *225, 500, and 1000 meter antennas at 35 Mc.*

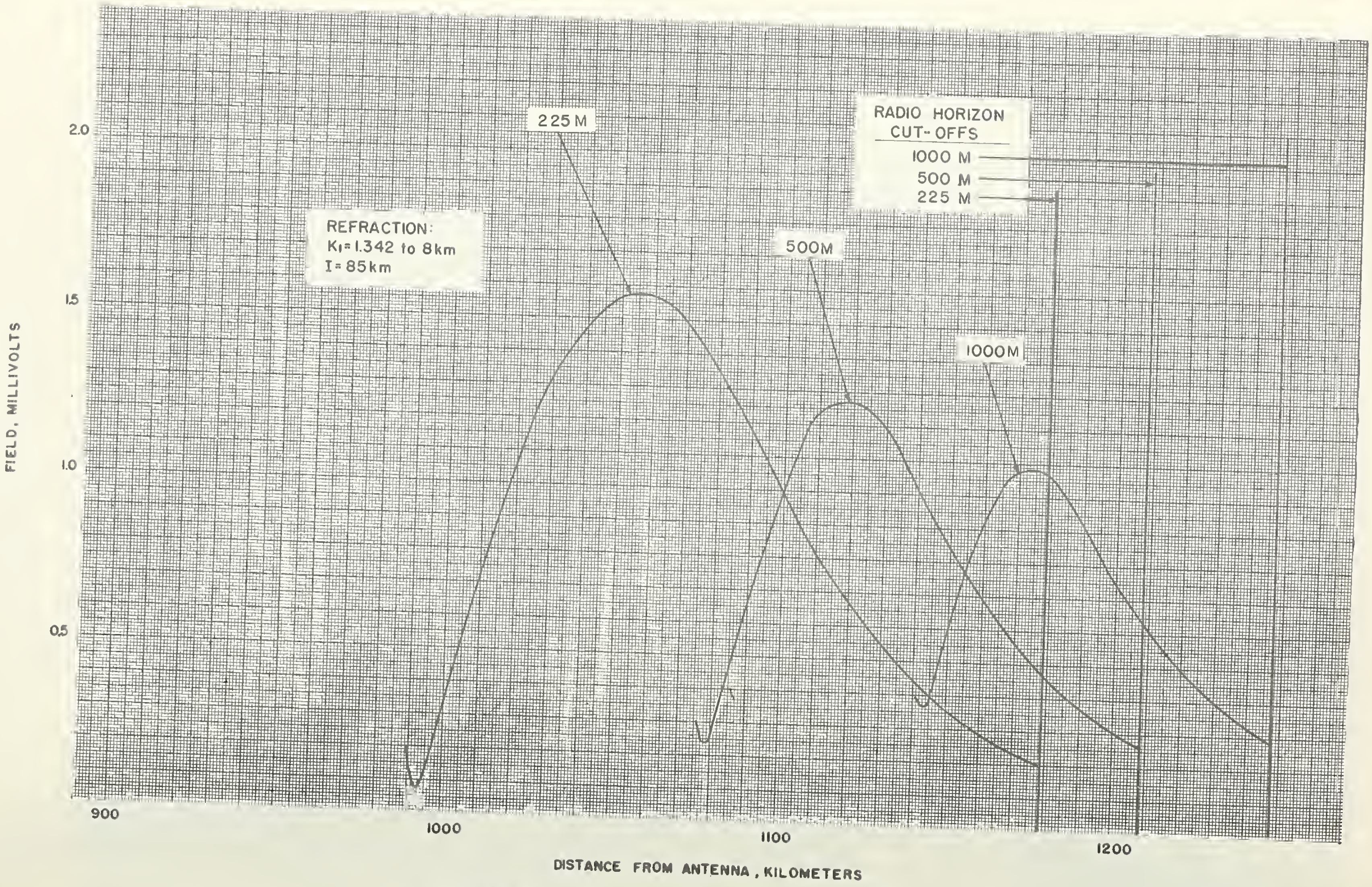

FIGURE 29. *225, 500, and 1000 meter antennas at 40 Mc.*

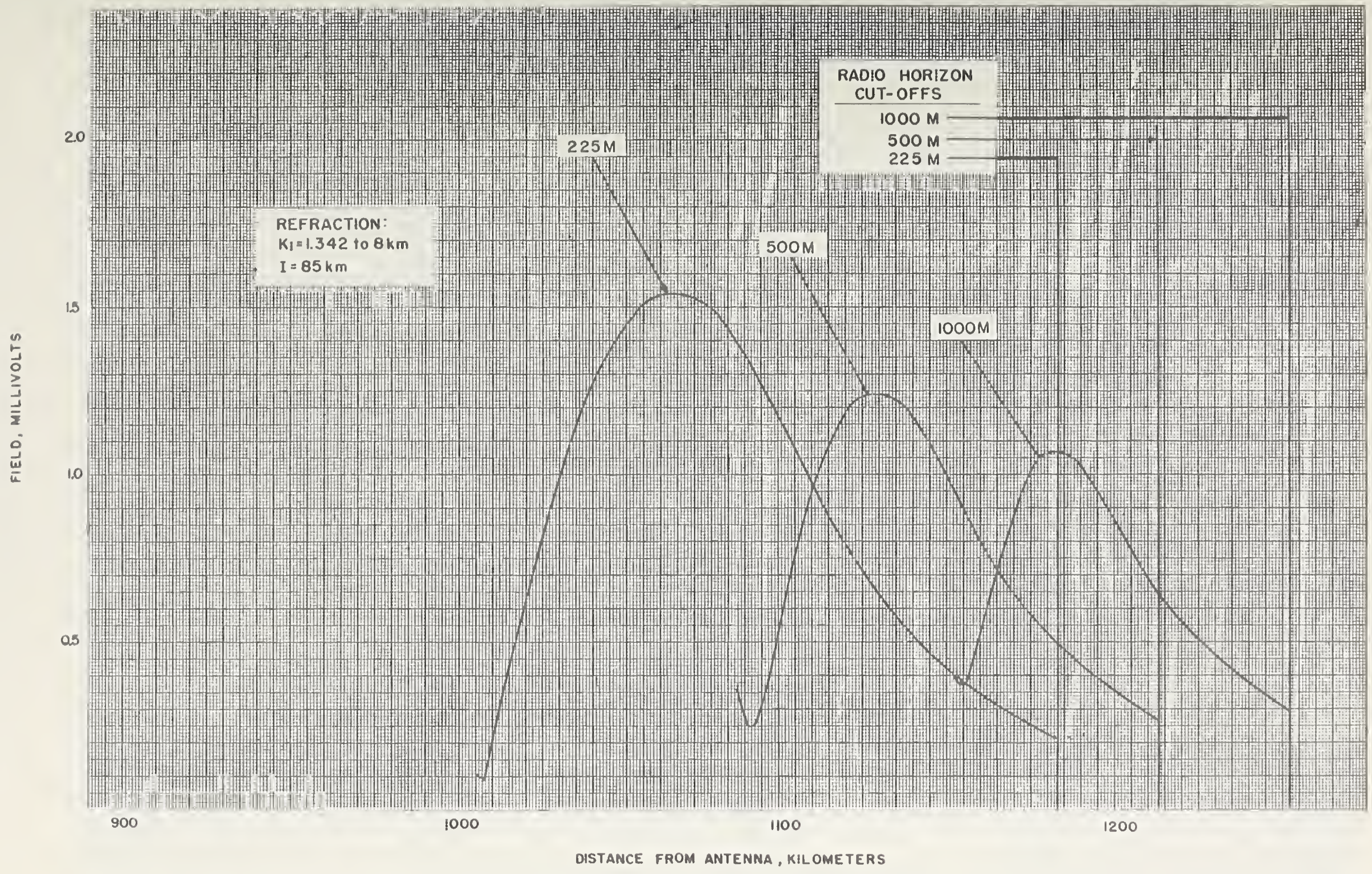

Figure 30. *225, 500, and 1000 meter antennas at 45 Mc.*

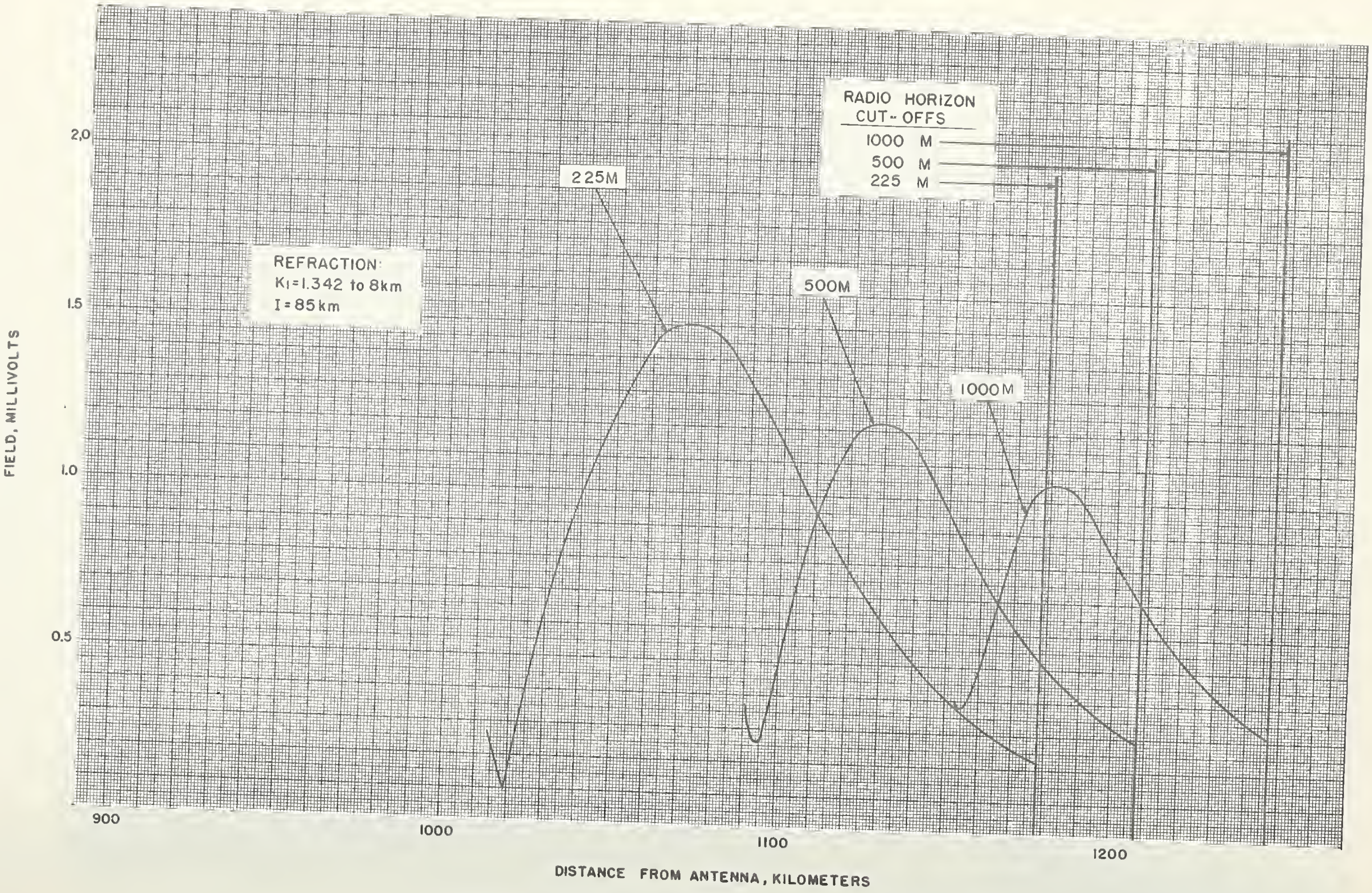

FIGURE 31. *225, 500, and 1000 meter antennas at 50 Mc.*

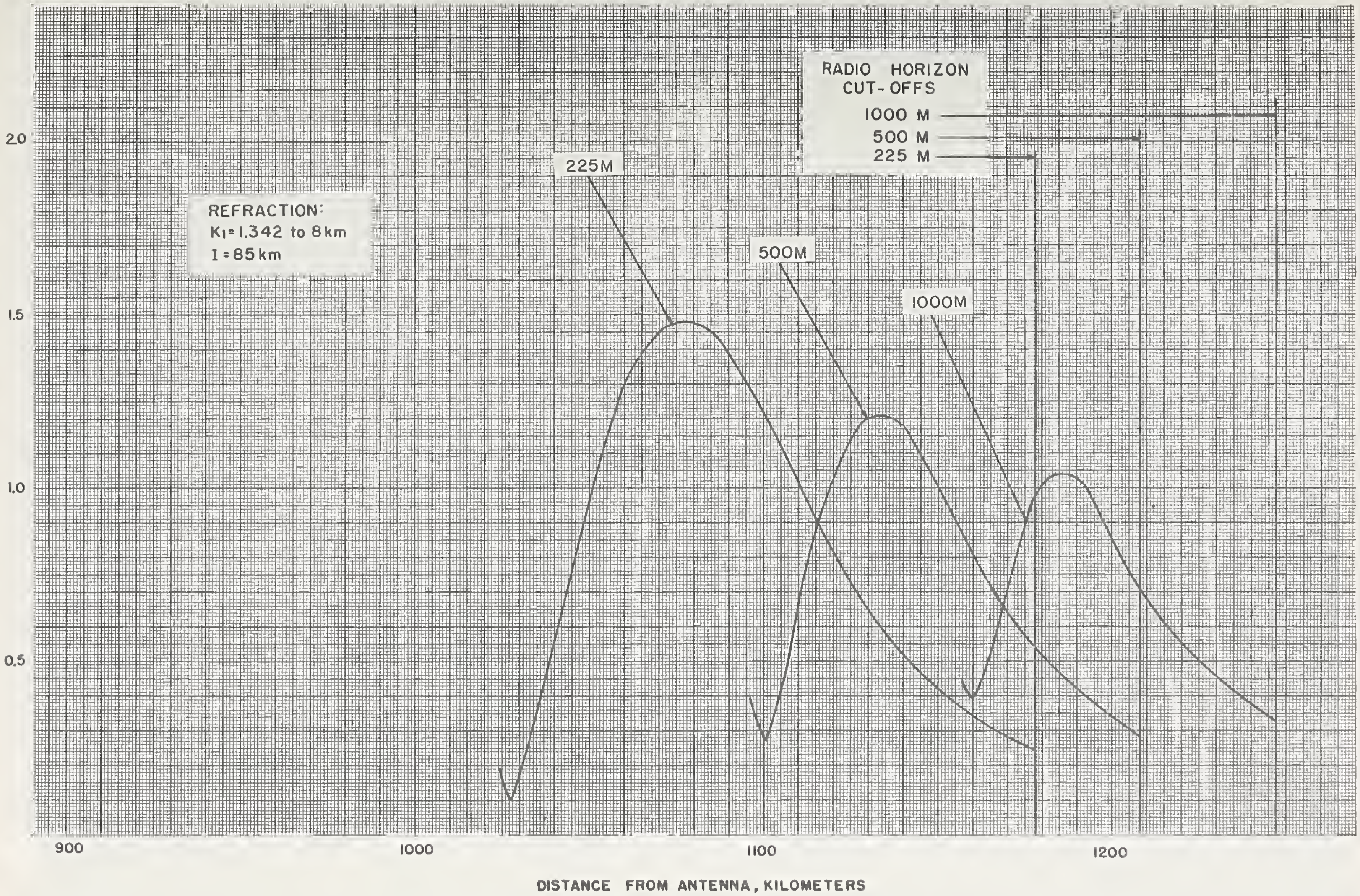

Figure 32. *225, 500, and 1000 meter antennas at 55 Mc.*

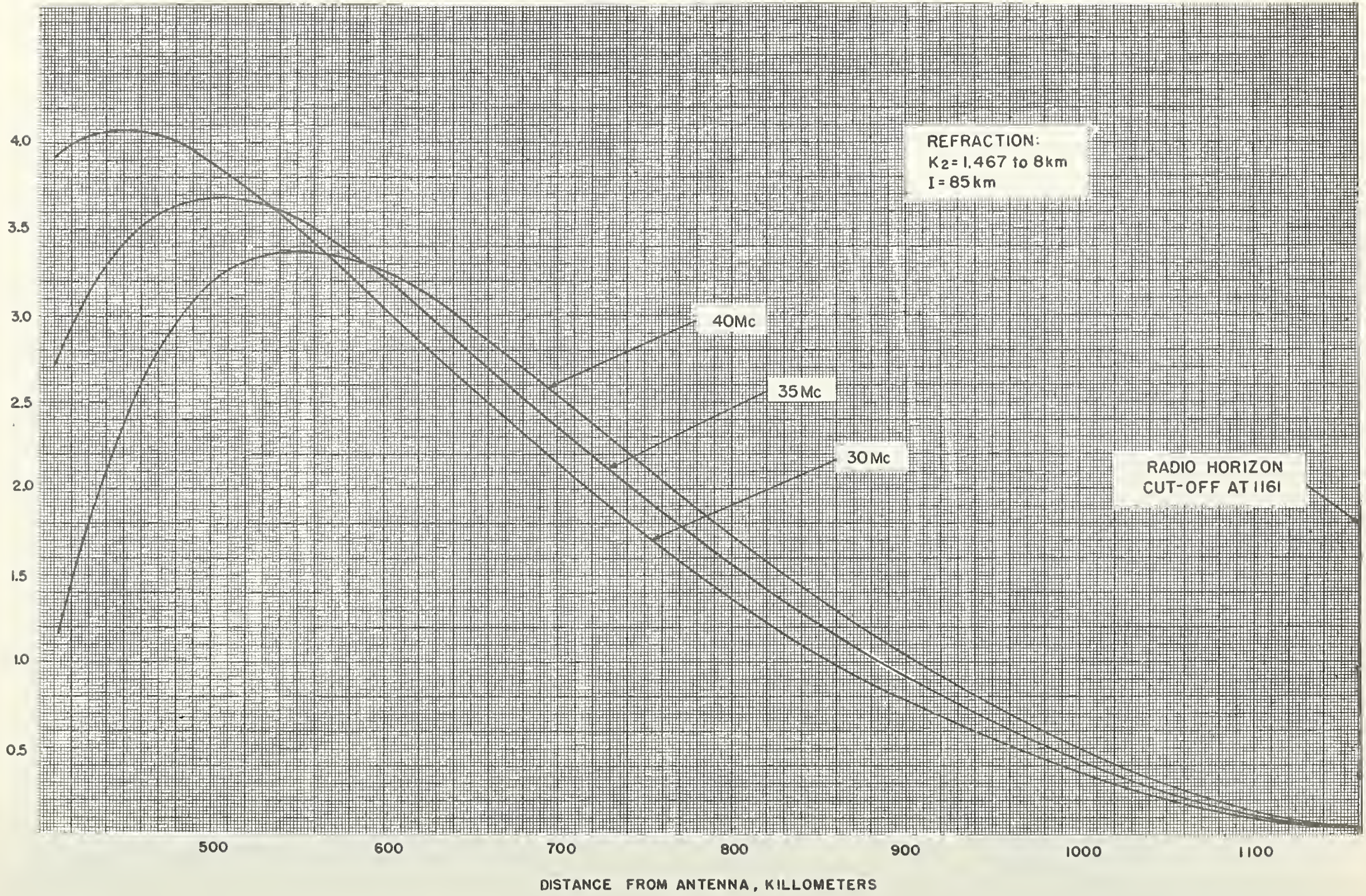

FIGURE 33. *20 meter antenna.*

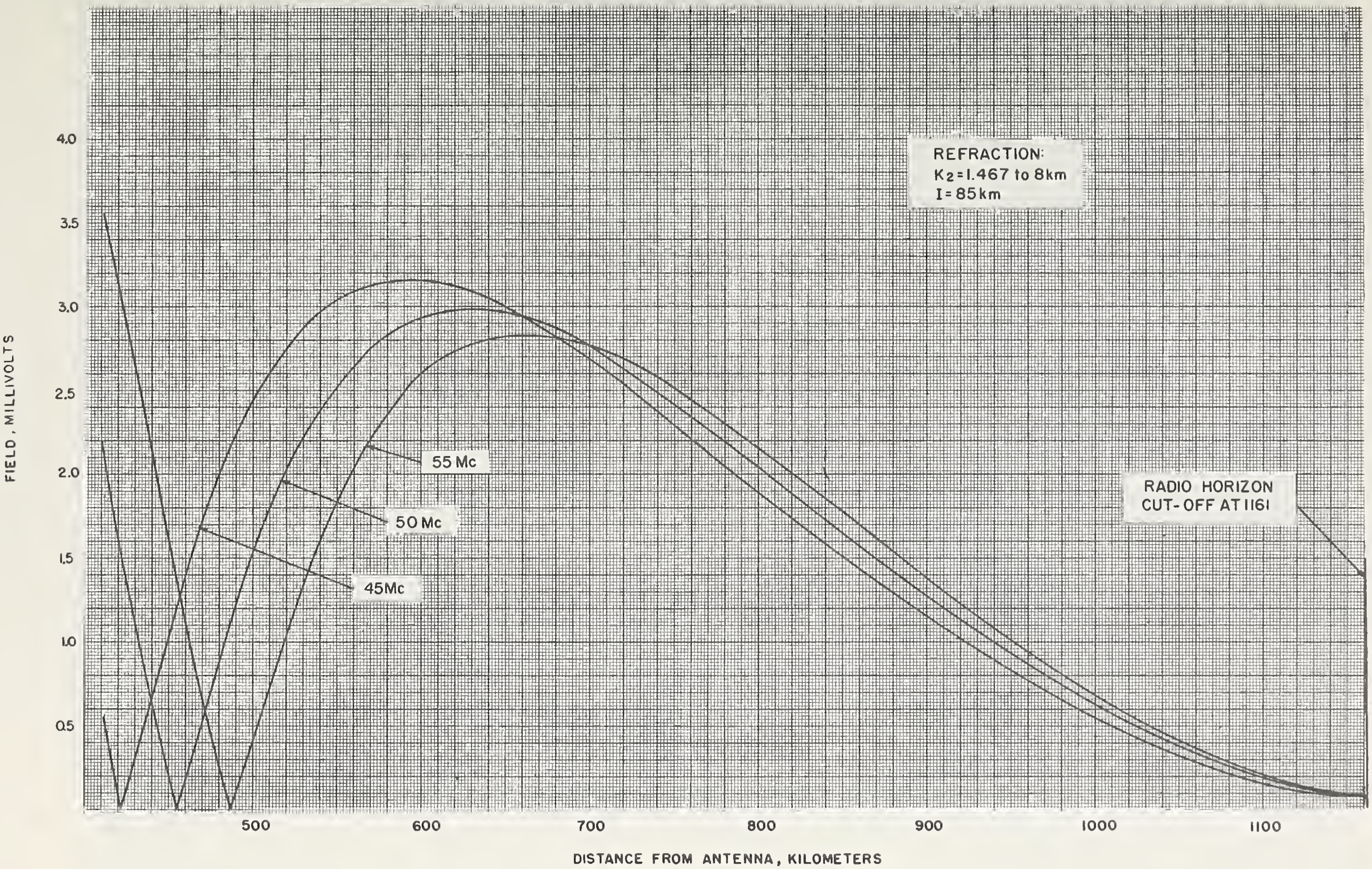

FIGURE 34. *20 meter antenna.*

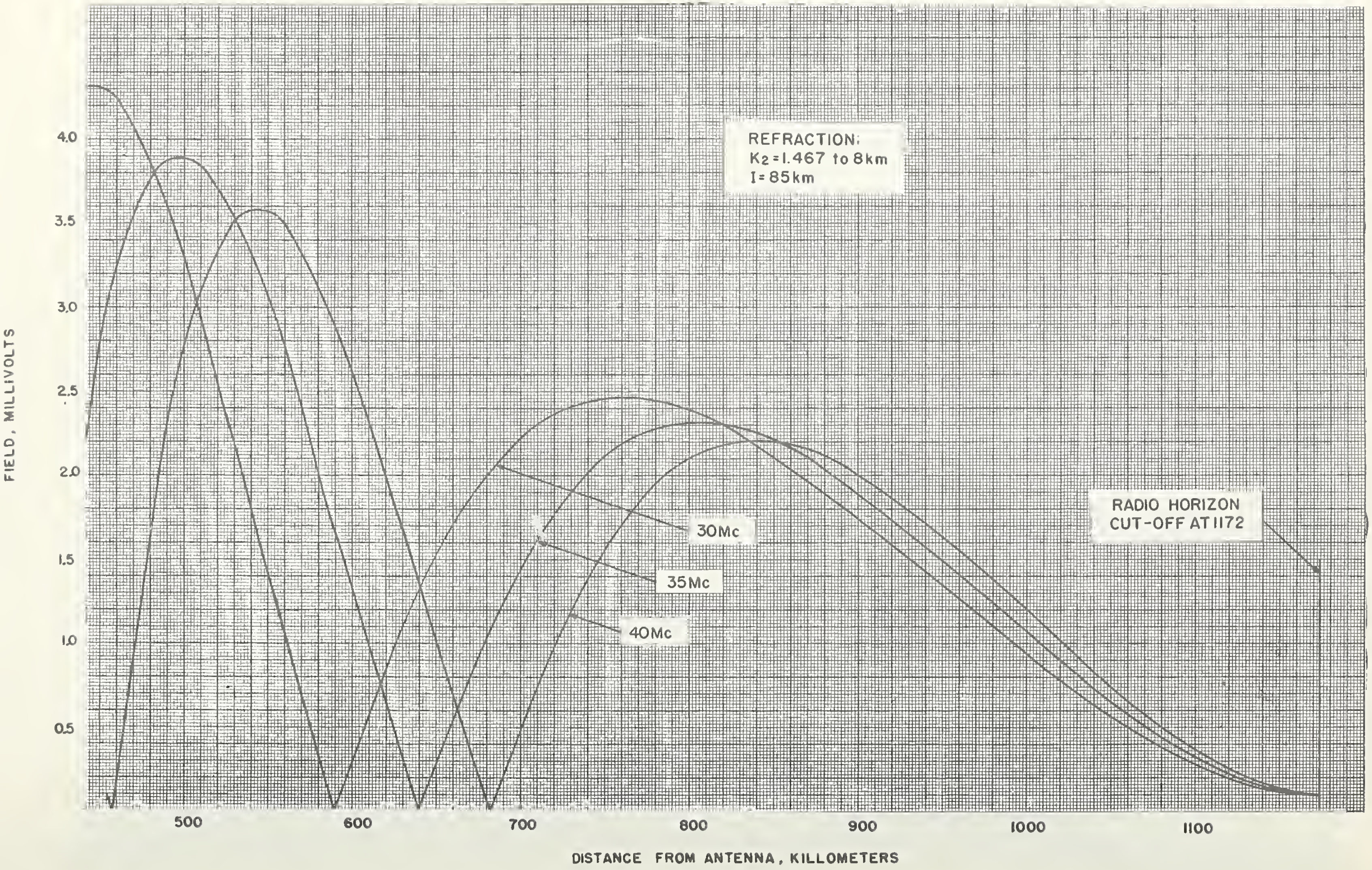

FIGURE 35. *50 meter antenna.*

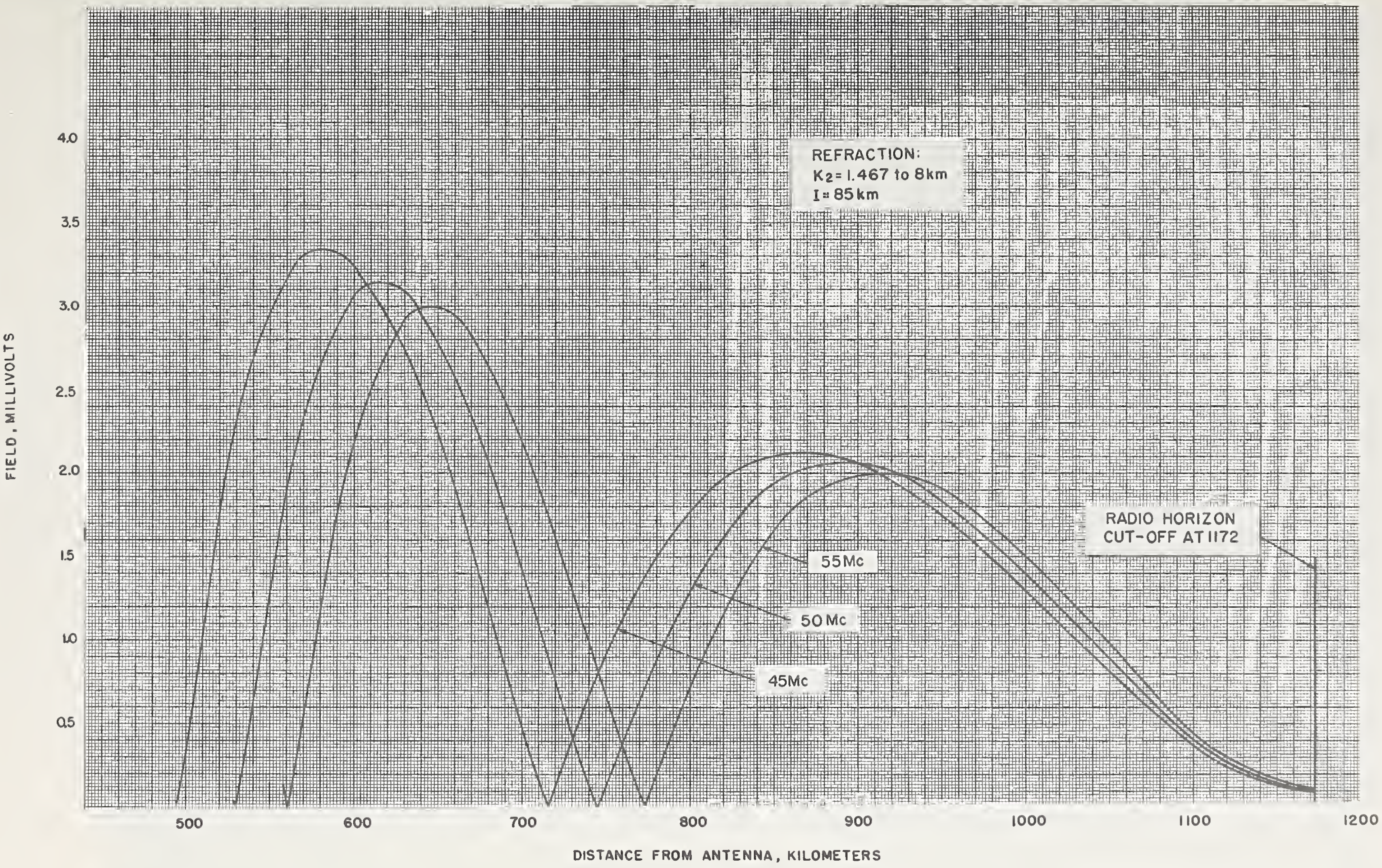

FIGURE 36. *50 meter antenna.*

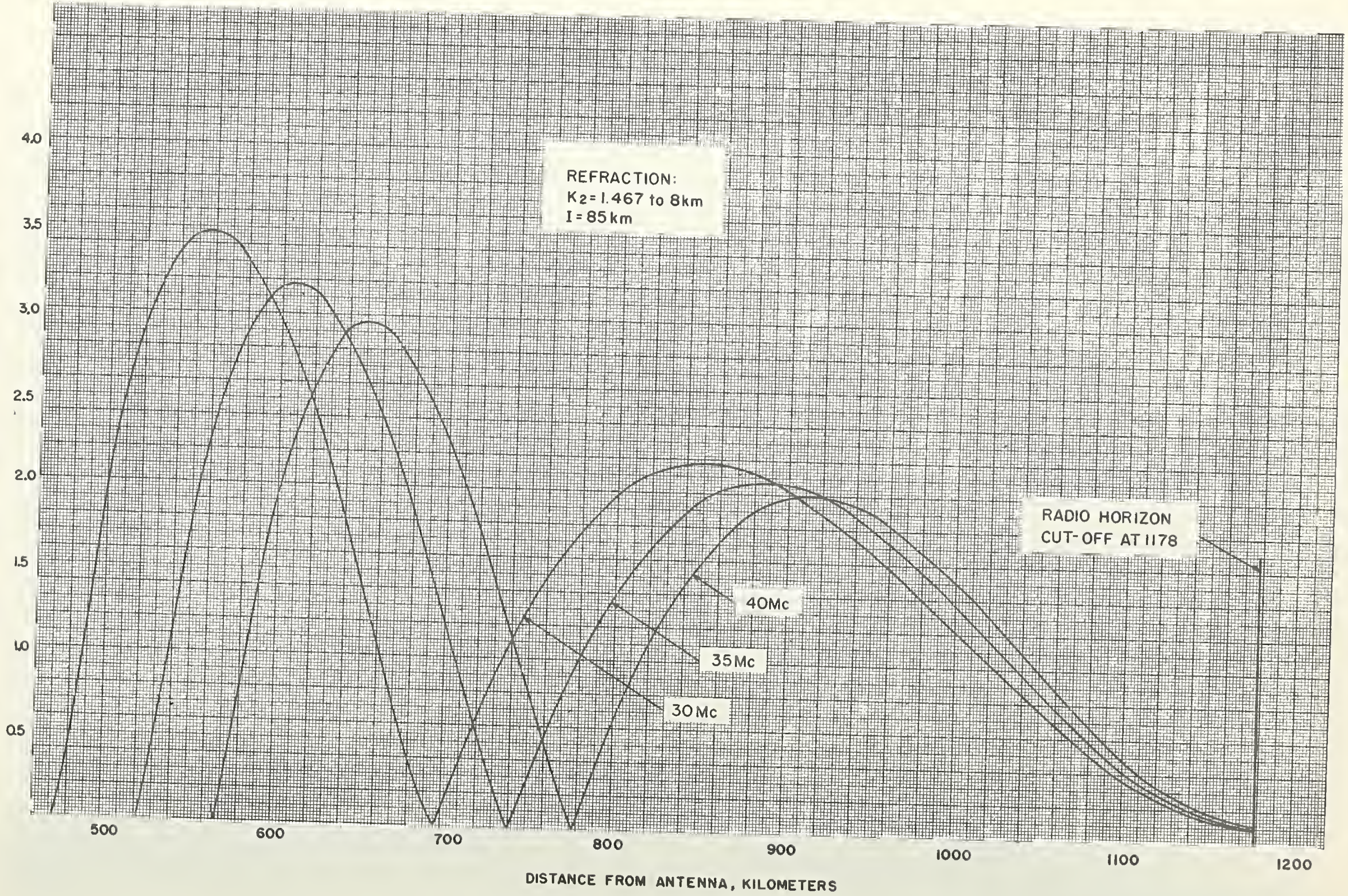

FIGURE 37. *70 meter antenna.*

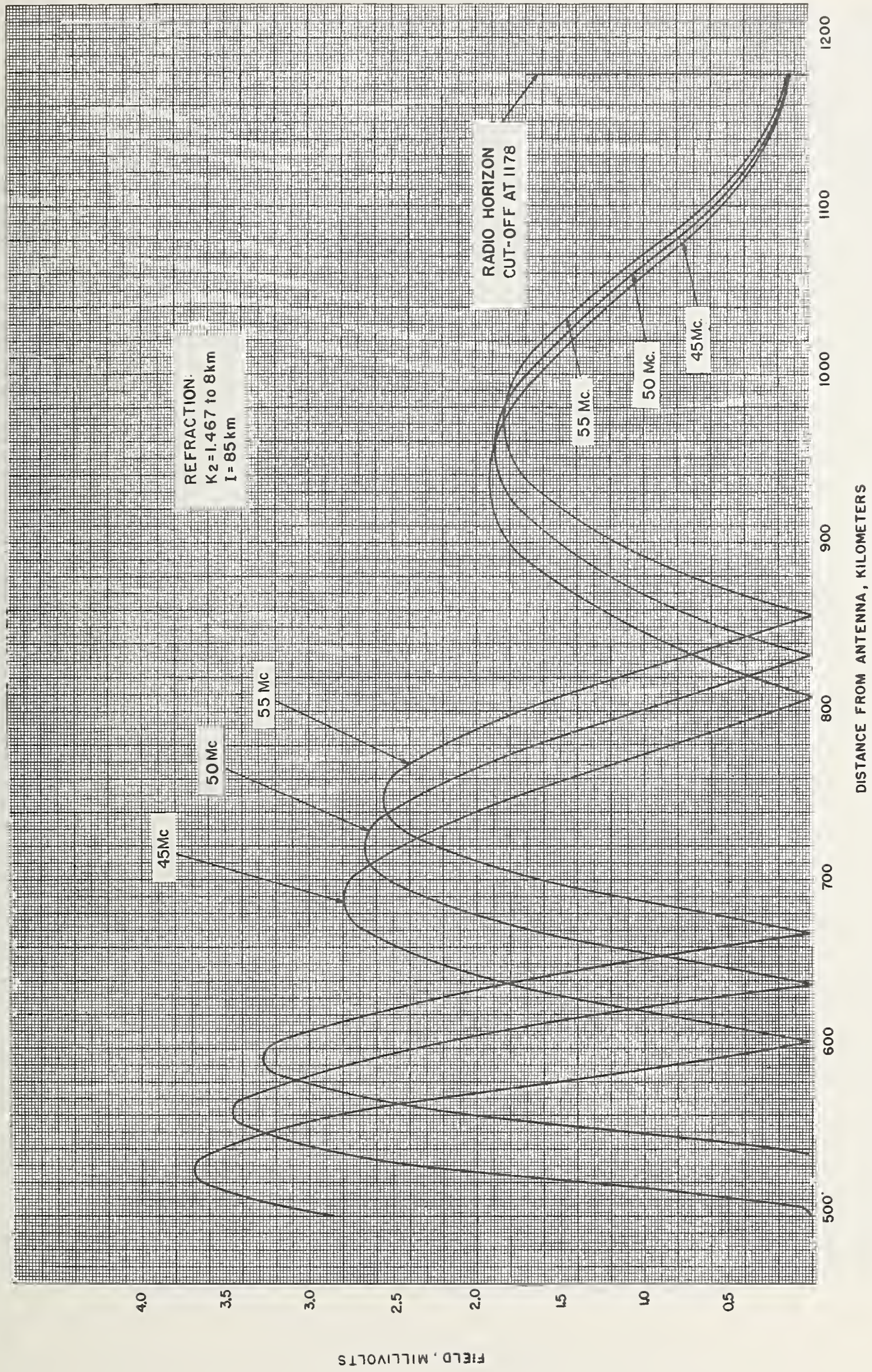

FIGURE 38. *70 meter antenna.*

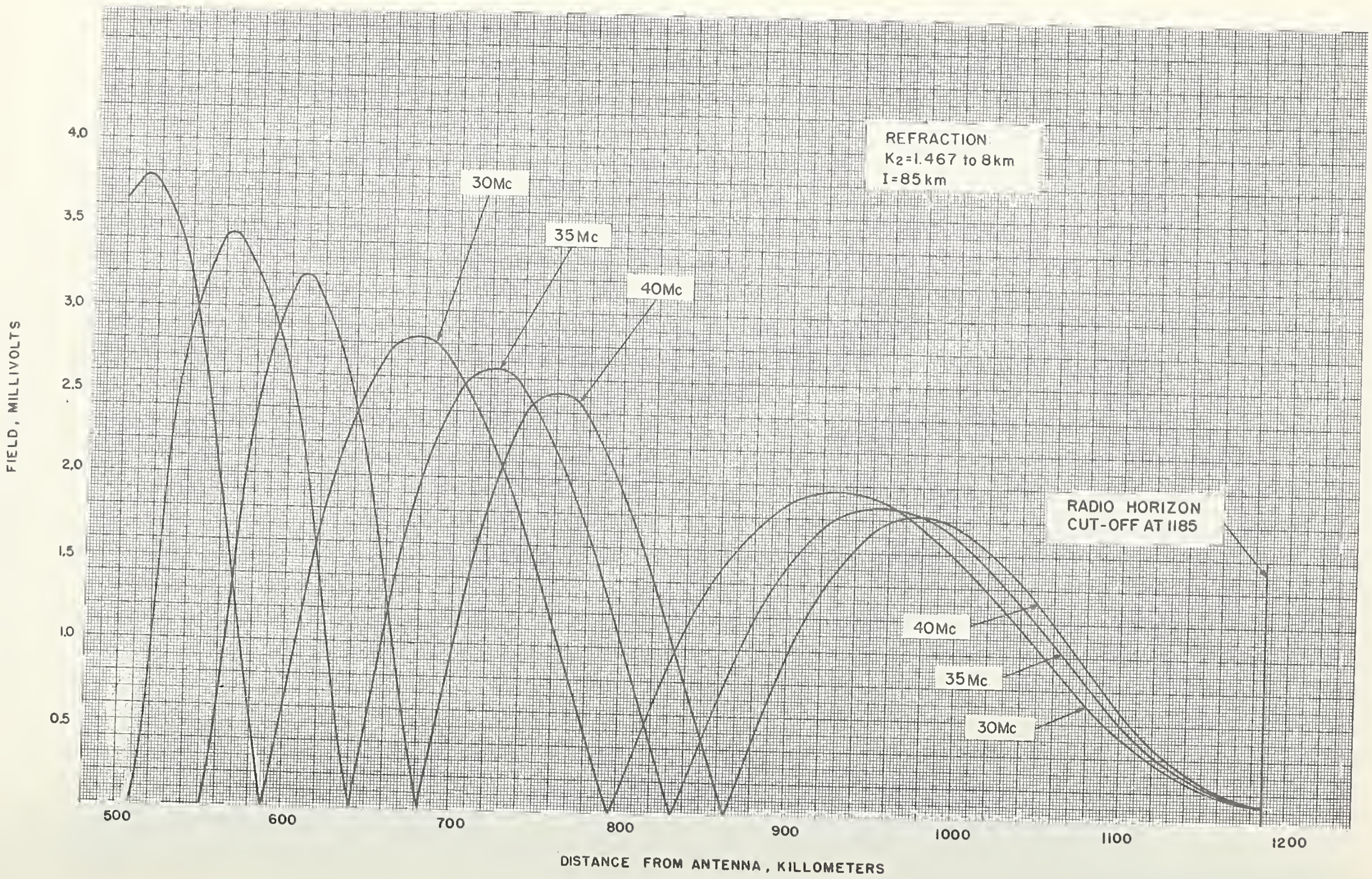

FIGURE 39. *100 meter antenna.*

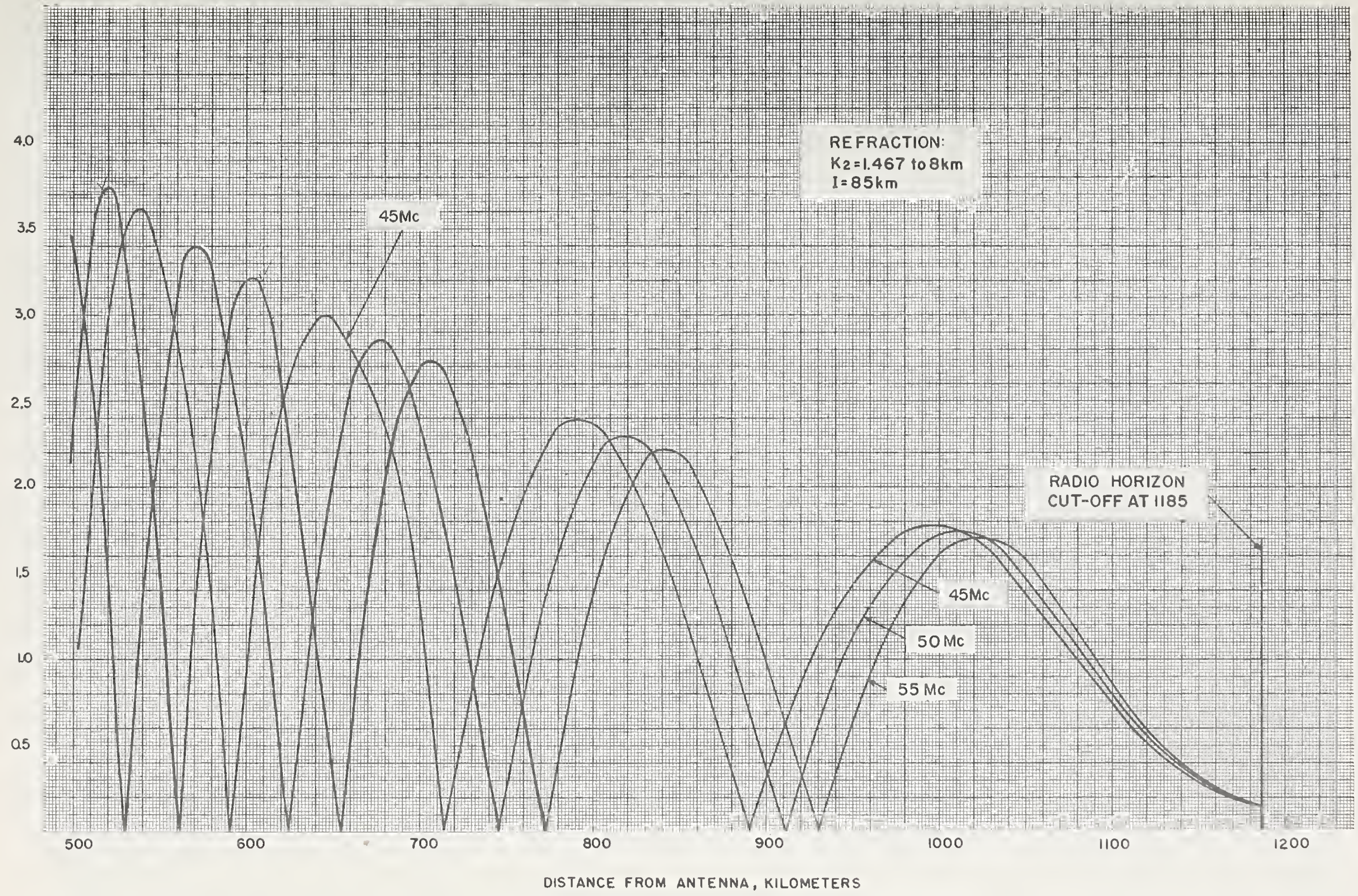

FIGURE 40. *100 meter antenna.*

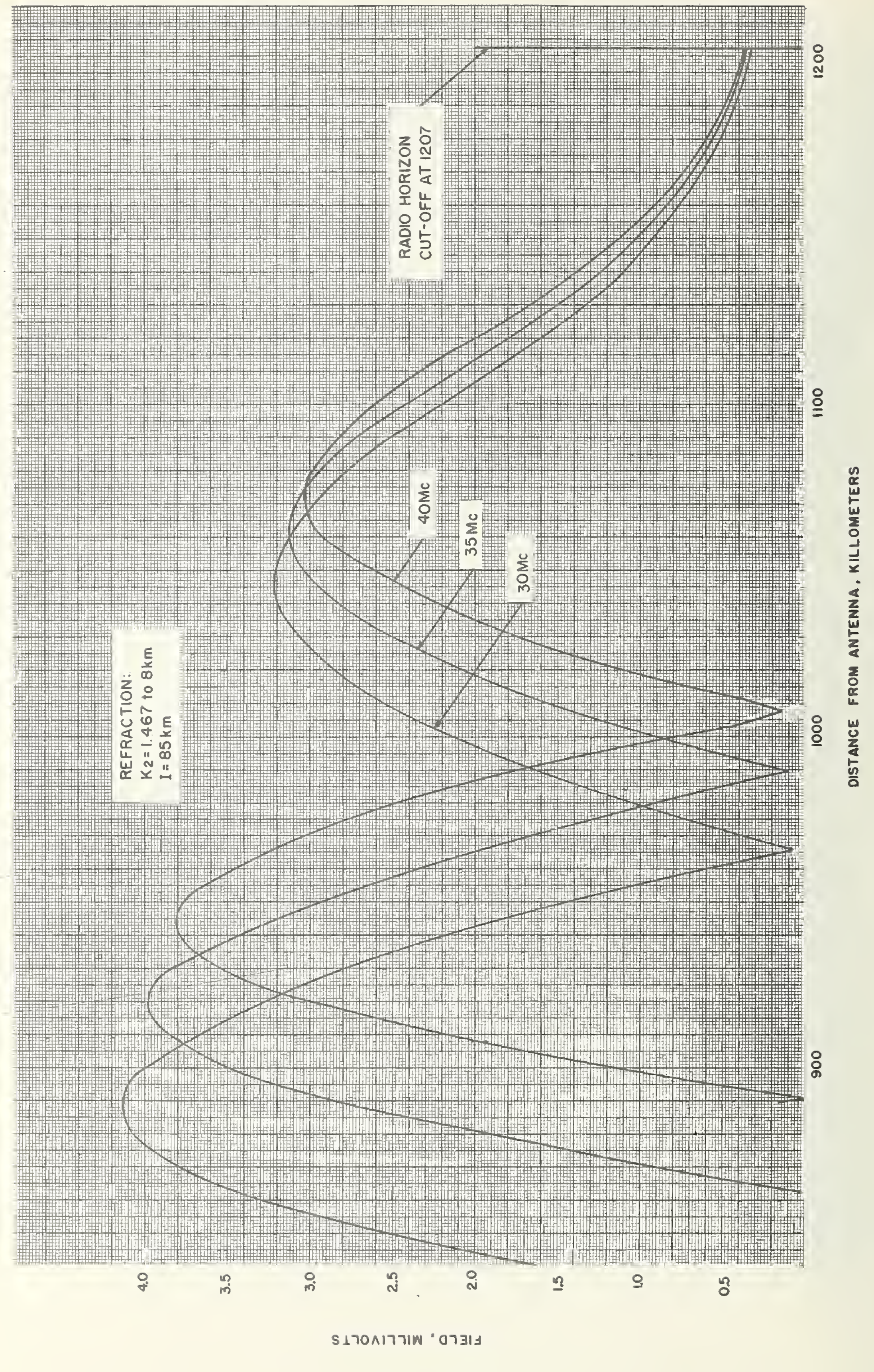

FIGURE 41. *225 meter antenna.*

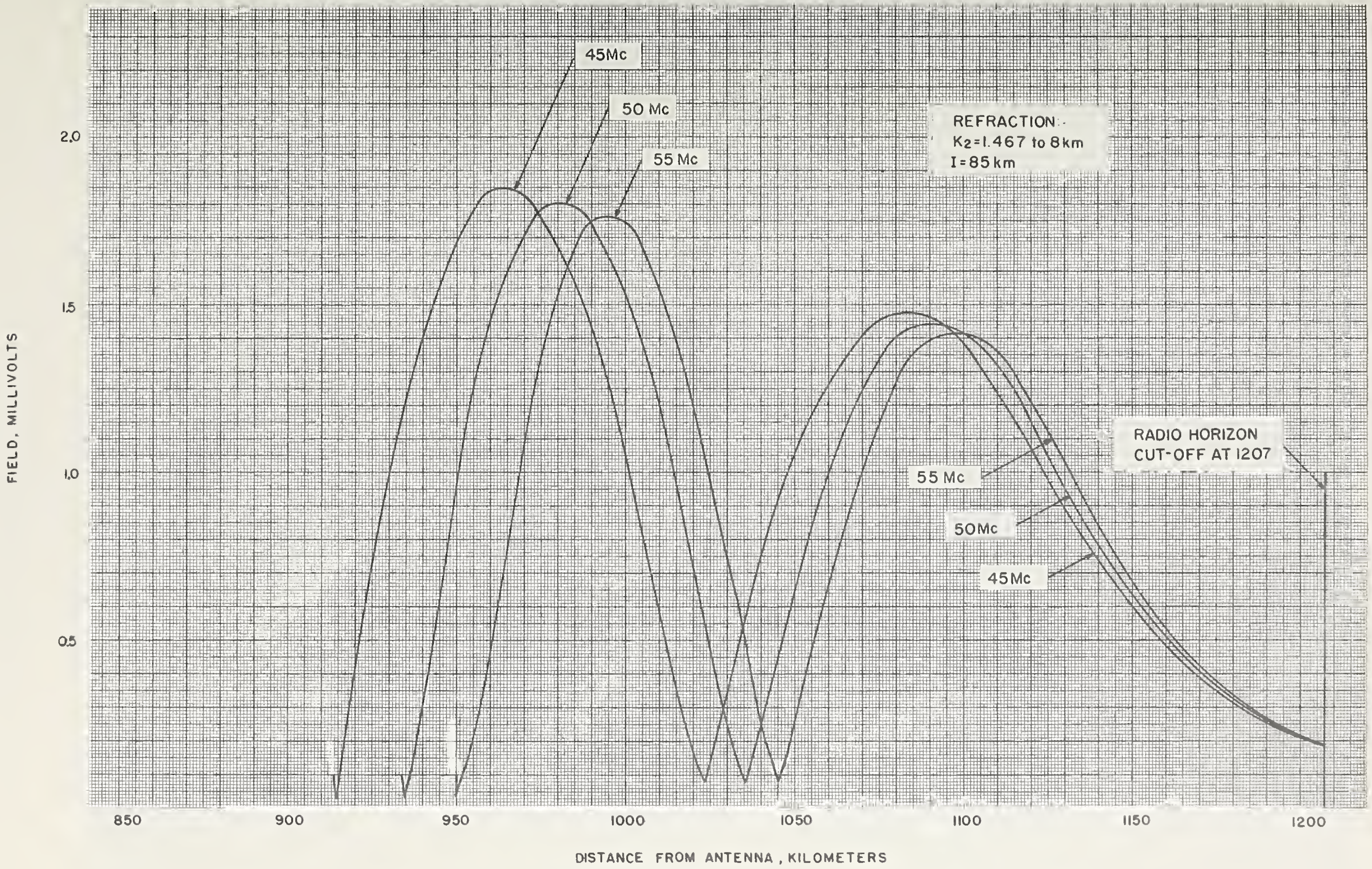

FIGURE 42. *225 meter antenna.*

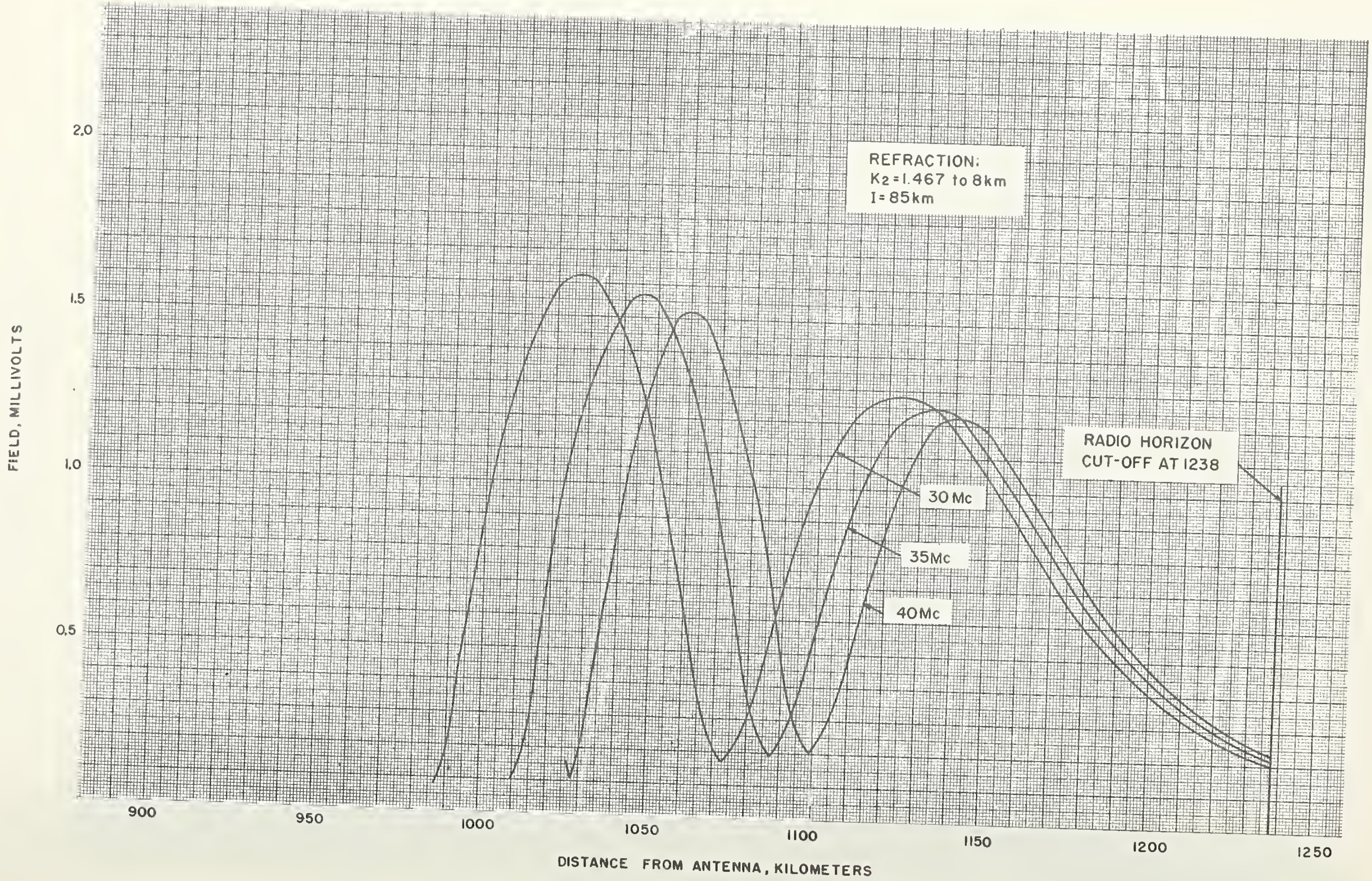

FIGURE 43. *500 meter antenna.*

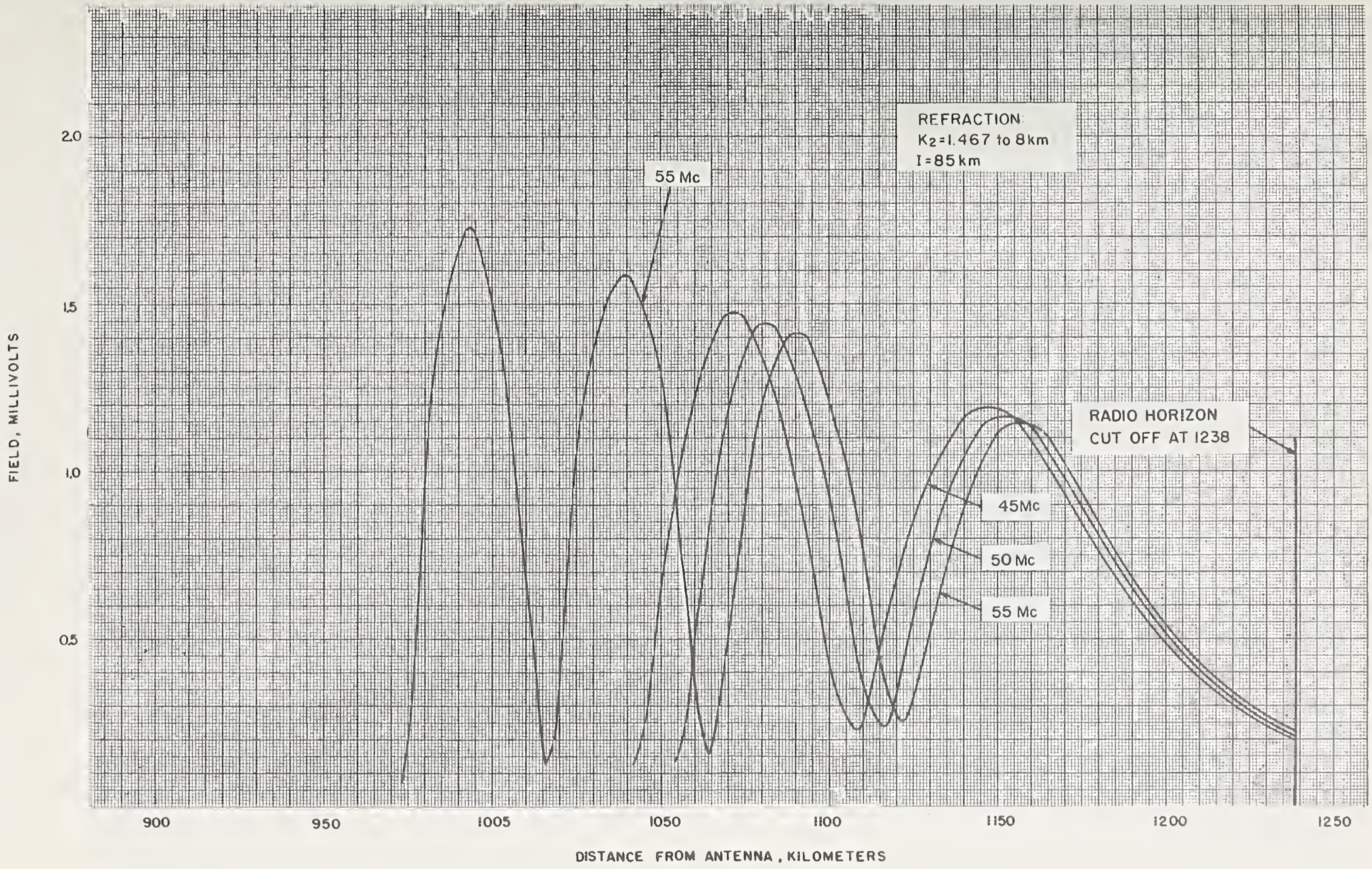

FIGURE 44. *500 meter antenna.*

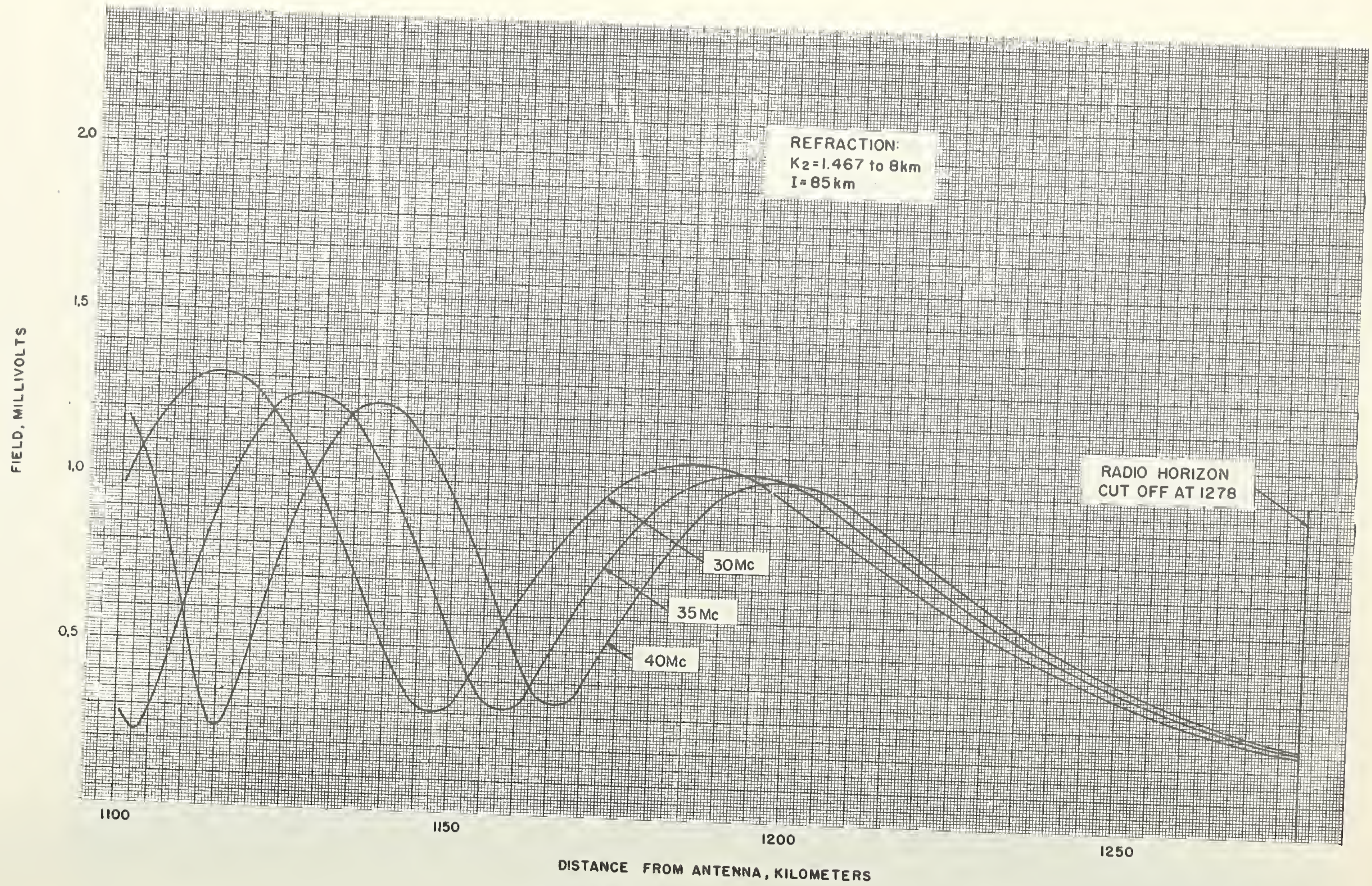

FIGURE 45. *1000 meter antenna.*

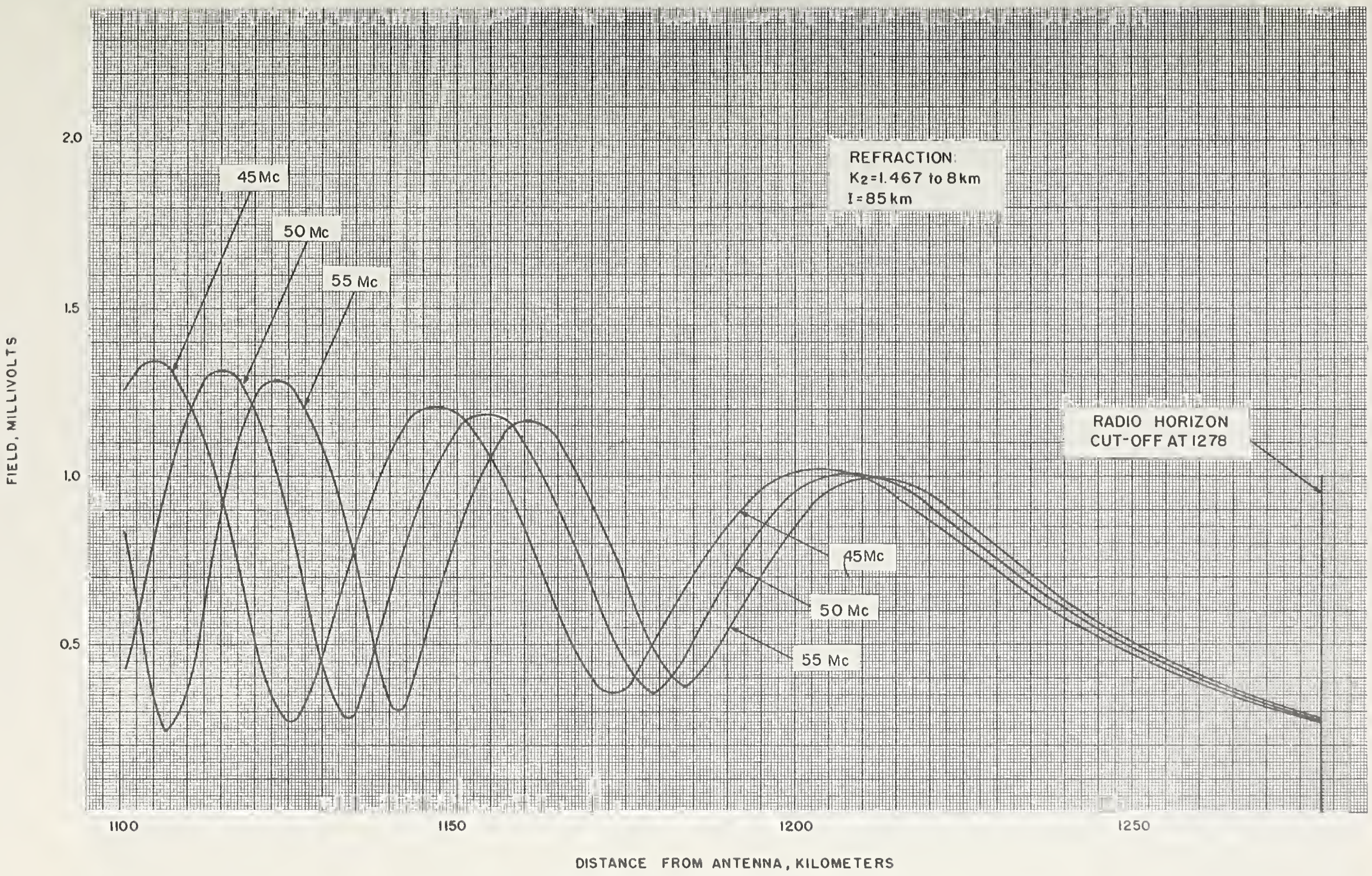

FIGURE 46. *1000 meter antenna.*

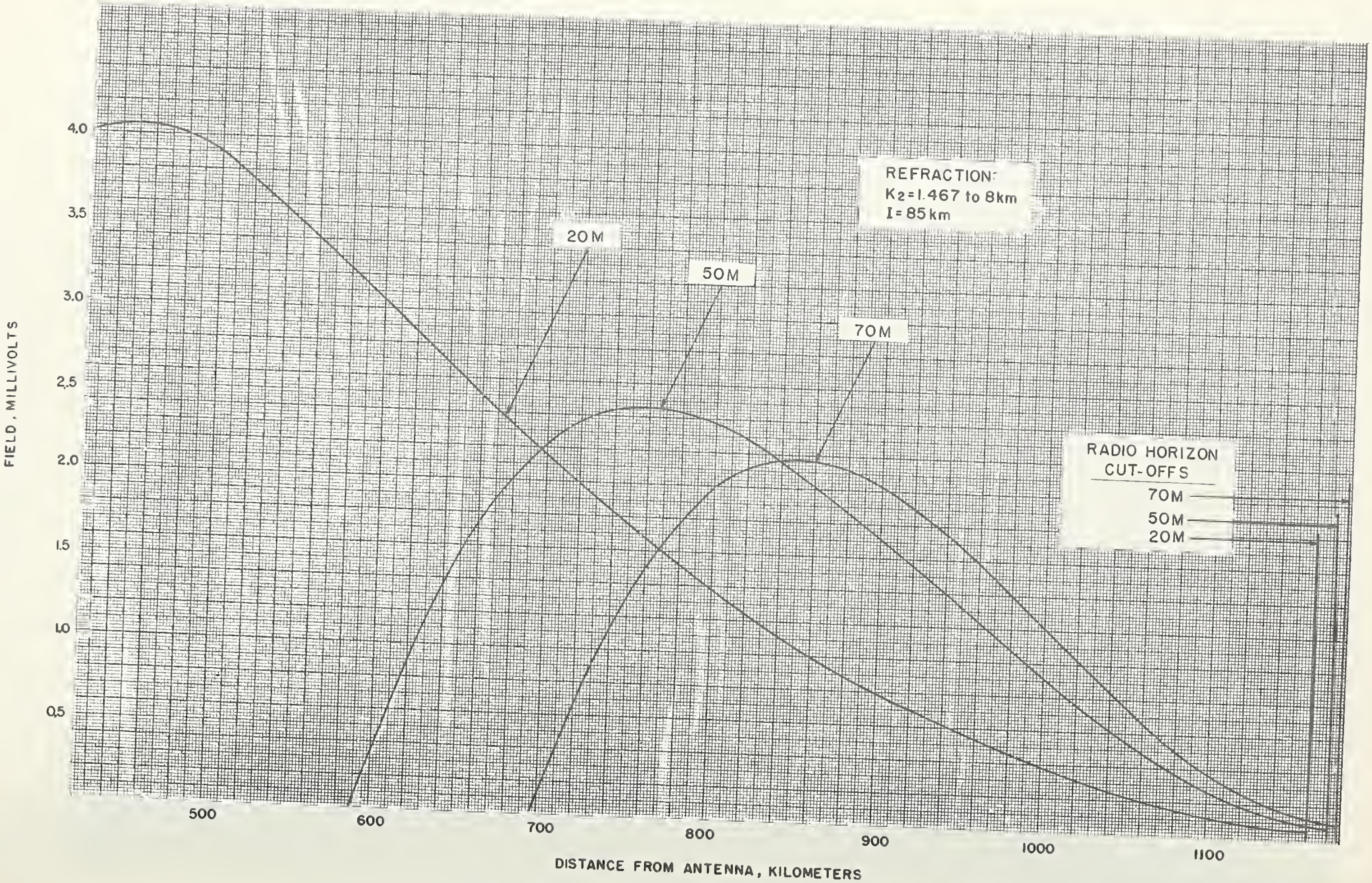

FIGURE 47. *20, 50, and 70 meter antennas at 30 Mc.*

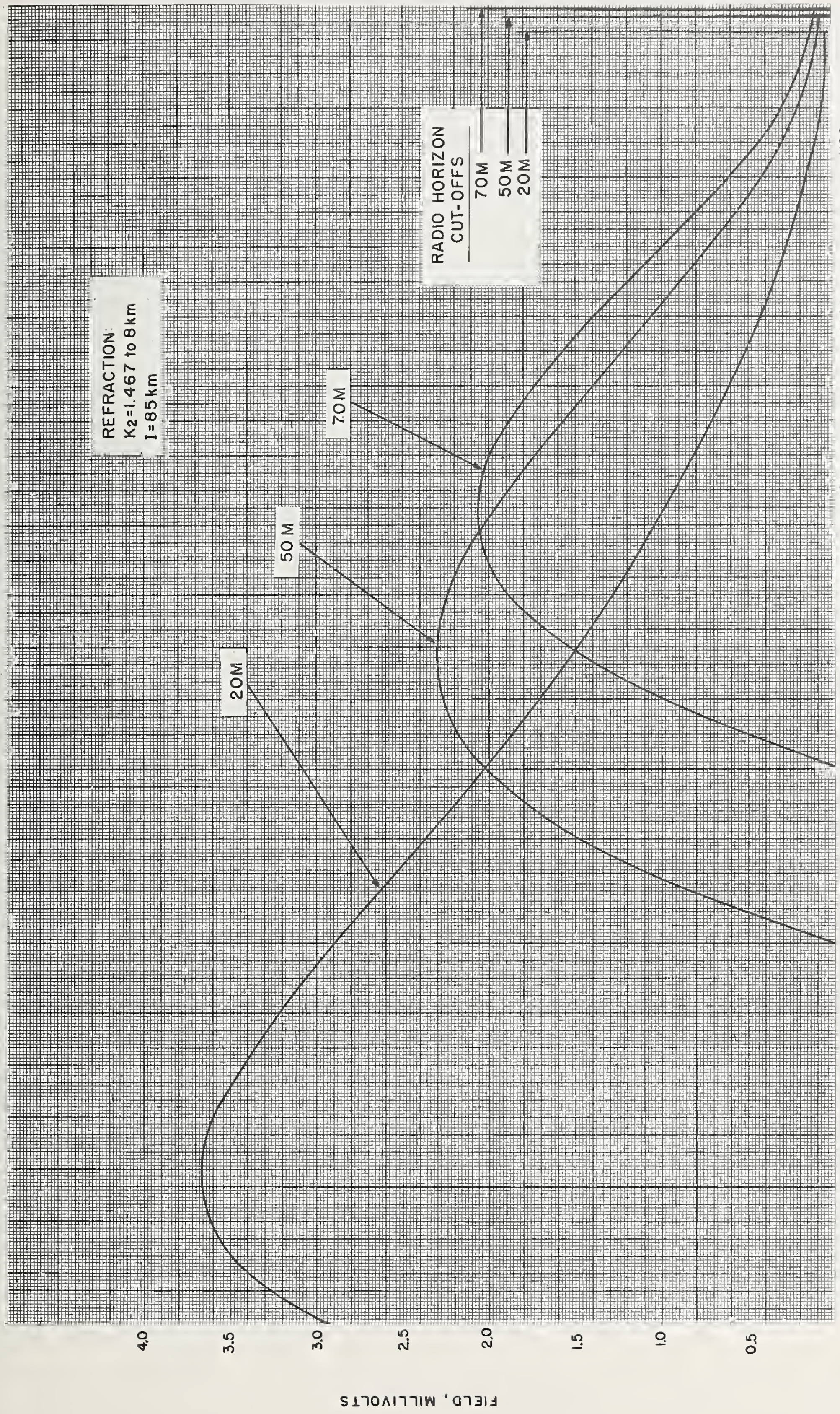

Figure 48. *20, 50, and 70 meter antennas at 35 Mc.*

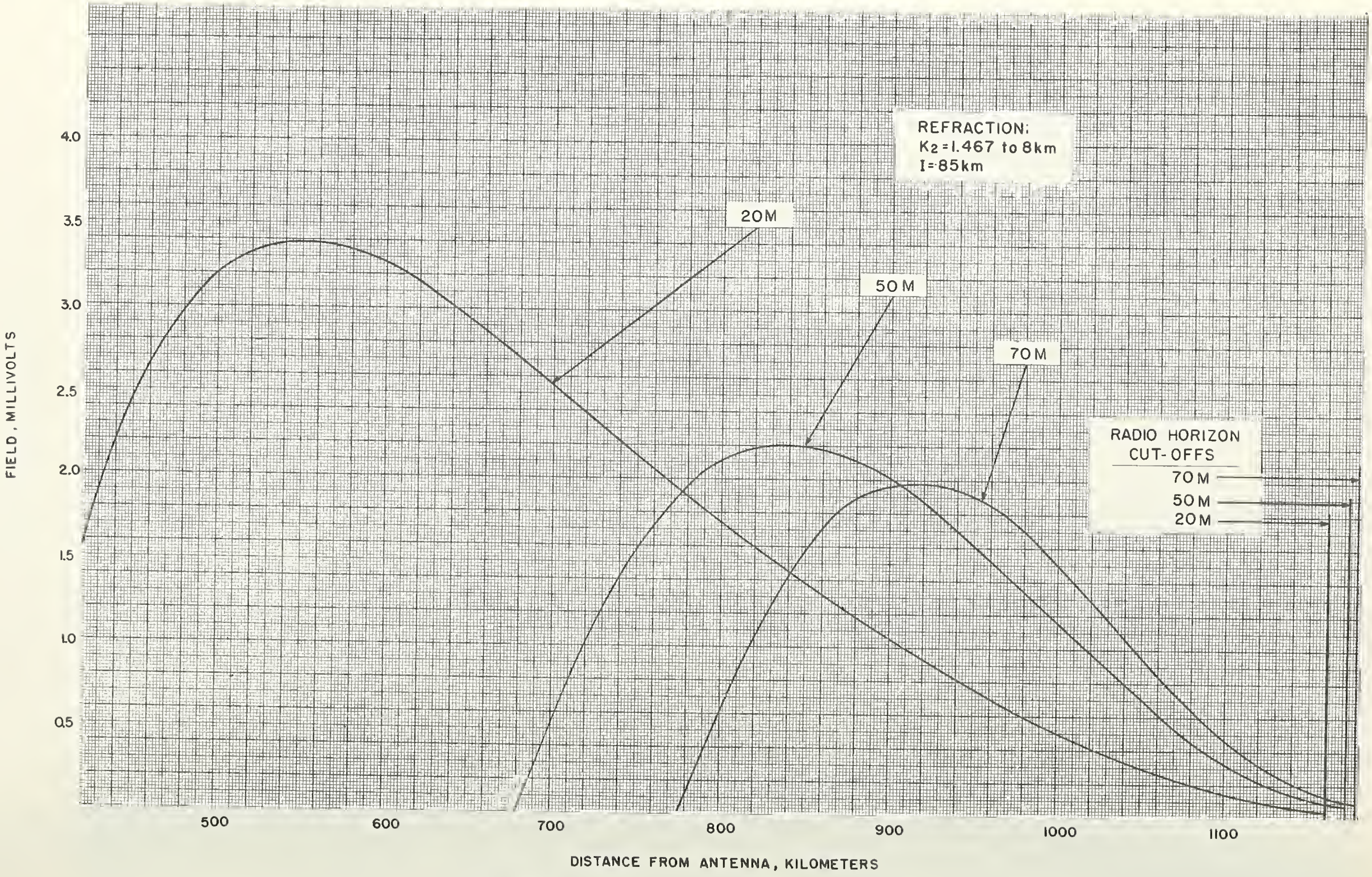

Figure 49. *20, 50, and 70 meter antennas at 40 Mc.*

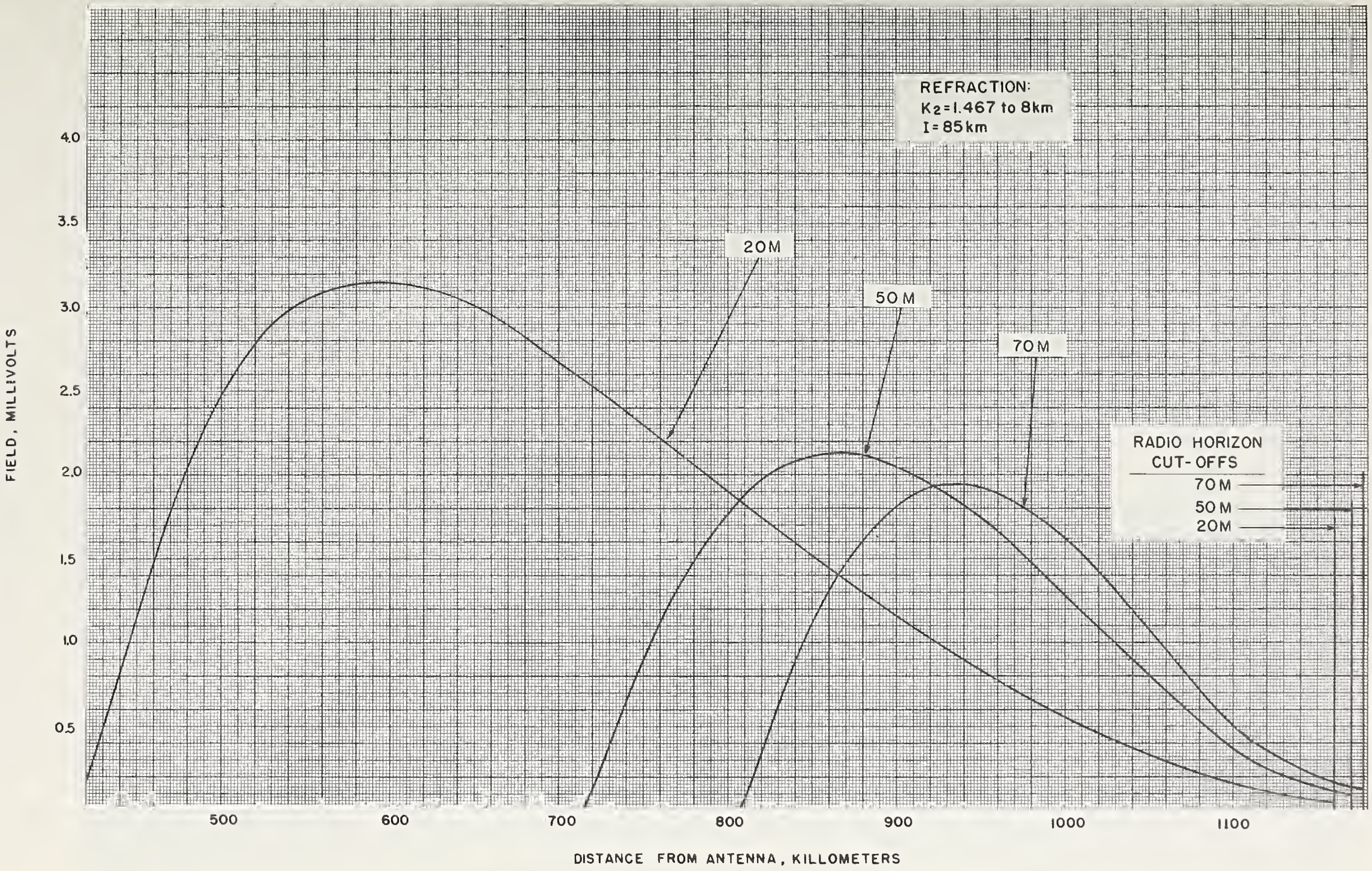

FIGURE 50. *20, 50, and 70 meter antennas at 45 Mc.*

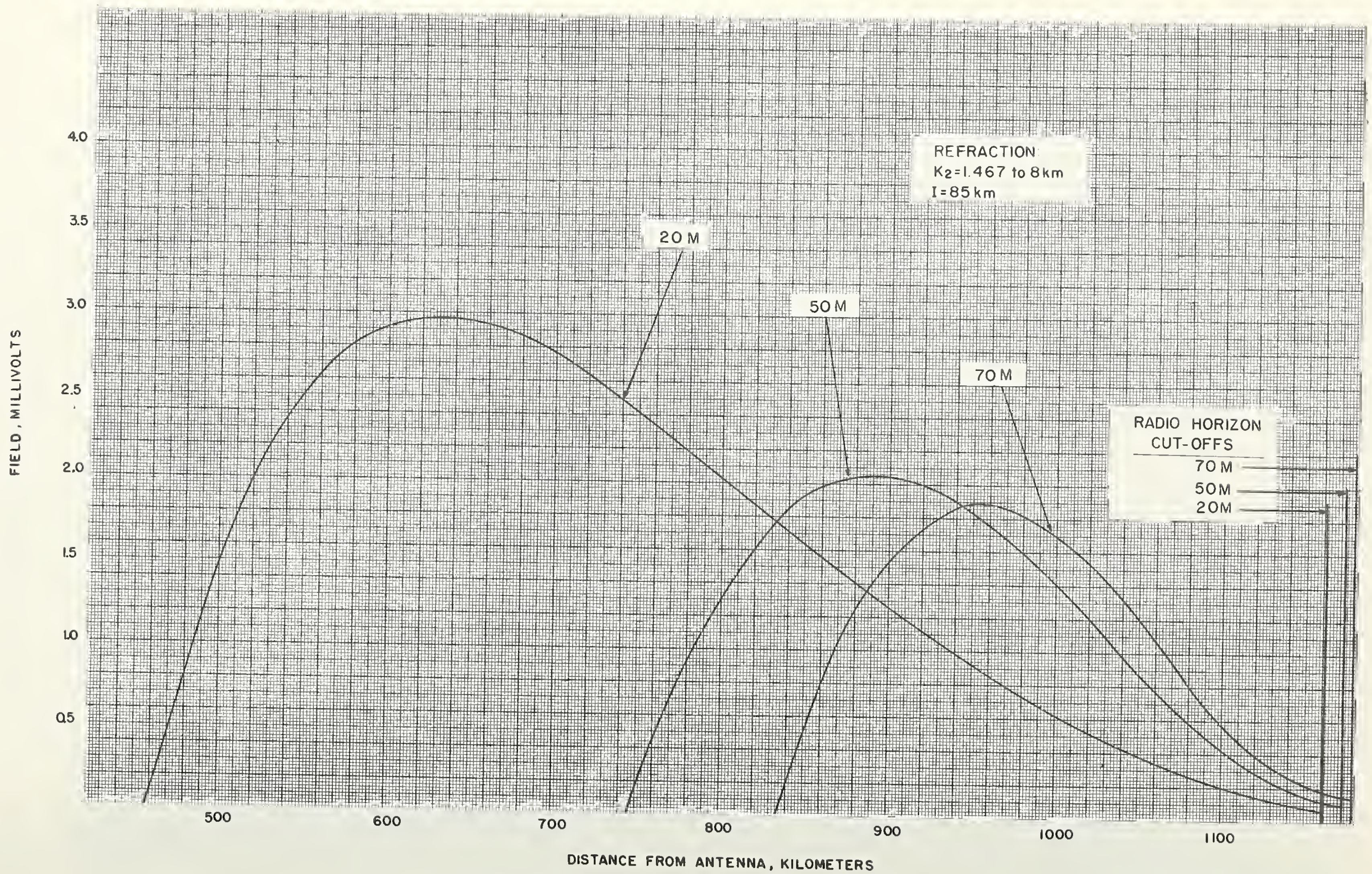

FIGURE 51. *20, 50, and 70 meter antennas at 50 Mc.*

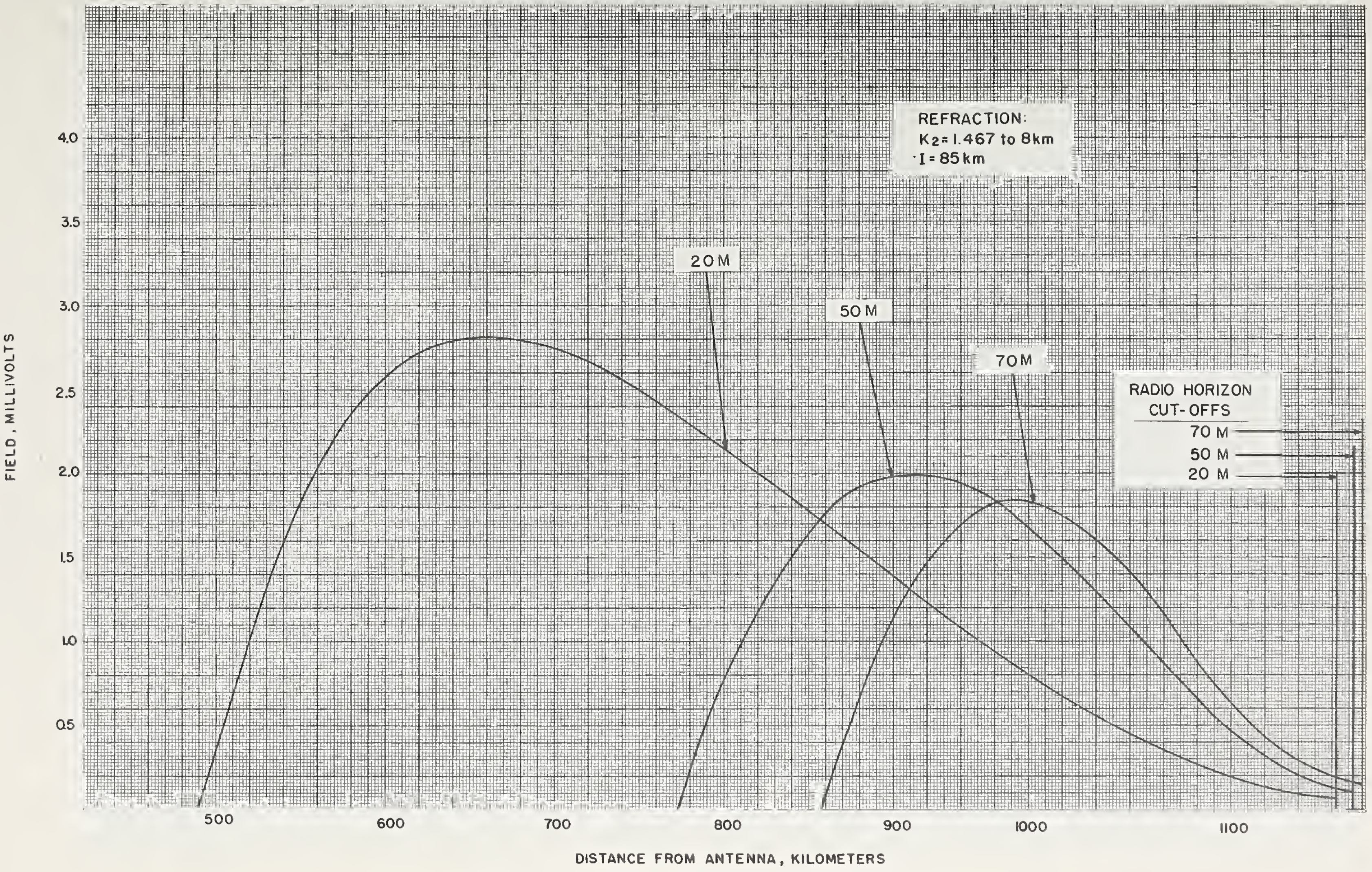

FIGURE 52. *20, 50, and 70 meter antennas at 55 Mc.*

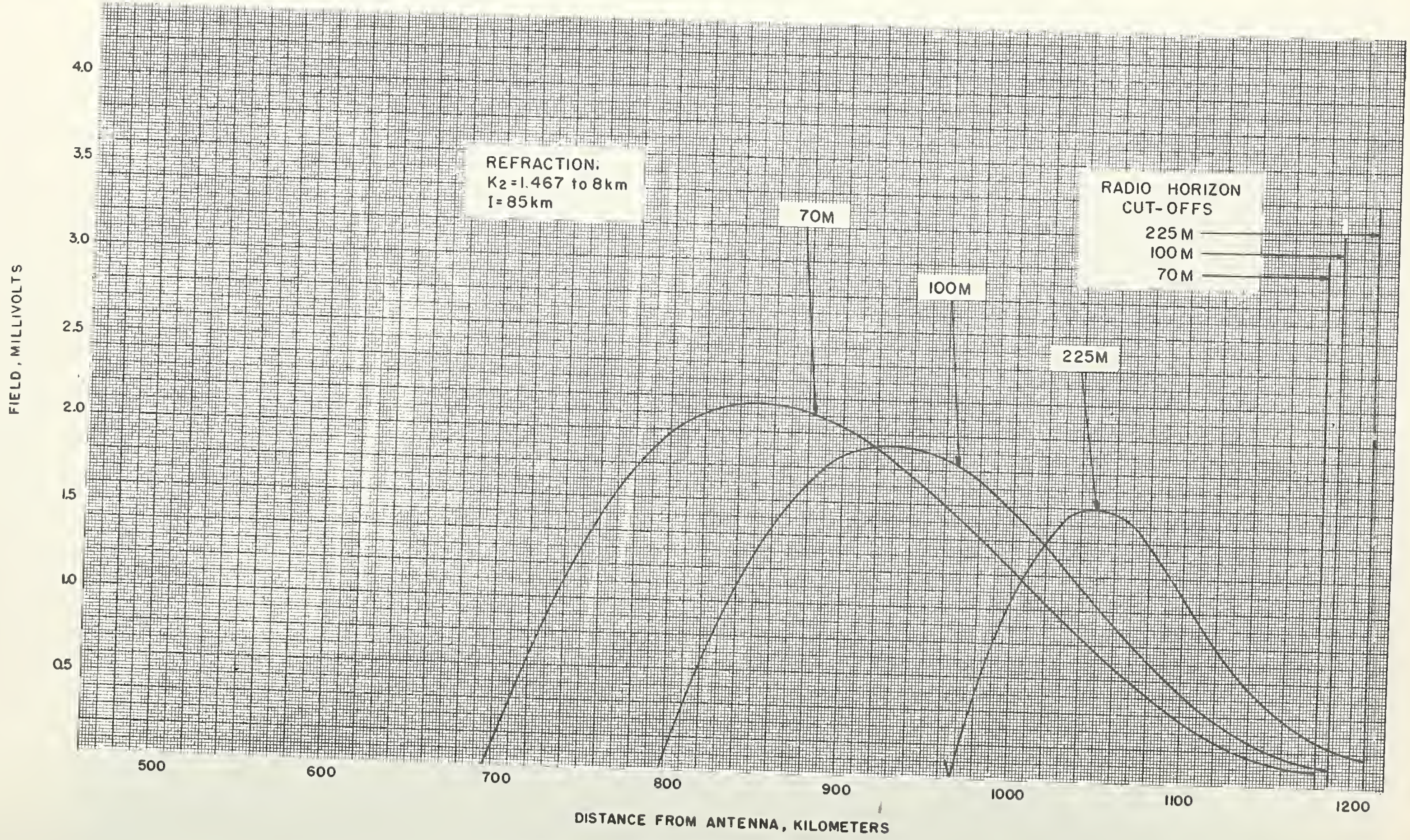

FIGURE 53. *70, 100, and 225 meter antennas at 30 Mc.*

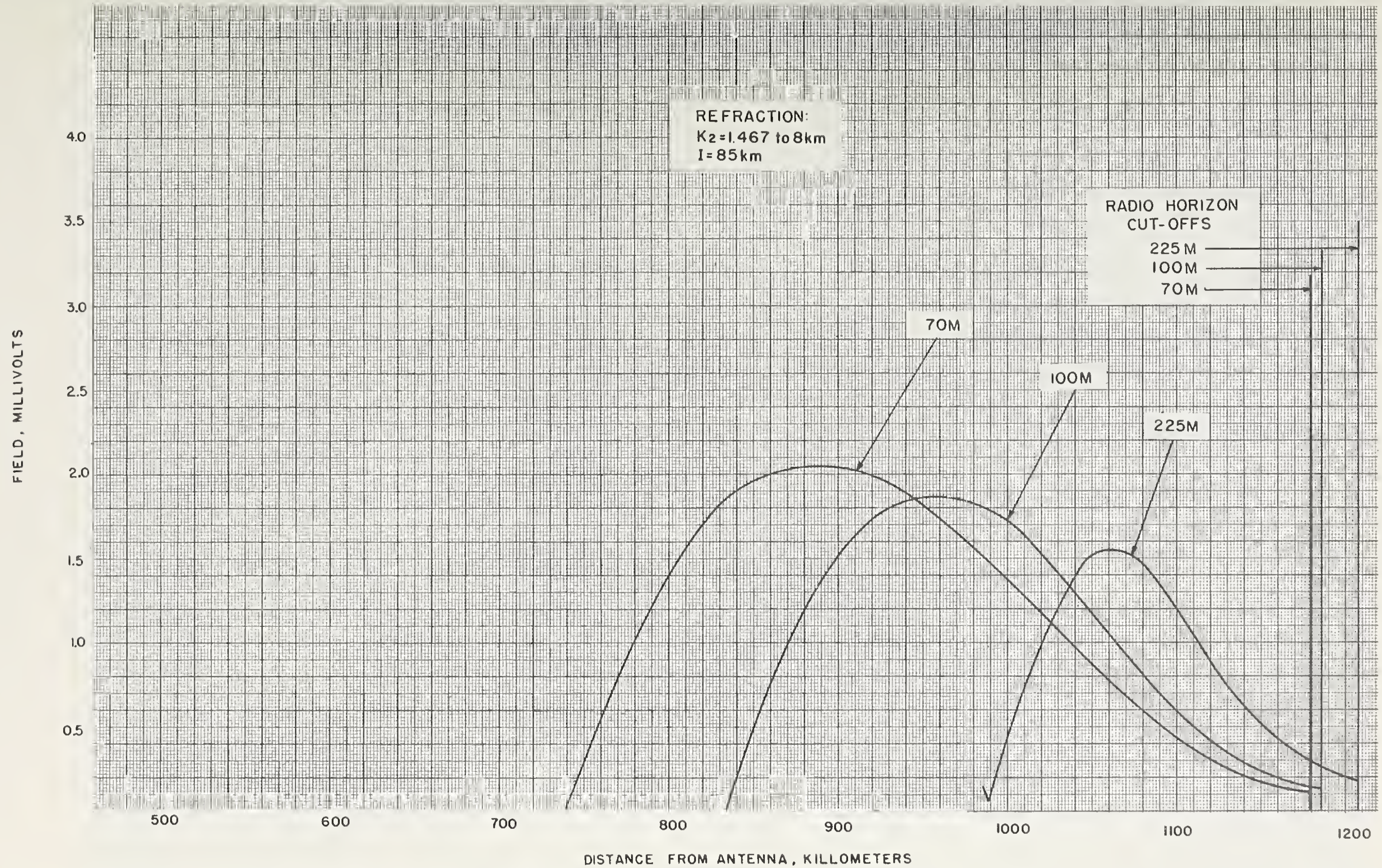

FIGURE 54. *70, 100, and 225 meter antennas at 35 Mc.*

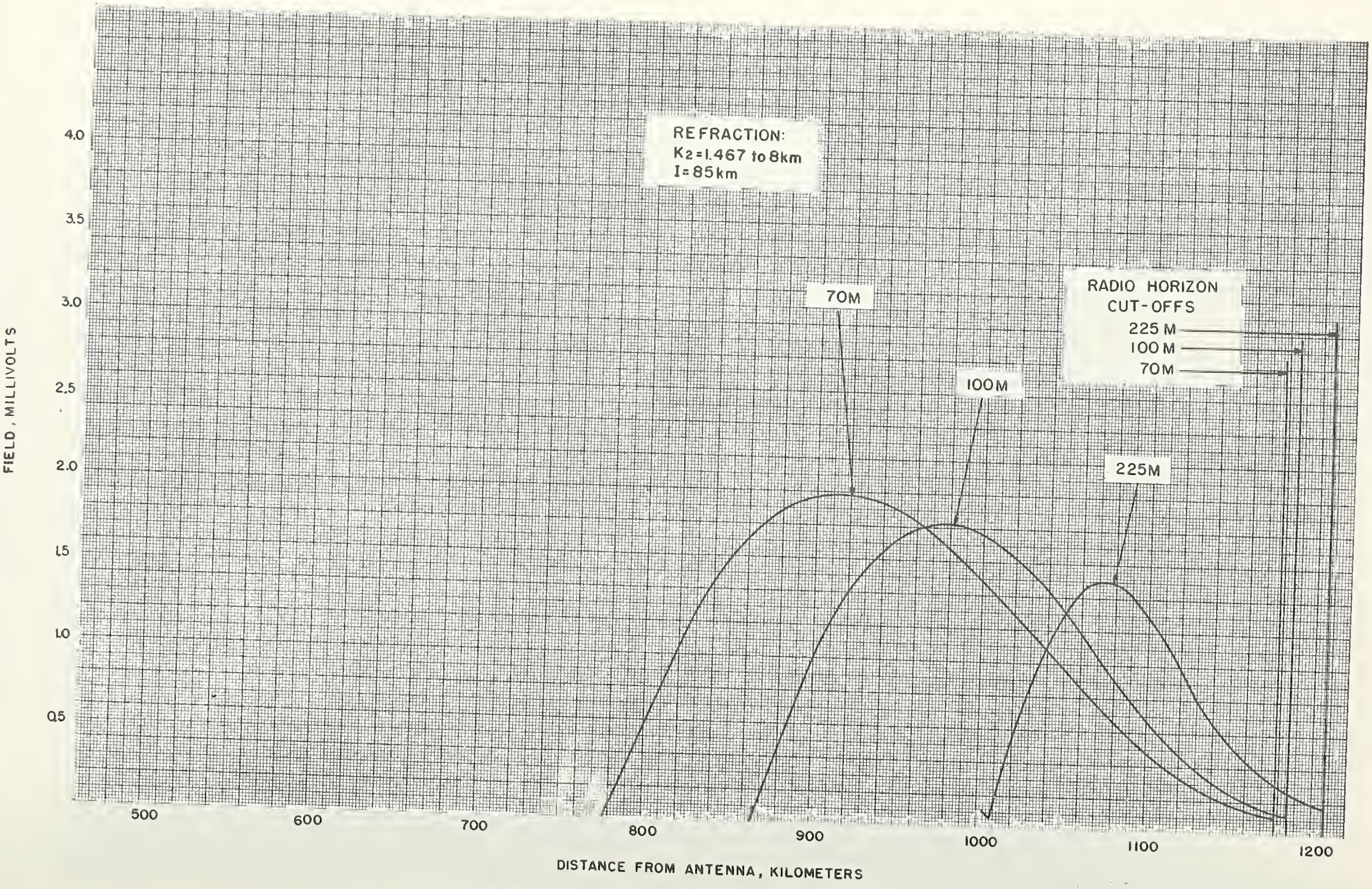

FIGURE 55. *70, 100, and 225 meter antennas at 40 Mc.*

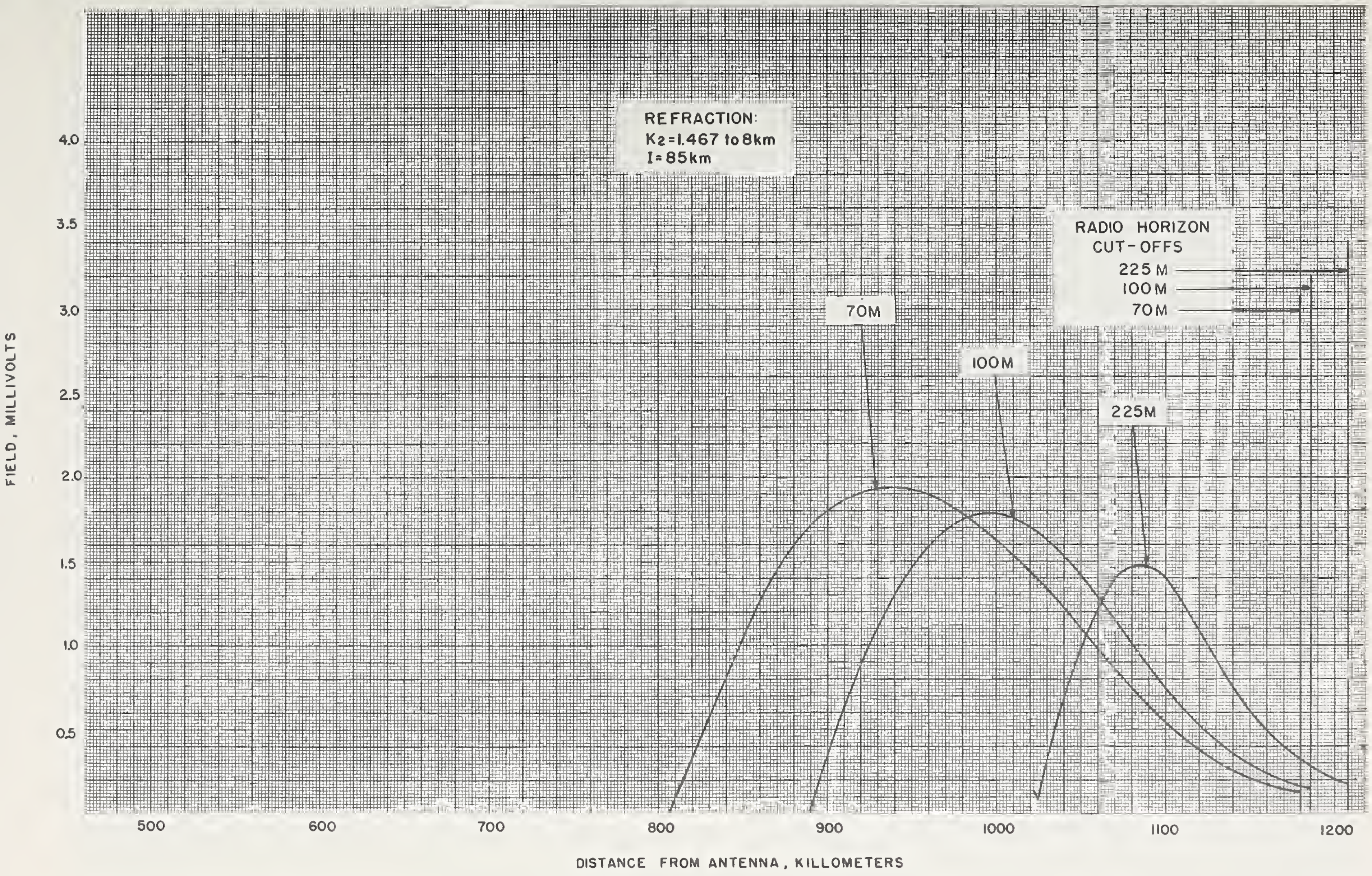

FIGURE 56. *70, 100, and 225 meter antennas at 45 Mc.*

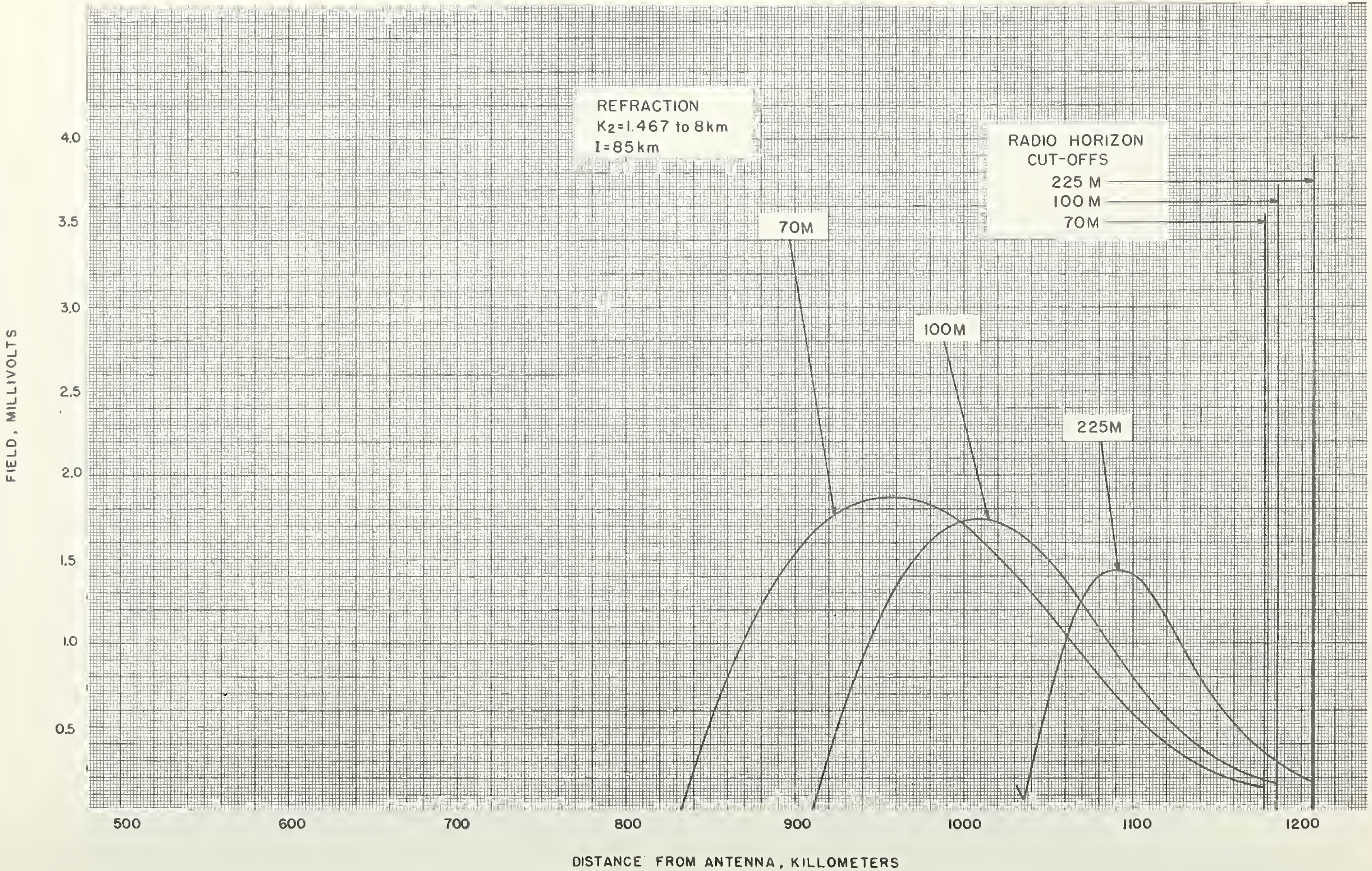

FIGURE 57. *70, 100, and 225 meter antennas at 50 Mc.*

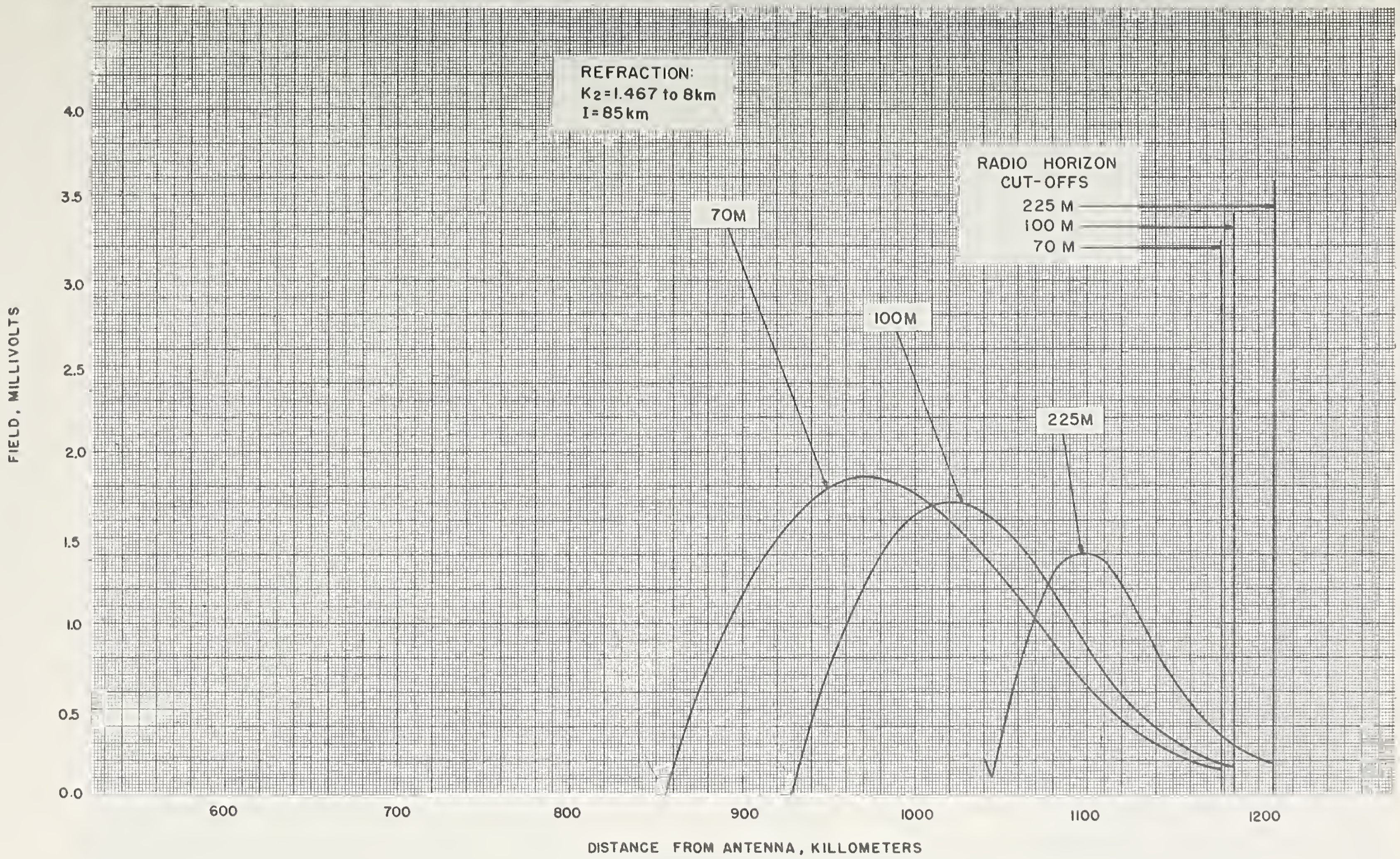

FIGURE 58. *70, 100, and 225 meter antennas at 55 Mc.*

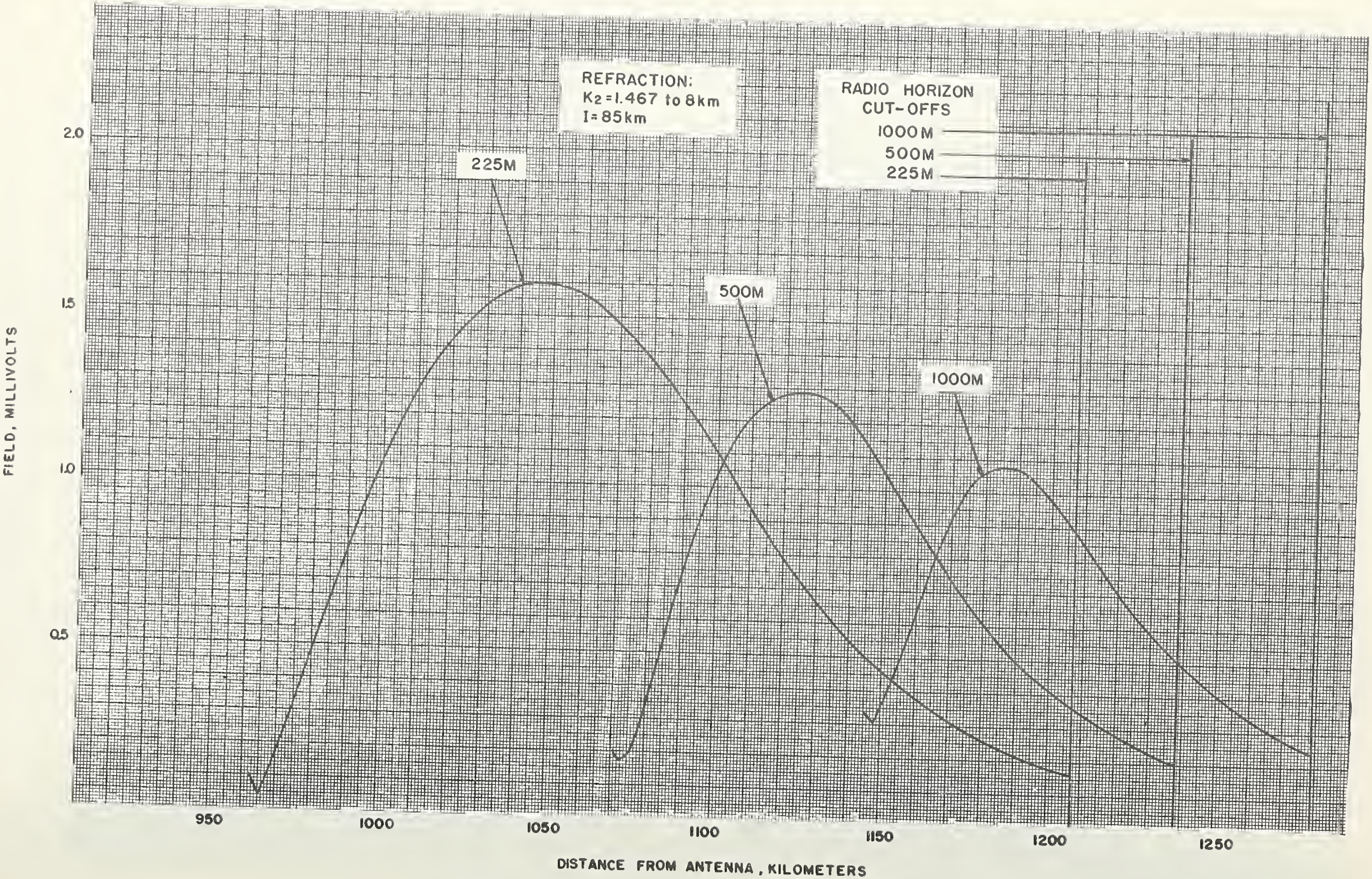

FIGURE 59. *225, 500, and 1000 meter antennas at 30 Mc.*

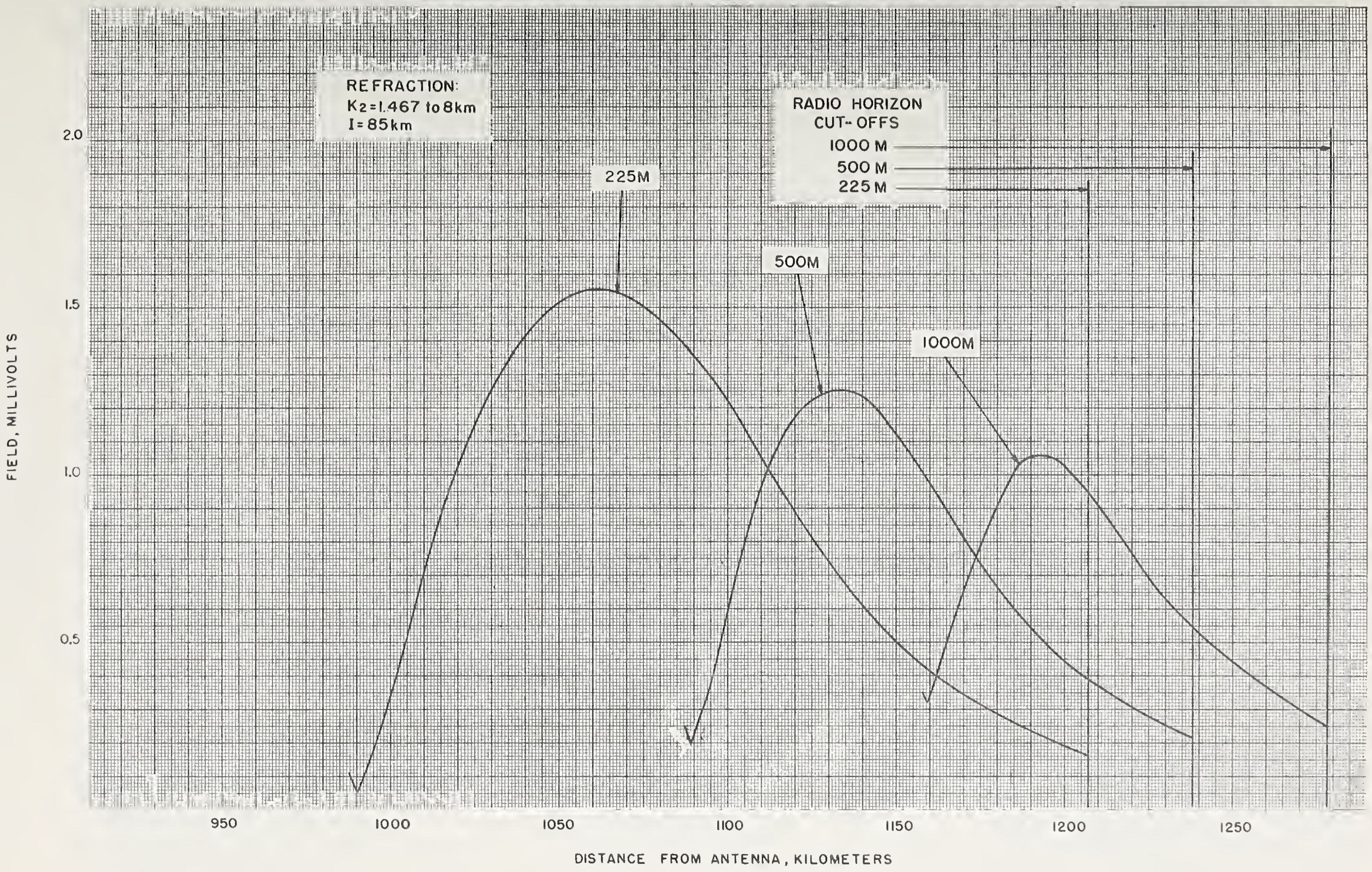

FIGURE 60. *225, 500, and 1000 meter antennas at 35 Mc.*

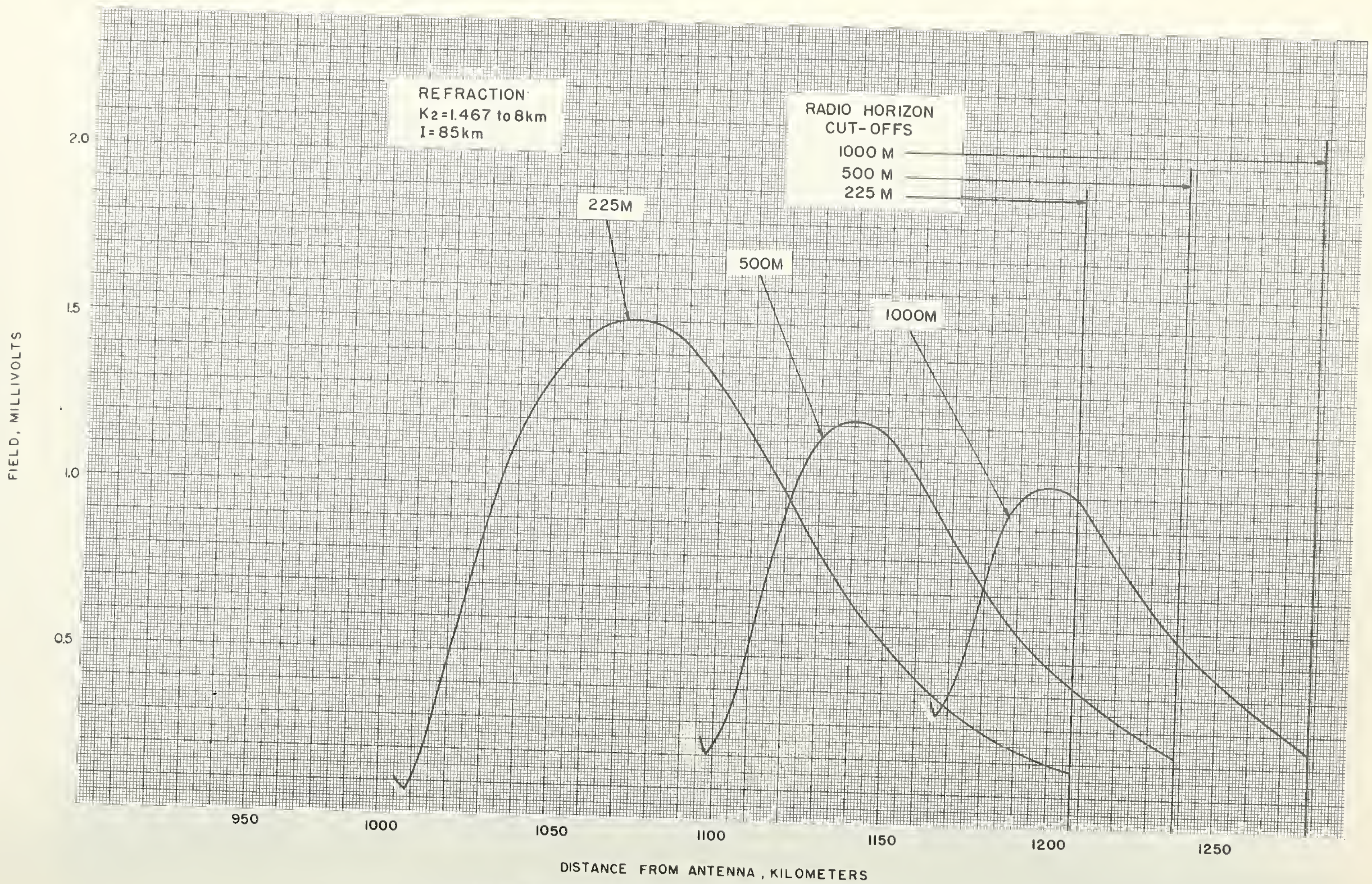

FIGURE 61. *225, 500, and 1000 meter antennas at 40 Mc.*

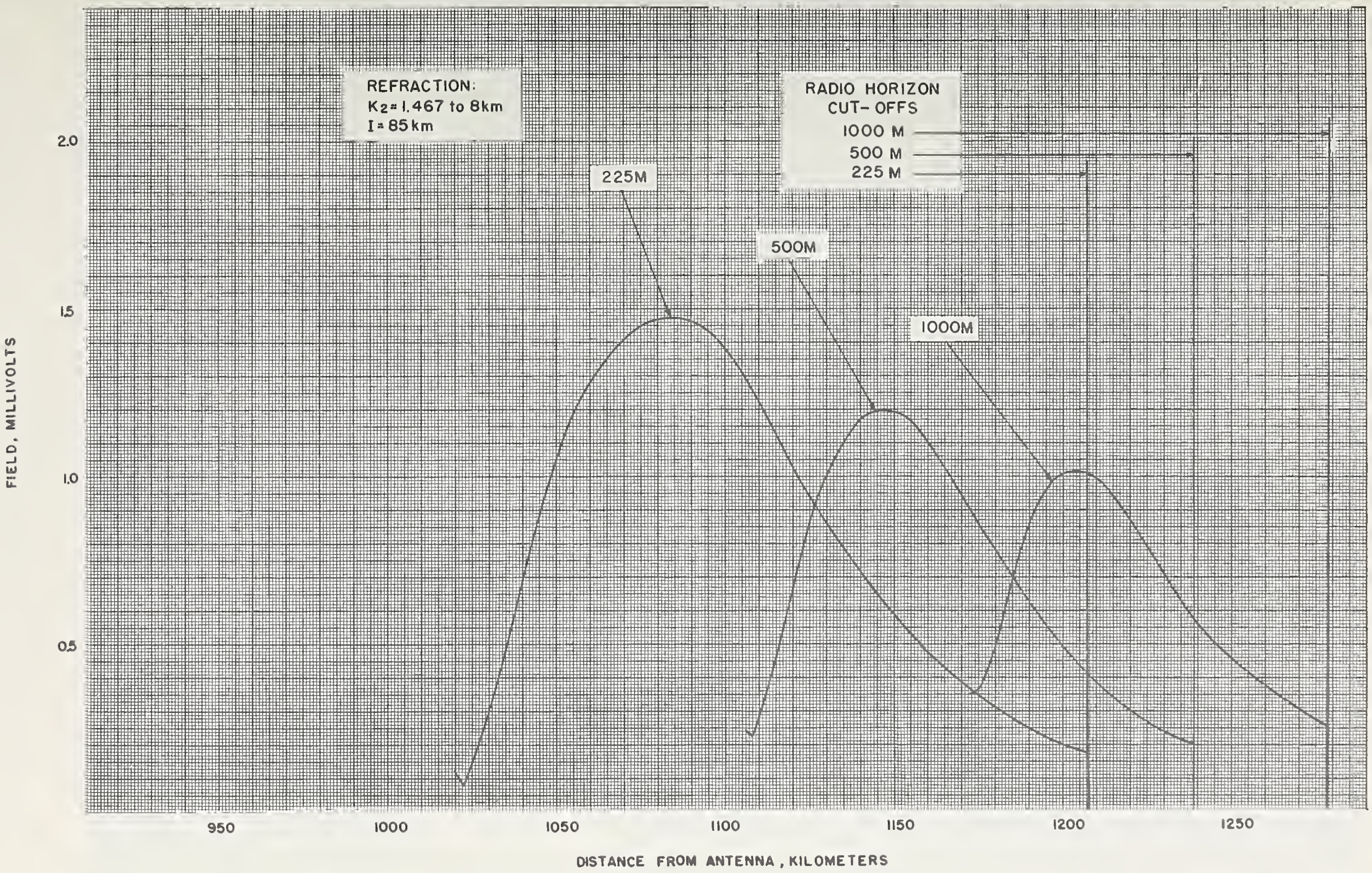

FIGURE 62. *225, 500, and 1000 meter antennas at 45 Mc.*

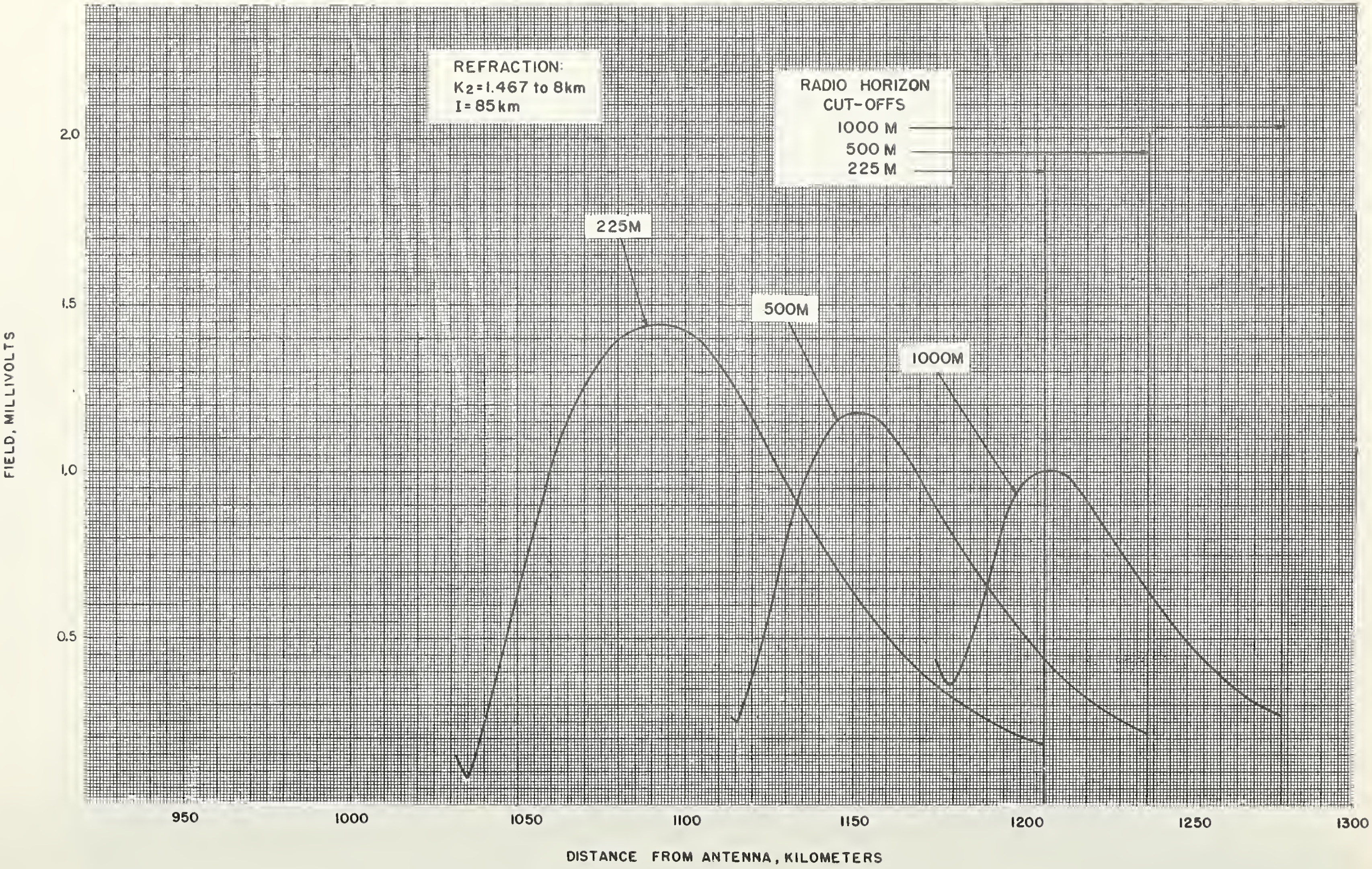

FIGURE 63. *225, 500, and 1000 meter antennas at 50 Mc.*

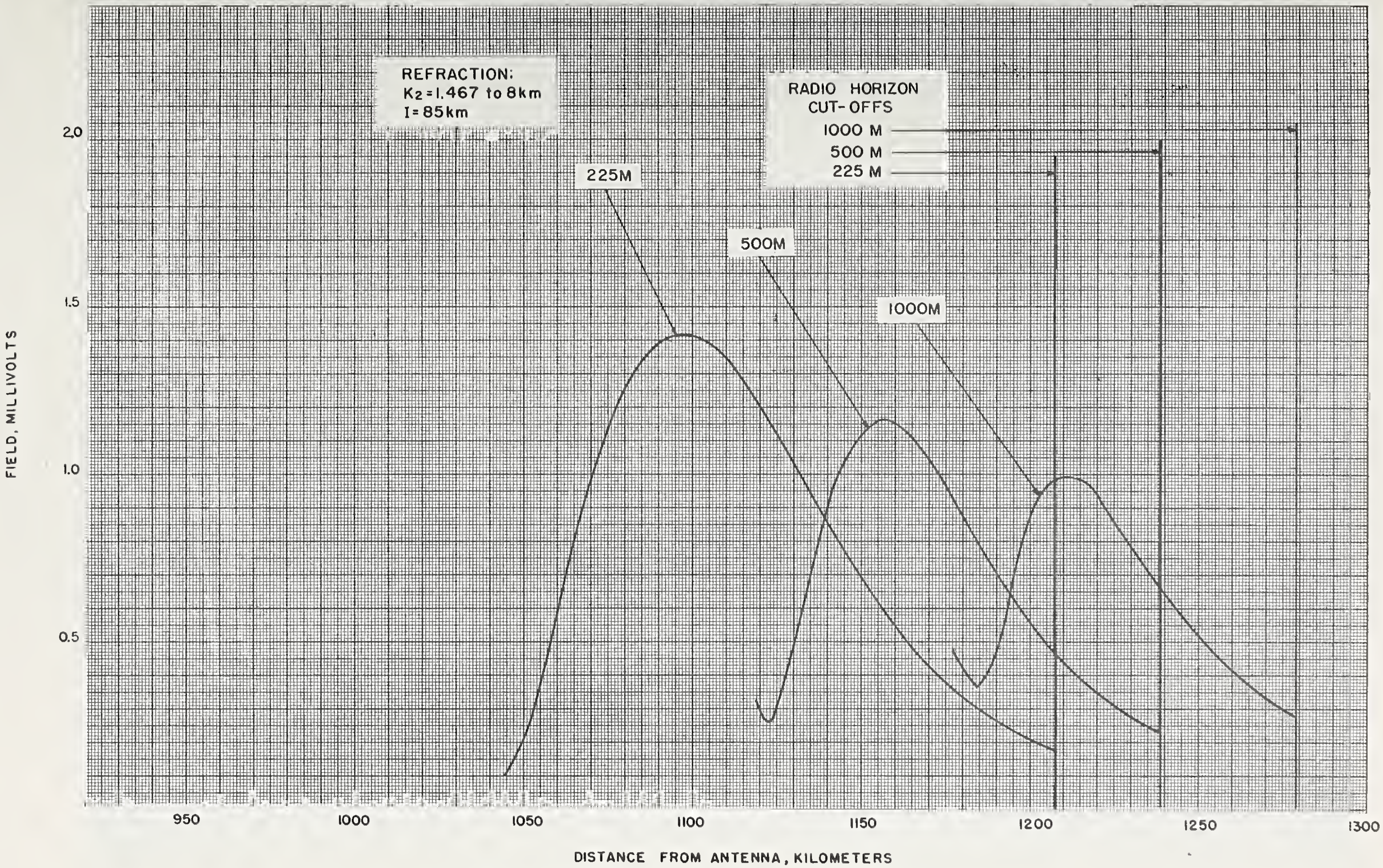

FIGURE 64. *225, 500, and 1000 meter antennas at 55 Mc.*

Appendix III. Comparison of Patterns for k_1 and k_2

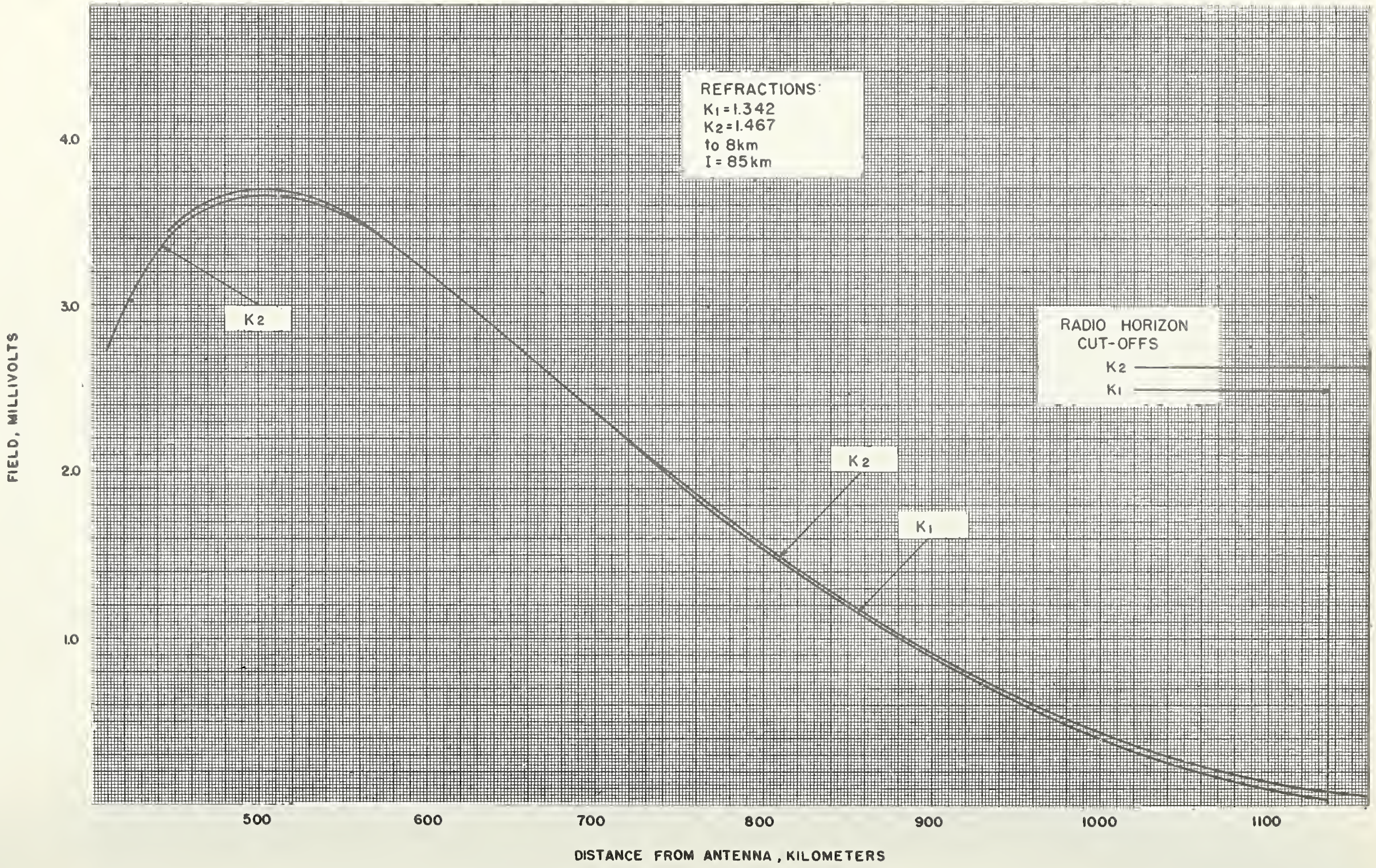

FIGURE 65. *20 meter antenna at 35 Mc for k_1 and k_2.*

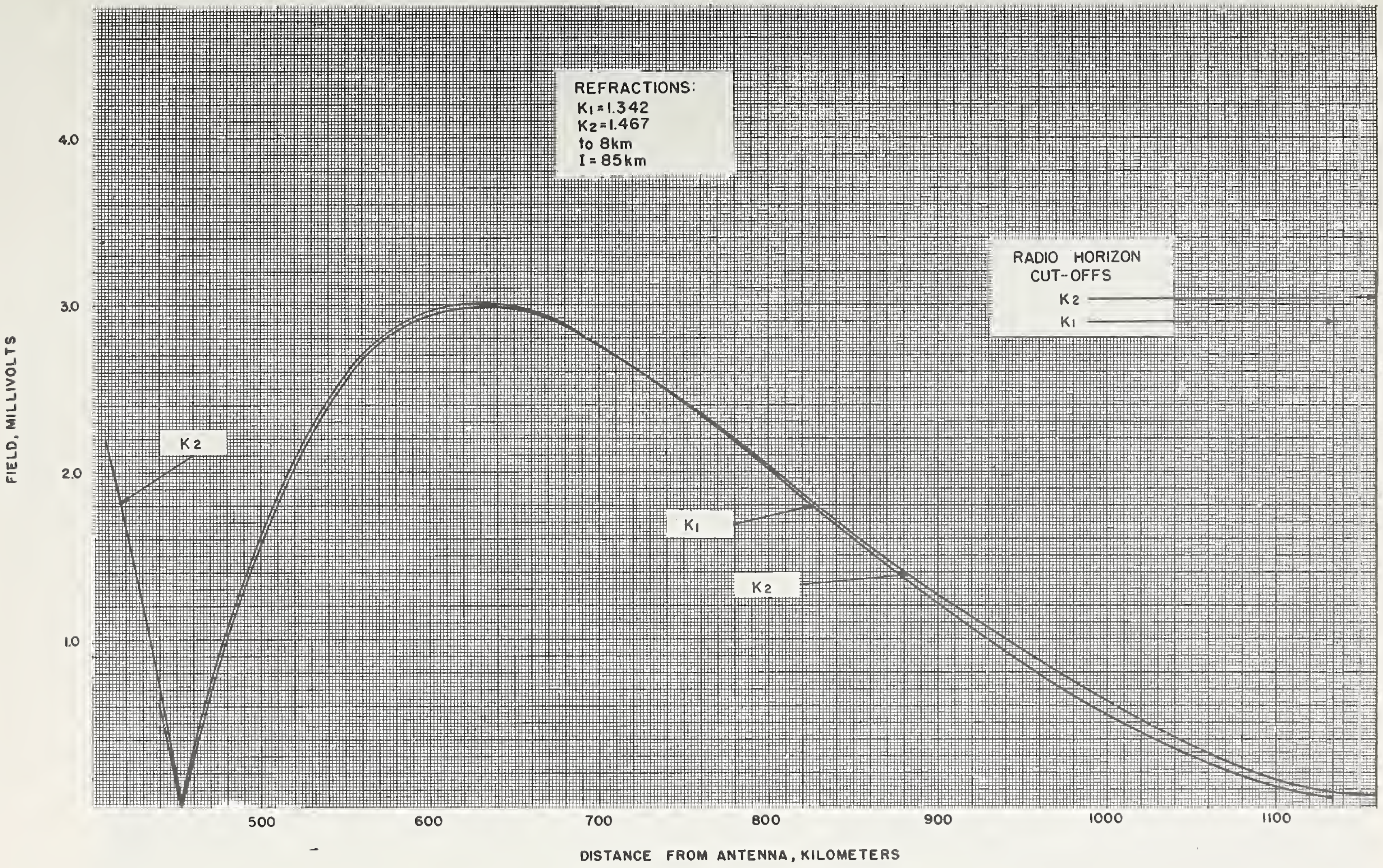

FIGURE 66. *20 meter antenna at 50 Mc for k_1 and k_2.*

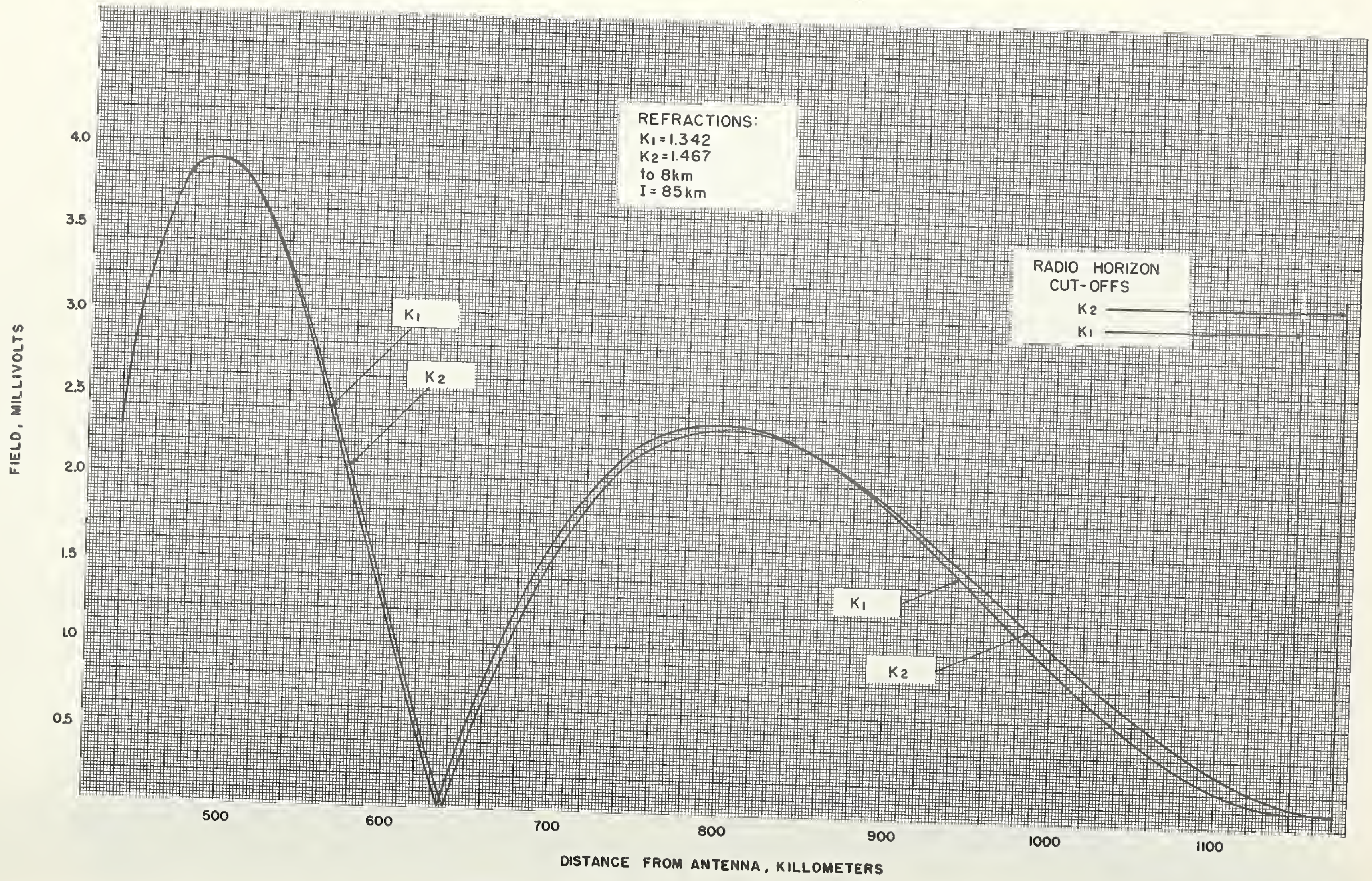

FIGURE 67. *50 meter antenna at 35 Mc for k_1 and k_2.*

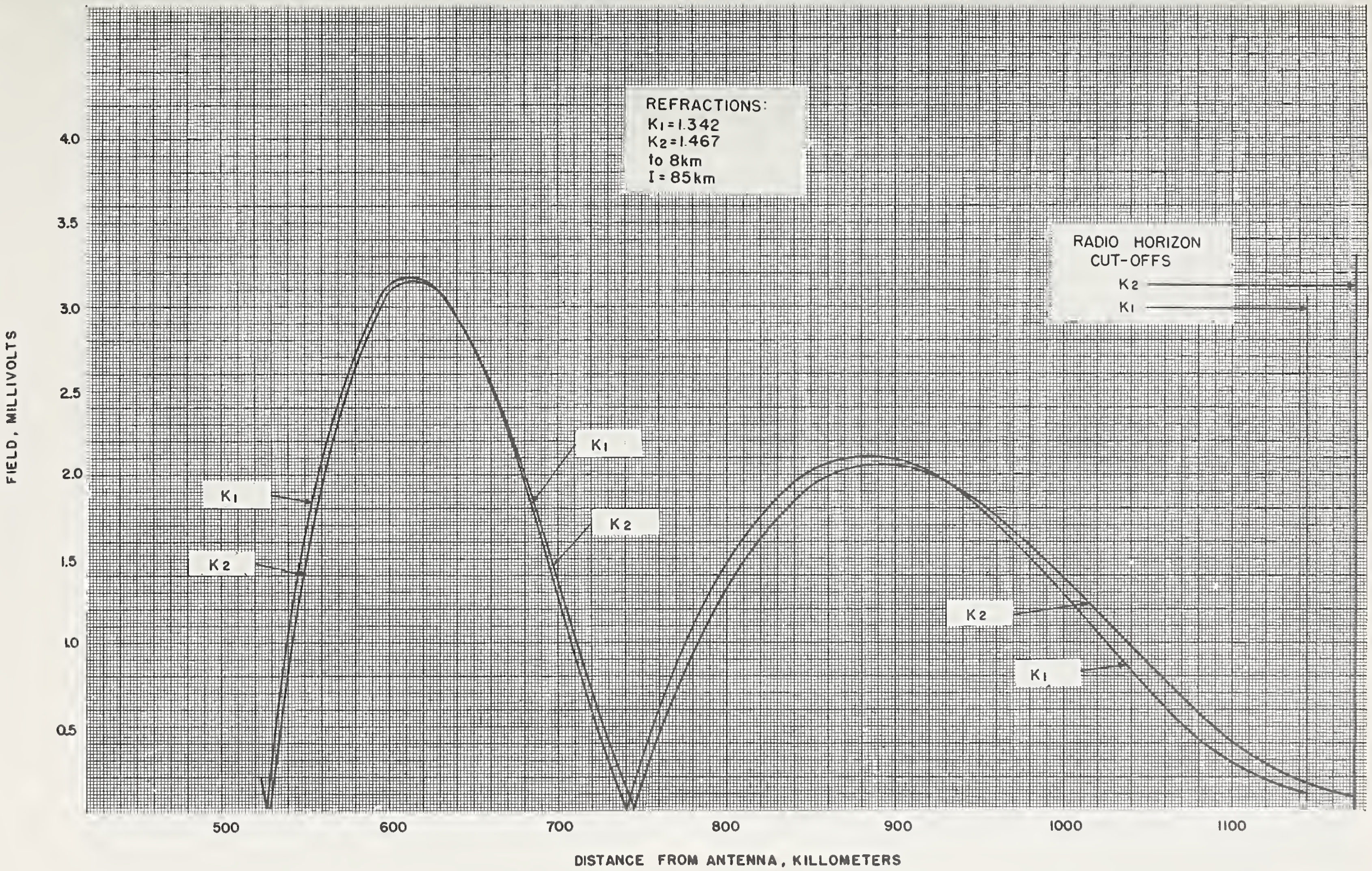

FIGURE 68. *50 meter antenna at 50 Mc for k_1 and k_2.*

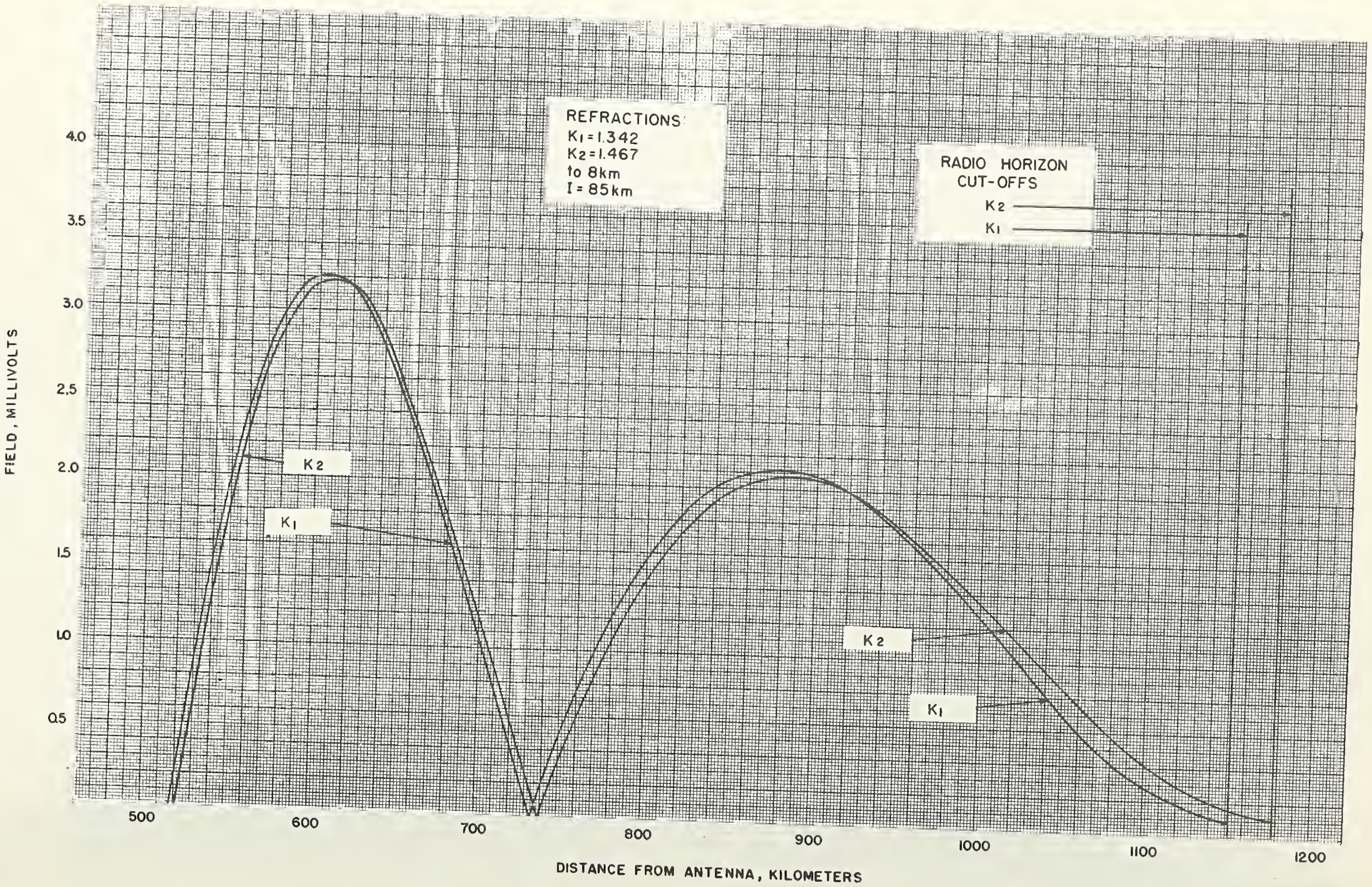

FIGURE 69. *70 meter antenna at 35 Mc for k_1 and k_2.*

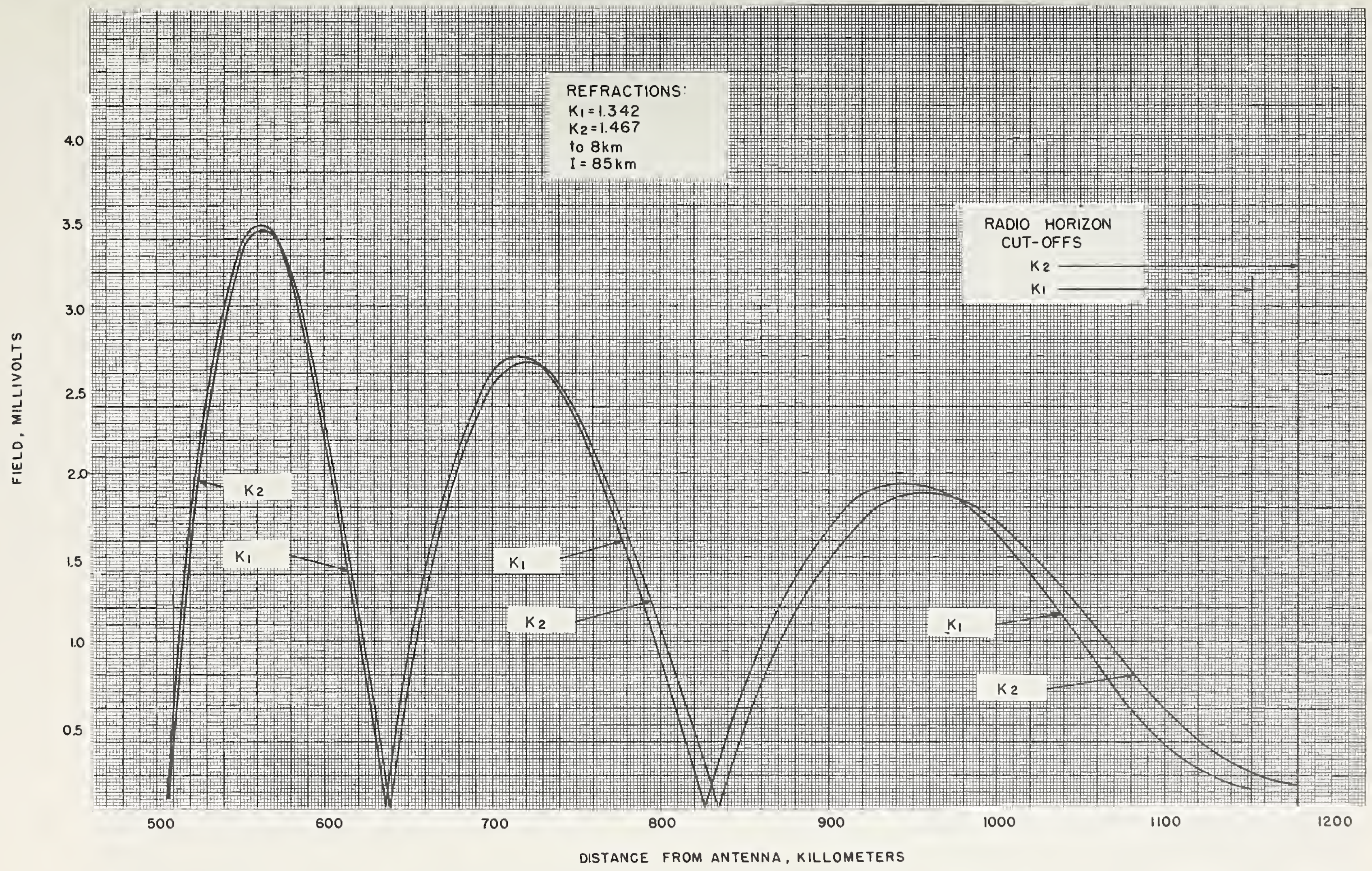

FIGURE 70. *70 meter antenna at 50 Mc for k_1 and k_2.*

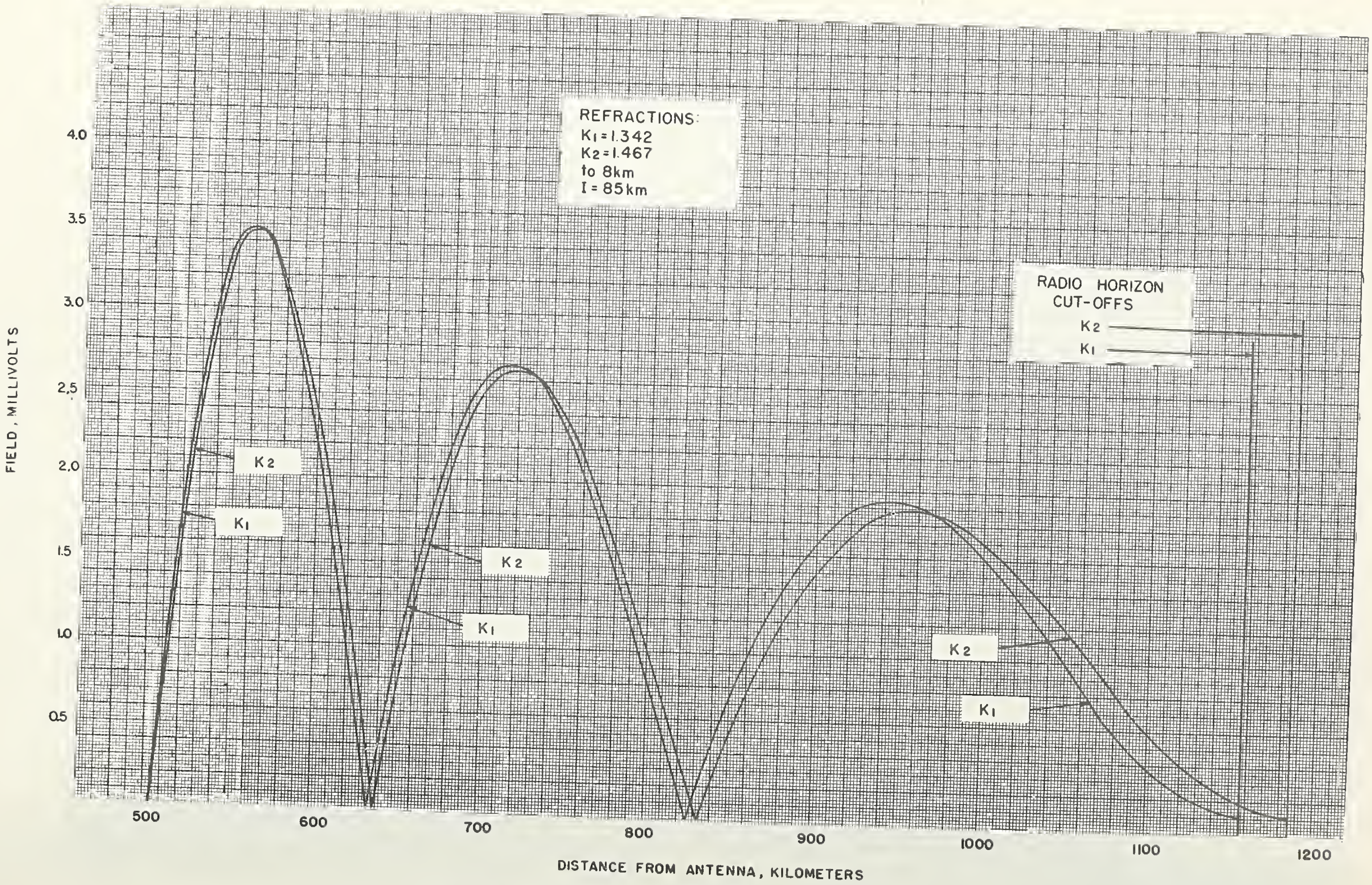

FIGURE 71. *100 meter antenna at 35 Mc for k_1 and k_2.*

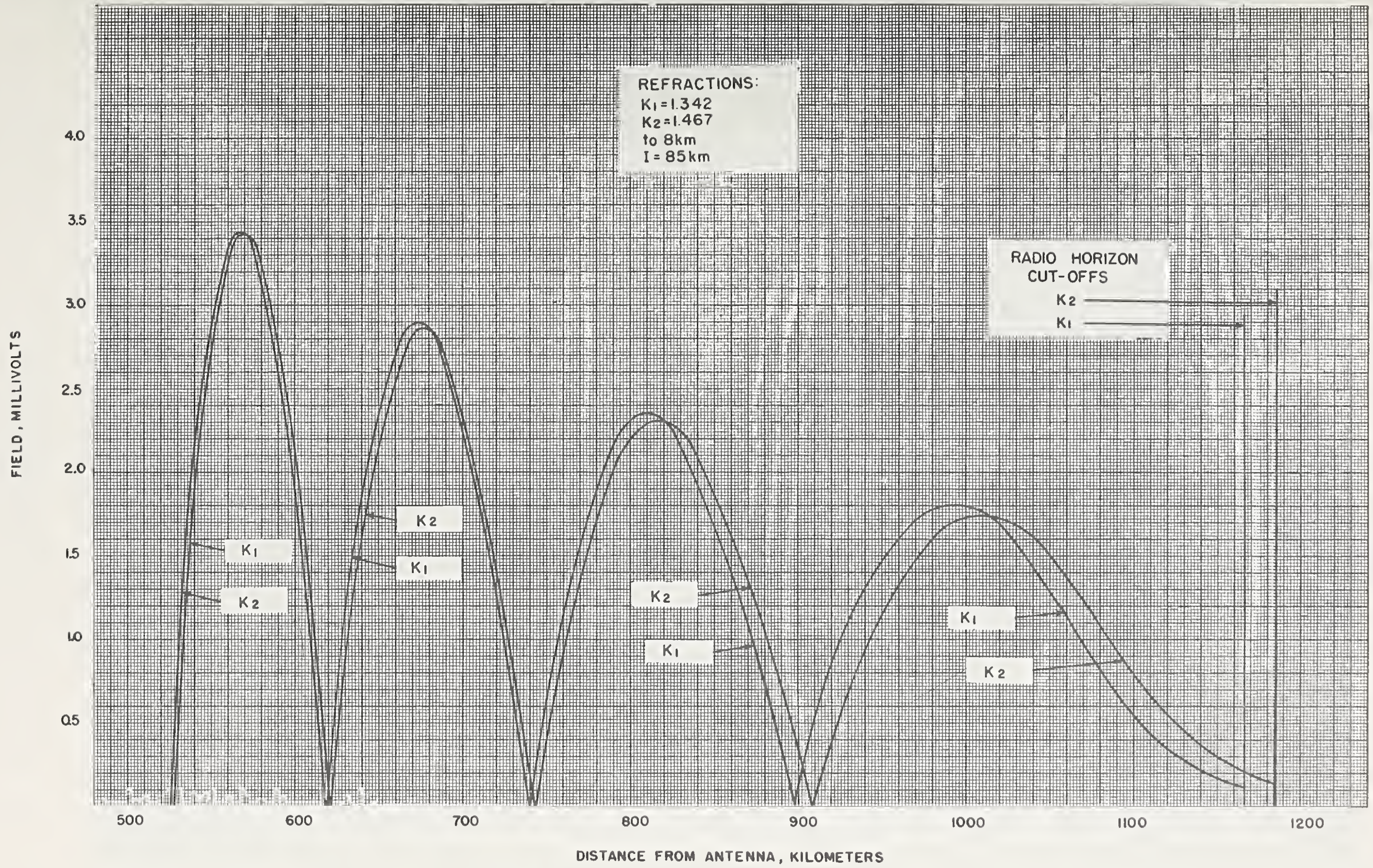

FIGURE 72. *100 meter antenna at 50 Mc for k_1 and k_2.*

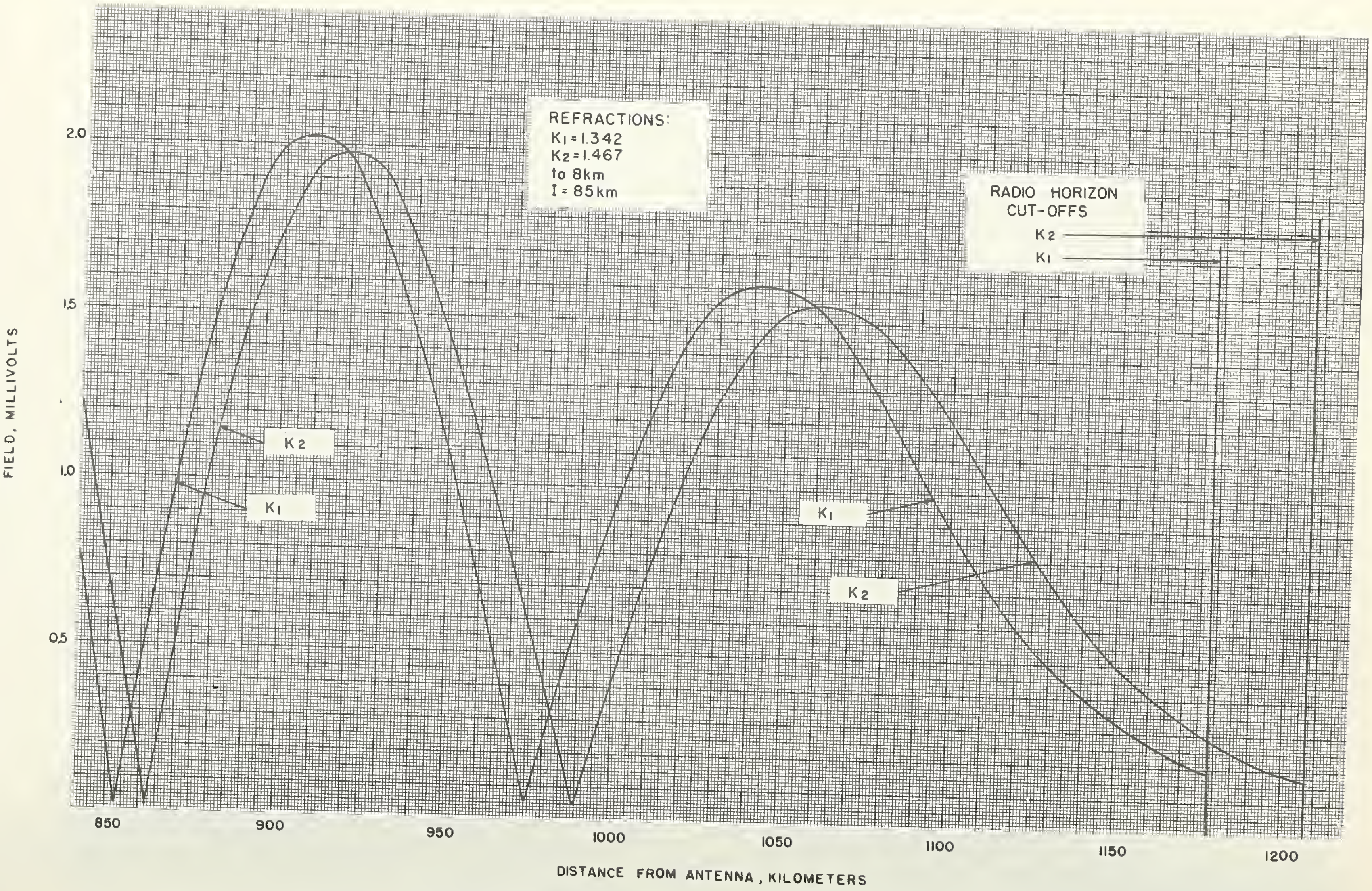

FIGURE 73. *225 meter antenna at 35 Mc for k_1 and k_2.*

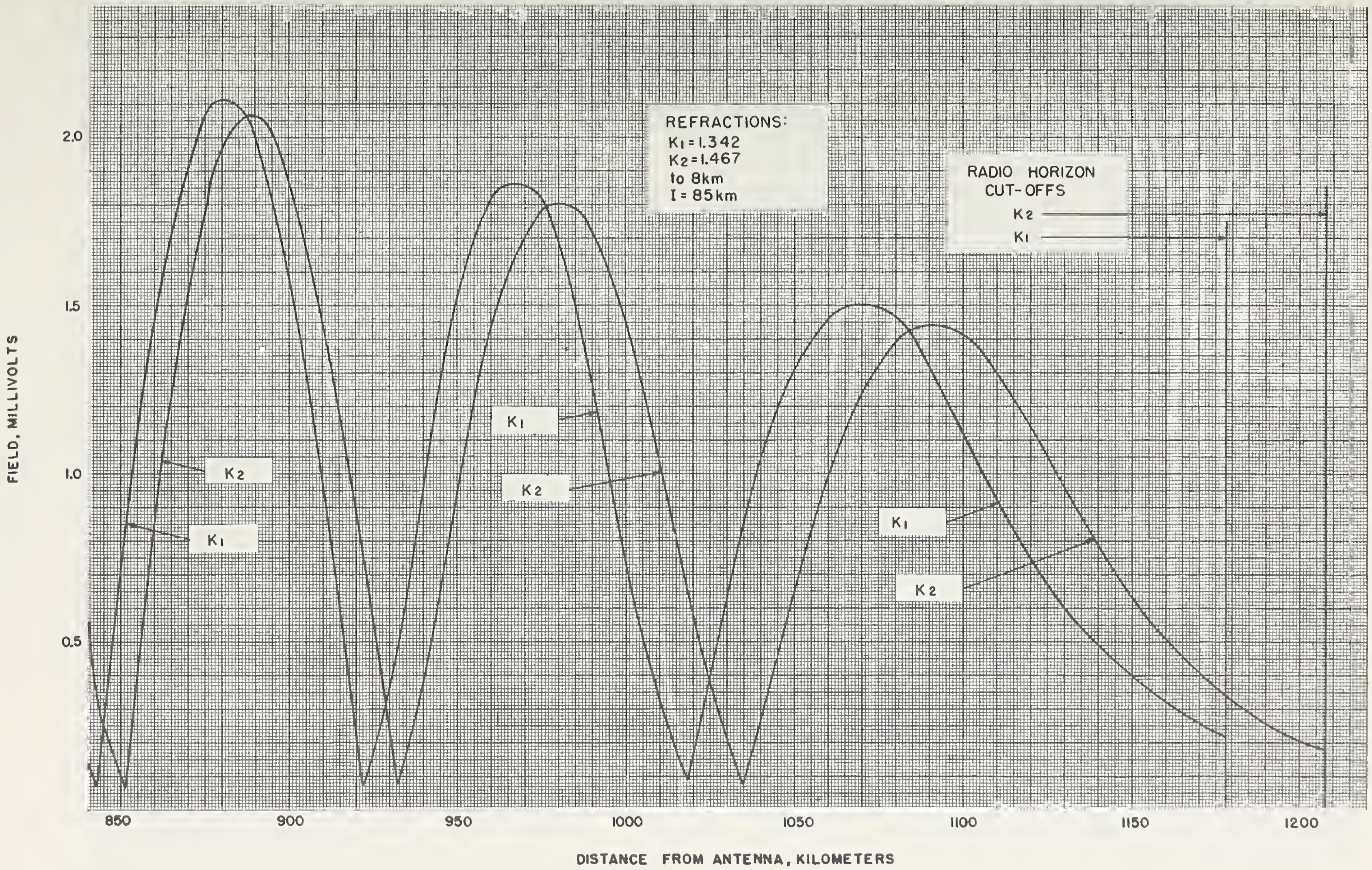

FIGURE 74. *225 meter antenna at 50 Mc for k_1 and k_2.*

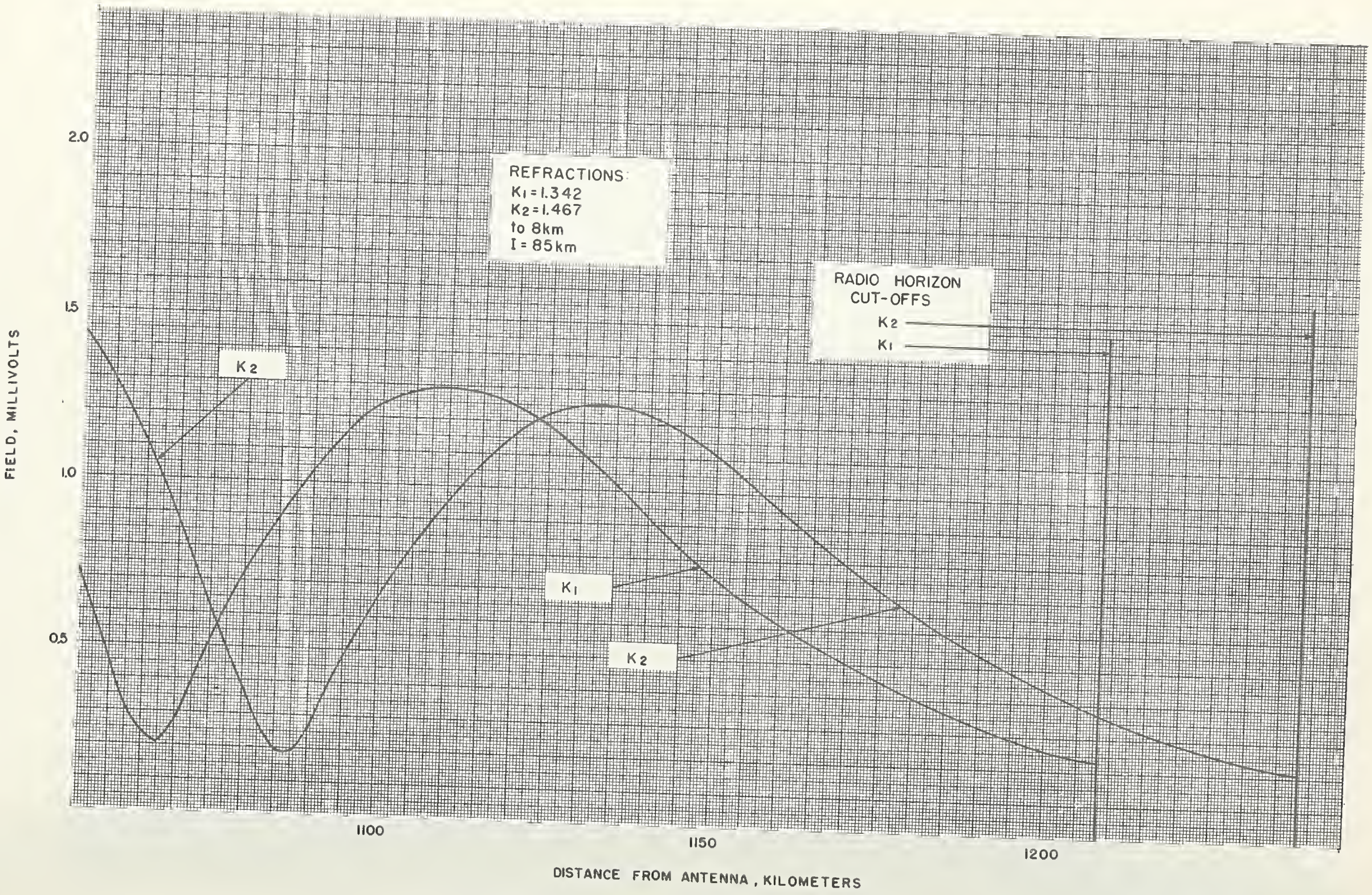

FIGURE 75. *500 meter antenna at 35 Mc for k_1 and k_2.*

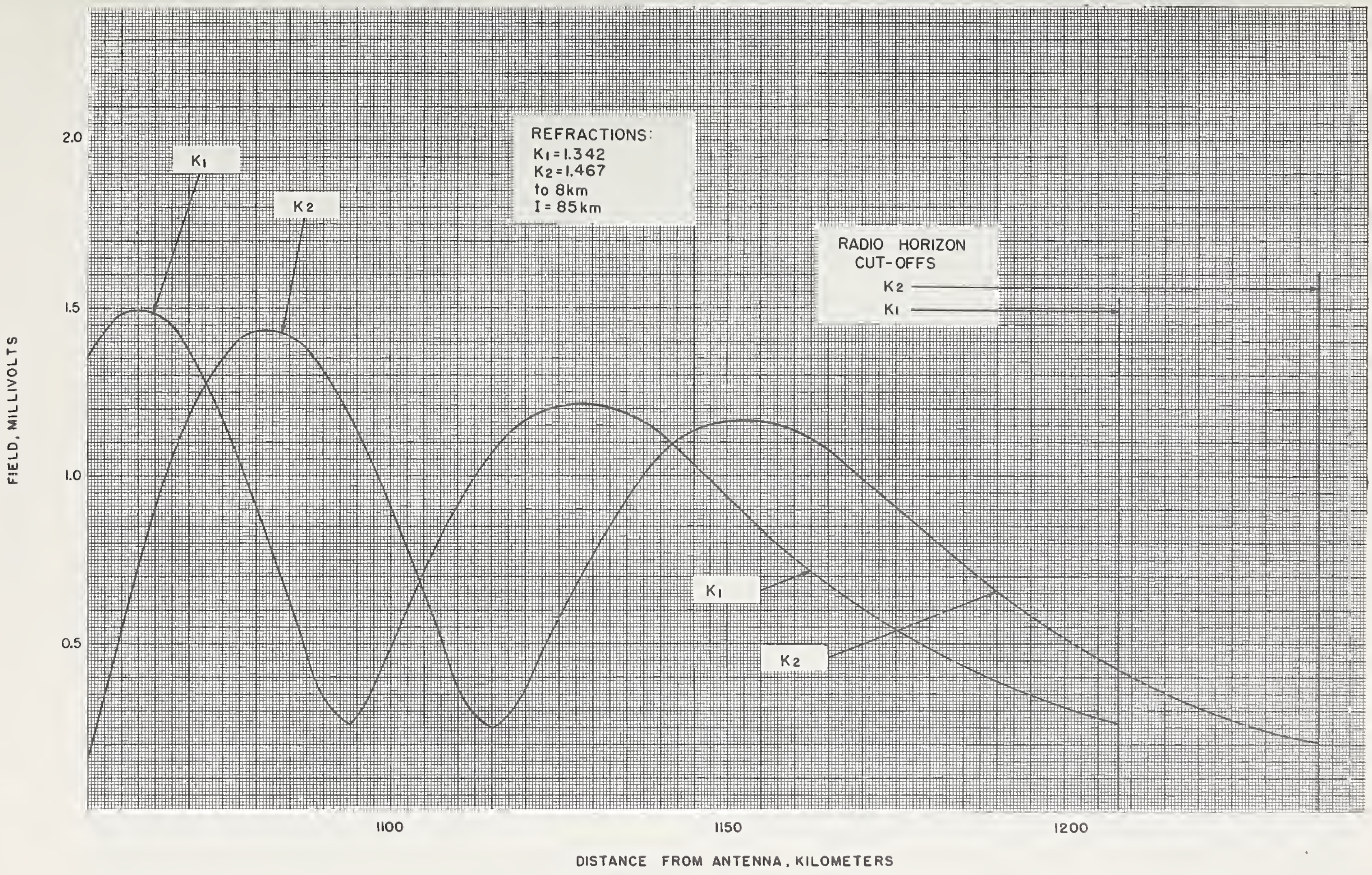

FIGURE 76. *500 meter antenna at 50 Mc for k_1 and k_2.*

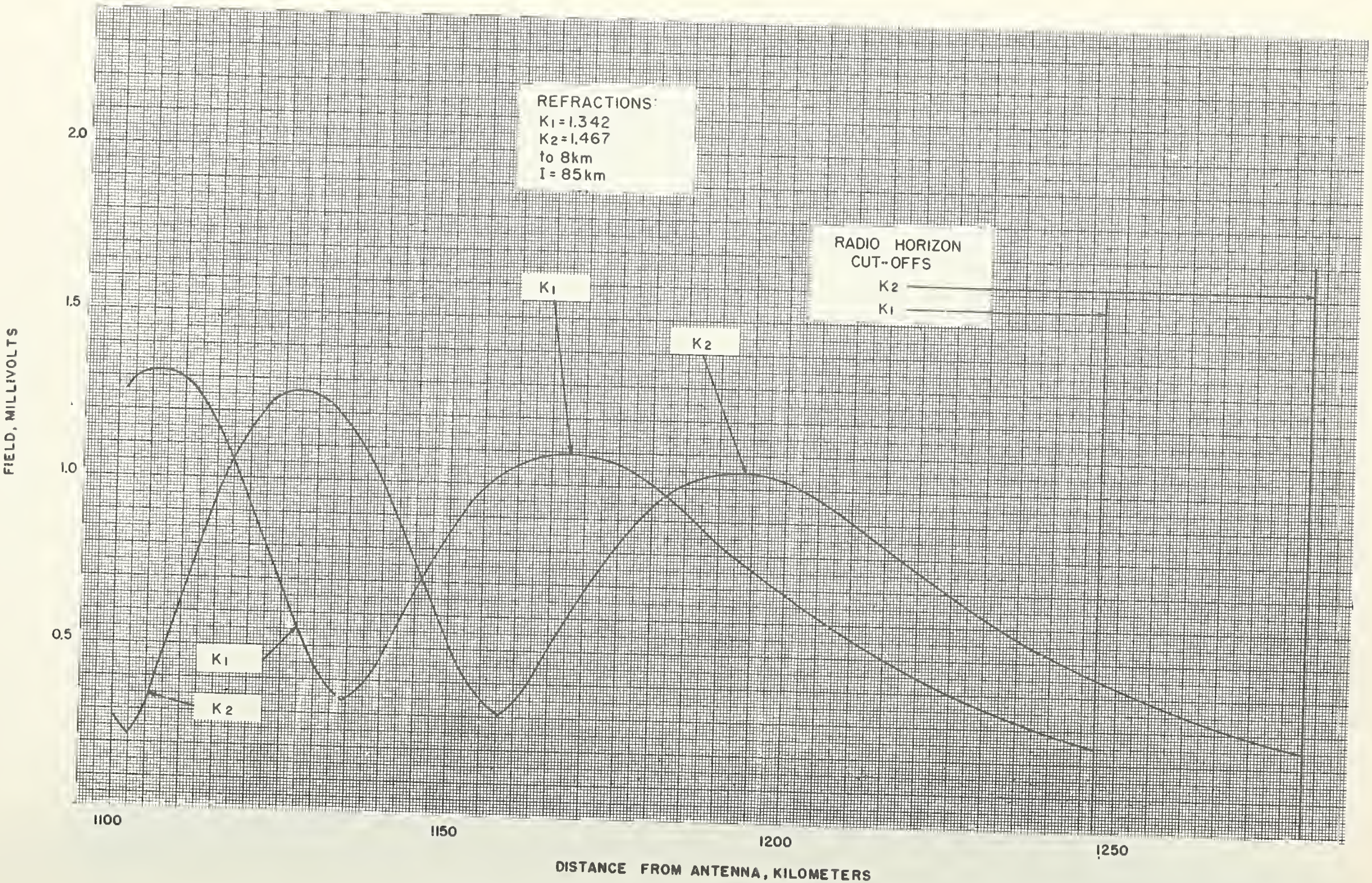

FIGURE 77. *1000 meter antenna at 35 Mc for k_1 and k_2.*

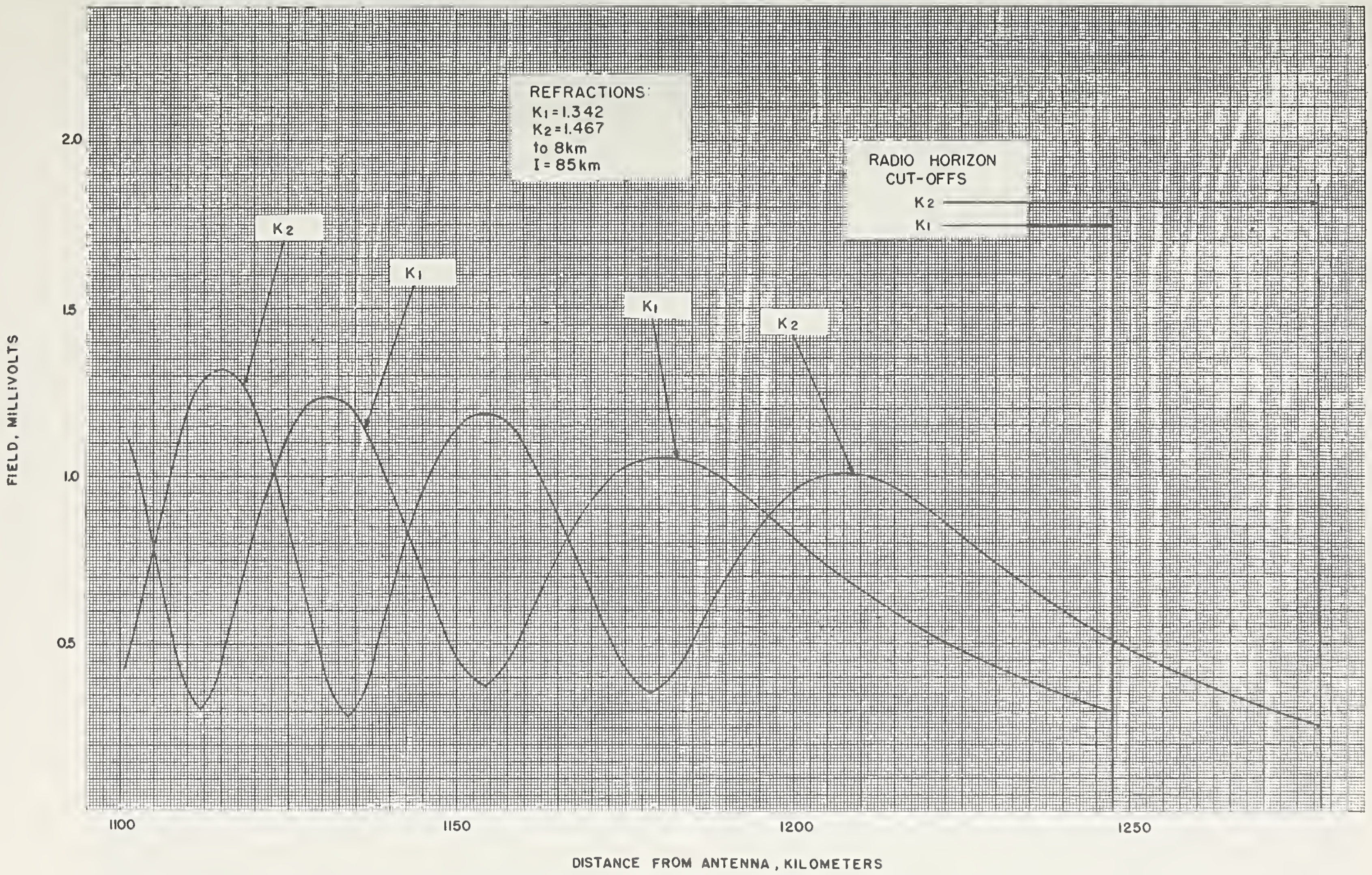

FIGURE 78. *1000 meter antenna at 50 Mc for k_1 and k_2.*

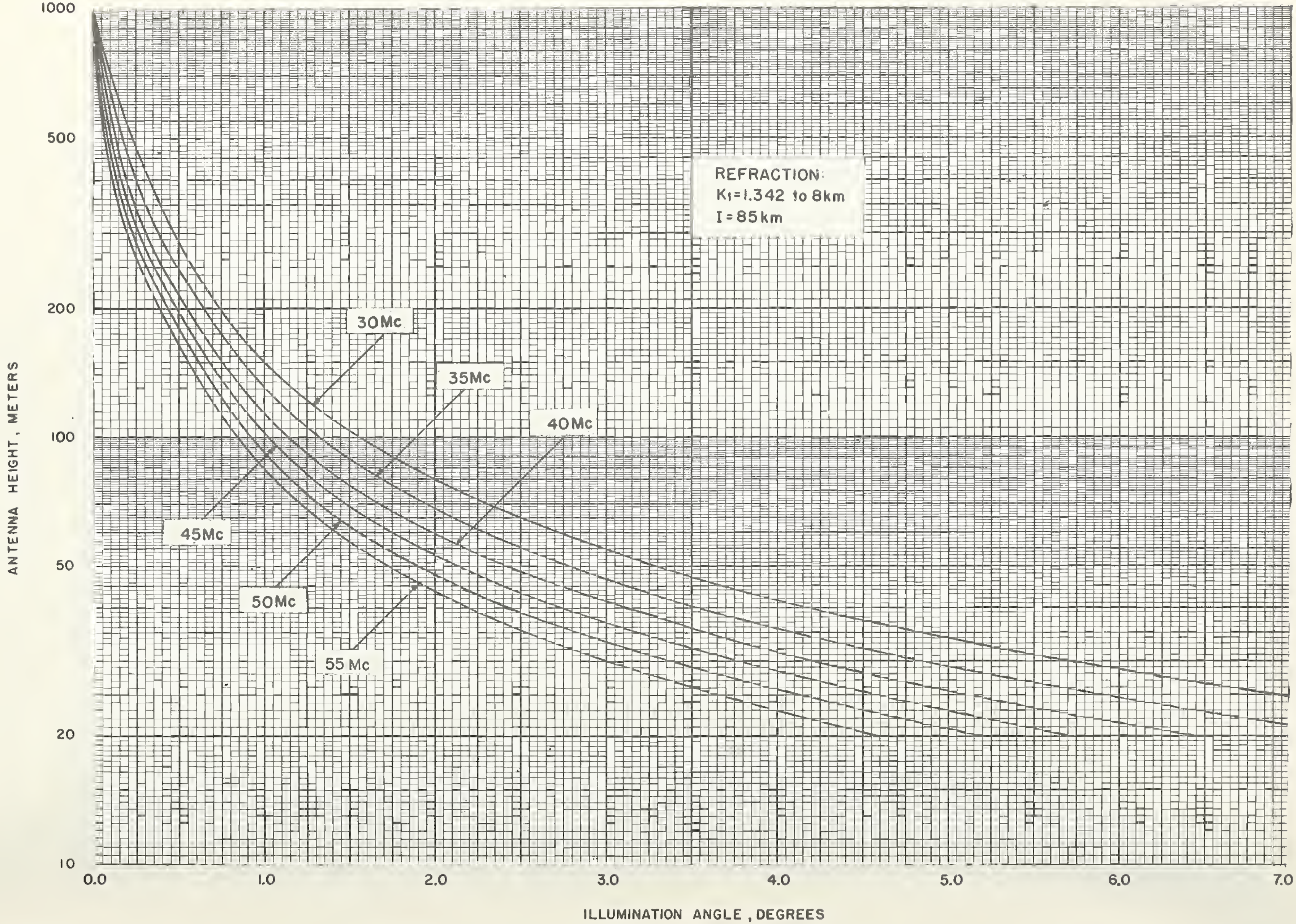

FIGURE 1A. *Angle of illumination at near edge of first Fresnel zone.*

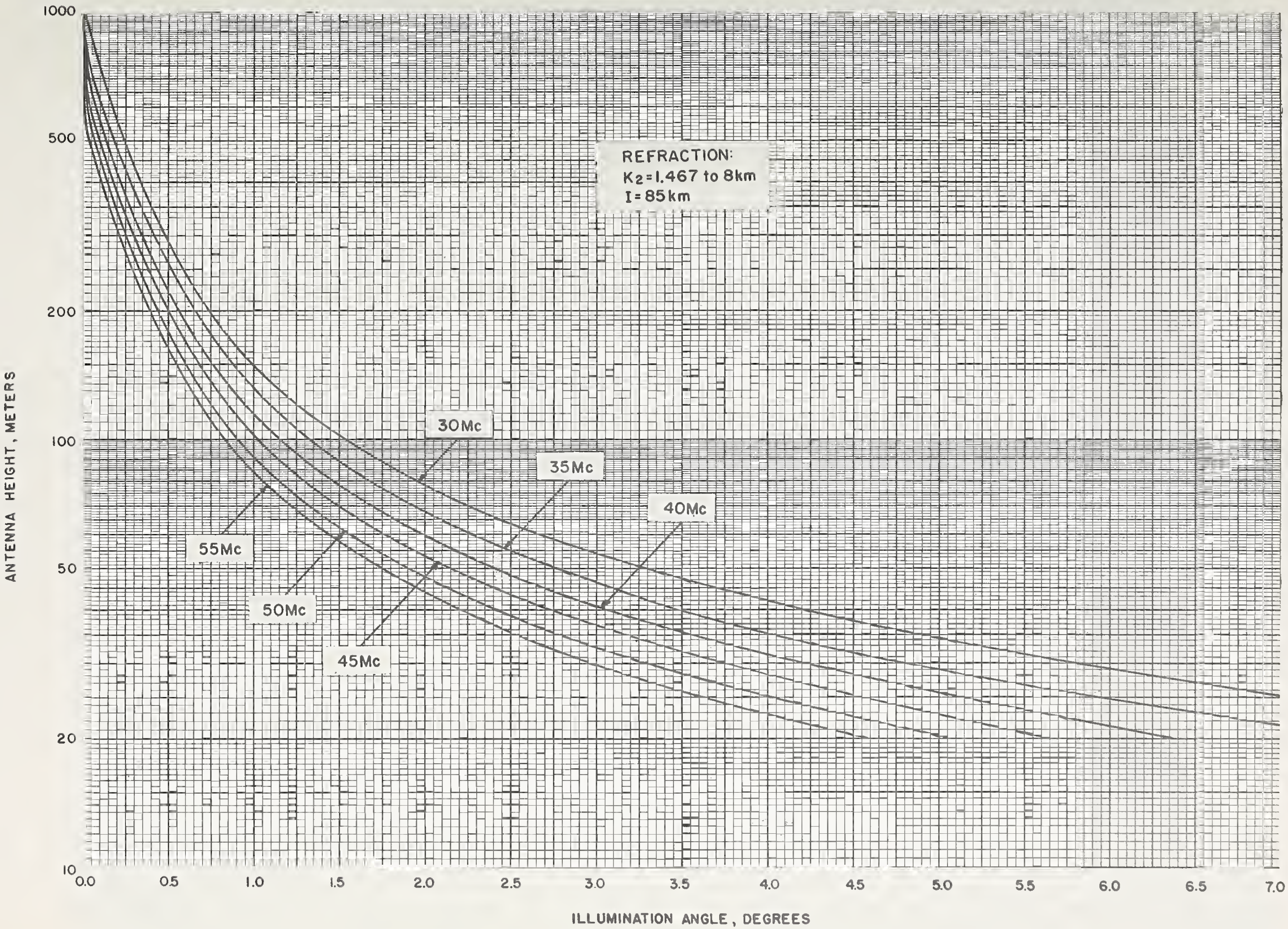

FIGURE 1B. *Angles of illumination at near edge of first Fresnel zone.*

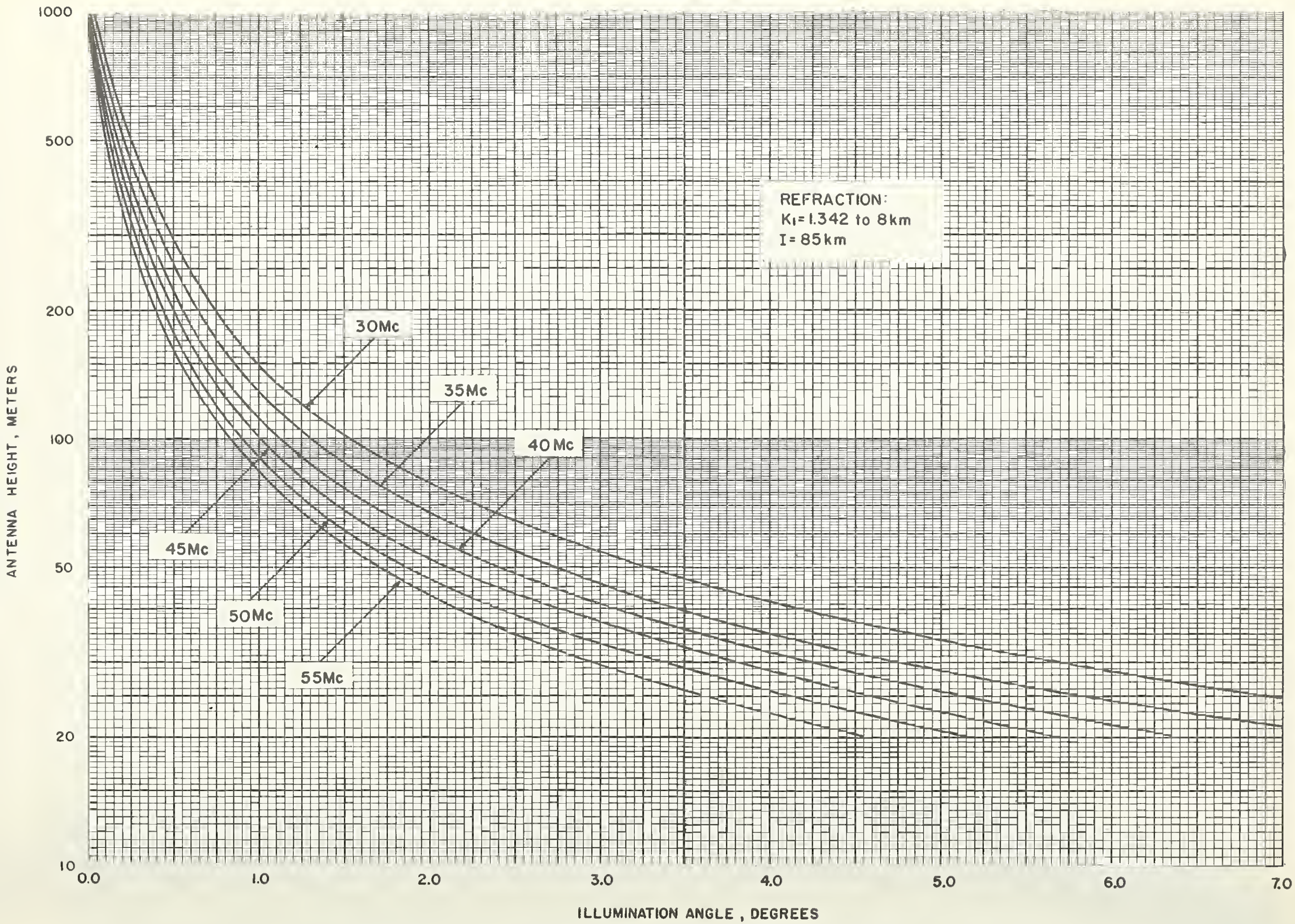

FIGURE 2A. *Angle of illumination at near λ/4 distance in first Fresnel zone.*

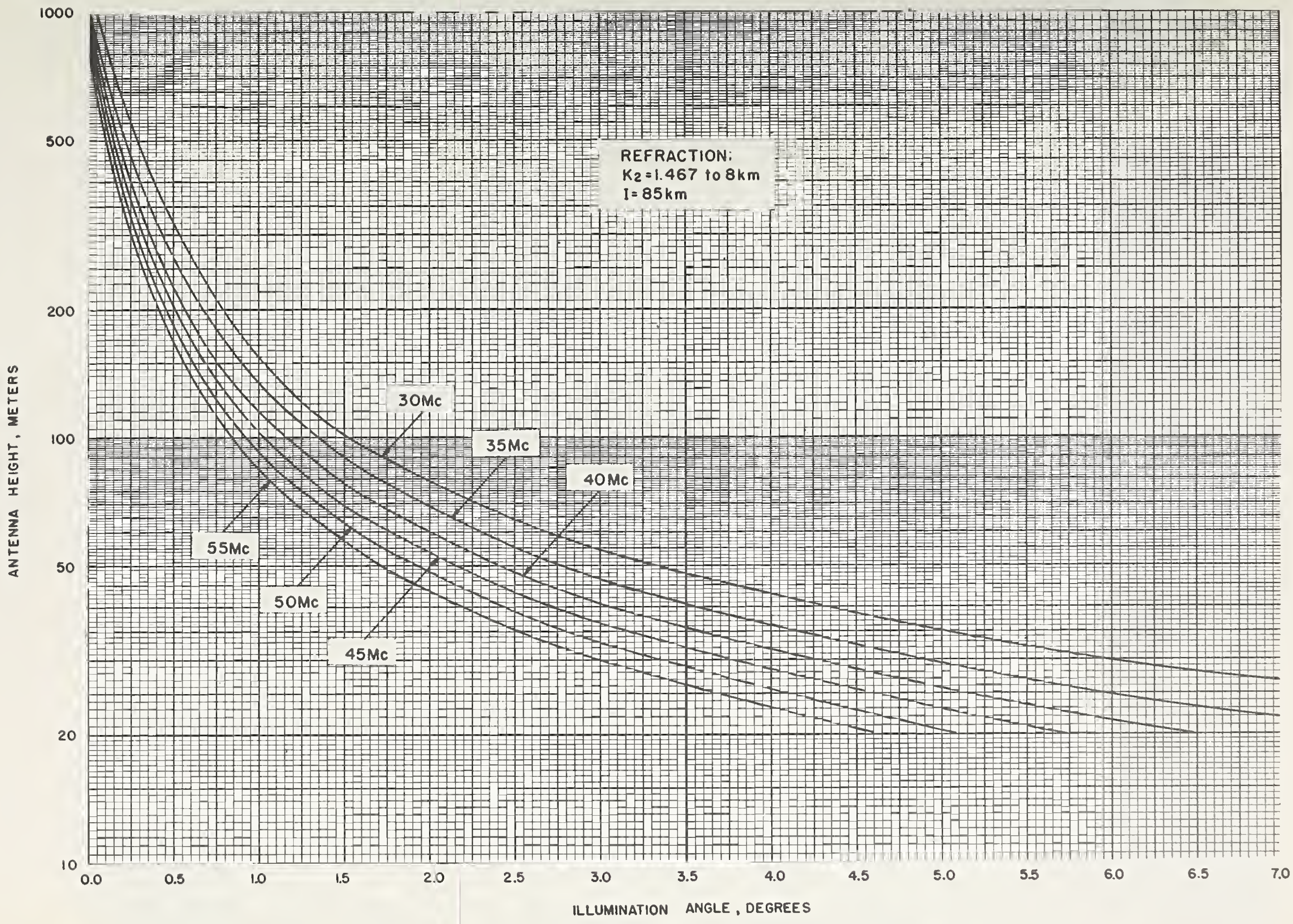

FIGURE 2B. Angles of illumination at near $\lambda/4$ distance in first Fresnel zone

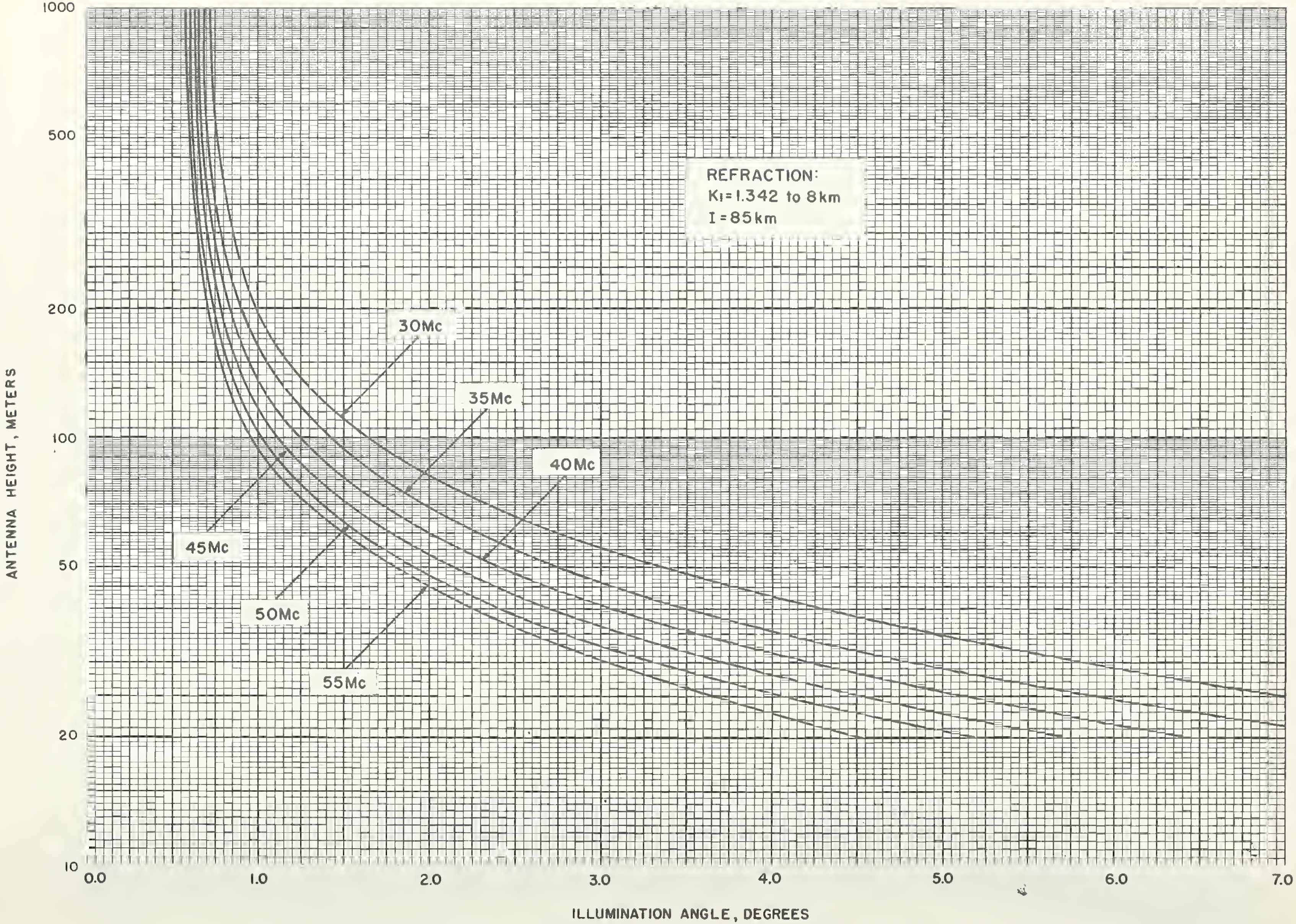

FIGURE 3A. *Angles of illumination at far λ/4 distance in first Fresnel zone.*

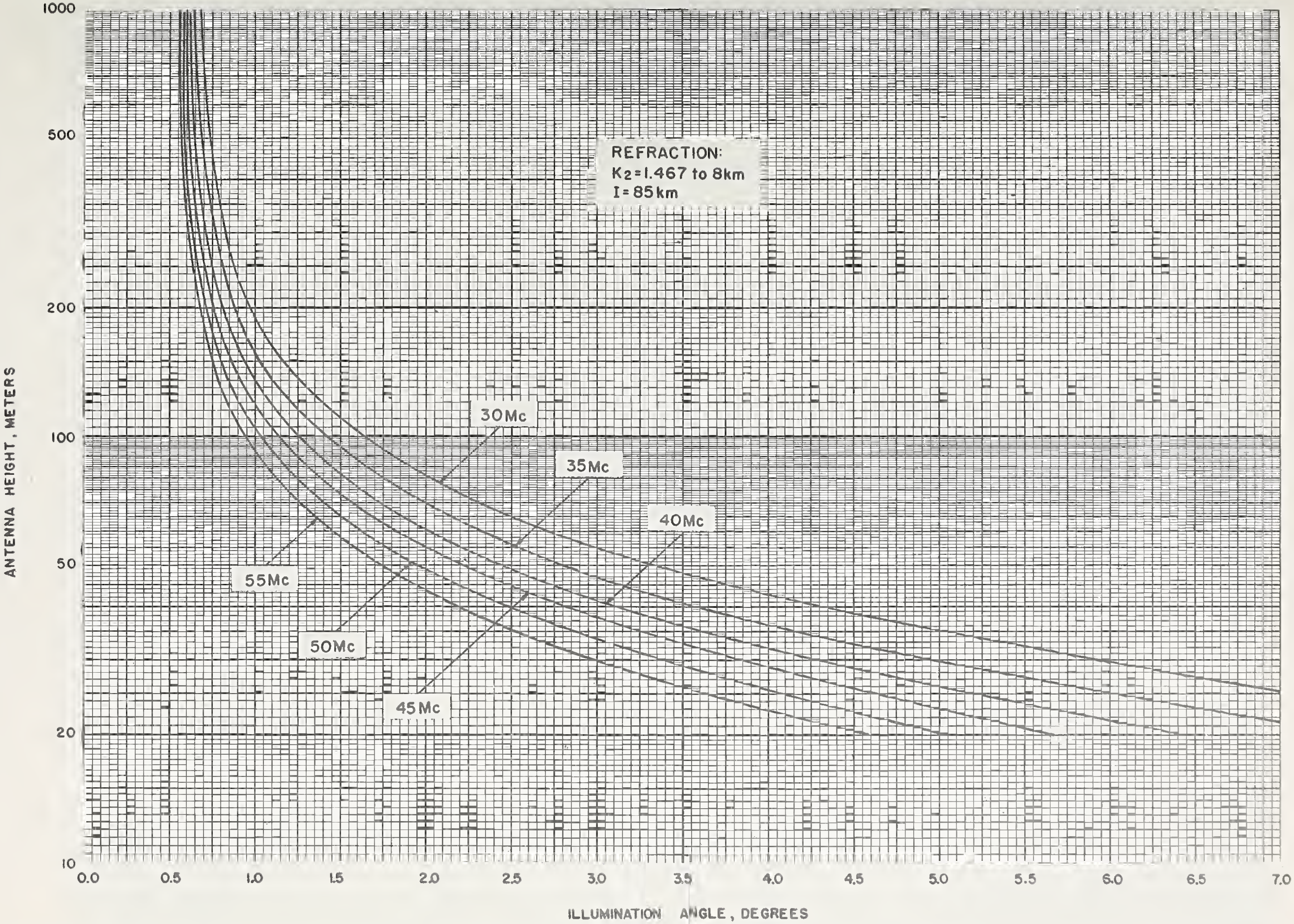

FIGURE 3B. *Angles of illumination at far λ/4 distance in first Fresnel zone.*

608365 O—62——9

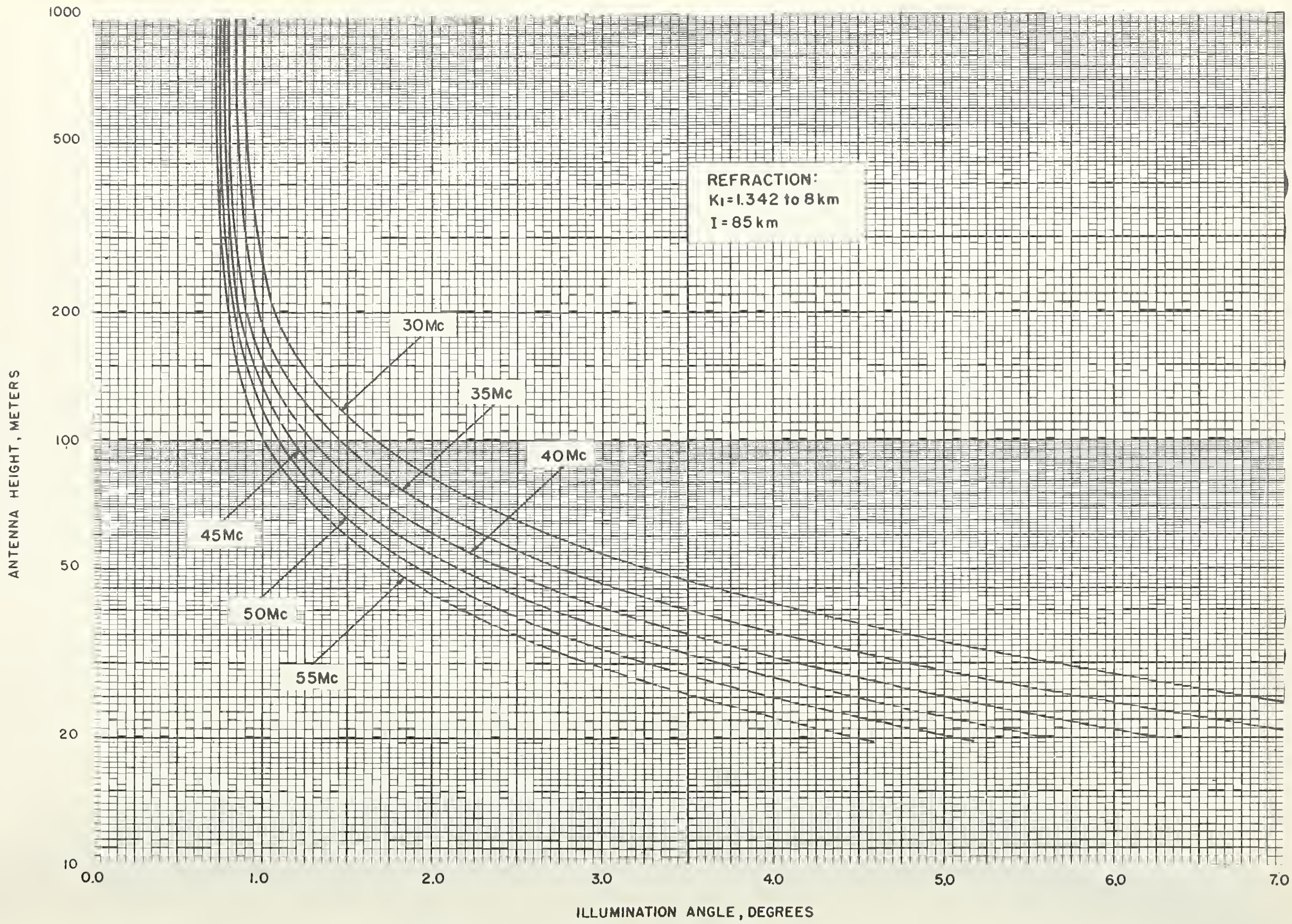

FIGURE 4A. *Angles of illumination at far edge of first Fresnel zone.*

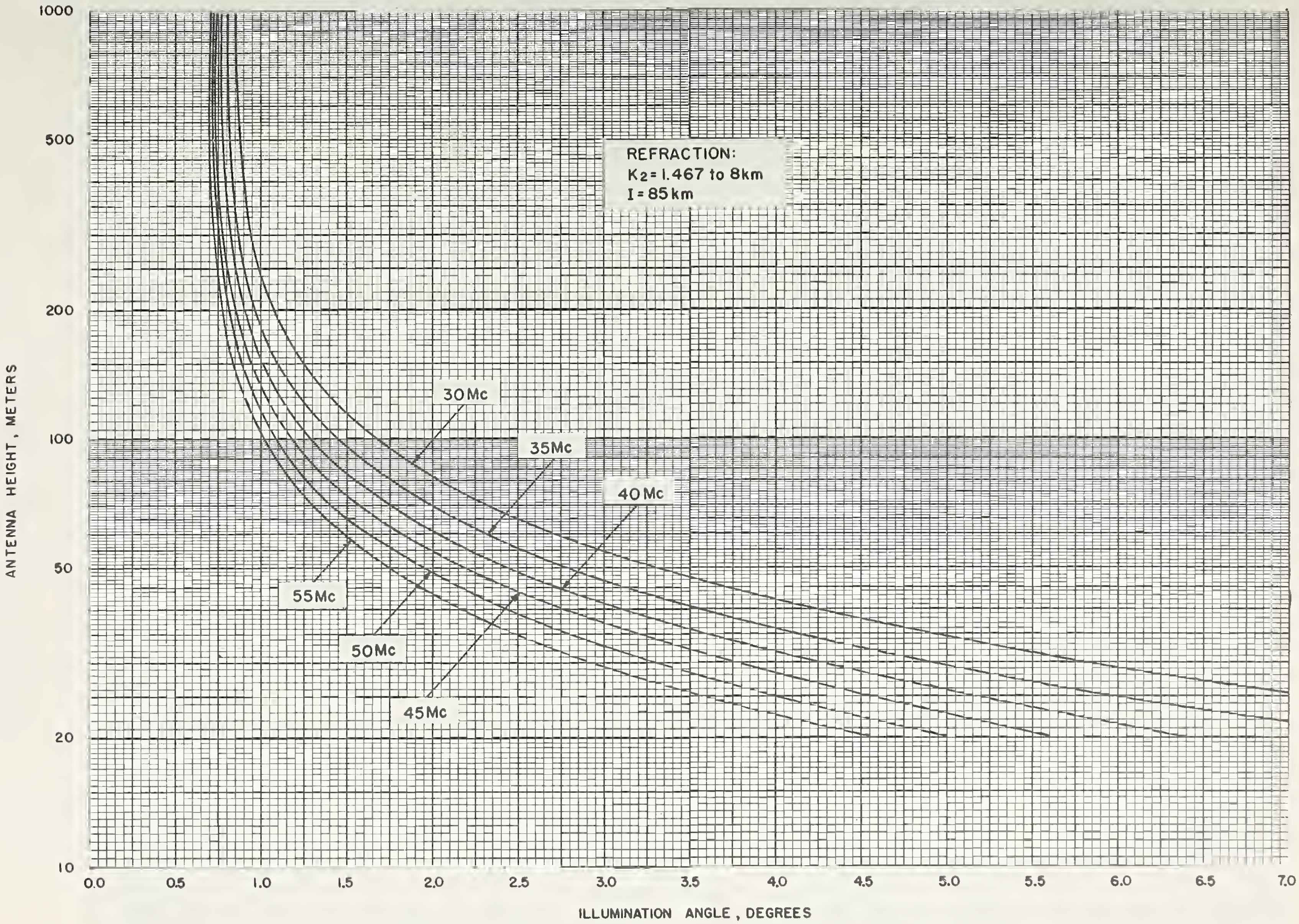

FIGURE 4B. *Angles of illumination at far edge of first Fresnel zone.*

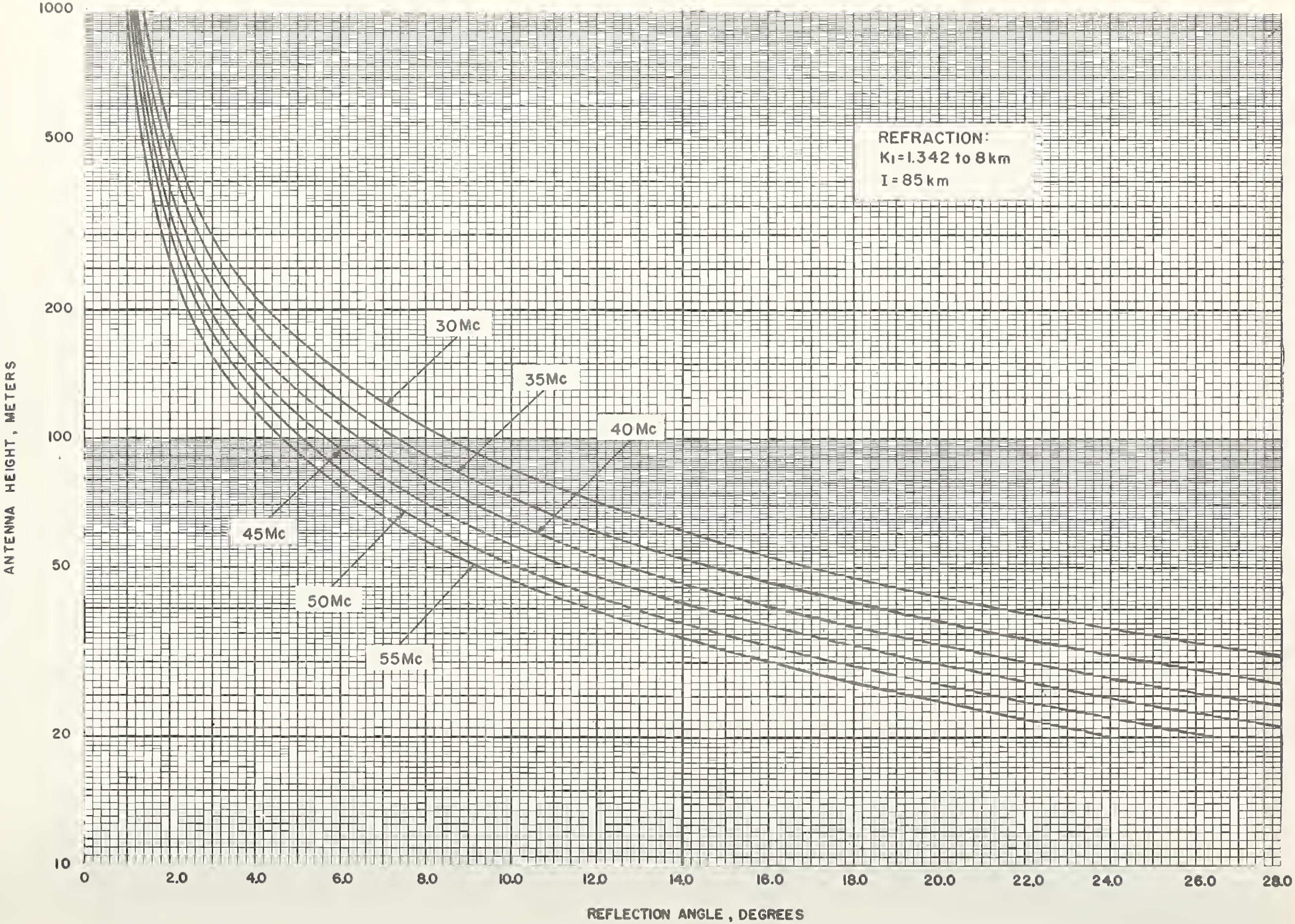

FIGURE 5A. *Angles of reflection at near edge of first Fresnel zone.*

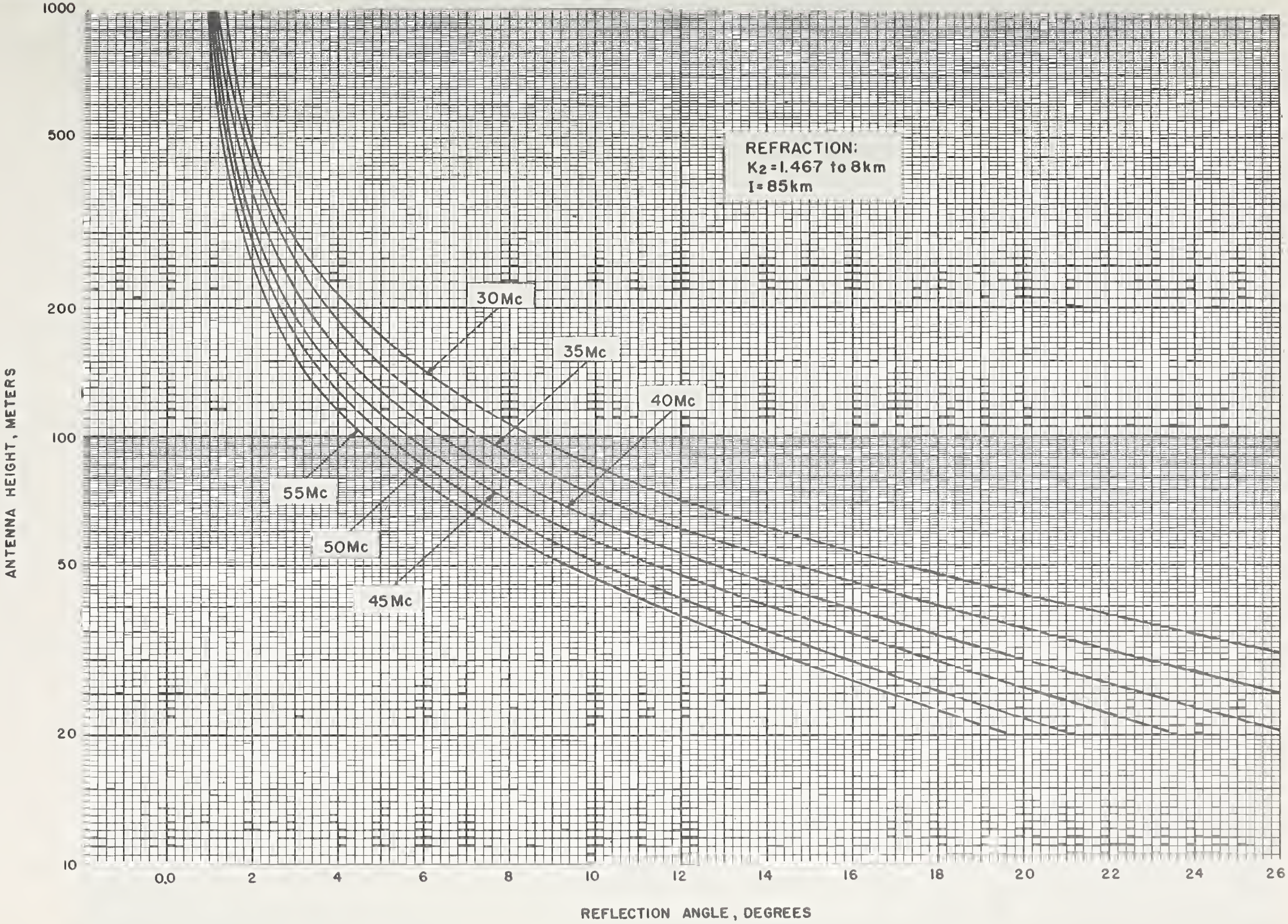

FIGURE 5B. *Angles of reflection at near edge of first Fresnel zone.*

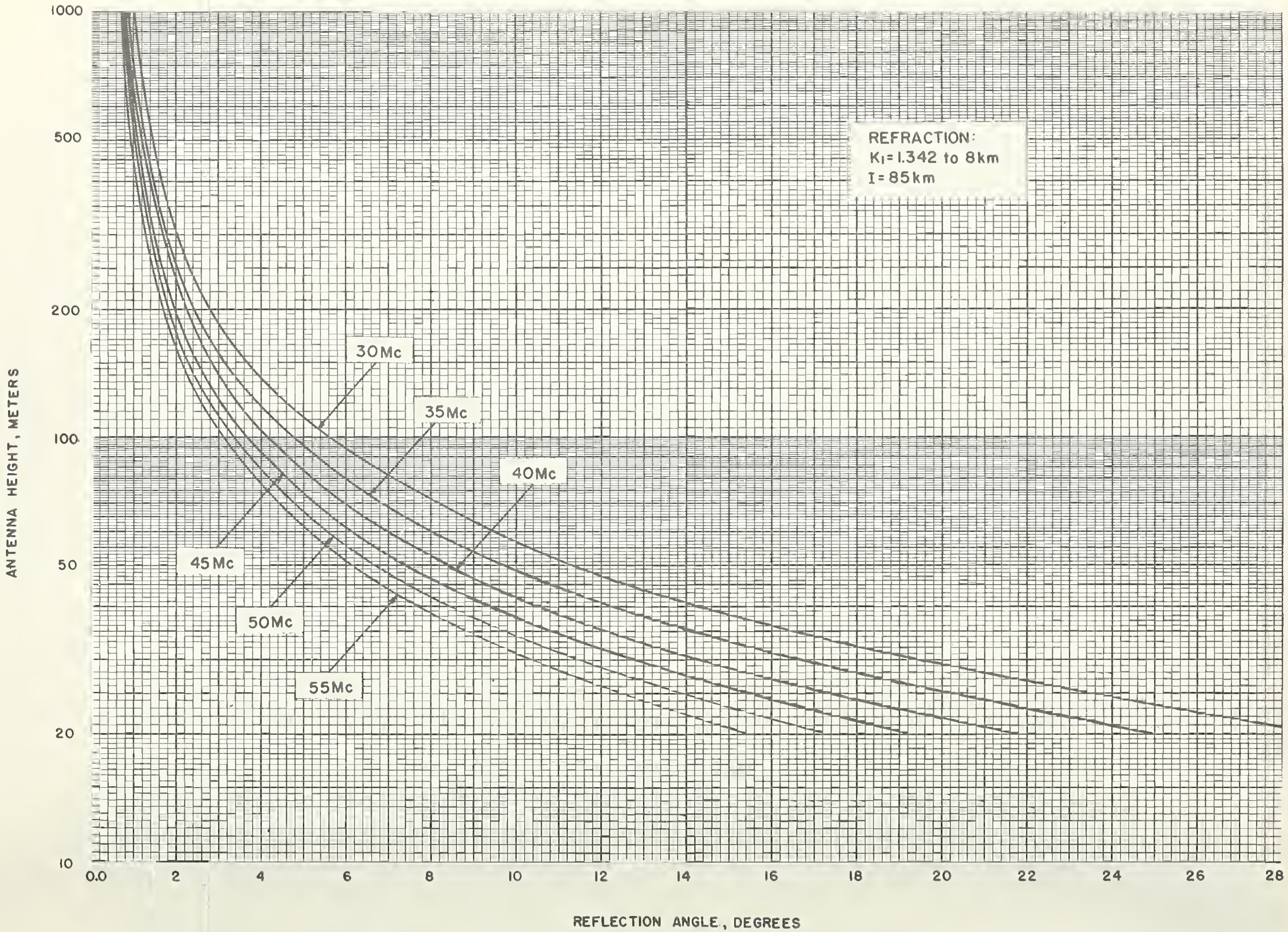

FIGURE 6A. *Angles of reflection at near $\lambda/4$ distance in first Fresnel zone.*

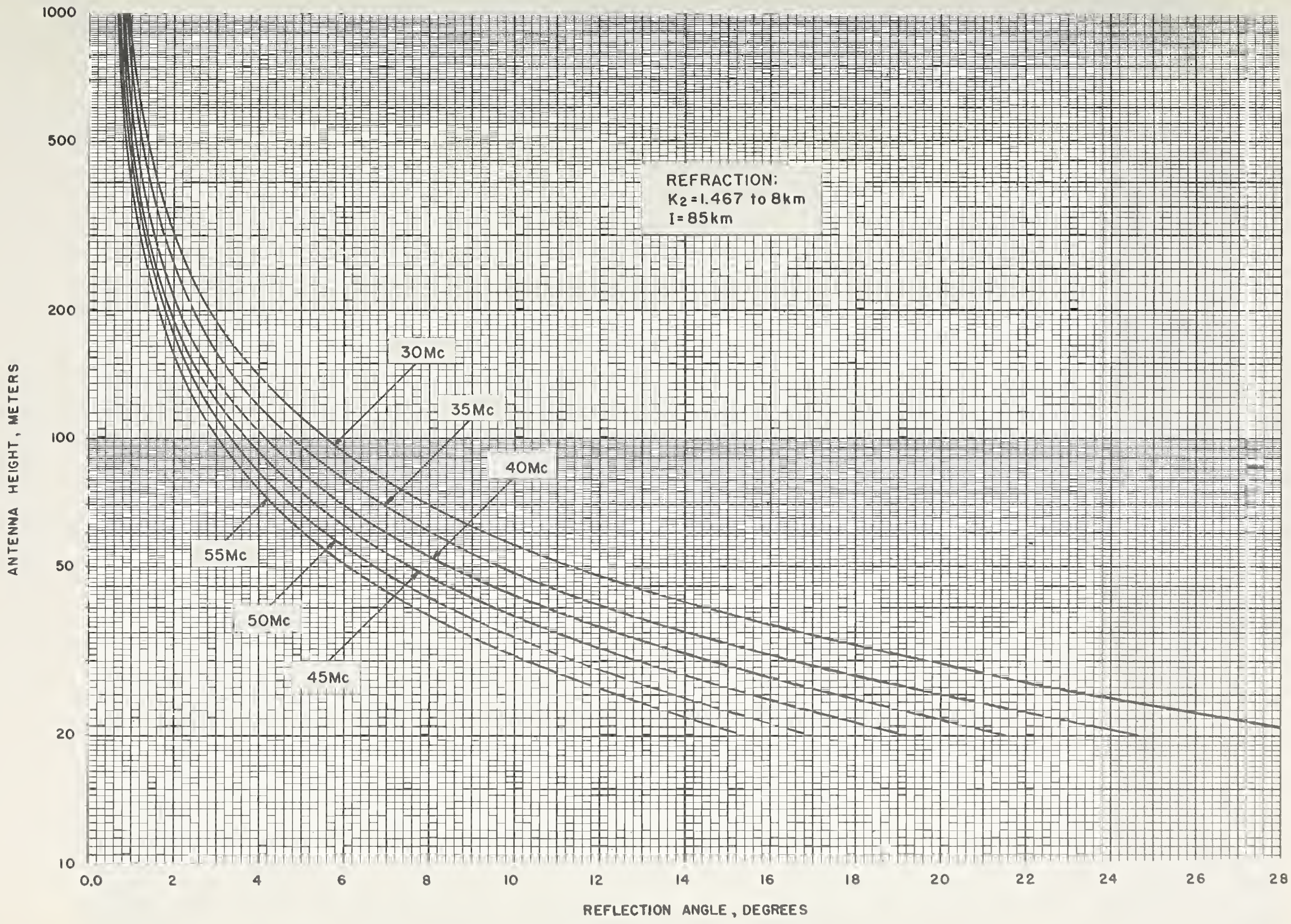

FIGURE 6B. *Angles of reflection at near $\lambda/4$ distance in first Fresnel zone.*

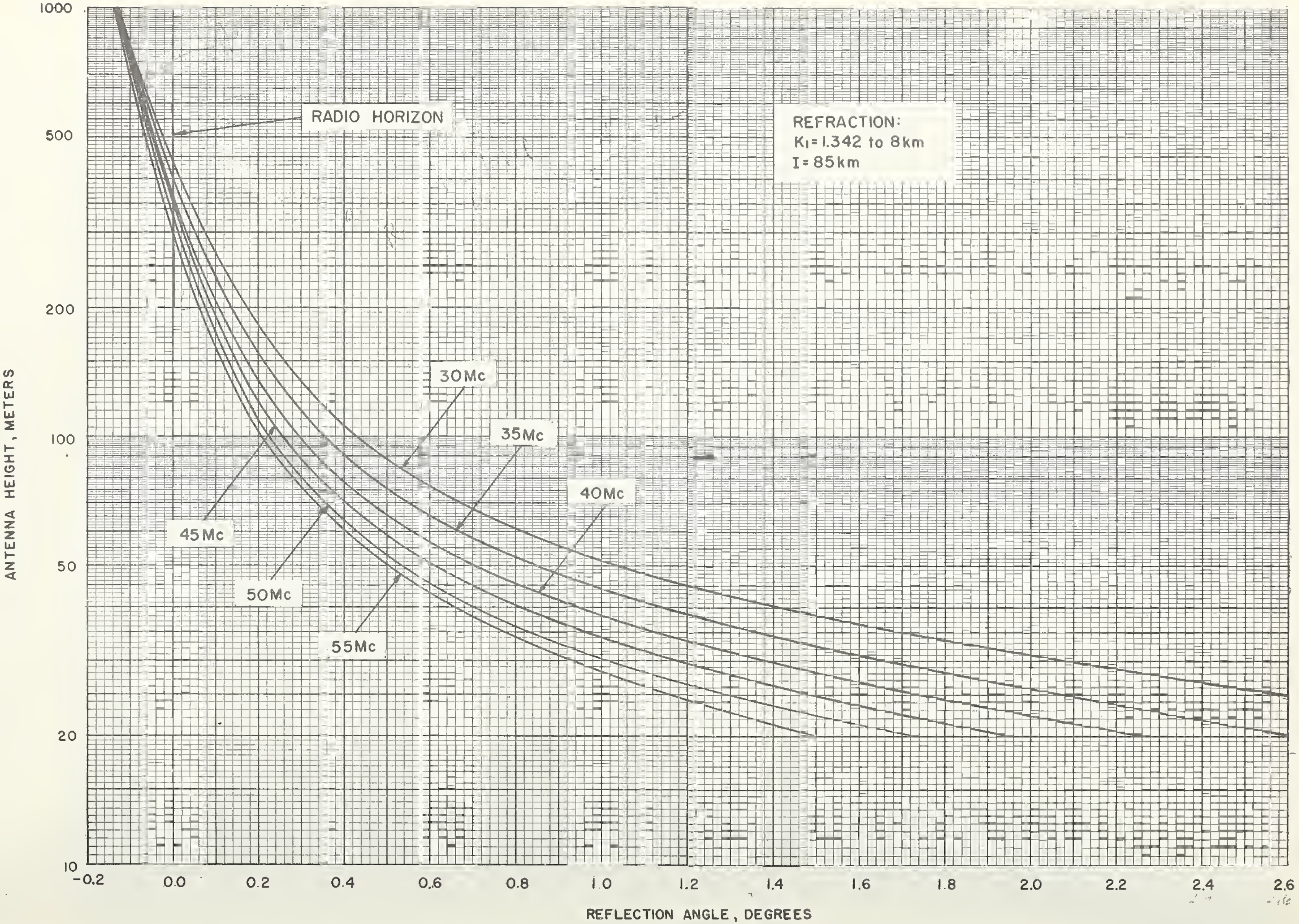

FIGURE 7A. *Angles of reflection at far λ/4 distance in first Fresnel zone.*

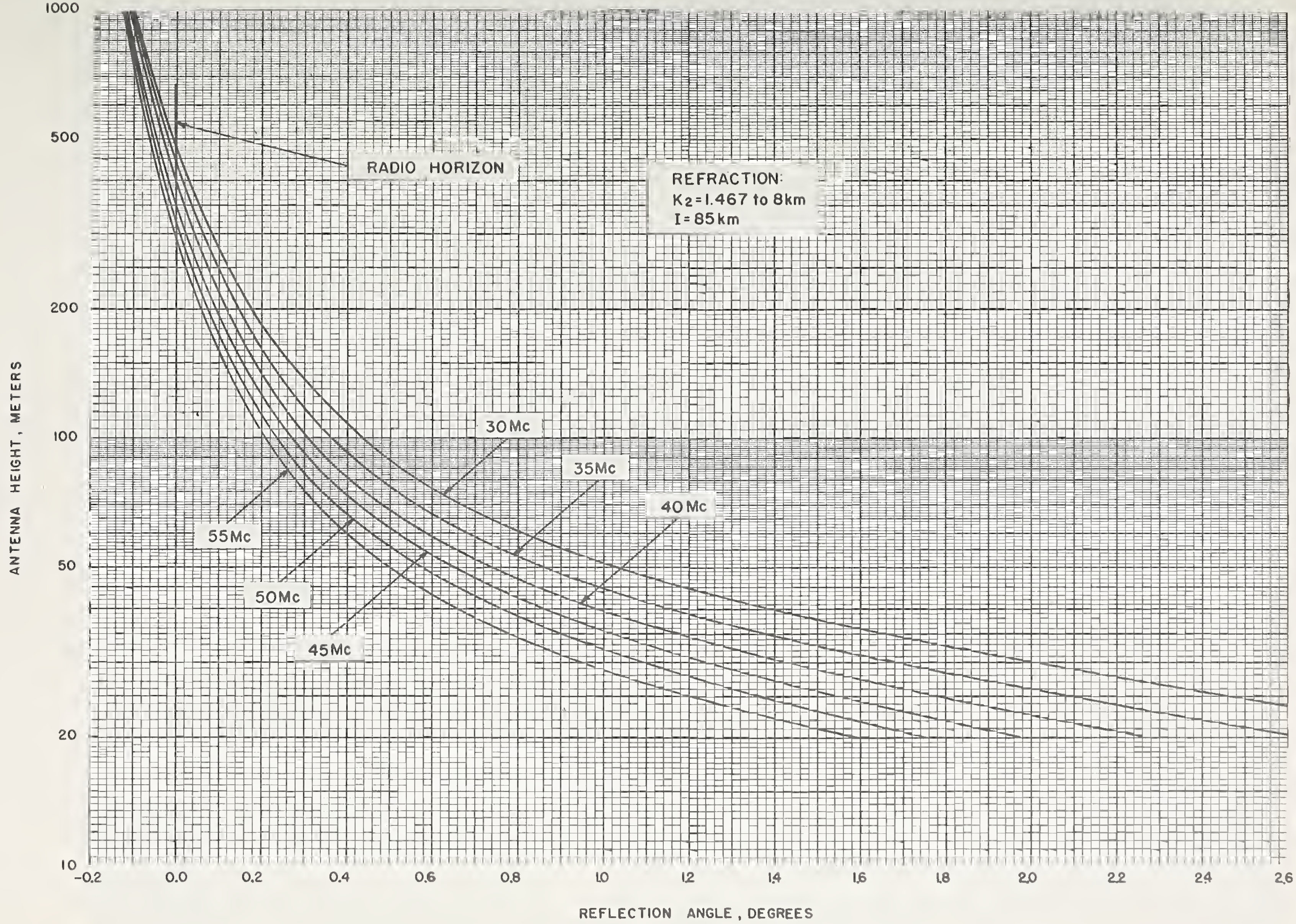

FIGURE 7B. *Angles of reflection at far λ/4 distance in first Fresnel zone.*

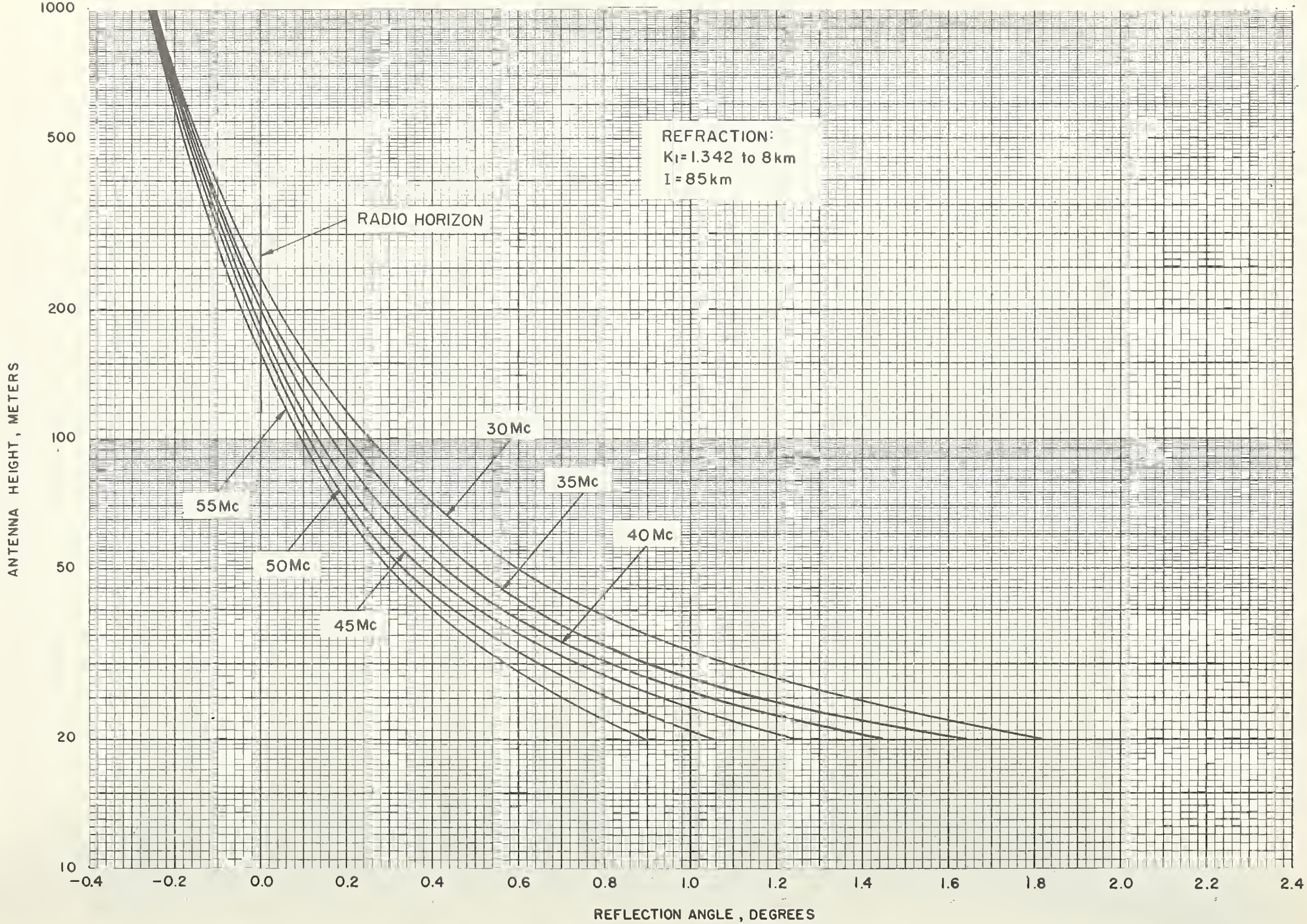

FIGURE 8A. *Angles of reflection at far edge of first Fresnel zone* (k_1).

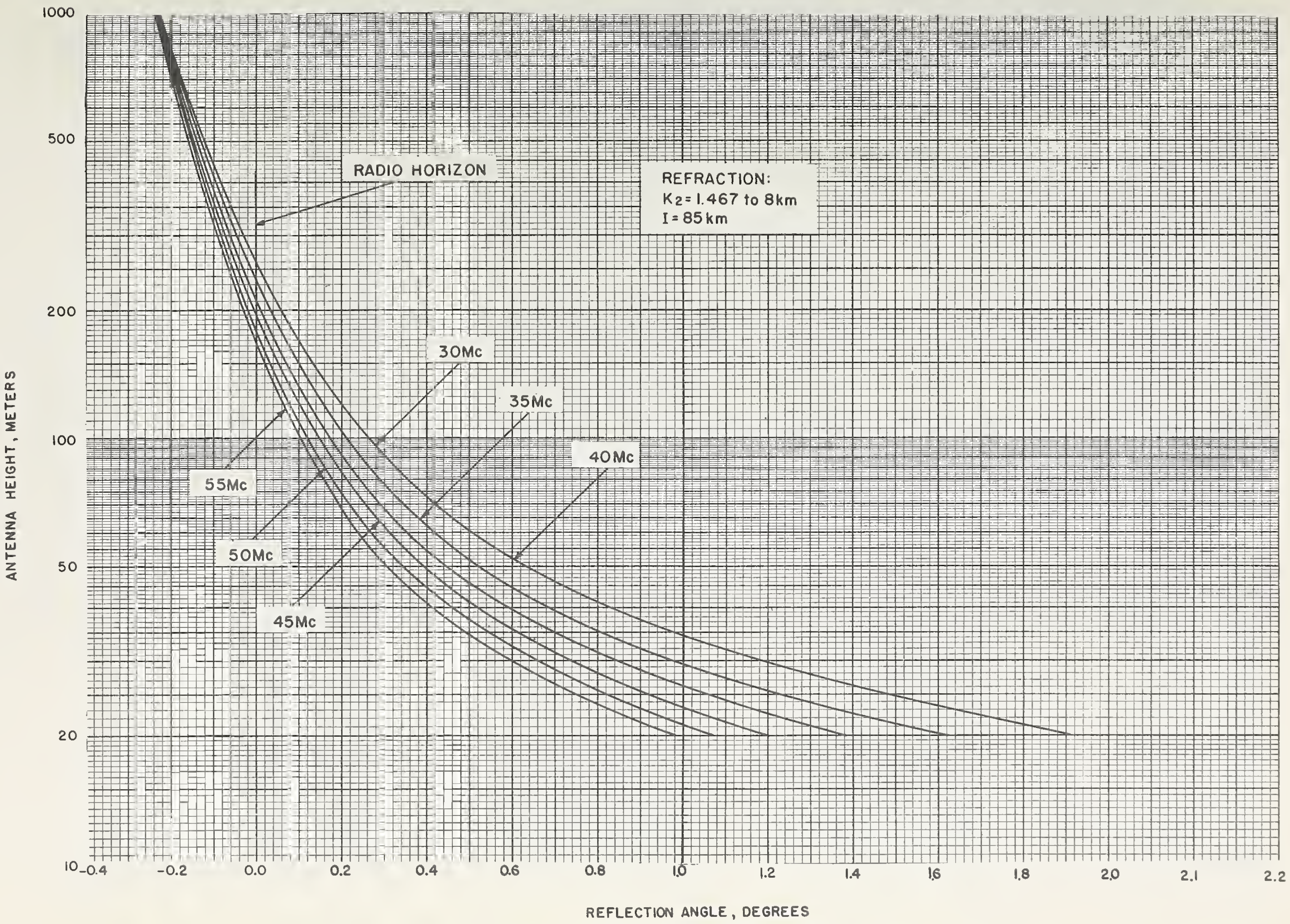

FIGURE 8B. *Angles of reflection at far edge of first Fresnel zone* (k_2).

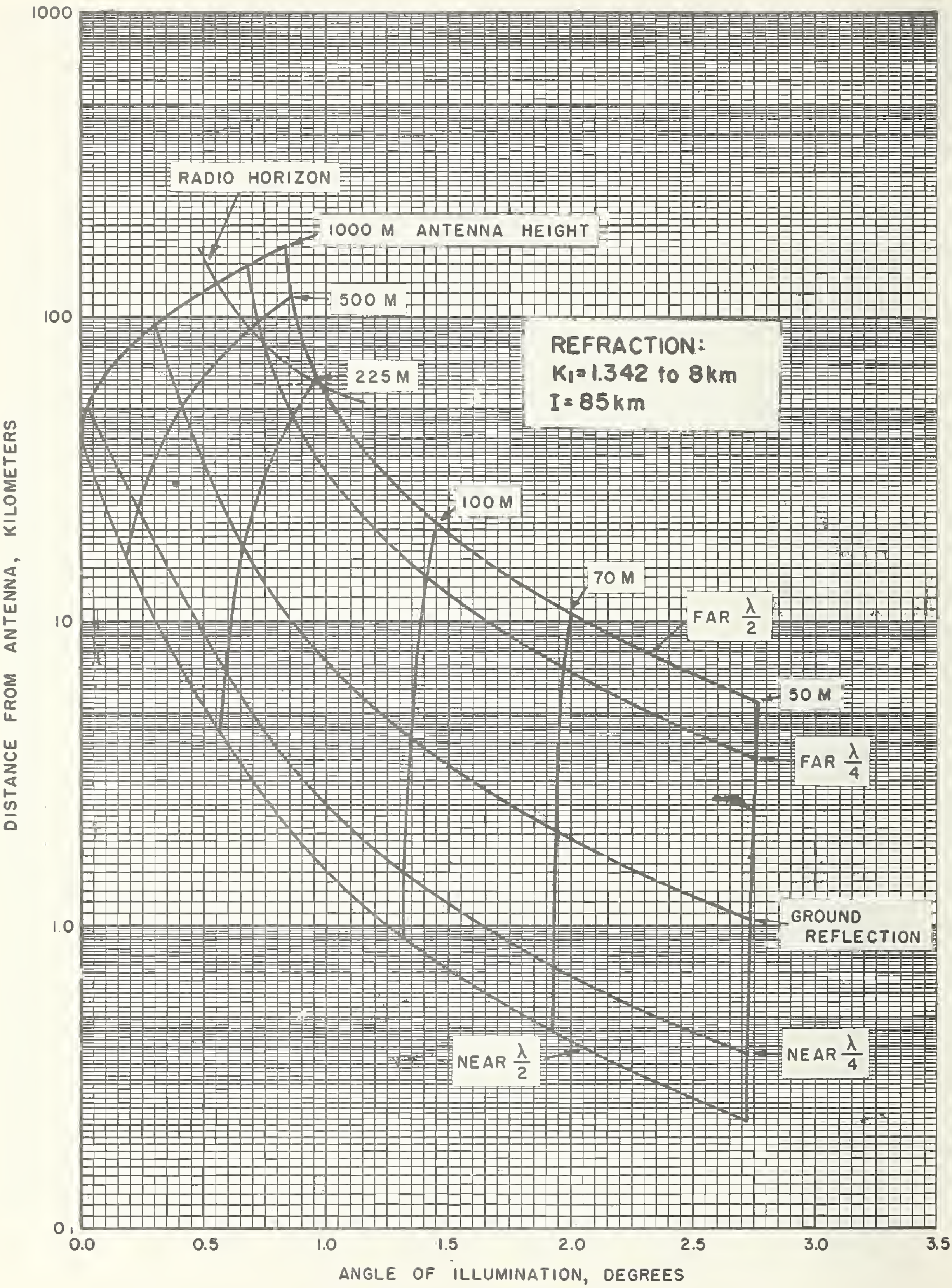

Figure 9. *Angles of illumination at 35 Mc.*

Appendix V. Tables

TABLE 1. *Lobe alinement antenna height, m*

Path length	Frequency (Mc)					
	30	35	40	45	50	55
Part A: k_1 refraction						
km						
1000	23.1	19.9	17.4	15.5	14.0	12.8
1100	26.6	22.8	19.9	17.7	16.0	14.7
1200	30.8	26.4	23.1	20.6	18.6	16.8
1300	35.9	30.8	26.9	23.9	21.5	19.4
1400	41.8	35.8	31.3	27.9	25.2	22.7
1500	49.5	42.5	37.2	33.1	29.7	26.6
1600	59.2	50.7	44.3	39.4	35.4	31.8
1700	72.9	62.2	54.3	48.4	43.7	39.3
1800	92.0	78.5	68.4	60.9	55.1	50.1
1900	122.0	103.5	90.3	80.8	73.5	66.8
2000	174.0	150.0	131.0	116.3	105.0	96.3
2100	285	246	216	193	175	161
2200	495	441	401	370	345	322
2300	883	819	763	715	675	643
Part B: k_2 refraction						
900	20.2	17.8	15.5	13.5	11.9	10.8
1000	22.9	20.2	17.7	15.5	13.7	12.4
1100	26.4	23.2	20.3	17.8	15.8	14.3
1200	30.7	26.7	23.3	20.6	18.3	16.6
1300	35.5	30.9	27.1	24.0	21.5	19.6
1400	41.6	36.1	31.6	28.0	25.2	23.0
1500	49.0	42.2	37.0	33.0	29.8	27.1
1600	58.0	49.9	43.9	39.4	35.7	32.2
1700	69.9	60.2	53.1	47.7	43.2	38.7
1800	87.0	74.7	65.6	58.8	53.2	47.8
1900	113.9	97.5	84.9	75.3	68.0	62.3
2000	157	135	117.3	103.4	93.0	85.6
2100	233	203	179	159	143	130
2200	376	334	299	271	248	228
2300	658	593	540	496	459	427
2350	890	806	736	679	633	595

TABLE 2. *Distance from antenna to ground reflection point, km*

Antenna height	Frequency (Mc)					
	30	35	40	45	50	55
Part A: k_1 refraction						
m						
20	0.130	0.154	0.179	0.203	0.228	0.252
50	.898	1.036	1.193	1.351	1.509	1.666
70	1.74	2.06	2.38	2.69	3.01	3.32
100	3.60	4.23	4.84	5.42	5.98	6.51
225	16.2	17.9	19.6	21.1	22.5	23.8
500	47.7	50.4	52.7	54.7	56.4	57.8
1000	90.9	93.4	95.6	97.6	99.3	100.7
Part B: k_2 refraction						
20	0.128	0.152	0.176	0.200	0.224	0.247
50	.866	1.023	1.179	1.336	1.493	1.650
70	1.74	2.04	2.35	2.65	2.95	3.26
100	3.52	4.13	4.74	5.36	5.97	6.58
225	16.3	18.3	20.2	21.9	23.5	25.0
500	48.7	51.9	54.6	56.8	58.7	60.2
1000	93.8	96.6	99.1	101.3	103.2	104.8

TABLE 3. *Distance from antenna to near edge of first Fresnel zone, km*

Antenna height	Frequency (Mc)					
	30	35	40	45	50	55
Part A: k_1 refraction						
m						
20	0.022	0.027	0.032	0.036	0.041	0.046
50	.161	.190	.218	.247	.276	.304
70	.321	.378	.434	.490	.545	.599
100	.662	.777	.890	1.001	1.111	1.219
225	3.28	3.79	4.29	4.77	5.24	5.69
500	13.7	15.3	16.8	18.2	19.4	20.5
1000	37.0	39.8	42.3	44.6	46.6	48.4
Part B: k_2 refraction						
20	0.022	0.027	0.032	0.036	0.041	0.046
50	.160	.189	.217	.245	.274	.303
70	.321	.376	.432	.487	.543	.598
100	.661	.773	.885	.996	1.108	1.220
225	3.29	3.80	4.31	4.80	5.29	5.76
500	13.9	15.6	17.1	18.5	19.8	21.0
1000	38.0	40.8	43.4	45.7	47.8	49.7

TABLE 4. *Distance from antenna to near quarter wave point, km*

Antenna height	Frequency (Mc)					
	30	35	40	45	50	55
Part A: k_1 refraction						
m						
20	0.037	0.044	0.051	0.058	0.065	0.072
50	.250	.295	.339	.383	.427	.470
70	.496	.585	.672	.758	.842	.924
100	1.02	1.20	1.37	1.54	1.71	1.88
225	5.05	5.73	6.42	7.10	7.79	8.47
500	19.6	21.5	23.3	24.9	26.4	27.8
1000	48.1	51.1	53.8	56.1	58.1	59.8
Part B: k_2 refraction						
20	0.036	0.043	0.050	0.058	0.065	0.072
50	.250	.294	.337	.380	.424	.468
70	.497	.582	.668	.753	.839	.925
100	1.02	1.19	1.36	1.53	1.71	1.88
225	5.04	5.75	6.47	7.18	7.90	8.62
500	19.7	21.8	23.7	25.5	27.1	28.5
1000	49.3	52.4	55.2	57.7	59.9	61.7

TABLE 5. *Distance from antenna to far quarter wave point, km*

Antenna height	Frequency (Mc)					
	30	35	40	45	50	55
	Part A: k_1 refraction					
m						
20	0.37	0.44	0.52	0.60	0.68	0.76
50	2.78	3.34	3.89	4.44	5.00	5.55
70	5.93	7.00	8.07	9.14	10.21	11.27
100	12.2	14.2	16.1	17.8	19.3	20.7
225	45.2	47.5	49.8	52.1	54.4	56.7
500	96.0	97.4	98.8	100.1	101.5	102.9
1000	149	150	151	151	152	153
	Part B: k_2 refraction					
20	0.36	0.43	0.50	0.57	0.64	0.71
50	2.71	3.25	3.80	4.35	4.89	5.44
70	5.84	6.90	7.95	9.00	10.05	11.10
100	12.0	14.0	15.9	17.7	19.4	20.9
225	45.5	48.8	51.9	54.6	56.9	58.8
500	98.1	100.1	102.1	104.1	106.1	108.1
1000	154	155	156	158	159	160

TABLE 6. *Distance from antenna to far edge of first Fresnel zone, km*

Antenna height	Frequency (Mc)					
	30	35	40	45	50	55
	Part A: k_1 refraction					
m						
20	0.63	0.75	0.86	0.97	1.08	1.19
50	4.51	5.43	6.32	7.17	7.99	8.77
70	9.02	10.81	12.46	13.97	15.34	16.57
100	18.2	21.1	23.7	26.0	28.0	29.7
225	60.0	63.4	66.2	68.5	70.3	71.6
500	117	118	119	120	121	122
1000	173	173	173	173	174	174
	Part B: k_2 refraction					
20	0.58	0.70	0.81	0.93	1.04	1.16
50	4.45	5.30	6.14	6.99	7.84	8.69
70	9.17	10.65	12.13	13.60	15.08	16.65
100	17.9	20.7	23.3	25.7	27.9	29.9
225	61.3	64.7	67.9	70.8	73.4	75.7
500	120	121	123	125	126	128
1000	179	179	180	180	181	181

Appendix VI. Mathematical Discussion of the Lobe Shift

The difference between the lobe alinement heights given in reference 2 and those given in figure 6 is due primarily to the incorporation of divergence and defocusing in the latter results. These quantities cause the first few lobe maximums to occur at phase differences other than $\phi=2\pi k$ ($k=0, 1, 2, \ldots$) between the direct and reflected rays. This is shown mathematically as follows:

Differentiating E_r (37) with respect to ψ we obtain

$$\frac{dE_r}{d\psi}=\frac{1}{E_r}\left[d_R\frac{d(d_R)}{d\psi}+d_D\frac{d(d_D)}{d\psi}+d_Dd_R(-\sin\phi)\frac{d\phi}{d\psi}+\cos\phi\left(d_D\frac{d(d_R)}{d\psi}+d_R\frac{d(d_D)}{d\psi}\right)\right]. \qquad \text{(A1)}$$

When $\phi=2\pi k$, $E_r=d_R+d_D$ and

$$\left.\frac{dE_r}{d\psi}\right]_{\phi=2\pi k}=\frac{d(d_R)}{d\psi}+\frac{d(d_D)}{d\psi},\ k=0,1,2,\ldots \qquad \text{(A2)}$$

Maximums occur at $\phi=2\pi k$ only when this derivative vanishes. Similarly, minimums occur only when

$$\left.\frac{dE_r}{d\psi}\right]_{\phi=\pi(2k+1)}=\frac{d(d_D)}{d\psi}-\frac{d(d_R)}{d\psi} \qquad \text{(A3)}$$

vanishes.

Using eq (35) and (36) and letting r_D and r_R be the lengths of the direct and reflected rays, we obtain

$$\frac{d(d_R)}{d\psi}=\frac{d}{d\psi}\left(\frac{\sqrt{D_R}}{r_R}\right)=\frac{1}{2r_R\sqrt{D_R}}\cdot\frac{d(D_R)}{d\psi}+\frac{\sqrt{D_R}}{(r_R)^2}\left|\frac{d(r_R)}{d\psi}\right| \qquad \text{(A4)}$$

and

$$\frac{d(d_D)}{d\psi}=\frac{d}{d\psi}\left(\frac{\sqrt{D_D}}{r_D}\right)=\frac{1}{2r_D\sqrt{D_D}}\cdot\frac{d(D_D)}{d\psi}+\frac{\sqrt{D_D}}{(r_D)^2}\left|\frac{d(r_D)}{d\psi}\right|, \qquad \text{(A5)}$$

knowing that the derivatives of r_R and r_D are negative.

The behavior of $d(D_R)/d\psi$ and of $d(D_D)/d\psi$ is independent of ϕ and can be quickly deduced from figure 8. Successive differences show that r_R and r_D (also independent of ϕ) are exponentially decreasing functions of ψ which asymptotically approach 85+0.002h km and 85 km, respectively, as ψ approaches $\pi/2$. Thus the two derivatives vanish as ψ increases. Since the derivatives of D_D and D_R vanish almost immediately, the difference in lobe alinement heights with increasing ψ (i.e., with decreasing antenna height), decreases exponentially as shown in reference 1, figures 7 and 8.

Similarly, since eq (A2) and (A3) are non-zero, they show that the minimums differ from zero voltage between the first few lobes, but by less than the maximums differ from the in-phase sums of the two components. This effect on the lobe shape is greatest for small ψ and is plainly evident in appendix I, figures 27–32 and in appendix II, figures 59–64.

Appendix VII. Symbols and Equations

List of Symbols

A: Observed angle of elevation of direct ray at antenna (fig. 1).
$A_{n(c)}$: Interpolated value of A.
$A_{n(dc)}$: Interpolated and corrected value of A.
a: Mean earth's radius (6368 km).
c: Velocity of light in vacuo ($2.99790 \cdot 10^{10}$ cm/sec).
D_D: Refractive defocusing of direct ray.
D_R: Product of spherical divergence and refractive defocusing of the direct ray.
d_D: Voltage contribution of direct ray.
d_R: Voltage contribution of reflected ray.
E_r: Voltage resultant (eq. 37).
E: Elevation of "radio tropopause" (eq. 2).
f: Frequency (Mc).
G: Direct ray segment (fig. 2).
H_R: Distance to radio horizon.
h: Antenna height.
h_D: Difference of arithmetic progression of ψ (eqs 19 and 21).
I: Ionospheric scattering layer height.
k: Effective earth's radius factor for linear atmosphere.
L_e: Electrical path length difference.
L_R: Path difference between Fresnel zone surface and obstacle surface.
L_w: Path length difference in wavelengths.
M: Reflected ray segment (fig. 2).
N: Reflected ray segment (fig. 2).
N_s: Surface refractivity.
R: Direct ray segment (fig. 1).
R_0: Elevation of zero phase surface.
SR_f: Total reflected ray length at frequency f in Fresnel zone calculation.
T: Reflected ray segment (fig. 1).
u_u: "Upper" inverse interpolation factor (eqs 19–20).
u_l: "Lower" inverse interpolation factor (eqs 21–22).
w: Width of first Fresnel zone over plane earth.
α: True angle of elevation (fig. 1).
β: Elevation of reflected ray from antenna (figs. 2 and 3).
ΔN: Gradient of refractivity.
Δ^1, Δ^2: First and second order central differences.
δ: Angle used in spherical divergence computation (figs. 1 and 3).
ζ: Angle used in nonparallactic geometry (fig. 10).
θ: Angular surface distance from antenna to point in the ionosphere.
$\theta_E, \theta_h, \theta_I$: Angular surface distances (fig. 2).
λ: Wavelength.
ϕ: Phase angle between direct and reflected rays.
ϕ_{ED}: Phase of voltage resultant with respect to direct ray.
ψ: Angle of ground reflection (grazing angle).
ψ_F: Angle of illumination in first Fresnel zone (elevation of ionospheric scattering volume).
ψ'_F: Angle of reflection in first Fresnel zone (elevation of antenna).

Equations

Given N_s and ΔN:

$$k=\frac{1}{1-\Delta N \cdot a \cdot 10^{-6}} \tag{1}$$

$$E=\frac{N_s}{\Delta N} \tag{2}$$

Given ψ:

$$\theta_h=\cos^{-1}\left(\frac{ka}{ka+h}\cdot\cos\psi\right)-\psi \tag{3}$$

$$N=\frac{\sin\theta_h}{\cos\psi}(ka+h) \tag{4}$$

$$\theta_E=\cos^{-1}\left(\frac{ka}{ka+E}\cdot\cos\psi\right)-\psi \tag{5}$$

$$M=\frac{\sin\theta_E}{\cos\psi}(ka+E) \tag{6}$$

$$\theta_I=\cos^{-1}\left[\frac{a+E}{a+I}\cos(\psi+\theta_E)\right]-\psi-\theta_E \tag{7}$$

$$T=\frac{\sin\theta_I}{\cos(\psi+\theta_E)}(a+I) \tag{8}$$

$$\theta=k(\theta_h+\theta_E)+\theta_I=\theta(\psi) \tag{9}$$

Given A:

$$\theta_E'=\cos^{-1}\left(\frac{ka+h}{ka+E}\cos A\right)-A \tag{10}$$

$$\alpha=A-\theta_E'(k-1) \tag{11}$$

$$G=\frac{\sin\theta_E'}{\cos A}(ka+E) \tag{12}$$

$$\theta'=\cos^{-1}\left[\frac{a+E}{a+I}\cos(A+\theta_E')\right]-\alpha=\theta(A) \tag{13}$$

$$R=\frac{\sin(\theta'-k\theta_E')}{\cos(A+\theta_E')}(a+I) \tag{14}$$

Given $\theta=0$:

$$\theta_E=\cos^{-1}\left(\frac{ka}{ka+E}\right) \tag{15}$$

$$\theta_h=\cos^{-1}\left(\frac{ka}{ka+h}\right)=-A_0 \text{ (Horizon } A) \tag{16}$$

$$\theta_I=\cos^{-1}\left(\frac{a+E}{a+I}\cdot\frac{ka}{ka+E}\right)-\cos^{-1}\left(\frac{ka}{ka+E}\right)$$

$$=\cos^{-1}\left(\frac{a+E}{a+I}\cos\theta_E{}'\right)-\theta_E{}' \tag{17}$$

Given ψ and A:

$$\cos^{-1}\left[\frac{a+E}{a+I}\cdot\frac{ka+h}{ka+E}\cdot\cos A\right]$$

$$+(k-1)\cos^{-1}\left[\frac{ka+h}{ka+E}\cdot\cos A\right]-A$$

$$=(k-1)\cos^{-1}\left(\frac{ka}{ka+E}\cos\psi\right)$$

$$+k\left[\cos^{-1}\left(\frac{ka}{ka+h}\cos\psi\right)-2\psi\right]$$

$$+\cos^{-1}\left(\frac{a+E}{a+I}\cdot\frac{ka}{ka+E}\cos\psi\right) \tag{18}$$

Inverse Interpolation:

$$A_{n(c)}=h_D u_u+A_n \tag{19}$$

$$u_u=\frac{-\Delta^1\theta'_{n-2}-\Delta^1\theta'_n-\sqrt{(-\Delta^1\theta'_{n-1}-\Delta^1\theta'_n)^2+8\Delta^2\theta'_{n-1}(\theta_n-\theta'_n)}}{2\Delta^2\theta'_{n-1}} \tag{20}$$

$$A_{n(c)}=h_D u_l+A_{n-1} \tag{21}$$

$$u_l=\frac{-\Delta^1\theta'_{n-2}-\Delta^1\theta'_{n-1}-\sqrt{(-\Delta^1\theta'_{n-2}-\Delta^1\theta'_{n-1})^2-8\Delta^2\theta'_{n-2}(\theta'_{n-1}-\theta_n)}}{2\Delta^2\theta'_{n-2}} \tag{22}$$

where $\theta'_n<\theta_n<\theta'_{n+1}$, for θ_n nearer θ'_n in u_u and nearer θ'_{n-1} in u_l

Derivative Correction:

$$\frac{d(A_{n(c)})}{d\theta_n}\cdot\Delta\theta=\Delta A_{n(c)} \tag{23}$$

$$A_{n(dc)}=A_{n(c)}+\Delta A_{n(c)} \tag{24}$$

$$\Delta\theta=\theta(A_{n(c)})-\theta(\psi_n) \tag{25}$$

$$\frac{d(A_{n(c)})}{d\theta_n}=\frac{2h_D}{\Delta^1\theta'_{n-1}+\Delta^1\theta'_n+2u_u\Delta^2\theta'_{n-1}} \tag{26}$$

$$\frac{d(A_{n(c)})}{d\theta_n}=\frac{2h_D}{\Delta^1\theta'_{n-2}+\Delta^1\theta'_{n-1}+2u_l\Delta^2\theta'_{n-2}} \tag{27}$$

where u_u and u_l are defined above.

Divergences of Direct and Reflected Rays:

$$D_{R_{n+\frac{1}{2}}}=\frac{[\psi_{n+1}-\psi_n-(\theta_{h_n}-\theta_{h_{n+1}})]}{2[\sin(\psi_n+\theta_{E_n}+\theta_{I_n})]}$$

$$\frac{[(N_n+N_{n+1}+M_n+M_{n+1})\,n_s+T_n+T_{n+1}]}{(a+I)\,(\theta_n-\theta_{n+1})} \tag{28}$$

$$D_{R_n}=\tfrac{1}{2}(D_{R_{n+\frac{1}{2}}}+D_{R_{n-\frac{1}{2}}}),\ D_{R_o}\equiv 0 \tag{29}$$

$$D_{D_{n+\frac{1}{2}}}=\frac{(A_{n+1(dc)}-A_{n(dc)})[(G_n+G_{n+1})n_s+R_n+R_{n+1}]}{2[\sin(\alpha_n+\theta_n)](a+I)(\theta_n-\theta_{n+1})} \tag{30}$$

$$D_{D_n}=\tfrac{1}{2}(D_{D_{n+\frac{1}{2}}}+D_{D_{n-\frac{1}{2}}}),\ D_{D_o}\equiv D_{D_{0+\frac{1}{2}}} \tag{31}$$

Path Length Difference:

$$L_e=(N_n+M_n)n_s+T_n-(G_n\cdot n_s+R_n)$$

$$\text{where } n_s=1+|N_s|\cdot 10^{-6} \tag{32}$$

Frequency Dependent Quantities:

$$\frac{L_e f}{c}=L_w \tag{33}$$

$$\phi=\left\{L_w+0.5-[L_w+0.5]-\binom{0.0}{1.0}\right\}2\pi,$$

where $-\pi\leq\phi\leq+\pi$. (34)

Lobe number$=[L_w]+1$

N.B. In (34) [ ] is the integral part of the improper fraction.

$$d_{D_n}=\frac{\sqrt{D_{D_n}}}{G_n\cdot n_s+R_n} \tag{35}$$

$$d_{R_n}=\frac{\sqrt{D_{R_n}}}{(N_n+M_n)n_s+T_n} \tag{36}$$

$$E_r=\sqrt{d_R{}^2+d_D{}^2+2d_Dd_R\cos\phi} \tag{37}$$

$$\phi_{ED}=\sin^{-1}\left[\frac{\sin\phi\cdot d_R}{E_r}\right] \tag{38}$$

U. S. GOVERNMENT PRINTING OFFICE: 1962 O - 608365

U.S. DEPARTMENT OF COMMERCE
Luther H. Hodges, *Secretary*

NATIONAL BUREAU OF STANDARDS
A. V. Astin, *Director*

THE NATIONAL BUREAU OF STANDARDS

The scope of activities of the National Bureau of Standards at its major laboratories in Washington, D.C., and Boulder, Colorado, is suggested in the following listing of the divisions and sections engaged in technical work. In general, each section carries out specialized research, development, and engineering in the field indicated by its title. A brief description of the activities, and of the resultant publications, appears on the inside of the front cover.

WASHINGTON, D.C.

Electricity. Resistance and Reactance. Electrochemistry. Electrical Instruments. Magnetic Measurements. Dielectrics.

Metrology. Photometry and Colorimetry. Refractometry. Photographic Research. Length. Engineering Metrology. Mass and Scale. Volumetry and Densimetry.

Heat. Temperature Physics. Heat Measurements. Cryogenic Physics. Equation of State. Statistical Physics.

Radiation Physics. X-ray. Radioactivity. Radiation Theory. High Energy Radiation. Radiological Equipment. Nucleonic Instrumentation. Neutron Physics.

Analytical and Inorganic Chemistry. Pure Substances. Spectrochemistry. Solution Chemistry. Standard Reference Materials. Applied Analytical Research.

Mechanics. Sound. Pressure and Vacuum. Fluid Mechanics. Engineering Mechanics. Rheology. Combustion Controls.

Polymers. Macromolecules: Synthesis and Structure. Polymer Chemistry. Polymer Physics. Polymer Characterization. Polymer Evaluation and Testing. Applied Polymer Standards and Research. Dental Research.

Metallurgy. Engineering Metallurgy. Microscopy and Diffraction. Metal Reactions. Metal Physics. Electrolysis and Metal Deposition.

Mineral Products. Engineering Ceramics. Glass. Refractories. Enameled Metals. Crystal Growth. Physical Properties. Constitution and Microstructure.

Building Research. Structural Engineering. Fire Research. Mechanical Systems. Organic Building Materials. Codes and Safety Standards. Heat Transfer. Inorganic Building Materials.

Applied Mathematics. Numerical Analysis. Computation. Statistical Engineering. Mathematical Physics. Operations Research.

Data Processing Systems. Components and Techniques. Digital Circuitry. Digital Systems. Analog Systems. Applications Engineering.

Atomic Physics. Spectroscopy. Infrared Spectroscopy. Solid State Physics. Electron Physics. Atomic Physics.

Instrumentation. Engineering Electronics. Electron Devices. Electronic Instrumentation. Mechanical Instruments. Basic Instrumentation.

Physical Chemistry. Thermochemistry. Surface Chemistry. Organic Chemistry. Molecular Spectroscopy. Molecular Kinetics. Mass Spectrometry.

Office of Weights and Measures.

BOULDER, COLO.

Cryogenic Engineering. Cryogenic Equipment. Cryogenic Processes. Properties of Materials. Cryogenic Technical Services.

Ionosphere Research and Propagation. Low Frequency and Very Low Frequency Research. Ionosphere Research. Prediction Services. Sun-Earth Relationships. Field Engineering. Radio Warning Services.

Radio Propagation Engineering. Data Reduction Instrumentation. Radio Noise. Tropospheric Measurements. Tropospheric Analysis. Propagation-Terrain Effects. Radio-Meteorology. Lower Atmosphere Physics.

Radio Standards. High Frequency Electrical Standards. Radio Broadcast Service. Radio and Microwave Materials. Atomic Frequency and Time Interval Standards. Electronic Calibration Center. Millimeter-Wave Research. Microwave Circuit Standards.

Radio Systems. High Frequency and Very High Frequency Research. Modulation Research. Antenna Research. Navigation Systems.

Upper Atmosphere and Space Physics. Upper Atmosphere and Plasma Physics. Ionosphere and Exosphere Scatter. Airglow and Aurora. Ionospheric Radio Astronomy.

Radio Physics.

Circuit Standards.